SYNTHESIS OF SOME NOVEL CHEMICAL SENSOR FOR CYANIDE ION SENSING *VIA* DIFFERENT MECHANISM

Ph. D. THESIS

by

NIRMA MAURYA

DEPARTMENT OF CHEMISTRY
INDIAN INSTITUTE OF TECHNOLOGY ROORKEE
ROORKEE-247667 (INDIA)
OCTOBER, 2017

SYNTHESIS OF SOME NOVEL CHEMICAL SENSOR FOR CYANIDE ION SENSING *VIA* DIFFERENT MECHANISM

A THESIS

Submitted in partial fulfilment of the Requirement for the award of the degree

of

DOCTOR OF PHILOSPHY

in

CHEMISTRY

by

NIRMA MAURYA

DEPARTMENT OF CHEMISTRY
INDIAN INSTITUTE OF TECHNOLOGY ROORKEE
ROORKEE-247667 (INDIA)
OCTOBER, 2017

INDIAN INSTITUTE OF TECHNOLOGY ROORKEE
ROORKEE

CANDIDATE'S DECLARATION

I hereby certify that the work is being presented in the thesis entitled, **"SYNTHESIS OF SOME NOVEL CHEMICAL SENSOR FOR CYANIDE ION SENSING *VIA* DIFFERENT MECHANISM"** in the partial fulfilment of the requirement of the award of the Degree of Doctor of philosophy and submitted in the Department of chemistry of the Indian Institute of Technology Roorkee, Roorkee is an authentic record of my own work during a period from January 2014 to October 2017 under the supervision of Dr. A. K. Singh, Professor, Department of Chemistry, Indian Institute of Technology Roorkee, Roorkee.

The matter presented in this thesis has not been submitted by me for award of any other degree of this or any other Institution.

(**NIRMA MAURYA**)

This is to certify that above statement made by the candidate is correct to the best of my knowledge.

(A. K. Singh)
Supervisor

Dated:

ABSTRACT

Structure of noble organic molecular scaffolds for recognition and sensing of environmentally and biologically important ions with high sensitivity and selectivity are constantly important for practical research in different fields of science. In current years there has been developed for constructing chemical sensors for on time, fast and cost-operative monitoring of environmental samples. Associated with the traditional analysis instruments, chemical sensors are convenient, modest to use, *in-situ* and minuscule in size. These topographies are perfect for real-time on field measurements, hence the inaccuracies instigated by the sample transference and storage can be generally condensed. Over current years the progress of a plethora of potential chemosensors has concerned substantial consideration in supramolecular chemistry. The most appropriate properties for development of chromogenic and fluorogenic sensors is the capability to react to useful perturbation in a highly selective and sensitive method by dramatic variations in color and emission intensity due to simplicity, convenience, low-cost, sensitivity, immediate response, and naked-eye visualization.

The present thesis entitled **"SYNTHESIS OF SOME NOVEL CHEMICAL SENSOR FOR CYANIDE ION SENSING *VIA* DIFFERENT MECHANISM",** describes the design, synthesis and photophysical properties of some receptors based on salicylaldehyde, azo-dye, coumarin and napthylamine systems. The molecules were characterized by FT-IR, ^{1}H, ^{13}C NMR, and APCI-MS data. The photophysical behaviors of these receptors were observed through UV-vis and fluorescence spectroscopy. The receptors were developed for studying the interaction with cyanide ions.

The thesis has been divided into five chapters, the first chapter deals with **"General Introduction",** which defines numerous aspects comprising cyanide sources and lethal effects, brief discussion of electrochemical sensors (cyclic voltammetry) and optical sensor, principle of optical chemosensors, some common photophysical mechanisms like charge transfer (CT), photoinduced electron transfer (PET), intramolecular charge transfer (ICT), energy transfer (ET), excimer/exciplex, excited state intramolecular proton transfer (ESIPT), Aggregation-induced emission (AIE)/Aggregation-caused quenching (ACQ) and C=N isomerization, principles and general approach for CN^{-} sensing and molecular logic gates.

Second chapter presents; **"Hydrogen Bonding Based Cyanide Sensor",** describes four Nobel azo linked [(3-methylpyridin-2-yl) iminomethyl-((4nitrophenyl) diazenyl) phenol (B1), (furan-2-yl methyl) iminomethyl-4-((4nitrophenyl) diazenyl) phenol (B2) and Enone based ((6-Fluoro-4-Oxo-4H-cromen-3-yl)methylene) isonicotinohydrazide (B3), and N-((4-oxo-4H-cromen-3yl)methylene)isonicotinohydrazide (B4)] anion receptors synthesis and characterized by FT-IR, ^{1}H NMR, ^{13}C NMR. Ligands B1-B4 displays large extent of selectivity toward CN^{-} resulting instant color change expressions witnessed in 10% aq. medium. Job's plot displays 1:1 stoichiometry along with all ligands. The limit of detection diagnosed for CN^{-} ion is down to 0.48 (B1), 1.66 µM, (B2) 0.76 µM (B3) and 0.68 µM (B4) that is below the WHO level. The anion binding property of the receptors (*via* deprotonation mechanism) was monitored by FTIR, ^{1}H NMR & hydroxyl titration and DFT calculation. The coated paper test strip was served as a mini colorimetric device for finding of CN^{-} in aqueous solution. It can be practiced for quantitative assurance of CN^{-} concentrations in water samples. The reversible behavior of B-CN complex with H^{+} also applied as a logic gate (in case of B3).

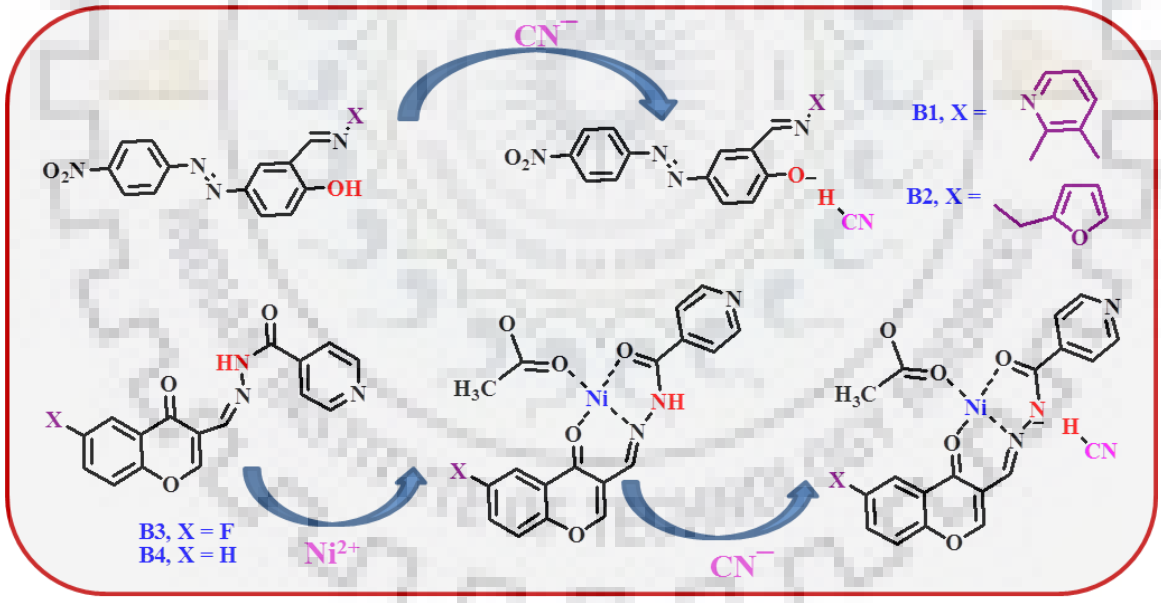

Third chapter presents; "**Metal Complexation Based Cyanide Sensor",** describes the synthesis of a novel effectual molecular receptor 2a [4hydroxy-6-methyl-3-(1-(-3methylpyridin-2-ylimine) ethyl)-2H-chromene-2-one] and characterized by spectroscopic techniques like, CHNS, FT-IR, ^{1}H NMR, ^{13}C NMR, and APCI-MS. Ligand 2a was the selective fluorescence turn-off sensor for the recognition of Co^{2+} *via* Photo-induced electron transfer quenching. Job's Plot analysis reveals the 2:1 stoichiometry

between the ligand-Co^{2+} complex. The resultant matallo-supramolecular complex of 2a-Co^{2+} exhibits the change in optical properties with CN^{-} (0.12 μM LOD) over complexation method in 1:2 stoichiometry. The possible binding mode was confirmed by FTIR, NMR and mass spectroscopic studies. Further, CN^{-} binding sturdily perturbs the redox properties of 2a-Co^{2+} complex. The 'On-Off-On' emission variation outlines the working principle of IMPLICATION logic gate. Besides, ligand 2a and 2a-Co^{2+} complex also exhibit antimicrobial activity against Gram negative bacteria *P. diminuta* and Gram positive bacteria: *S. aureus*, *B. brevis* using disc diffusion method.

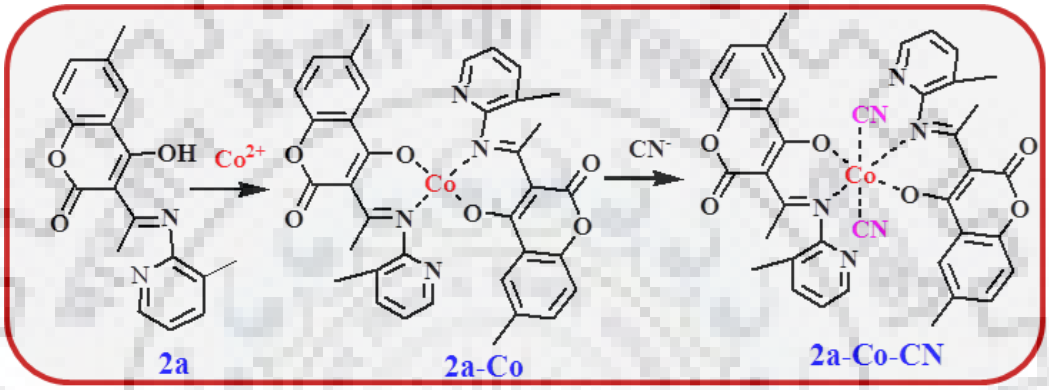

Fourth chapter presents; **"Nucleophilic Addition Based Cyanide Sensor",** describes synthesis of doubly activated Michael type receptors 2-((2-methoxynaphthalene-1-yl) methylene) -2H-indene-1-3dione (L1), 2-cyano-3-(2-methoxynaphthalene-1-yl) acrylic acid (L2) and indolium based spiropyran type receptors 1,3,3-trimethylspiro[indoline-2,2'-pyrano[3,2-c]chromen]-6-ium (L3), 9'fluoro-1,3,3-trimethylspiro[indoline-2,2'-pyrano[3,2-c]chromen]-6-ium (L4). In case of L1-L2 the donor-acceptor molecular arrangement was interrupted by Michael addition of CN^{-} on electron-deficient alkene bridge, which blocks intramolecular charge transfer and showed colorimetric blue shift and fluorescence enhancement. On the other hand, in case of receptors L3-L4 emerging red shift in absorption and emission enhancement is a consequence ring opening with conversion of enolate chromophore as merocyanine forms with CN^{-}. The 1 : 1 stoichiometry of L-CN- complex was proved by Job's plot and pseudo first-order rate constant were calculated found to be 0.025 s^{-1} (L1), 0.029 s^{-1} (L2) and 0.022 S^{-1} (L4). The detection limit analysed for CN^{-} is 1.2 nm (L1), 1.15 nm and 57.9 nM (L4) that is very below the WHO level. The FTIR, NMR, mass spectroscopy and DFT (Density functional theory) further supported the suggested mechanism of interaction between receptors and CN^{-}. Cyclic

Voltammetry studies were also confirmed the recognition of CN^- with all lignds L1-L4. Thus, ligands for the spectroscopic identification of CN^- can principal to the practical application as in paper strips and biological activities (antifungal, antibacterial).

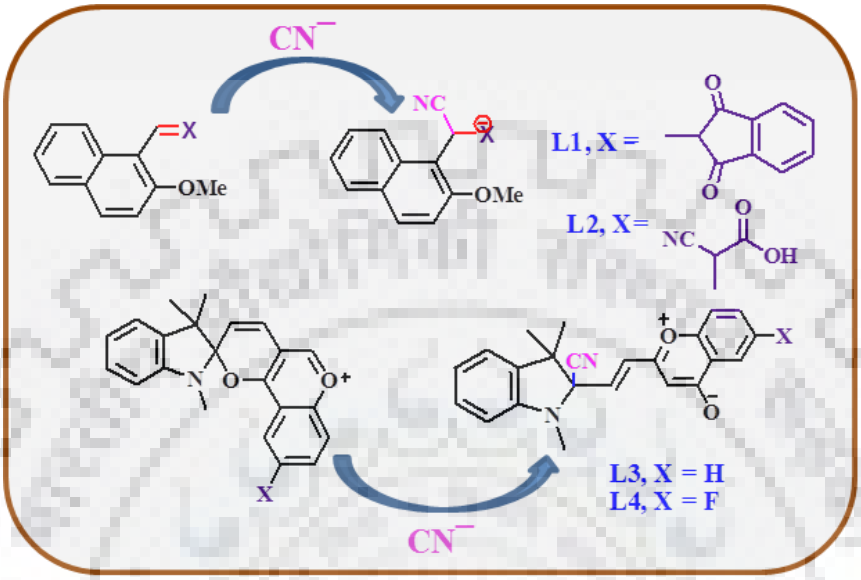

Fifth chapter presents; **"Metal Displacement Based Cyanide Sensor (Indirect Approach)",** describes synthesis of excited state intramolecular proton transfer (ESIPT) based four Nobel receptors S1- (2-ethoxy-3-((p-nitrophenyl-1-ylimino)methyl) -2H-chromen-4-ol) S2- (2-methoxy-3-((p-nitrophenyl-1-ylimino)methyl) -2H-chromen-4-ol), S3- (2-methoxy-3-((naphthalen-1-ylimino) methyl) -2H-chromen-4-ol) and S4- 2-ethoxy-3-((naphthalen-1-ylimino) methyl) -2H-chromen-4-ol), which are shown the remarkable aggregation-induced emission enhancement (AIEE) in aqueous medium. ON basis of this phenomenon further developed fluorescent organic nanoparticles of S3. All receptors express good water solubility and subsequent *in-situ* sensing of Cu^{2+} and CN^- in aqueous and biological settings. Cu^{2+} displayed a blue shift in absorption wavelength and efficiently quenches the emission intensity. Under the optimised conditions, the fluorescence intensity change established the feasibility for quantifiable analysis of ultra-trace concentrations of Cu^{2+} as inferred from an absolutely low detection limit 1.69 μM, 12.3 nM with S1 and S3-FONs respectively. Standardized exercise revealed the *in-situ* formed S-Cu^{2+} assembly acted as a secondary sensor for CN^- *via* regeneration of fluorescence intensity with a limit of detection 0.168 μM, 21.4 nM with S1-Cu^{2+} and S3-FONs-Cu^{2+} respectively. Additionally the receptors were

mimic as the function of a sequential logic circuit at molecular level based on "On–Off–On" sensing behavior by the inputs of Cu^{2+} and CN^{-}. The recovery analysis executed by spiking the known concentrations of Cu^{2+} and CN^{-} in deionised water, tap water and river water samples. Further, S1 and S1-Cu^{2+} complex shows the antimicrobial activities against fungi: *Bipolaris oryzae* and *Rhizoctonia solani* using the agar well diffusion method. Similarly S3-FONs express promising applications in intracellular recognition of Cu^{2+} and CN^{-} *via* cellular imaging in HeLa cells.

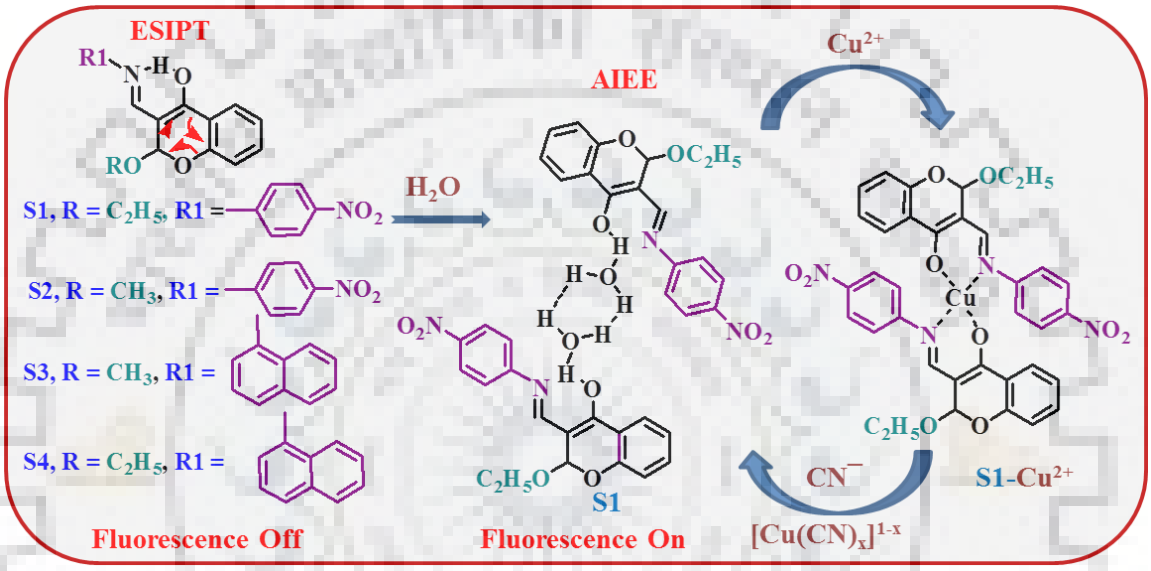

ACKNOWLEDGEMENTS

PhD is a project complemented by great efforts, struggle and support of many people. The completion of my Ph.D. thesis led me very close to achieving the title for 'Doctorate', one of my biggest dreams. It is a teamwork that proves fruitful after a long visage. At this moment, I take the opportunity to pay my kind gratitude to everyone who helped me directly or indirectly.

First and foremost, I thank the incessant source of divine blessings, the almighty GOD, who always motivate me to move forward with his omens and love.

I would like to express my deepest gratitude to my supervisor Prof. Ashok Kumar Singh for his excellent guidance, prudent support throughout the period of my research work. Without his support I have not been able to complete my research work. I further extend my thanks to him for providing all the facilities and keeping me free to do research up to the maximum possible extent. I tried to learn many qualities from him, but still I have to develop and learn so many things because he is library of reference to me in all aspects.

I am highly obliged and express my sincere thanks to, Prof. Mannar Ram Maurya, Head, Department of Chemistry and all other faculty members of the Chemistry Department for providing the basic infrastructural ease for accomplishing this research work. I am also thankful to my SRC (Student Research Committee) members, Prof U. P. Singh (Department of Chemistry, IIT Roorkee), Prof Anil Kumar (Department of Chemistry, IIT Roorkee) and Prof V. K. Agrawal (External member, Department of Chemical Engineering, IIT Roorkee) for their helpful suggestions, constant support and encouragement. I express my sincere thanks to Mr. S. P. Singh and Mr. Madan Pal, Department of Chemistry for their needful help.

"I owe my deepest gratitude to my husband Dr. Akhilesh Kumar Kushwaha, who loves me, a lot, without their support I cannot suppose to be here and writing this. They form the backbone and the origin of my happiness. I am very fortunate to have him in my life. In spite of his own duty, he has always encouraged me to work harder and do

my best. He has been very patient with me in all my ups and downs. A special thanks to my newborn baby Nitya Kushwaha, who delighted me with her yells and smiles". Both are the most important people in my life, and I love you both more than anything".

I have no words to express my feeling towards my parents Hooblal Maurya & Jairaji Maurya, parents-in-law, uncles and aunties for their love, blessings and continuous motivation throughout my Ph.D. work. Love and support which I got from my sister, brother-in-law, brother and sister-in-law are beyond the scope of any acknowledgement, yet I would like to express my heartfelt gratitude to them. I would like to give a special thanks to my uncle Dr. G. D. Verma and aunties Mrs. Usha Maurya and Mrs. Rama Verma, who helped me for successful realization of this thesis.

I express my sincere thanks to Sahajyoga family specially Versha Pradhan, Vikas Shrivastava, Diksha Dey and Dr. Rekha Singh, who gave me moral support in all the tough times.

I would like to give my gratitude to my seniors who taught me research skills such as synthetic and analytical techniques and their selfless help and moral support: Dr. Manoj Kumar Sahani, Dr. Shubhrajyotsna Bhardwaj, Dr. Neha Gupta, Dr. Divya Singhal, Shaily and labmate Neetu Yadav, who gave me moral support in all the tough times and a bunch of advices during my whole research work.

I specially express my sincere thanks to my BHU seniors Dr. Syed Sibtay Razi, Dr. Rashid Ali and Ramesh Chandra Gupta, department of chemistry for their valuable suggestions. I highly appreciate the constant encouragement.

I consider myself truly blessed as I have always been in a good company of friends. Their daily smiles and laughter have made my time intensely delightful and certainly unforgettable. I would like to express thanks to my special friends Iram Parveen, Mandeep Kaur Chahal, Tawseef Ahmad, Ankita Saini, Kiran Mowai, Aanand Ratnam, Rashmi Natawat, Urvashi Sharma, Tanu Gupta, Jyoti Maurya, Firoz Khan, Korra Praveen and Bhartendupati Tripathi for their constant encouragement, support and necessary guidance. I would like to convey my deepest gratitude to my junior Mohammed Wahid, Danish Khan, Muzey and Jatin Mahajan. Thank you all for your encouragement, support and most of all your humour.

I am highly grateful to acknowledge the funding source MHRD (Ministry of Human Resource Development) and UGC (University Grant commission, New Delhi, India) for providing financial support.

With profound gratitude, love and devotion, I dedicate this Thesis to my family.

Date: (NIRMA MAURYA)

Roorkee

LIST OF ABBREVIATIONS

A.U.	Arbitrary Unit
LOD	Limit of Detection
gm	Gram
µ	Micro
cm	Centimeter
hr	Hour
M	Molar
Mol	Mole
nM	Nanomolar
nm	Nanometer
^{o}C	Degree Centigrade
ppm	Parts Per Million
δ	Chemical Shift
Φ	Quantum Yield
conc.	Concentration
EtOH	Ethanol
MeOH	Methanol
ACN	Acetonitrile
DMF	N,N′-Dimethylformamide
DMSO	Dimethylsulphoxide
$CDCl_3$	Deuterated Chloroform
DMSO d_6	Deuterated Dimethylsulphoxide
equiv.	Equivalents
HEPES	4-(2-Hydroxyethyl)-1-Piperazineethanesulfonic Acid
TBAS	Tetrabutylammonium Salts
nBu_4NPF_6	Tetrabutylammonium Hexafluorophosphate
CN^-	Cyanide Ion
HCl	Hydrochloric Acid
TMS	Tetramethylsilane

FESEM	Field Emission Scanning Electron Microscope
AFM	Atomic Force Microscopy
APCI-MS	Atmospheric Pressure Chemical Ionization Mass Spectrometry
WHO	World Health Organization

LIST OF SCHEMES

LIST OF FIGURES

LIST OF TABLES

LIST OF PUBLICATIONS

1. **N. Maurya**, S. Bhardwaj, A. K. Singh, A modest colorimetric chemosensor for investigation of CN^- in semi-aqueous environment with high selectivity and sensitivity, *Sens. Actuators, B* 229 (2016) 483-491.
2. **N. Maurya**, S. Bhardwaj, A. K. Singh, Selective and sensitive colorimetric sensor for CN^- in the absence and presence of metal ions (Cu^{2+}/ Ni^{2+}): mimicking logic gate behavior, *RSC Adv.* 6 (2016) 71543-71549.
3. S. Bhardwaj, **N. Maurya**, A. K. Singh, R. Varshney, P. Roy, Promising ESIPT-based fluorescence sensor for Cu^{2+} and CN^- ions: investigation towards logic gate behaviour, anticancer activities and bioimaging application, *RSC Adv.* 6 (2016) 102096-102101.
4. **N. Maurya**, S. Bhardwaj, A. K. Singh, Selective colorimetric and fluorescence 'turn-on' sensor for Ag^+ and *in-situ* sensing of CN^- (off-on-off) *via* displacement approach, *Mater. Sci. Eng., C* 74 (2017) 55–61.
5. **N. Maurya**, A. K. Singh, Selective naked eye and "turn-on" fluorescence chemodosimeter for CN^- by activated Michael acceptor possessing different polar substituents: Reduced ICT-based signal transduction, *Sens. Actuators, B* 245 (2017) 74-80.
6. **N. Maurya**, A. K. Singh, Effective ensemble system for the identification of CN^- based on a cobalt (II) complex: a logic gate mimic. *New J. Chem.* 41 (2017) 4814-4819.
7. **N. Maurya**, A. K. Singh, Indirect approach for CN^- detection *via* Cu^{2+} induced turn-off sensor: using Novel AIEE fluorophore with Logic gate and antimicrobial application, *Dyes Pigm.* 147 (2017) 484-490.
8. **N. Maurya**, A. K. Singh, A novel chromogenic and fluorogenic chemodosimeter for selective detection of CN^- with antimicrobial activity. (Communicated).
9. S. Bhardwaj, **N. Maurya**, A. K. Singh, Chromone based fluorescent organic Nanoparticles for high-precision *in-situ* sensing of Cu^{2+} and CN^- ions in 100% aqueous solutions. (Communicated).
10. S. Bhardwaja, **N. Maurya**, S. Dubey, A. K. Singh, R. P. Singh, Potent "turn off" fluorescence sensor based on AIE organic nanoparticles for Hg^{2+} recognition in aqueous solutions. (Communicated).

POSTER PRESENTED IN CONFERENCES

1. "A simple colorimetric approach for CN^- investigation in semi-aqueous medium" in ***18th CRSI National Symposium in Chemistry (NSC 18)*** organized by Punjab University; 5-7 February 2016.
2. "Colorimetric and turn on fluorescence sensor for Ag^+ and *in-situ* sensing of CN^- *via* displacement approach" in ***2nd International Conference on recent advances in analytical sciences (RAAS),*** organized by Department of Chemistry, IIT BHU Varanasi; 7-9 April 2016.

WORKSHOPS

1. Participate "***Science Academic Lecture workshop on Molecular Spectroscopy: Theory and Instrumentation"*** organized by Department of Chemistry BHU, 2^{th}-3^{th} March, 2012.
2. Attend "***Indian Roadshow Workshop"*** organized by IIT Delhi, 4^{th} Nov. 2014.
3. Attend One Day Workshop on "***Nano Drug Delivery Systems (Industry-Academia Interaction)"*** organized by the Centre of Excellence: Nanotechnology, IIT Roorkee, 10^{th} Jan. 2015.

TABLE OF CONTENTS

CHAPTER 4: NUCLEOPHILIC ADDITION BASED CYANIDE SENSOR

CHAPTER 5: METAL DISPLACEMENT BASED CYANIDE SENSOR (INDIRECT APPROACH)

CHAPTER 1

General Introduction

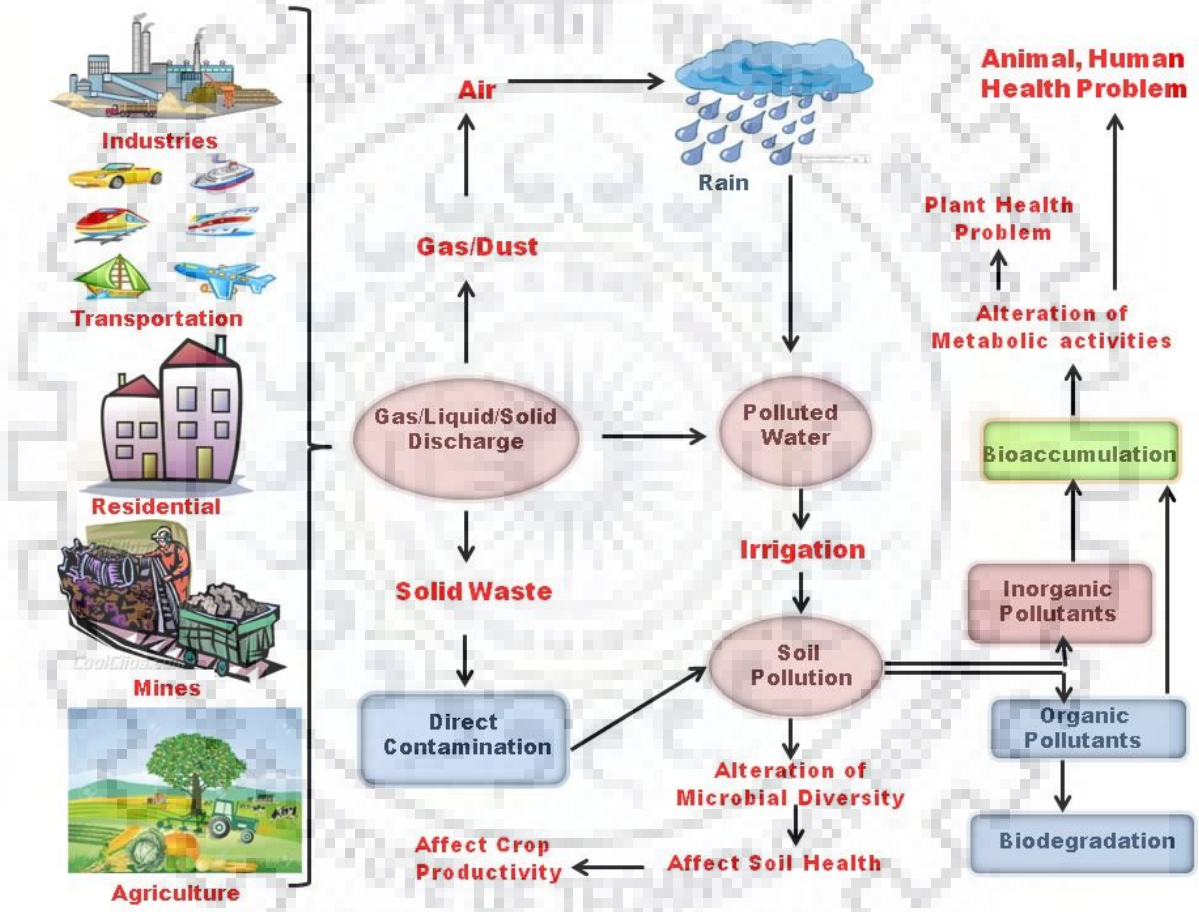

1.1 INTRODUCTION

Cations and anions have substantial significance in chemical, biological, and environmental processes [1-4]. Heavy metals (Cu^{2+}, Pd^{2+} etc.) and anions extensively practiced in industrial, biological, agricultural and military purposes for decades of time [5-8]. Some anions are extremely toxic such as CN^{-}, AsO_2^{-} [9-12] and some have vital role in biological system like F^{-}, $H_2PO_4^{-}$, SO_4^{2-}, NO_3^{-}, PO_4^{3-} [13-15]. Such type of poisonous and oncogenic anions also permits for precise measurement in numerous environmental systems. Thus anion recognition conventional little attention in the prompt years owing to complications characteristic in binding for example, their large size (less effective electrostatic binding exchanges due to lower charge to radius ratio) than isoelectronic cations, pH sensitivity (the function of sensor within low pH range due to protonation at low pH), obligation of a higher degree of sensor design complementarity with an anion and the solvent properties which are to be contended by the sensors for the anions in assured solvents. Opposing all these limitations, anion binding has now materialized as an advanced field of research, and has been a topic of a numeral of admirable articles in the last period. There are numerous conventional analytical methods are accessible for poisonous ions recognition comprising electrochemical methods like as; voltammetry [16-17], potentiometric as ion selective electrode [18-22], and spectrometric methods like as; atomic absorption spectroscopy [23-24], flow injection [25-29], and chromatography [30-31] but the new optical sensing approach are quick, portable and cost effective. Among all anions, CN^{-} is very toxic anion. Related to other types of anion selective chemosensors [32-36], CN^{-} chemosensors take lead of two substantial and characteristic properties, its robust nucleophilicity and strong binding affinity concerning to some transition metal ions such as Cu^{2+}, Hg^{2+}. Therefore this research work instigates with a brief discussion of CN^{-} sensors on the basis of different approach of mechanism.

1.2 CYANIDE SOURCES AND LETHAL EFFECTS

CN^{-} comprising salts are prevalent chemicals found in surface water patenting not only from industrial discarded however also from biological causes. CN^{-} is used in many chemical processes, such as plastics manufacturing, electroplating, gold and silver extraction, tanning, and metallurgy, which are accountable for CN^{-} contamination [37]. Biological sources consist of fungi, bacteria and algae, which release CN^{-} as part of their nitrogen metabolic pathway. Cyanogenic glycosides containing vegetables such as lima

beans, sorghum and linseed, kernels of fruits, sweet potatoes and bamboo shoots are causes of CN^- absorption in animals and humans. Tobacco smoke is also a mutual source of CN^- in the blood and other prospective sources are organic thiocyanates, sodium nitroprusside and succinonitrile [38]. CN^- disturbs the functions of visual, vascular, central nervous, endocrine, cardiac, and metabolic systems of the body [39]. In the bloodstream of humans being CN^- can inhibit t

he activity of enzyme cytochrome c oxidase *via* formation of stable complex, causing cellular asphyxiation and cytotoxic hypoxia [40-41]. Sub toxic doses of CN^- decreases the rate of glycolysis and obstruct the action of the TCA cycle thus anaerobic metabolism prompted by accumulation of lactate in the blood [39]. CN^- increases the Ca^{2+} concentration within the cell by which the level of reactive oxygen species (ROS) increases thus inhibit antioxidant defense systems [42-43]. CN^- also turns as an inhibitor of some non-metallo and metallo-enzymes that act *via* the intermediacy of Schiff bases [44].

The toxico-dynamic properties of CN^- are influenced by on the route, dose, speed of direction and chemical form. The lethal dose that is 50% of the presenting population (LD_{50}) of cyanogen chloride and hydrogen cyanide has been informed to be 2500-5000 mg-min/m^3 and 11000 mg-min/m^3 [39]. There are various local, national and international protocols and guidelines concerning to CN^- in water, air and other media. For example US EPA fixed the maximum toxic level in drinking water is 200 μg/L; whereas the lower limit set by European Union is 50 μg/L [45-46]. The Australian and New Zealand Environmental and Conservation Council set a standard of trigger values of lower limits for marine and freshwater (that provides for protection of 99% of the species) as 2 μg/L and 4 μg/L respectively [47]. The lethal concentration of CN^- has been suggested to be between 23-26 mM in blood of fire victims [39]. The WHO has set a determined tolerant level of CN^- limit is 1.9 μM in drinking water [38].

1.3 CONVENTIONAL METHODS FOR THE DETERMINATION OF CN^-

The improvement of very accurate and sensitive instruments is an enormous challenge for CN^-. A variability of analytical methods accomplishing these difficulties is present. Approved methods for the purpose of CN^- detection comprise titration [48], potentiomety [49], atomic absorption spectrometry (AAS) [50], amperometric [51], flow injection [52], chromatography [53] and surface enhanced Raman scattering (SERS) [54] methods. Though most constituted desires which seen by these techniques are operationally complex,

expensive in price, large in size, low detection limits, time-consuming and frequently involve substantial pre-concentration and/or organic solvents, thus are not suitable for use. Therefore, alternate and further sensitive methods that can openly measure CN^- in μM levels in diverse matrices, including water, soil, air, exhaled breath, food and biological fluids are reasonable. For the time being, the attentions in CN^- sensors are developed for naked eye detection (optical method) to practically all characteristics of recent instrumental analysis have performed during the last ten years. In recent times, Yoon *et al* [55] reviewed optical sensors and colorimetric measurement of CN^-.

1.4 CHEMOSENSOR FOR DETERMINATION OF IONS

A molecular chemosensor is well-defined as 'chemical structure being capable to bind an ionic or neutral guest species over supramolecular appreciation by a receptor and generating a visible variation of the systems'. Further recording the incidence of the guest species the receptor should be selective and also have the potential for giving out information. Now a day, configuration of chemical sensors for cost-effective real-time and fast observing of environmental tasters is an attractive emergent area of research. Chemosensors are handy for *in-situ* measurement and miniscule in size. Chemosensor can sense the incidence of ions with concentration, thus it is important in the environmental and medical area. Thus the economical sensors [56] can extensively use in diverse areas such as pollution, environmental, mining, geology, medicine etc. Such perfect chemosensors generally signifying three main constituents attached in a series: a chemical (molecular), transduction platform and signal processing step. Initially the receptor molecule interacts with analyte and then its analytical properties such as color, absorption spectra, emission spectra and electrical potential or altered in a manner, transducer leads to variations and transmute the extent of signal into valuable analytical information (Fig. 1.1).

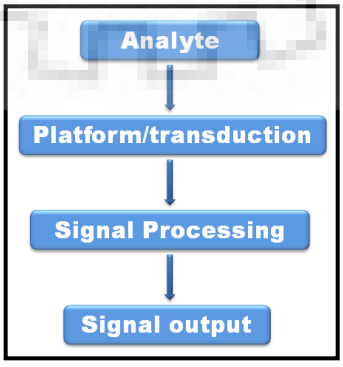

Fig. 1.1 Graphical representation of chemosensor.

1.4.1 Types of Chemosensors

Based on working principle chemosensors have been divided in various categories like as mass sensor, magnetic and thermal sensor, electrochemical sensor and optical sensor [57]. Mass sensor is constructed on mass loading concerning analyte *via* adsorption [58]. Magnetic sensors are depending on magnetic properties of analyte and receptor. Thermal sensor exploited thermal reaction consummate by adsorption process or chemical response. The electrochemical sensor displays electrochemical variations between the performed electrode and analytes [59]. Optical sensor exploits the optical alterations of chemosensor with target analyte [60].

1.4.1.1 Electrochemical Sensors

The modified form of the receptor can be used as an electrode which display a reaction concerning to selected ion (consenting to concentration purpose of ion in solution) *via* interaction between electrode-analyte and change into a convenient signal. The following subgroups may be well-known:

- In potentiometric sensors, observe the change of potential (Gibbs free energy of the electrons in equilibrium between two half-cells) on working electrode, counter to reference electrode. There is no need of external potential, thus no current flow arises. This difference is called the electrode potential difference, or the redox potential difference [61].

- Voltammetric sensors commonly consist on relating a controlled external current or potential to the cell and assessing the resulting flow potential or current. Further, it can be divided into two classes, the pulse or step methods (e.g. chronoamperometry), where the potential is stepped, consenting exclusion of the capacitive current and the second class is potential sweep methods (e.g. Cyclic Voltammetry), where the potential of the working electrode is linearly scanned [62-63].

These sensors are fabricated with chemically inert/active electrodes and modified electrodes.

1.4.1.1.1 Cyclic Voltammetry (CV)

CV is a potential-precise technique, generally using three electrode systems. The potential difference is applied amongst the working and reference electrode, while the current is concerning to the counter and working electrode. The working electrode subsists in numerous geometries and materials, commonly consists of gold, platinum (inert metals),

glassy carbon, pyrolytic carbon (inert carbon) or a mercury drop. The counter or auxiliary electrode must have a precise huge surface area to lower the current density and be prepared by inert metal like gold, platinum. The reference electrode, preferably non-polarizable, must have a persistent potential. Therefore the Standard Hydrogen Electrode (SHE), Standard Calomel Electrode (SCE) and the silver/silver chloride electrode are commonly used [64].

In CV the current is measured such as a function of the applied linear potential (different potentials and with different intensity) of reacting analyt (eq. 1.1), thus assists various recognitions in one measurement (qualitative), and valuation of their concentration in solution (quantitative). The current bring about from the applied potential is due to the incident of redox responses in the solution (Faradic current) and to the charging double layer (capacitive current). The correlation among the potential, E and current I is called the polarization curve (eq. 1.2).

$$\mathbf{E\,(t) = E\,(0) \pm vt} \qquad 1.1$$

$$\mathbf{I = f\,(E)} \qquad 1.2$$

where E (t) is the potential at time t, E (0) is the potential at time $t = 0$ and v is the scan rate, i.e. dE/dt (sometimes called polarization rate).

As CV name designates, uses a cyclic potential waveform, and comprises of two parts: a forward sweep anodic (increasing potential) and reverse sweep is cathodic (decreasing potential) or *vice versa*. Thus the species are sequentially oxidized and reduced (or *vice versa*). The voltage is scanned using a triangular waveform shown in Fig. 1.2. In this example the voltage is swept concerning to two values at a stationary rate, beginning from E_1; voltage reaches E_2 then the scan is reversed and swept back to E_1.

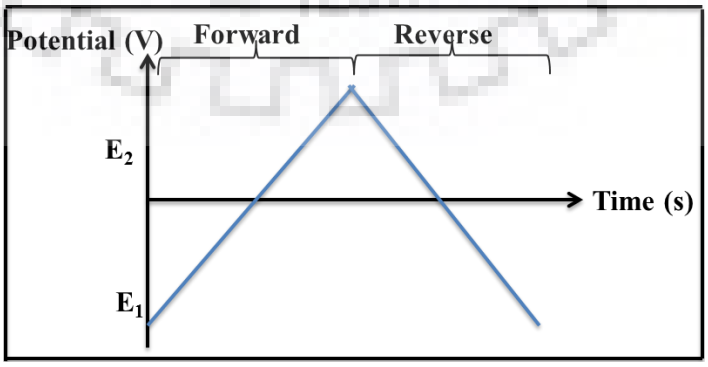

Fig. 1.2 Potential applied to the cell versus time.

The diffusion layer is linear at the electrode surface and the reversible electrochemical reaction (Fig. 1.3) can be described as follows:

- The ratio of the anodic (I_{pa}) and cathodic (I_{pc}) peak currents is equal to one:

$$[Ipa/Ipc] = 1$$

- The peak currents are proportional to the square root of the scan rate $\upsilon^{1/2}$, as expressed by the Randles-Sevcik equation [43]:

$$Ip = 0.4463(nF/RT)^{1/2}\, nFAeD^{1/2}{}_{redox}C_{redox}\, \upsilon^{1/2}$$

where n is the number of electrons for charge transfer, R is the universal gas constant (8.314 J mol^{-1} $K^{-1)}$, F is Faraday constant (96485 C mol^{-1}), T is temperature, Ae is the interfacial area between the working electrode and electrolyte solution, D_{redox} is the diffusion coefficient of the redox species in the electrolyte, C_{redox} is the concentration of the redox species and υ is the scan rate.

- The peak potential and the redox couple potential Ep (against SHE) are related as follows:

$$Ep = (Epa + Epc)/2$$

- The positions of peak potential are independent of the scan rate.

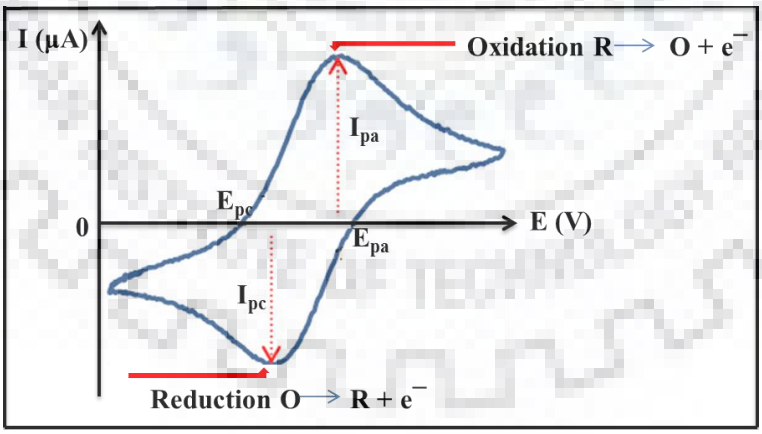

Fig. 1.3 Schematic diagram of a Cyclic Voltammogram in a redox couple system.

The diffusion layer size at the electrode surface will be reliant on the scan rate of voltage. Therefor at slow scan rates the electrode flux surface is considerably smaller (diffusion layer will grow much further from the electrode) as comparison to a fast scan. As the flux towards

the electrode is proportional to the current, the extent of the current will be lesser at slow scan rates and greater at high rates.

1.4.1.2 Optical Sensor

Optical chemosensor is a device, which observes the concentration of a specific analyte within the concern sample *via* alteration of the optical properties. The chemical reagent is ideal to react more precisely and perceptively to the ions. The dignified optical properties are absorbance, luminescence (phosphorescence, fluorescence), Raman spectroscopy, reflectance and light polarization [56, 66]. The most commonly used methods along with preferable approaches for chemical sensing are absorption and fluorescence spectroscopy.

1.4.1.2.1 Absorption Based Optical Sensor

The absorption based optical sensor can be spectroscopic and colorimetric in nature (analyte-induced color variation). The colorimetric sensors draw more devotion owing to their naked eye detection, without the use of expensive equipment's [67]. They also effects direct function of optodes and one-use dipstick arrays. The ultraviolet (190-400 nm) and visible (400-800 nm) regions are two main parts of electromagnetic radiations. The array of UV-vis absorption peaks is governed by numerous probable electronic transitions, which are arranged in the increasing energies order *viz.* $\mathbf{n \rightarrow \pi^* < n \rightarrow \sigma^* < \pi \rightarrow \pi^* < \sigma \rightarrow \pi^* < \sigma \rightarrow \sigma^*}$. The UV-vis spectrum of a compound would belong to one or more well distinct peaks with analogous transition due to stable amount of energy required. The upper energy transition implicates shorter wavelength (< 150 nm i.e. ultraviolet wavelength) whereas lesser energy transition relate to the longer wavelength (200-1000 nm i.e. UV-vis). The variation in color is imitated by the respective decrease or increase in the electron densities on the chromophore moiety by analyte interaction. If ground state is more polar than excited state, it becomes stable the non-bonding electrons by hydrogen bonding with its electrostatic interface or polar solvents. Thus absorption shifted to concern to shorter wavelength and this phenomenon known as **Hypsochromic Shift (blue shift).** On the reverse case, if excited state is more polar than the ground state then the absorption band shifted towards longer wavelength which is called as **Bathochromic Shift (red shift).**

1.4.1.2.2 Fluorescence Based Optical Sensor

The fluorescence based sensors are standard intensity built devices, in which intensity of the ligand varies in response to the analyte interaction. The fluorescent probe has two integrated components; a signaling fluorophore and another one is guest receptor which is connected by a spacer to create fluorophore-spacer-receptor scaffold. The photophysical feature of the fluorophore, such as emission intensity, emission wavelength, quantum yield and fluorescence lifetime will altered *via* a different mechanism after binding with analyte to the receptor. The practical mechanisms can expand the fabrication of fluorescent chemosensors to appreciate sensing system at the molecular level [68]. The fluorescence sensitivity is a very important concern, which is rises from the difference between the excitation and emission wavelength. The fluorescence recognition method has foremost advantage over former methods due to safety, high sensitivity and high speed. In absorption method the concentrations amount can determine in the micromolar range, on the other hand, in fluorescence method, precise concentration measured in picomolar and femtomolar range. Therefore, due to good output range (measure at lower concentration) fluorescent sensor is attractive and can be used properly for biological system.

1.5 PRINCIPLE OF OPTICAL CHEMOSENSORS

1.5.1 Photoluminescence

Maximum fundamental elements are in their ground state at room temperature. After an electromagnetic irradiation, the particles absorb photons of appropriate energy and goes to electronically excited state which is monitored by the absolution of other energy in different forms. Thus the Photoluminescence is definite as ‘the radiation of light from any procedure of molecules *via* absorption of photons’ [69]. Accountable on the nature of the excited state, generally the emitted light can be divided into two sets as phosphorescence and fluorescence. Specifics allied to the photoluminescence process will be considered in the following sections (Fig. 1.4)-

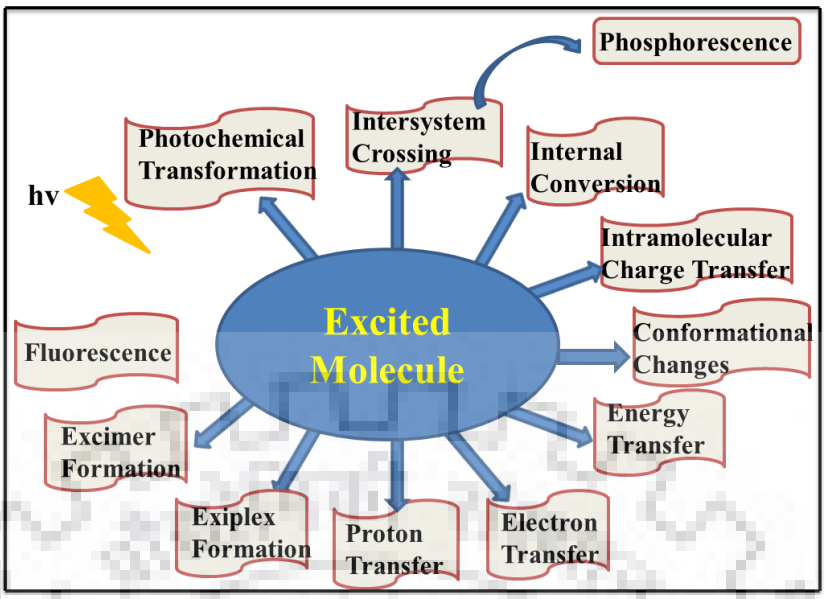

Fig. 1.4 Probable de-excitation ways of excited molecule.

1.5.2 Absorption of Light

Upon absorption of electromagnetic radiations light, a substance becomes reactive in an excited state (having dissimilar chemical reactivity with its ground state) and transition of electrons takes place from HOMO (highest occupied molecular orbital) to LUMO (lowest unoccupied molecular orbital). The irradiated light must be of abundant energy for transition between electronic energy levels and these photons of light found deceiving in UV-vis region (range of 200-800 nm), which is mentioned as "photochemical window". The wavelength of the spectrum and the product of absorption implicate are almost shortened in the Table 1.1. The wavelength range is divided into UV, visible and near IR region (able in prolonged conjugation or mixed-valence system [70]). The excitation between ground and excited states determine the shape and intensity of absorption spectra. The absorbance, conc. of the absorber and the path length is related to each other by the Lambert-Beer Law [71]:

$$A = \varepsilon \times c \times l = \log_{10} \frac{I_0}{I}$$

Where, A is absorbance, ε is the molar extinction coefficient, c is the concentration, l is absorption path length, I_0 is incident light and I is transmitted light of radiation.

Table: 1.1 Regions and effect of the electromagnetic spectrum on molecular structures.

Radiation	Scale of Wavelength	Absorption Results
Gamma rays	0.1 nm	Nuclear reactions
X–rays	0.01 – 10 nm	Transitions of inner atomic electrons
UV	10 – 400 nm	Transitions of outer atomic electrons
Visible	400 – 750 nm	Transitions of outer atomic electrons
Infrared	750 nm – 15μm	Molecular vibrations
Far Infrared	15μm – 1mm	Molecular rotations
Radar	1mm – 1m	Oscillation of mobile electrons

The asset of the absorption at a specific wavelength is depends upon concentration and molar absorption coefficient (probability of an electronic transition at a particular wavelength). The transition is referred as "fully allowed, where $\varepsilon > 10^5$ dm^3 mol^{-1} cm^{-1} and below ~100 dm^3 mol^{-1} cm^{-1} is mentioned as "forbidden" means the molecule does not absorb well the radiations of that wavelength and possibility of the transition taking place is precise low. The transitions are "partially allowed" when ε values between ~10^2 and ~10^4. Thus the selection rule (quantum mechanical rules) oversees the probability of transitions, which is based on spin and symmetry factors [72]. **Spin selection rule** states that simply electronic transitions are allowed where throughout the transition spin remains unchanged and forbidden if there is alteration in a spin during transitions *i.e.* singlet to triplet. The symmetry of molecules (in ground and excited states) may be distorted through the influence of environmental factor or the existence of heavy metal/solvents. It becomes very challenging to distinguish allowed or forbidden transition *via* symmetry analysis only due to the molecular geometry distortion. To overcome this condition, measured absorption coefficient values are divided by some parameters. Therefore, if a transition is spin-forbidden and symmetry allowed, then the possibility is very low, *i.e.* ε will be < 100, then significant absorption may be detected (10^2-10^4).

The renowned factor of transitions *i.e.* ε values, the natures of transitions and absorption intensity describes the shape of absorption spectra. For distinct transitions, vibration levels of each orbital may be having additional intensity than others. All of these transitions are ruled through the **Franck-Condon principle,** which states that electronic transitions in molecule takes place in a simple way and very fast, transitions are vertical. Potential energy diagrams

display that electronic orbitals comprise of their specific vibrational levels for HOMO-LUMO transitions. The internuclear spaces remain unaffected throughout the transition. There is an insignificant shifting among nuclear coordinates of the ground and excited states. These transitions are precise, intense transition in absorption spectra. The commonly organic system shows broad curves instead of fine or intense transitions in solution and solid media due to the enormous number of vibrational levels in electronic states. Moreover, the **Franck-Condon principle** is similarly valid to both absorption and fluorescence phenomenon [73-74].

1.5.3 Physical Deactivation of Excited States

When a molecule is exposed to light and forms an excited state, which is chemically altered species to their consistent ground states. Owing to the instability of these excited states, they lose their extra energy instantly *via* deactivation processes. The **Perrin-Jablonski diagram** is suggested to envision of the most distinctive processes in a simple way that generally arisen after photon absorption (Fig. 1.5) and validates the properties of excited states along with their relaxation procedures. After absorption of light the molecular vibrational levels in the excited states will be congested with electrons, which have high energy and starts to relax to the lowermost vibrational level of S_1 within a picosecond or less *via* vibrational relaxation and this phenomenon is called as the *"**internal conversion (IC)**"* (non-radiative loss of energy). The rest of all photochemical reactions will eternally originate from $\nu = 0$ of S_1 after excitation, as the relaxation rate is the fastest deactivation procedures at the lowest vibration levels of S_1 **(Kasha's rule)** [75]. Further the excited electrons at S_1 now may go through either ***fluorescence*** *via* emitting photons or convert to a triplet state by ***intersystem crossing (ISC)***. Commonly, ISC of triplet state T_1 from S_1 singlet state (by spin conversion process) is a forbidden transition process in the unrealistic environments. Electron relaxation from triplet state T_1 to ground singlet state S_0 is a radiative phenomenon and well-known as delayed process ***phosphorescence,*** which is much slower than the fluorescence process due to spin multiplicity and lower energetic radiation. Thus the fluorescence is a spin-allowed radiative relaxation phenomenon because of same spin multiplicity of the S_1 and S_0 states. Therefore, it occurs in a very short period (picoseconds to microseconds).

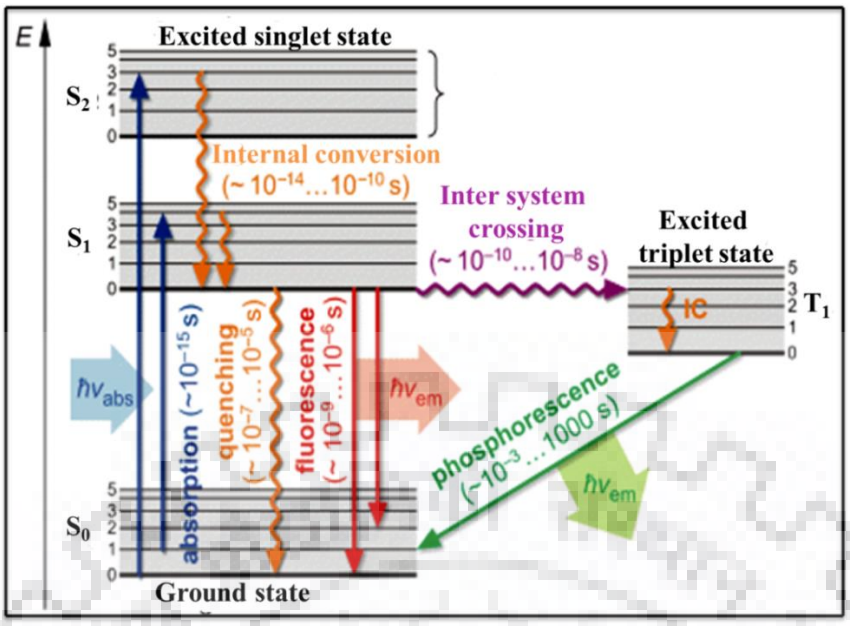

Fig. 1.5 The Perrin-Jablonski Diagram.

The emitted light continually has a longer wavelength (less energetic) as paralleled to absorb light due to loss of limited energy through the molecule throughout all above process. This λ_{max} difference between the absorption and emission spectral positions is called a **Stokes' shift** [76] (Fig. 1.6). The Stokes' shift occurs *via* prompt non-radiative decay to S_1 (lowest vibrational level). Furthermore the fluorescent molecules can exhibit an extra Stokes' shift owing to complex formation, excited-state reactions, energy transfer and solvent effects.

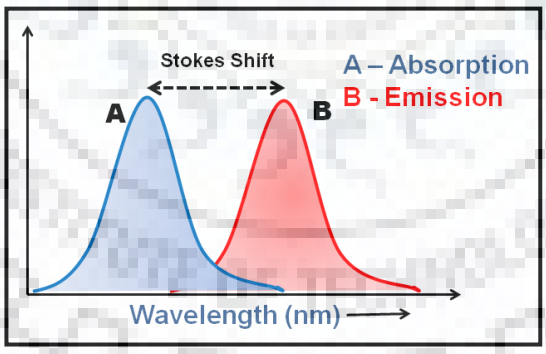

Fig. 1.6 Representation of Stokes' shift.

1.6 SOME COMMON PHOTOPHYSICAL MECHANISMS FOR SIGNAL TRANSDUCTION

Emission sensation proceeds from the excited state molecule, since of the high reactivity of the element which does not originate in the ground state. Communication amongst two elements gives rise to the signal transduction. Till the date various signaling

mechanisms have been well-known for applied in the area of optical detection of ions, which consist of charge transfer (CT), photoinduced electron transfer (PET), intramolecular charge transfer (ICT), chelation mechanism, energy transfer (ET), excimer/exciplex formation, excited state intramolecular proton transfer (ESIPT), C=N isomerization and aggregation emission process (AE).

1.6.1 Charge Transfer (CT)

Commonly, charge-transfer complexes contain electron transfer amongst metal atoms and ligands. The charge transfer band is result of alteration of charge density between molecular orbital (MO) of metal and ligand. If the electronic charge arisen from the MO with corresponding to ligand character to the metal-identical, then known as LMCT (ligand-to-metal charge-transfer) and *vice-versa* called as MLCT (metal-to-ligand charge-transfer). Thus, LMCT consequences in the reduction of the metal center while MLCT outcomes in oxidation of the metal center. **Baitalik *et al.*** [77-78] described MLCT centered some metalloreceptors **(1-2)** to sense anions. The N-H deprotonation of benzimidazole unit directed to a naked eye sensitive intense color. Similarly, **Lee *et al.*** [79] described heteroleptic complex **3** and **4**, with 4-(dimesitylboryl) benzoate (Bbz) auxiliary ligand. The intense phosphorescence spectra was observed with binding of F^- *via* inhibition of the PET procedure, whereas switching on $(C\wedge N)_2$ Ir-centered MLCT phosphorescence.

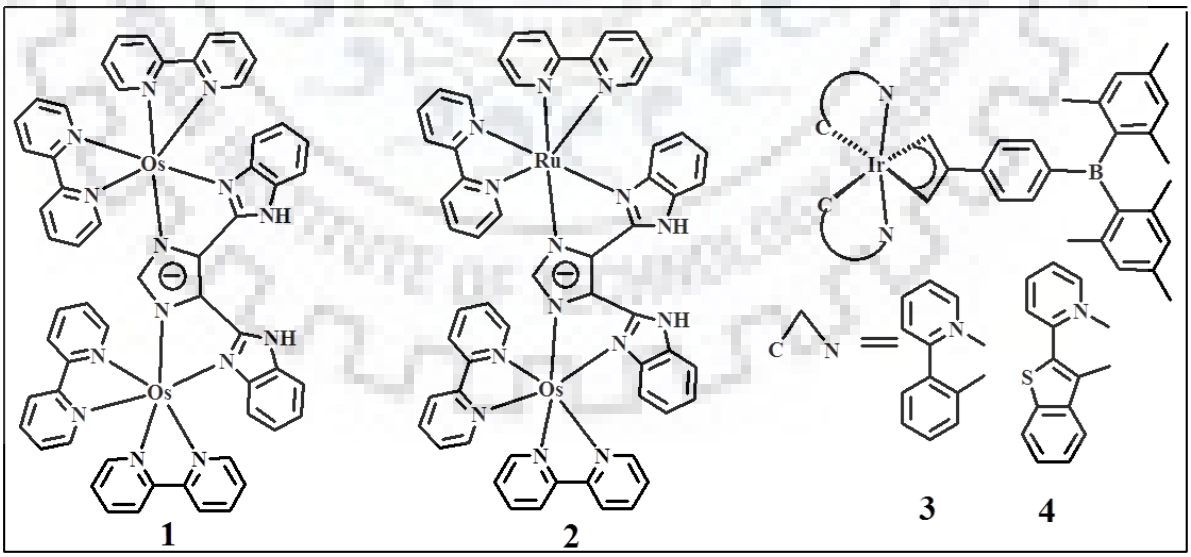

Fig. 1.7 CT based some chemosensors.

1.6.2 Photoinduced Electron Transfer (PET)

PET sensations are instigated from excited state, throughout this excited electron moved from donor to acceptor excited state. Close area in space and similar of oxidation reduction potentials of both accepter-donor site is the principal condition for this mechanism. Thus, PET sensors consist of both the chromophore/fluorophore and receptor units interconnected by the spacer (non-conjugated bridging). The behavior of receptor part oversees the reaction of the chromophore /fluorophore unit, which produce a signal upon analyte interface. Consequently the PET process can be divided in two manners (on the basis of nature of receptor unit).

❖ **A Reductive PET process** takes place when receptor unit has an electron donating group. Completely filled energy of the receptor (HOMO) located amongst the HOMO and LUMO of the fluorophore. Upon irradiation electronic conversion proceeds from fully occupied HOMO of the receptor to the HOMO of the fluorophore, thus the fluorescence quenching occurs *via* obstruction of the relaxation route of fluorophore follow a non-radiative path. After the interaction of analyte to the receptor unit, the HOMO of receptor transferred at the inferior energy site of fluorophore HOMO. Thus, transitions from the fully occupied receptor (HOMO) to unoccupied fluorophore (HOMO) are thermodynamically forbidden and typical reduction path proceeds, followed by electron existing in excited state LUMO of the fluorophore. Consequently, this type of sensing mechanism is recognized as "OFF-ON" trigger (Fig. 1.8 a).

❖ **The Oxidative PET process** proceeds while the receptor unit has an electron acceptor moiety. In this case HOMO and LUMO of fluorophore are located amongst fully occupied HOMO and vacant LUMO energy gap of the receptor. This alignment does not permissible for electronic transition from LUMO of an excited fluorophore to LUMO of the receptor and the characteristic relaxation pathway followed *via* the electron belong to an excited state of the fluorophore, thus output comes as fluorescence "ON" signal. Subsequently, relocalisation of receptor LUMO among HOMO-LUMO energy gap of fluorophore upon binding with the analyte. Therefore the electron moved from excited LUMO of a fluorophore to the unoccupied LUMO of receptor, causing fluorescence quenching signal with an "ON-OFF" trigger (Fig. 1.8 b).

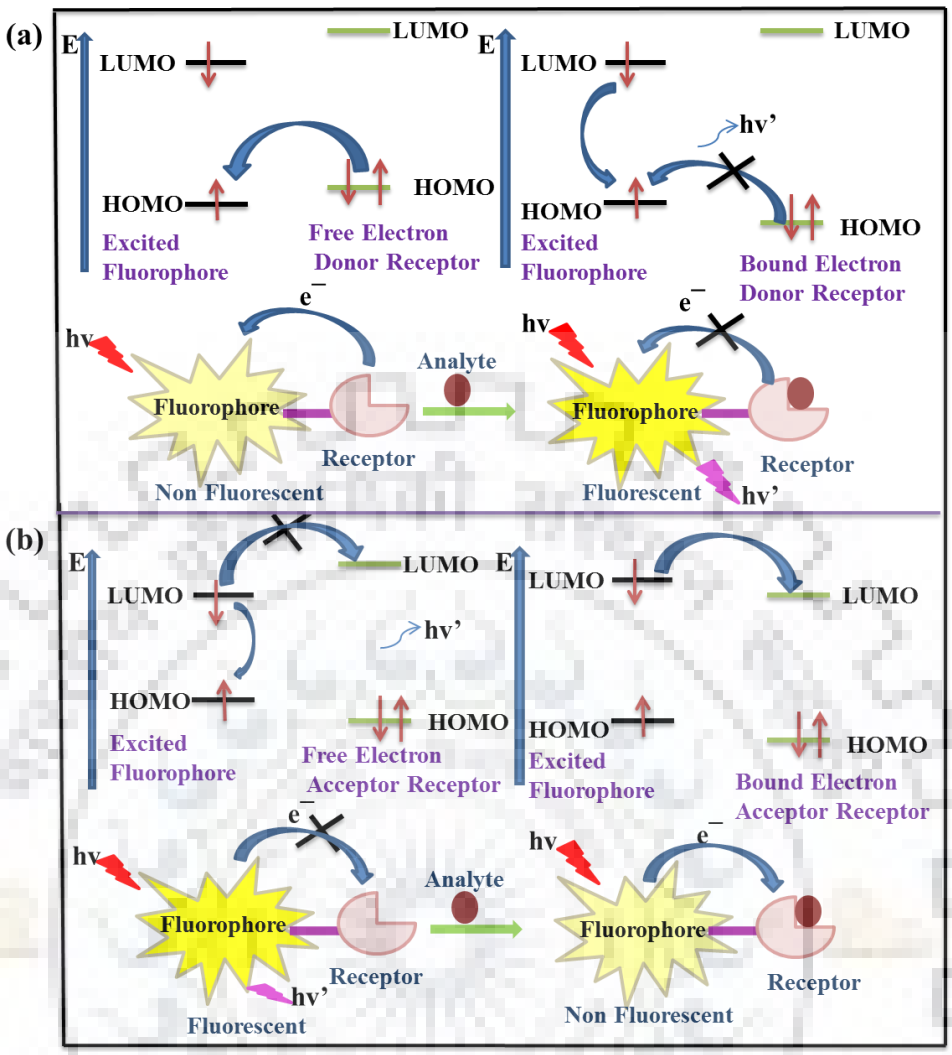

Fig. 1.8 Representation of PET mechanism.

Yoon *et al.* [80] described anthracene derivative containing thiourea moiety **5**. This is selective for F^- and showed a fluorescence quenching through PET. **Nagano *et al.*** [81-82] synthesized *N*,*N*-di-(2-picolyl) ethylenediamine (DPEN) based PET chemosensors **6, 7** which validated fluorescence turn-on reactions with Zn^{2+}.

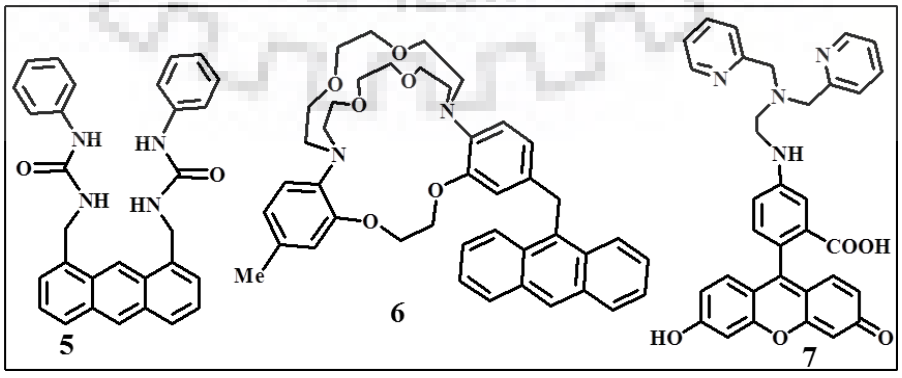

Fig. 1.9 PET based some chemosensors.

1.6.3 Intramolecular Charge Transfer (ICT)

ICT state rises due to a variation in the dipole moments of molecules having electron donor-acceptor (*D*-π-*A*) form of structural designs. For this method, chromophore/fluorophore openly attached to the receptor devoid of any spacer unit which forms a π–conjugated system, thus ICT improves from donor to acceptor unit. If receptor has electron donating property, then hypsochromic shift occurs upon binding with ions, on the other hand, when receptor plays electron acceptor property (reinforce push–pull effect), then hyperchromic shift observed upon interaction with ions [83-85]. Furthermore, the presence of donor (D) and acceptor (A) moieties could grant a π-conjugated luminogen with a solvatochromic conclusion, since the photophysics of the *D*-π-*A* conjugates in solutions are sturdily dependent on the solvent polarity (Fig. 1.10).

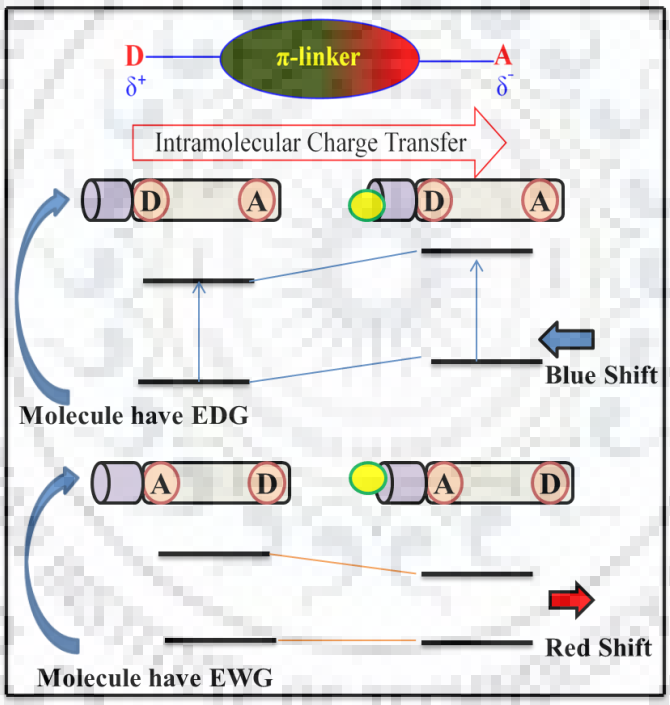

Fig. 1.10 Representation of ICT mechanism.

Guo *et al.* [86] produced novel coumarin-hemicyanine conjugates fluorophore **8** for the recognition of CN^- based on ICT mechanism. Basically, 2-C atom of hemicyanine is susceptible for nucleophilic CN^- addition, due to electron deficient nature, thus disturbed the π-conjugation and obstructed the ICT route of the coumarin ring to hemicyanine moiety. **Liu *et al.*** [87] deliberate a new dicyanovinyl containing ratiometric ICT sensor **9** for CN^- detection.

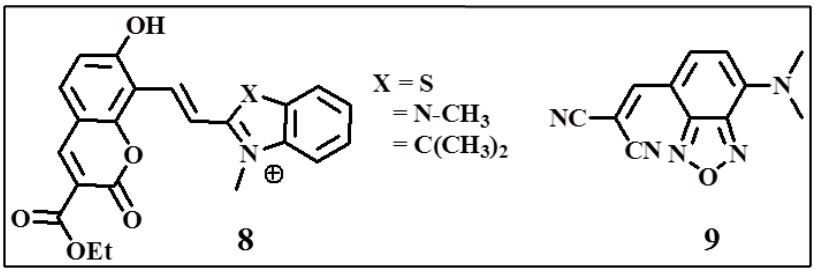

Fig. 1.11 ICT based some chemosensors.

1.6.4 Chelation Enhanced Emission (CHEF) and Chelation Enhanced Quenching (CHEQ)

CHEF (Chelation enhanced fluorescence) and CHEQ (Chelation enhanced quenching) both are precise conversant method in fluorescence sensors for recognition of ions. Quenching of fluorescence intensity arises due to paramagnetic nature of ions in the vicinity of the fluorophore and forbidden ISC (intersystem crossing) come to be faster, the conclusion are known as paramagnetic effect. The rigidity of molecular system becomes rises upon the chelation process over restricted variation of the fluorophore [88-89]. More recently, in 2016, **Misra *et al.*** [90] described a thiphene based selective sensor **10** for Hg^{2+} (based on CHEF) and Cu^{2+} (based on CHEQ) in H_2O-ACN (1:1, v/v).

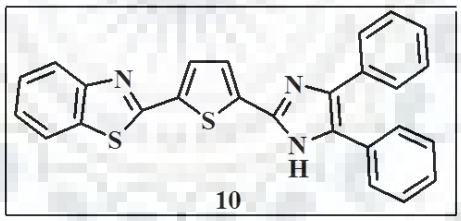

Fig. 1.12 CHEF and CHEQ based chemosensor.

1.6.5 Energy Transfer

Energy transfer is a significant mechanism of signal transduction by the multichromophoric systems because it is distant dependent on donor and acceptor moiety. In this procedure, donor unit constantly absorb radiation at higher energy then transmitted to acceptor unit which fluoresces at low energy [91-92]. Thus, this interface subject on distance and may be classified on the source of distance amongst donor and acceptor moieties during interaction:

1.6.5.1 Fluorescence Resonance Energy Transfer (FRET)

FRET is a non-radiative energy transmission procedure between two relating fluorophores in their excited state. The prerequisite of FRET is to have a definite degree of spectral overlap among the absorption and emission spectrum of the donor and acceptor moiety. Generally, FRET mechanism concerning to acceptor (A) and donor (D) molecule in the ground and excited state and rely on the distance between a fluorophore and excited state to another fluorophore (within the 10-100 Å range) [93]. Moreover, it can elucidate the relief of energy upon the electron relaxation from LUMO to HOMO (of donor part), is used in the excitation of electrons of receptor part from HOMO to LUMO [94] (Fig. 1.13). The FRET based system has some particular advantages, two well separated emission bands with comparable intensities, the enormous shift from excitation to emission and -+effects fluorescence recognition. Generally FRET mechanism is not applicable for a simple fluorescent molecule due to small Stokes' shift. This method is also known a Forster type energy transfer.

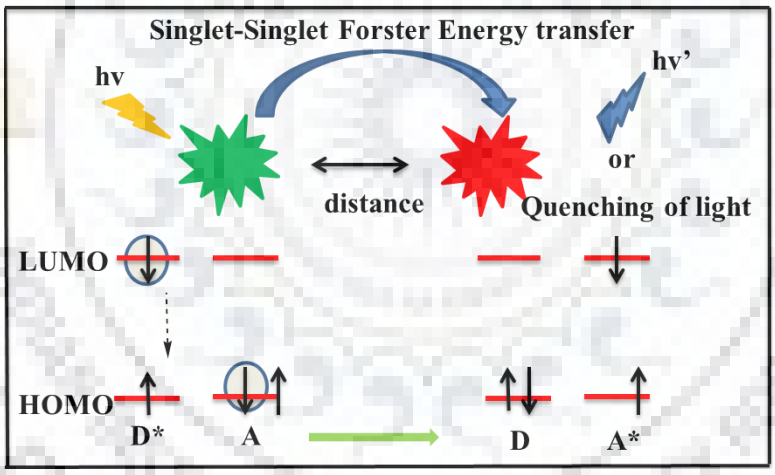

Fig. 1.13 Schematic representation of FRET mechanism.

Chan *et al.* [95] developed 8-aminoquinoline (donor) and spiropyran derivative (acceptor) **11** for Zn^{2+} by fluorescence turn on response. **Kaewtong *et al.*** [96] described a reversible Rhodamine-based probe **12** for Cu^{2+} and CH_3COO^- Molecule display excimer-fluorescence resonance energy transfer (E_m-FRET) consuming a ditopic receptor strategy. Cu^{2+} prompted a ring-open conformation of spirolactam (E_m-FRET ON), whereas CH_3COO^- was induced ring closure (E_m-FRET OFF).

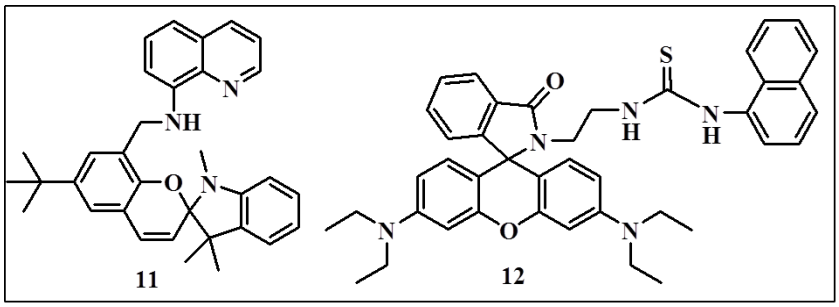

Fig. 1.14 FRET based some chemosensors.

1.6.5.2 Electronic Energy Transfer (EET)

EET mechanism is arisen when the donor and acceptor distance are within the range of 10 Å because the adjacent proximity of the fluorophore with cation and direct orbital interaction are basic requirements for direct energy transfers. Thus, it *is also* known as Dexter electron transfer (Fig. 1.15). This mechanism can be termed as exchange energy transfer and through bond energy transfer because it commonly takes place in conjugated linked donor and acceptor unit where electron exchange takes place between both HOMOs and LUMOs [97-99]. **Burges *et al.*** [100] reported anthracene-bodipy based ligand **13** for extending the energy transfer rate.

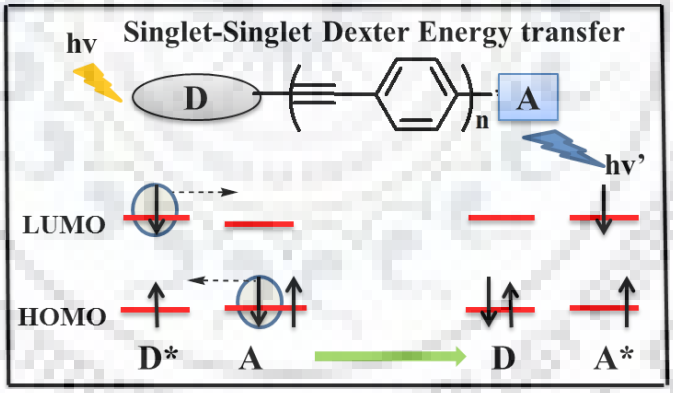

Fig. 1.15 Representation of EET mechanism.

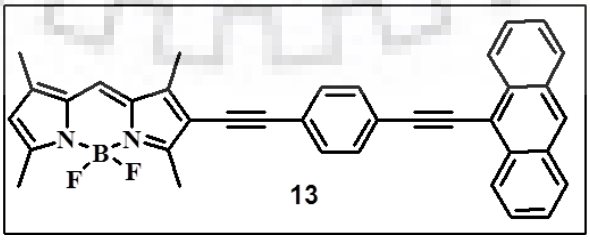

Fig. 1.16 EET based some chemosensor.

1.6.6 Excimer/Exciplex Formation

An excimer can be well-defined as a complex formed by an interaction of a fluorophore (excited state) with the same structure of a fluorophore (ground state), which displays altered emission spectrum from their monomer. A further necessity is close proximity of two monomers for excimer formation imperative to provide stacking exchange and the molecular excimer state. When collision perform amongst structurally dissimilar molecules (*e.g.* an acceptor and an electron donor), an excited state complex is formed, which is known as exciplex (from "excited complex"). Emission of an excimer/exciplex is constantly broad, shifted to longer wavelength paralleled to monomer emission and does not display vibrational resolution. The incidence of an analyte sturdily encourages or interrupts excimer/exciplex formation [101-102], alters the emission spectra. This is also known as "ratiometric sensors" because the ratio of excimer and monomer emission intensity provides a quantitative magnitude of ions present in solution. **Wu *et al***. [103] reported a novel pyrene based derivative **14**, having monomer/excimer alteration in the absence and presence of hypochlorite. The hypochlorite can break the conjugated moiety of sensor that freely forms excimer and emit the excimer emission of pyrene. **Teramae *et al.*** [104] developed a pyrene-guanidinium based sensor, **15** for pyrophosphate sensing *via* intramolecular excimer formation.

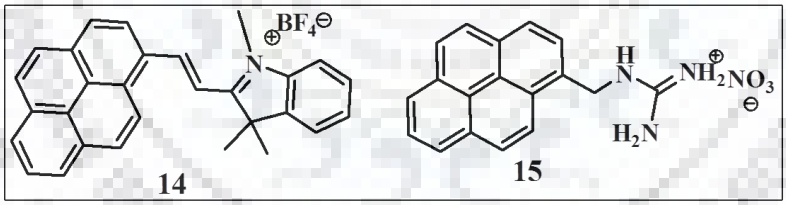

Fig. 1.17 Excimer/Exciplex based some chemosensors.

1.6.7 Excited State Intramolecular Proton Transfer (ESIPT)

Commonly, in this procedure a fast proton transfer occurs in an excited state from proton donor to proton acceptor captivated by intramolecular hydrogen bond. In a distinctive ESIPT process, photoexcitation leads to electron density shift that assists proton movement from a donor atom (usually -OH/-NH_2) to adjacent acceptor atom (O, N atom). Molecule survives in *cis enol* form (ground state) then able to conversion of *keto* isomer (K*- excited state) upon excitation of molecule. Large Stokes' shift observed in emission (up to 10,000 cm^{-1}) relatively absorption energy due to the variance in energy among absorption of the

original (*enol*) tautomer and emission from the secondary (*keto*) tautomer of the molecule. Thus, dual emission can be detected by fluorescence. The intersystem crossing (ISC) for *cis*–keto deactivation form primes to the triplet excited state of the keto tautomer. A different deactivation process is isomerization to the *trans-keto* form to the *cis-keto* form, which is a slow process due to an energy barrier (Fig. 1.18).

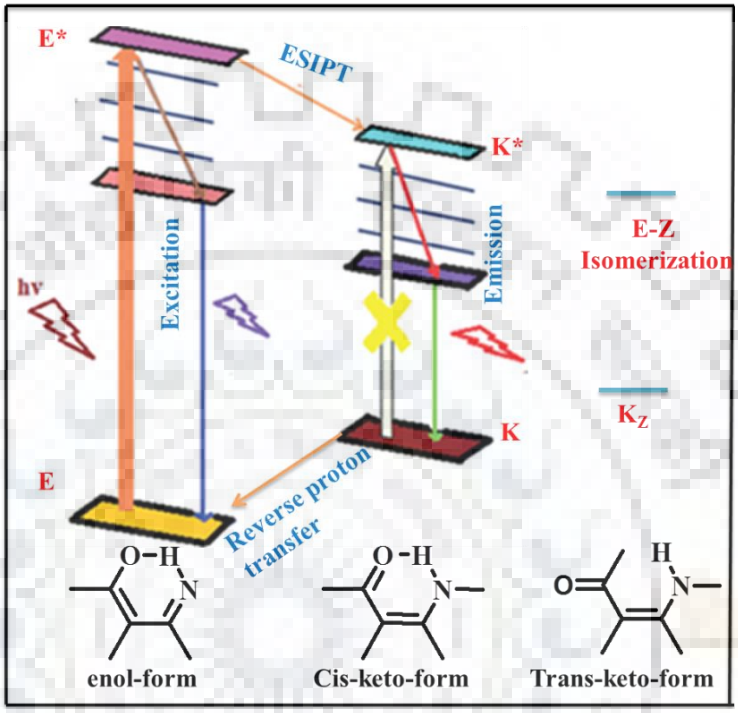

Fig. 1.18 Demonstration of ESIPT mechanism.

Goswami *et al*. [105] synthesized an effectual chemodosimeter **16** for Hg^{2+} and OCl^- recognition. Sensor **16** itself displays emission at 417, 514 nm due to ESIPT procedure. The emission intensity at 514 nm decreased and increased at 590 nm ratiometrically upon addition of Hg^{2+} or OCl^-. **Peng *et al.*** [106] reported **17** and **18** (TABO and PUBO) anion sensors by condensation reaction of 2-(2-aminophenyl) benzoxazole with *p*-toluene sulfonylchloride and phenylisocyanate. The ESIPT process of **17** and **18** is distressed by F^-, CH_3COO^- and $H_2PO_4^-$ anions owing to deprotonation of -NH proton.

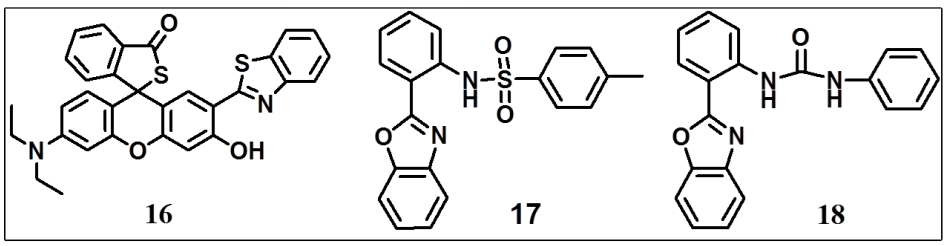

Fig. 1.19 ESIPT based some chemosensors.

1.6.8 Aggregation-Induced Emission (AIE) /Aggregation-Caused Quenching (ACQ)

Most organic luminescent constituents display very strong luminescence in dilute solutions and become non-luminescent in concentrated solution or aggregations in the solid state. This sensation, behavior is normally known as ACQ (aggregation-caused quenching). In this mechanism the aromatic rings of the adjacent luminophores have to capability of intense intermolecular π-π stacking interactions, thus the excited states frequently decay or relax back to the ground state through non-radiative process, causing the emission quenching [107]. On the other hand, in the AIE process, faintly luminescent chromogens are prompted to emit proficiently by the formation of aggregates. This phenomenon can be associated with reduced co-facial intermolecular π-overlapping, restricted intramolecular rotation (RIR), definite molecular arrangements, such as J-aggregation, or dimmer stacking and intramolecular charge transfer [108]. This unusual phenomena were firstly reported by **Tang *et al.*** in 2001 as of a solution of 1-methyl-1,2,3,4,5-pentaphenylsilole. The AIE is a profitable effect which makes it possible to actively develop the aggregation process, while ACQ is a detrimental effect and used to determine luminophore molecules from forming aggregates [109] (Fig. 1.20).

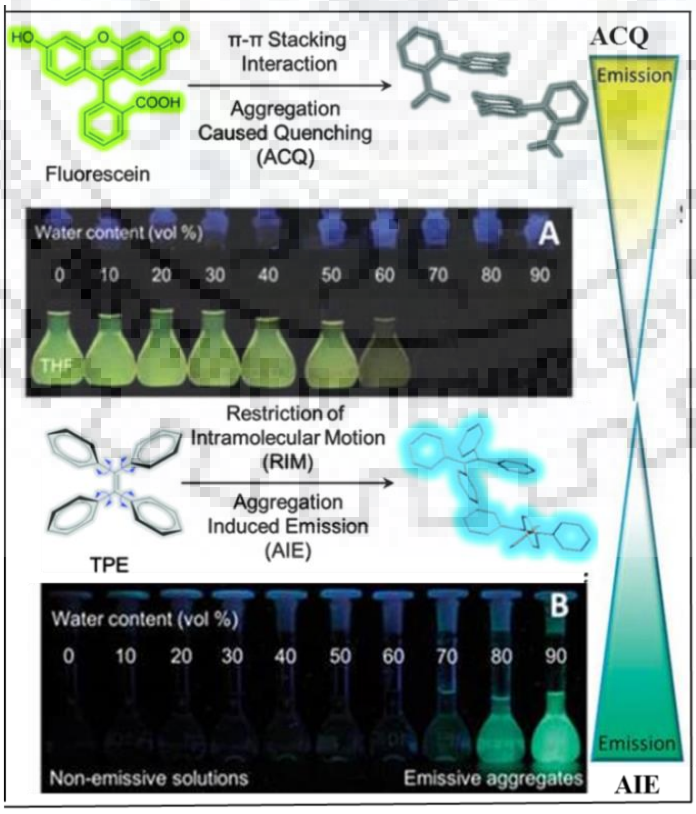

Fig. 1.20 Representation of AIE/ACQ mechanism.

Xiang and **Zhou *et al***. [110] reported salicylaldehyde-based Schiff base **19** and **20**. Sensor **19** displayed intense fluorescence while **20** showed very weak fluorescence in ACN. When the fraction of water volume was increased up to 70%, the emission intensity of the probe **19** reduced due to the aggregation quenching, while the intensity of **20** becomes higher because of the aggregation process. Similarly **Wu *et al***. [111] detected non-luminescent affect for derivatives of **21** in pure THF but upon addition of excess amount of water into its THF solution aggregation process start and molecule displays luminescence.

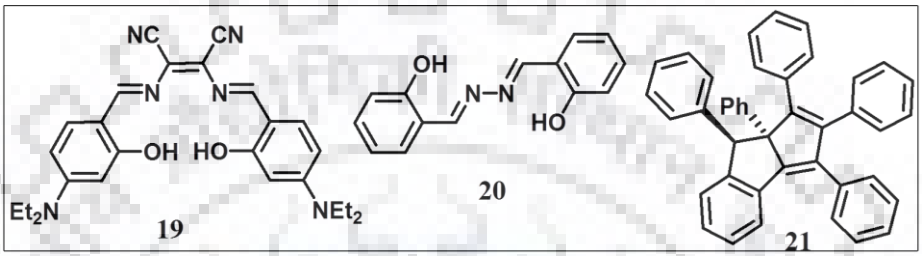

Fig. 1.21 AIE and ACQ based some chemosensors.

1.6.9 C=N Isomerization

This is the most recent described signaling mechanism, since 2007. This is applied on the photophysical properties of conformationally restricted compounds having an unabridged C=N group which are generally non-fluorescent. Upon binding with ions, quenching of C=N isomerization occur in molecular excited states and molecule exhibits emission enhancement (Fig. 1.22).

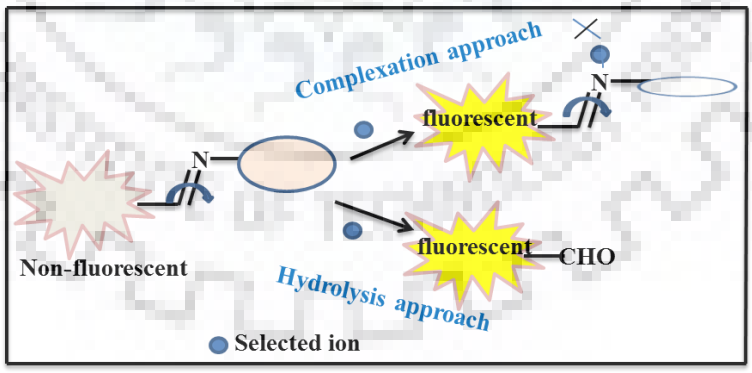

Fig. 1.22 "Turn ON" sensing approaches by C=N isomerization mechanism.

Chellappa *et al.* [112] reported anthracene centered Schiff base **22** to selectively turn on sensor for Ag^{+} in EtOH-H_2O (1:9, v/v) based on PET/C=N isomerization mechanisms. Further, **Lee *et al.*** [113] synthesized coumerin based chemosensor **23** for Zn^{2+} in ACN. The free ligand is almost nonfluorescent due to the isomerization of C=N double bond in the

excited state. However, the solution of ligand shows about a 200-fold increase of fluorescence quantum yield (about 30%) upon addition of $Zn(ClO_4)_2$.

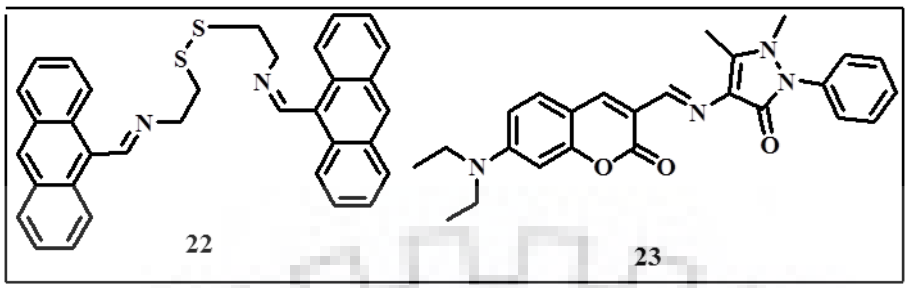

Fig. 1.23 C=N isomerization based some chemosensors.

1.7 DESIGN PRINCIPLES AND GENERAL APPROACH FOR CN^- SENSING

Associated with other types of anions, CN^- selective optical chemosensors have two substantial and specific properties, high binding affinity concerning to transition metal ions like Cu^{2+}, Co^{2+}, Ag^+ and strong nucleophilic character. Commonly, three different methodologies have been working to plan for CN^- optical sensors-

1.7.1 Sensors Based on the Covalently Linked Approach (Hydrogen Bonding)

A general approximation to develop an ion chemosensor is the coupling of at least two units, each one displaying a precise function: the binding site and the signaling subunit, which are linked covalently. In the former resides the function of coordination for CN^- whereas, the signaling unit exhibits change in spectroscopic characteristics (color or fluorescence) upon interaction with analyt. Though CN^- is not a robust hydrogen bonding acceptor paralleled to other anions, numerous CN^- selective sensors based on this approach have been described. The Benzimidazole unit has been used favorably due to deprotonation of the NH proton, which is made acidic by integration of proper electron withdrawing groups and observed the variation in absorption and emission bands by blocking ICT (Fig. 1.24).

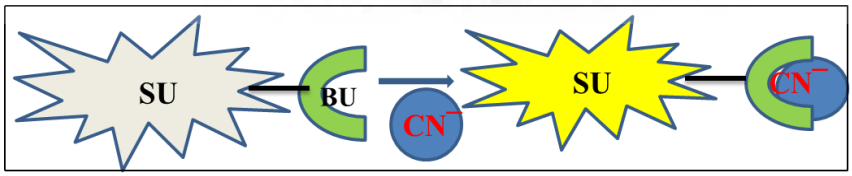

Fig. 1.24 General depiction of binding site signaling approach.

Using this method **Das *et al.*** [114] designed an anthraquinone conjugated imidazole moiety (**24, 25**) with high selectivity in ACN-HEPES buffer (1:1, v/v). The limits of detection were determined to be 0.06 ppm. **Zhang *et al.*** was developed as a proton transfer based compond 4-Amino-3-hydroxynaphthalene-1-sulfonic acid **26** for CN^- [115] based on proton transfer methodology with 0.32 μM detection limit. Chemosensor **26** form a zwitterion complex in aqueous medium due to self-assembly process *via* NH_3^+ and SO_3^- electrostatic interaction and p-p stacking between naphthalene moiety. Upon addition of CN^- interruption of the intramolecular charge exchanges takes place due to deprotonation reactions and quenching observed.

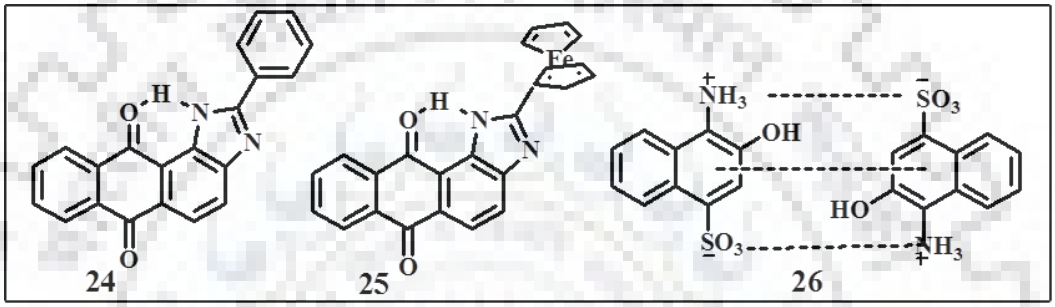

Fig. 1.25 Proton based some CN^- chemosensors.

1.7.2 Chemodosimeter Approach

Chemodosimeters are precise chemical reaction base technique which displays substantial variation in photophysical properties (absorption or emission) of a ligand upon interface with appropriate target ions. These types of sensors depend on the incidence of precise, frequently irreversible chemical reactions and have numerous advantages such as more specific and faster recognition. Thus, it is furthermost significant methods for CN^- detection due to the exceptional nucleophilic character (Fig. 1.26). Numerous classes of chemodosimeters have been reported for CN^- recognition [116].

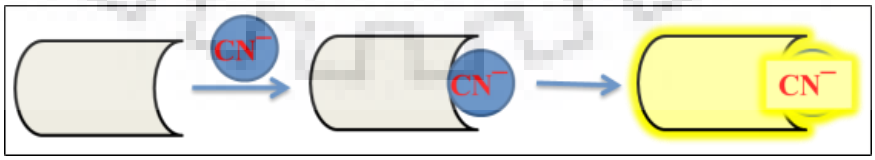

Fig. 1.26 General representation of the chemodosimeter approach.

1.7.2.1 C–C Bond Formation

Carbonyl compounds are well-known to react with CN^- and form analogous cyanohydrins, which can be improved by intramolecular hydrogen bonding interfaces. Using this strategy **Goswami *et al.*** [117] was developed 2-(20 hydroxyphenyl) benzothiazole containing ESITP based ratiometric sensor **27** for CN^- in aqueous solution. The absorbance and emission changes are recognized *via* addition of CN^- to the o-aldehyde group, which leads to inhibition of the ESIPT process. Electron-withdrawing groups like CF_3 boosted the reactivity of carbonyl compounds with CN^-. Using this phenomenon, **Guo *et al.*** [118] developed colorimetric and fluorogenic trifluoroacetylamino **28** containing Rhodafluore based CN^- sensor in MeOH-H_2O (4:1, v/v) *via* ring opening of spirolactam.

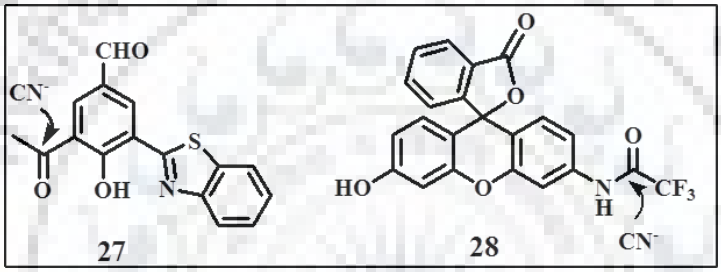

Fig. 1.27 Cyanohydrin forming some CN^- chemosensors.

The 1,1-dicyanovinyl selected reactive moiety has also been engaged in design of CN^- (due to prolonged conjugation) and produce a stabilized anionic adduct. Addition of CN^- interrupts the ICT that produces color and spectral variations. Using this approach, **Jang *et al.*** [119] synthesized BODIPY based turn-on fluorophore **29** for detection of CN^- in THF-H_2O (1:99, v/v) solution. **Li *et al.*** [120] synthesis a novel biindenyl-based D–A derivatives **30**, for prompt detection (100 s) of CN^- in aqueous medium based on aggregation-induced emission.

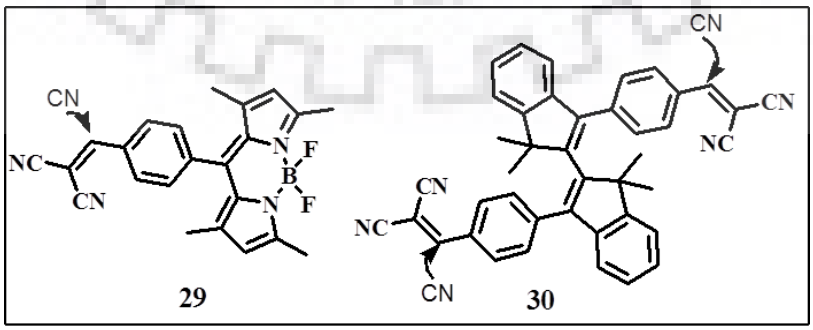

Fig. 1.28 Dicynovinyl based some CN^- chemosensors.

Cyanide discriminating sensors have been developed *via* Michael addition approach. Based on a design with the conjugate addition scheme **Kim *et al.*** designated diethylamino containing α-β unsaturated carbonyl compound **31** that go through rapid reaction with CN^- [121] in ACN solvent (PET process) with a 1.7 μM detection limit and 3 signal-to-noise ratio. **Li *et al.*** [122] developed iridium (III) complex **32** using nano-phosphors (UCNPs) for CN^- detection based on FRET mechanism in DMF-H_2O (9:1, v/v) solution. The detection limit of the OA-41-UCNPs was calculated below 0.18 μM.

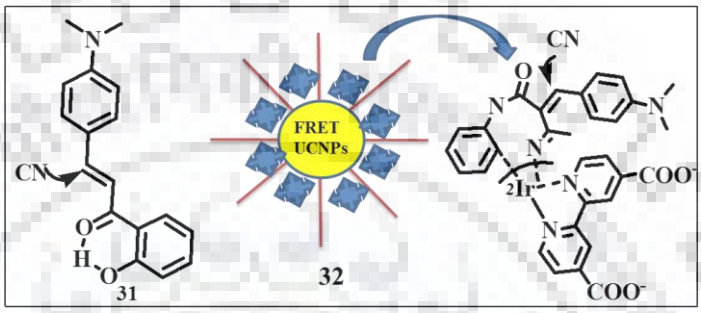

Fig. 1.29 Michal type some CN^- chemosensors.

Because of the simple synthesis Schiff base is a significant class of compound for nucleophilic attack of strong nucleophile CN^- on imine carbon. **Wei *et al.*** [123] reported a naplthylamine based Schiff base **33** for CN^- detection in DMSO-H_2O (9:1, v/v). The nucleophilic addition reaction of CN^- at C=N of the ketoeamine form to generate a cyanohydrin type compound. More recently, **Misra *et al.*** [124] synthesized a tetra-substituted imidazole based selective sensor **34** (based on ESIPT). The nucleophilic addition of CN^- (at immine carbon) induces the cyclisation with formation of benzoxazoline derivative.

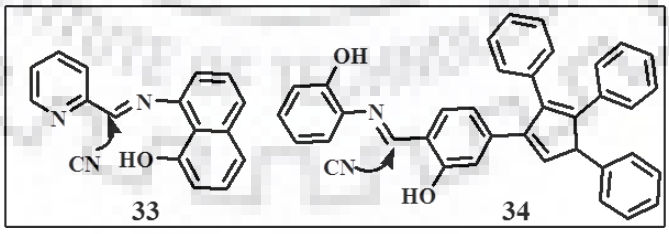

Fig. 1.30 Immine based some CN^- chemosensors.

The electrophilicity of sp^2 hybridized carbon atoms concerning to CN^- can be improved by connection of a positively charged nitrogen/oxygen atom to form iminium/oxonium group respectively. Using this approach, **Kim *et al.*** [125] developed the indole conjugated coumarin **35** as ICT based sensor for CN^- in H_2O-ACN (5:95, v/v) solution. Operating with

the same approach, along with the AIE feature of the tetraphenylethylene (TPE) group, **Zhang *et al.*** [126] designed a fluorescence probe **36** for CN^- detection in aqueous solution with a 91 nM detection limit. The aggregate formation by CN^- addition was validated *via* both DLS (dynamic light scattering) and CLSM (confocal laser scanning microscopy). Recently **Tae *et al.*** [127] reported the acridine moiety based CN^- sensor **37** in DMSO-H_2O (95:5, v/v). The nucleophilic addition of CN^- takes place at the 9-position of the N-methyl acridinium group.

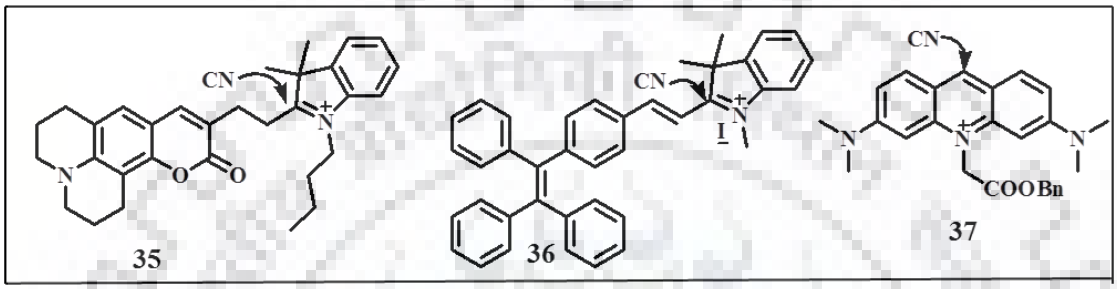

Fig. 1.31 Positively charged heteroatom based some CN^- chemosensors.

Some ring opening reactions containing spiropyran groups also assist as the chemical sensor for CN^-. For example, **Tian *et al.*** [128] syntesize a highly selective oxazine based chemosensor **38** derivatives in which the C–O bond of the oxazine moiety cleaves at the Spiro center by CN^- addition in ACN-H_2O solution (9:1, v/v) with a 26 ppb detection limit. Simiarly, **Zou *et al.*** [129] synthesized polymerization of spiropyran linked diacetylene **39** vesicles reversing fluorometric sensor for CN^- with a very low detection limit (0.5 μM).

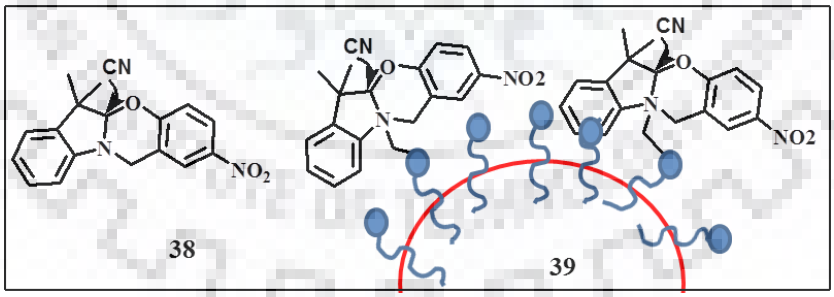

Fig. 1.32 Oxazines based some CN^- chemosensors.

1.7.2.2 C–B Bond Formation

Because of vacant p-orbital, boron center (electron deficient) has a strong affinity for electron donating species like CN^-. Thus, another method for cyanide sensors depends on C–B forming reactions. One example of this approach was developed by **Akkaya *et al.*** [130] based on boron dipyrrin dye **40** to distinguish both F^- and CN^- in chloroform solvent. The

spectral variation arising *via* detachment of the difluoroboron bonds by CN^- and F^- substitution reactions at boron center. Cationic boranes are proficient of undergoing effectual complexation with CN^-, due to the promising Coulombic CN-receptor. **Gabbaı *et al*.** [131] devised this type of sensor based on 9-thia-10-boraanthracene moiety substituted at boron by the cationic anilinium group **41.** This sensor can sense both CN^- and F^- in THF to give the corresponding zwitter ionic cyanoborate and fluoroborate species, but in nitromethane-water it is selective for CN^- rather than F^-.

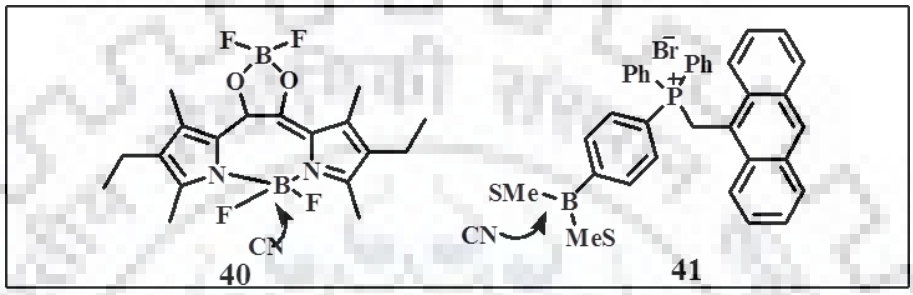

Fig. 1.33 C-B bond forming based some CN^- chemosensors.

1.7.2.3 C–S Bond Formation

Wang *et al.* [132] described donor-acceptor type chromophores **42** with well-tuned reactivity for CN^-. The triple signaling properties are valuable for the extremely quantitative recognition of CN^- in DMF-H_2O (99:1, v/v). The mechanism was proved *via* a model system, implicates CN^- attack on the benzothiadiazole ring sulfur, trailed by a second CN^- attack. The subsequent imidosulfite adduct is willingly oxidized to form a more stable sulfamide.

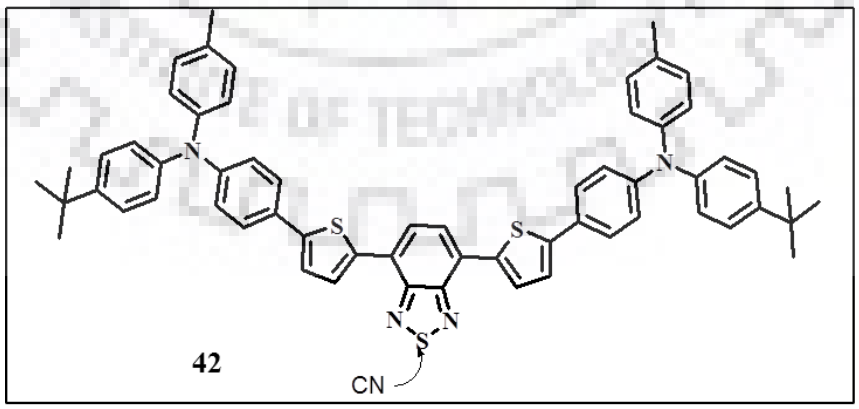

Fig. 1.34 C-S bond forming based CN^- chemosensor.

1.7.2.4 M–C Bond Formation (M-metal)

It is well recognized that CN^- have a strong binding affinity with transition metal cations, because of the instantaneous back donation and the electron pair donation effect. Furthermore, the ligand field splitting (low to high or high-to-low spin changes), induces marked variations in the absorption spectra of the complexes, resulting from CN^- coordination. Similarly, the fluorescence spectra (containing luminescent moieties) are also frequently tuned by exogenous co-ligands CN^-, which sturdily affect the electronic states of metal complex. For example, **Hong *et al.*** [133] synthesized the Co (II)-salen based fluorescent CN^- sensor **43** in ACN on PET based phenomenon, which is withdrawn due to the formed cyanoligated complex having a higher energy LUMO level. Further **Tian *et al.*** [134] developed Cu (II)-based complex **44** containing unsymmetrical dithienylethene moiety and naphthalene group as a fluorophore for CN^- detection in ACN solution with a 22.5 nM detection limit.

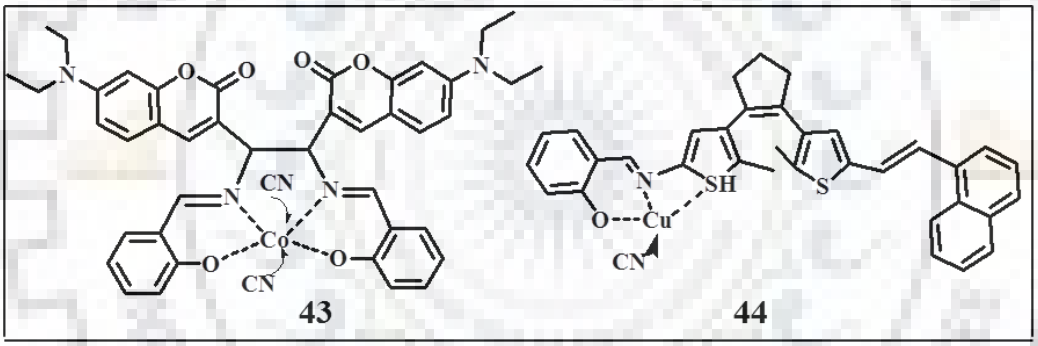

Fig. 1.35 Metal coordinated based some CN^- chemodosimeters.

1.7.2.5 Electron Transfer Reactions

A SET (single electron transfer) interested reaction based advance approach for CN^- recognition has been described. The distinctive HOMO-LUMO electronic transition, multidimensional signal outputs and potential use in practical electronic devices are advantages of this method. **Mukhopadhyay *et al.*** [135-136] described a series of SET-based CN^- sensor created by naphthalenediimide **45** (NDI) and 7,7,8,8-tetracyano quinodimethane **46** (TCNQ) moieties by using their low-LUMO properties. Specially, a CN^- addition to the sensors leads to the development of the equivalent air-stable radical anions and detect 0.67 and 1.3 μM detection limit in THF and DMF, respectively. The sensors **45** can be rejuvenated by usage $NOBF_4$ as oxidizing agent. Similarly the TCNQ sensor **46** produces differentiable signal outputs in both UV-vis-NIR absorption and scattering-based

spectroscopic methods such as Raman and hyper Rayleigh scattering with CN^- in ACN-H_2O (9:1, v/v). The intense NIR absorption peak suggests the potential detection of CN^- in biological samples.

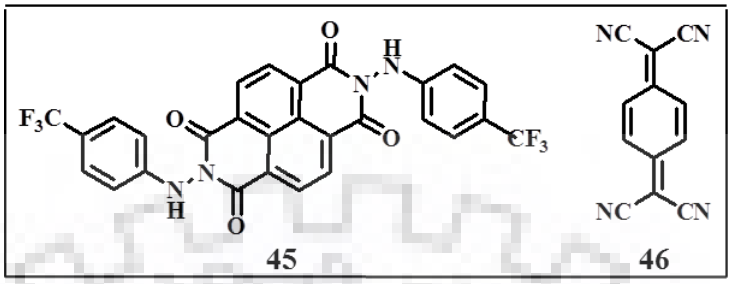

Fig. 1.36 SET based some CN^- chemodosimeters.

1.7.3 Displacement Approach (Indirect Method)

Unlike the first (hydrogen bonded) and second (chemodosimeter) methods, the displacement method consuming anion binding sites and signaling subunits, which forms a coordination complex instead of covalently attachment (one part of the host-indicator associations that are used in indicator displacement). An indicator has moved from the binding position upon anions addition, resultant a non-coordinated state from a coordinated state with different spectroscopic characteristics. The displacement sensing procedure depends on the basis of two main approaches: (i) the two or more units consist of organic-indicator, organic-organic or organic-metal-indicator mixtures, form an addition complex and a displacement reaction takes place with the addition of the analyte i.e. the interface of analyte (with one of the earlier two cases and organic-metal unit in the second case) discharges the other into the solution associated with spectral variations and, (ii) protocol is constructed upon the demetallation, the receptor binds through metal and varies the signal. The first methodology is most generally employed due to noncovalent contact between the groups which consents much enhanced tuning of the sensing methods. For this approach the stability constant of the designed complex amongst the anions and binding site should be greater than that concerning the signaling subunits and binding site. The advantages of the displacement method are that it does not requisite to integrate the indicator into receptors structures or analytes and the recognition mechanism is independent of the analyte structure. Displacement analyses have been broadly used for chromogenic sensor development as sketched in Fig.1.37. Many metal complexes are used for CN^- sensing *via* this method. In these chemosensors, the taster CN^- form stable $[M(CN)x]_n^{1-x}$ species (M-Ag^+, Cu^{2+}, Hg^{2+})

and regenerates the spectroscopic activities of the noncoordinated sensors, thus it is acting as an indirect approach for the CN^- sensing [137-138].

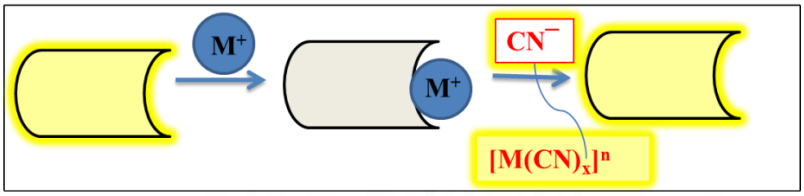

Fig. 1.37 General representation of the displacement approach.

Utilizing this strategy **Misra *et al.*** [139] reported acenapthene based Cu complex **47** for CN^- detection in H_2O-ACN (4:1, v/v) with 2 μM detection limit. Further, **Kim *et al.*** [141] synthesized coumarin Cu^{2+} system **48** for CN^- in aqueous medium. Biological application was also effectively accomplished in $HepG_2$ cells to display ''Off-On'' fluorescence cellular pictures. Also, some Zn complex **49** is replaced by CN^- from the complex. Moreover, this Zn^{2+} complex was effectively applied for CN^- analysis in the cultured plants [141].

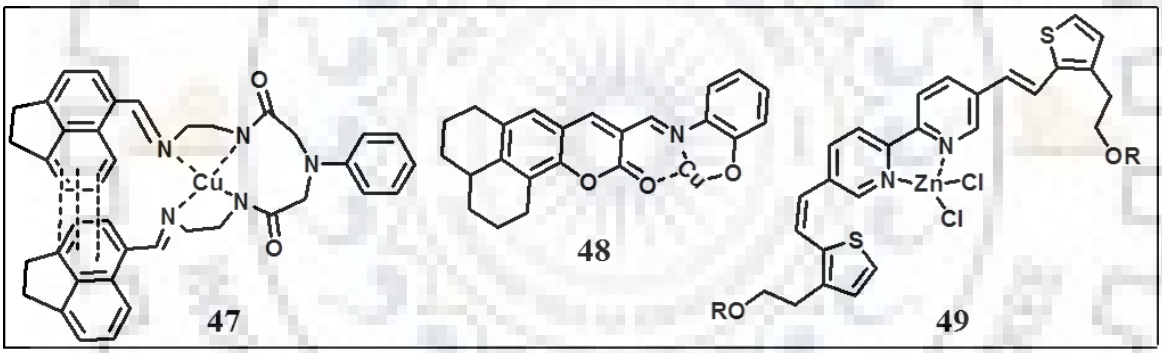

Fig. 1.38 Displacement based some CN^- chemosensors.

1.8 MOLECULAR LOGIC GATES

In the area of supramolecular chemistry, assembly of simple electronic and photonic systems as molecular devices function integrating logic gates were great interest. The most common molecular logic gates are constructed on the optical assets of the molecular switches, coding the guest molecules such as inputs and the absorption/emission signals as outputs. The inputs and outputs are assigned as 0 (low-off) and 1 (high-on). A furthermost case, the base of logic gates is accomplished when the chemically coded data are altered into fluorescent (quenching or enhancement) outputs. While the first suggestion to accomplish logic operations at the molecular level was reported in 1988 [142], but it was in fact implemented when analogy among molecular switches and logic gates was experimentally

validated by **de Silva** [143]. Meanwhile, there are a number of logic gates have been described which depends upon the number of inputs and outputs. The assimilated operations of molecular logic gates have become a significant application of chemistry which is marked from the development of basic (YES, NOT, AND and OR) as well as slightly complex two-integrated logic functions such as NAND, NOR, XOR, IMPLICATION and INHIBIT [141-147]. Here in this portion of this chapter, we have partial discussion to some characteristic molecular logic gates described in recent times as Table 1.2 & 1.3.

Table: 1.2 Truth tables for single input logic gate.

Input	**YES**	**NOT**
0	0	1
1	1	0

Table: 1.3 Truth tables for two input logic gates.

I	**O**	**OR**	**AND**	**XOR**	**XNOR**	**NOR**	**NAND**	**INH**	**IMP**
0	0	0	0	0	1	1	1	0	1
0	1	1	0	1	0	0	1	1	0
1	0	1	0	1	0	0	1	0	1
1	1	1	1	0	1	0	0	0	1

The pyrene attached calix [4] crown **50** go through fluorescence quenching with Pb^{2+} [148] *via* the photo induced electron transfer from pyrene moiety to the electron deficient amide group. Also the quenching phenomenon also observed with the addition of, either $HClO_4$/Et_3N, into **50** solutions. Thus, on the origin of the emission behavior displayed by **50** in the presence of Pb^{2+}, $HClO_4$ and Et_3N, the logic gates NOR, XNOR and INHIBIT were produced. **Jang *et. al.*** [149] reported benzimidazole-based fluorescent probe **51** for Fe^{3+} and Cu^{2+}, to develop a molecular 'OR' gate. The probe showed dual emissions at 320 and 420 nm in aqueous ACN, which got quenched with the development of new emission band at 490 nm upon accumulation of Fe^{3+} and Cu^{2+}. Hence, with Fe^{3+} and Cu^{2+} as two inputs and emission as output, the probe **51** presented a remarkable molecular 'OR' logic gate. The metal ion based sensors have also been working for the recognition of analytes, particularly for heavy metal ions. For example, iridium (III) complex with N-O donor moiety **52** has been developed as an 'AND' and 'INHIBIT' logic gate with Hg^{2+} and histidine as chemical

inputs and phosphorescence signal as output [150]. More recently, in 2016, **Misra *et al.*** [90] described a thiphene based selective sensor **10** for Hg^{2+} and Cu^{2+} in ACN-H_2O (1:1, v/v). Subsequently the probe exhibited different emission behavior with Hg^{2+} (On) and Cu^{2+} (Off) ions tried to construct two chemical input. On behalf of the first input sequence order such as, In1 (Hg^{2+}) followed by In2 (Cu^{2+}) emission enhancement occurred (at 500 nm) and lead to in an INHIBIT logic function. Moreover, on reversing the input sequences quenching occurred and this "Off-state" using the output signal as, '0' and mimic an IMPLICATION logic gate.

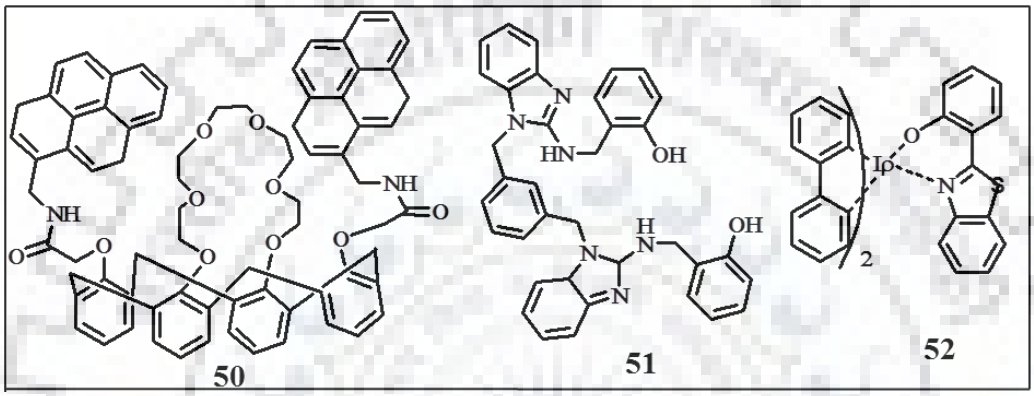

Fig. 1.39 Logic gate applied some chemosensors.

1.9 AIM OF THE THESIS

Further, literature survey discloses that the utmost of the reported CN^- sensor are not with precise high sensitive, selective and good response time. Owing to their hazardous and biotoxicity to the environment, recognition of CN^- is praiseworthy. Numerous challenges have been made to improve new sensing material for CN^-, which display enhanced performance paralleled to the prevailing ones. Most of them reported as a dual sensor in organic solvents. In order to overawed the modern challenges which have been revealed above, this study will be to increase the sensitivity of the CN^- sensor by coupling its reaction with different chemosensors in aqueous medium. The research in this thesis focuses on the synthesis of some simple, novel, highly selective and sensitive chromogenic and fluorogenic sensors for CN^-, which demonstrated by absorption, emission, spectroscopy, electrochemical variation. The binding and sensing mechanisms have been analyzed *via* NMR, IR, Mass spectroscopy and advanced DFT. Further the whole scheme applied as a logic gate and antimicrobial behavior.

The present work is summarized in five chapters. The **first chapter** deals with 'general introduction' which defines numerous aspects comprising cyanide sources and lethal effects, brief discussion and principle of optical sensors, some common photophysical mechanism, a general approach for CN^- sensing and molecular logic gates. **Second chapter** presents; 'hydrogen bonding based cyanide sensor' in H_2O-ACN/DMSO (1:9 v/v, pH-7.4 HEPES buffer). The reversible behavior of receptors applied as INHIBIT logic gate. **Third chapter** presents; 'metal complexation based cyanide sensor' in H_2O-DMF (1:9 v/v, pH-7.4 HEPES buffer). The 'On-Off-On' emission variation outlines the working principle of IMPLICATION logic gate. The receptor and its metal complex exhibit antimicrobial activity against Gram negative bacteria *P. diminuta* and Gram positive bacteria: *S. aureus, B. brevis*. **Fourth chapter** presents; 'nucleophilic addition based cyanide sensor' in H_2O-DMF (9:1 v/v, pH-7.4 HEPES buffer). The spectroscopic identification of CN^- applied as paper strips and biological activities (antifungal, antibacterial). **Fifth chapter** presents; 'metal displacement based cyanide sensor (indirect approach)' which describes the synthesis of excited state intramolecular proton transfer (ESIPT) based Nobel chemosensors. They show the remarkable aggregation-induced emission enhancement (AIEE) in aqueous medium. ON basis of this phenomenon further developed fluorescent organic nanoparticles. All chemosensors express good water solubility and *in-situ* sensing of CN^- in aqueous medium. "On-Off-On" sensing behaviour was mimic as the function of a sequential logic circuit at molecular level. Ligands show the antimicrobial activities against fungi: *Bipolaris oryzae* and *Rhizoctonia solani* and nanoparticle S3-FONs express promising applications in cellular imaging in HeLa cells.

References

1. Bianchi, K. B. James, E. G. Espana, Eds., Supramolecular chemistry of anions, Wiley-VCH (1997) 461.
2. M. Vàzquez, L. Fabrizzi, A. Taglietti, R. M. Pedrido, A. M. Gonzàlez-Noya, M. R. Bermejo, A colorimetric approach to anion sensing: A selective chemosensor of fluoride ions, in which color is generated by anion-enhanced π delocalization, Angew. Chem. Int. Ed. 116 (2004) 1996-1999.
3. Valeur, I. Leray, Design principles of fluorescent molecular sensors for cation recognition, Coord. Chem. Rev. 205 (2000) 3-40.
4. M. K. Jaiswal, P. K. Muwal, S. Pandey, P. S. Pandey, A novel hybrid macrocyclic receptor based on bile acid and calix[4]arene frameworks for metal ion recognition, Tetrahedron Lett. 58 (2017) 2153-2156.
5. M. Asthana, R. Kumar, T. Gupta, R. M. Singh, Facile synthesis of functionalized 1H-pyrrolo[2,3-b]quinolines via Ugi four-component reaction followed by Cu-catalyzed aryl-amide, C-N bond coupling, Tetrahedron Lett. 56 (2015) 907-912.
6. R. M. Singh, R. Kumar, K. C. Bharadwaj, T. Gupta, Pd catalyzed facile synthesis of cyclopenta[b]- quinolin-1-one *via* sequential Sonogashira coupling and annulation. An unusual mode of ring closure, using sulphur as a soft nucleophile, Org. Chem. Front. 3 (2016) 1100-1104.
7. J. B. Singh, K. C. Bharadwaj, T. Gupta, R. M. Singh, Ligand-free palladium-catalyzed facile construction of tetra cyclic dibenzo[b,h][1,6]naphthyridine derivatives: domino sequence of intramolecular C-H bond arylation and oxidation reactions, RSC Adv. 6 (2016) 26993-26999.
8. M. M. Antonijevic, S. M. Milic, M. B. Petrovic, Films formed on copper surface in chloride media in the presence of azoles, Corros. Sci. 51 (2009) 1228-1237.
9. R. Gracia, G. Shepherd, Cyanide poisoning and its treatment, Pharmacotherapy, 24 (2004) 1358-1365.
10. M. F. Hughes, Arsenic toxicity and potential mechanisms of action, Toxicol. Lett. 133 (2002) 1-16.
11. M. S. Razzaque, Phosphate toxicity: new insights into an old problem, Clin. Sci. 120 (2011) 91-97.
12. M. Fukagawa, Y. Hamada, S. Nakanishi, M. Tanaka, The kidney and bone metabolism: Nephrologists' point of view, J. Bone Miner. Metab. 24 (2006) 434-438.

13. Z. H. Chohan, M. Praveen, Biological role of anions (sulphate, nitrate, oxalate and acetate) on the antibacterial properties of cobalt (II) and nickel (II) complexes with pyrazinedicarboxaimide derived, furanyl and thienyl compounds, Met.Based Drugs 6 (1999) 95-99.
14. G. Pizzo, M. R. Piscopo, I. Pizzo, G. Giuliana, Community water fluoridation and caries prevention: a critical review, Clin. Oral Invest. 11 (2011) 189-193.
15. S. Ayoob, A. K. Gupta, Fluoride in drinking water: A review on the status and stress effects, Crit. Rev. Environ. Sci. Technol. 36 (2006) 433-487.
16. S. K. Mittal, R. Sharma, M. Sharma, N. Singh, J. Singh, N. K. M. Chhibber, Voltammetry of nanoparticle coupled imine linkage based receptors for sensing of Al(III) and Co(II) ions, J. Appl. Electrochem. 44 (2014) 1239-1251.
17. Desmond, B. Lane, J. Alderman, M. Hill, D. W. M. Arrigan, J. D. Glennon, An environmental monitoring system for trace metals using stripping voltammetry, Sens. Actuators, B 48 (1998) 409-414.
18. R. Mihajlovic, Z. Stanica, M. Antonijevic, Natural monocrystalline pyrite, chalcopyrite and galena as electrochemical sensors for potentiometric redox titrations in acetonitrile, Electrochim. Acta 51 (2006) 3707-3713.
19. N. R. Gupta, S. K. Mittal, S. K. Sonkar, Trace level detection of nickel ions in chocolate samples using novel N4 macrocycle based potentiometric sensor, Adv. Sci. Eng. Med. 5 (2013) 1-6.
20. S. K. Mittal, P. Kumar, S. K. A. Kumar, L. F. Lindoy, A comparative study of linked 2, 2’-dipyridylamine ligand system as an ion selective electrode for Ag(I) ions, Int. J. Electrochem. Sci. 5 (2010) 1984-1995.
21. S. K. Mittal, S. K. A. Kumar., N. Gupta, S. Kaur, S. Kumar, 8-Hydroxyquinoline based neutral tripodal ionophore as a copper(II) selective electrode and the effect of remote substituents on electrode properties, Anal. Chim. Acta 585 (2007) 161-170.
22. M. G. Fallon, D. Mulcahy, W. S. Murphy, J. D. Glennon, Cesium ion-selective electrodes based on crowned benzoquinones, Analyst 121 (1996) 127-131.
23. M. Cuartero, M. M. Montoya, M. S. Garcia, D. Curiel, J. A. Ortuno, New carbazolo[1,2-a]carbazole derivative as ionophore for anion-selective electrodes: Remarkable recognition towards dicarboxylate anions, Talanta 123 (2014) 200-206.
24. M. M. Antonijevic, M. Maric, Determination of the content of heavy metals in pyrite contaminated soil and plants, Sensors 8 (2008) 5857-5865.

25. T. Senior, J. D. Glennon, Use of acetohydroxamic acid in the direct spectrophotometric determination of iron(III) and iron(II) by flow-injection analysis, Anal. Chim. Acta 196 (1987) 333-336.
26. S. Pedreno, M. S. Garcia, J. A. Ortuno, M. I. Albero, R. Exposito, Kinetic methods for the determination of cadmium(II) based on a flow-through bulk optode, Talanta 56 (2002) 481-489.
27. A. S. Pedreno, M. S. Garcia, J. A. Ortuno, M. I. Albero, E. Ballester, Development of a new flow-through bulk optode for the determination of manganese(III), Fresenius J. Anal. Chem. 369 (2001) 680-683.
28. A. S. Pedreno, J. A. Ortuno, M. I. Albero, M. S. Garcia, J. C. G. Bayonas, A new procedure for the construction of flow-through optodes; Application to determination of copper(II), Fresenius J. Anal. Chem. 366 (2000) 811-815.
29. M. I. Albero, J. A. Ortuno, M. S. Garcia, C. S. Pedreno, R. Exposito, Determination of zinc(II) in pharmaceuticals based on a flow-through bulk optode, J. Pharm. Biomed. Anal. 29 (2002) 779-786.
30. Merly, B. Lynch, P. Ross, J. D. Glennon, Selective ion chromatography of metals on porous graphitic carbon, J. Chromatogra. A 804 (1998) 187-192.
31. N. Ryan, J. D. Glennon, Trace metal preconcentration in ion chromatography using biochelating silicas, Anal. Proceedings 29 (1992) 21-23.
32. A. Kumar, P. S. Pandey, Anion recognition by 1,2,3-triazolium receptors: application of click chemistry in anion recognition, Org Lett. 10 (2008) 165-168.
33. V. K. Khatri, S. Upreti, P. S. Pandey, Novel bile acid-based cyclic bisimidazolium receptors for anion recognition, Org. Lett. 8 (2006) 1751-1758.
34. A. Nayal, P. S. Pandey, Bile acid-based triazole and triazolium receptors for colorimetric sensing of anions, Tetrahedron 71 (2015) 6991-6996.
35. S. K. Kim, D. H. Lee, J. I. Hong, J. Yoon, Chemosensors for pyrophosphate, Acc. Chem. Res. 42 (2009) 23-31.
36. H. N. Lee, Z. Xu, S. K. Kim, K. M. K. Swamy, Y. Kim, S. J. Kim, J. Yoon, Pyrophosphate-selective fluorescent chemosensor at physiological pH: formation of a unique excimer upon addition of pyrophosphate, J. Am. Chem. Soc. 129 (2007) 3828-3829.

37. G. Liu, W. Cai, L. Kong, G. Duan, Y. Li, J. Wang, Z. Cheng, Trace detection of cyanide based on SERS effect of Ag Nano plate-built hollow microsphere arrays, J. Hazard. Mater. 248 (2013) 435-441.
38. World Health Organization, Guidelines for drinking-water quality, 3rd, Geneva, 2008, pp.188, http://www.who.int/water sanitation health/dwq/fulltext.pdf (accessed January 9, 2010).
39. S. L. Baskin, T. G. Brewer, Medical aspects of chemical and biological warfare, ed. F. R. Sidell, E. T. Takafuji, D. R. Franz, TMM Publications, Washington, DC (1997) 271-286.
40. F. J. Baud, Cyanide: critical issues in diagnosis and treatment, Toxicology 26 (2007) 191-201
41. H. B. Leavesley, L. Li, K. Prabhakaran, J. L. Browitz, G.E. Isom, Interaction of cyanide and nitric oxide with cytochrome c oxidase: implications for acute cyanide toxicity, Toxicol. Sci. 101 (2008) 101-111.
42. J. D. Johnson, T. L. Meisenheimer, G. E. Isom, Cyanide-induced neurotoxicity: role of neuronal calcium, Toxicol. Appl. Pharmacol. 84 (1986) 464-469.
43. B. K. Ardent, J. L. Borowitz, G. E. Isom, Brain lipid peroxidation and antioxidant protectant mechanisms following acute cyanide intoxication, Toxicological. 56 (1989) 147-154.
44. K. W. Kulig, Cyanide Toxicity; U.S. Department of health and human services: Atlanta, GA, (1991).
45. United States Environmental Protection Agency (EPA), Methods for chemical analysis of water and wastes, Environmental monitoring and support laboratory, Cincinnati, OH, 1983, http://www.epa.gov/ogwdw000/ contaminants/basicinformation/cyanide.html (2010).
46. Official Journal of the European Union, Commission Directive 1998/83/EC, 1998, pp. L30-42, http://eur-lex.europa.eu/LexUriServ/LexUriServ.do?uri=OJ: L:1998:330:0032:0054:EN:PDF (2010).
47. Australian and New Zealand Environmental and Conservation Council (ANZECC), Agriculture and resource management council of Australia and New Zealand, Australian water quality guidelines for fresh and marine water, (2000) 4-5, http://www.mincos.gov.au/ data/assets/pdf file/0019/316126/wqg-ch3.pdf (2010).

48. P. Anzenbacher, D. S. Tyson , K. Jursíková, F. N. Castellano, Luminescence lifetime-based sensor for cyanide and related anions, J. Am. Chem. Soc. 124 (2002) 6232-6233.
49. A. Abbaspour, M. Asadi, A. Ghaffarinejad, E. Safaei, A selective modified carbon paste electrode for determination of cyanide using tetra-3,4-pyridinoporphyrazinatocobalt(II), Talanta 66 (2005) 931-936.
50. M. Noroozifara, M. K. Motlagh, S. N. Hosseini, Flow injection analysis-flame atomic absorption spectrometry system for indirect determination of cyanide using cadmium carbonate as a new solid-phase reactor, Anal. Chim. Acta 528 (2005) 269-273.
51. Z. F. Kovačević, M. M. D. Šalamon, Cyanide determination in fruit brandies by an amperometric biosensor with immobilised *Saccharomyces cerevisiae*, Eur. Food Res. Technol. 215 (2002) 347-352.
52. A. T. Haj-Hussein, G. D. Christian, J. Ruzicka, Determination of cyanide by atomic absorption using flow injection conversion method, Anal. Chem. 58 (1986) 38-42.
53. A. Ishii, H. Seno, K. W. Suzuki, O. Suzuki, Determination of cyanide in whole blood by capillary gas chromatography with cryogenic oven trapping, Anal Chem. 70 (1998) 4873-4876.
54. B. Ren, D. Y. Wu, B. W. Mao, Z. Q. Tian, Surface-enhanced Raman study of cyanide adsorption at the platinum surface, J. Phys. Chem. B 107 (2003) 2752-2758.
55. F. Wang, L. Wang, X. Chen, J. Yoon, Recent progress in the development of fluorometric and colorimetric chemosensors for detection of cyanide ions. Chem. Soc. Rev. 43 (2014) 4312-4324.
56. C. McDonagh, C. S. Burke, B. D. MacCraith, Opical chemical sensors, Chem. Rev. 108 (2008) 400-422.
57. A. Hulanicki, S. Geab, F. Ingman, Chemical sensors definitions and classification, Pure & Appl. Chem. 63 (1991) 1247-1250.
58. S. Olcum, N. Cermak, S. C. Wasserman, S. R. Manalis, High-speed multiple-mode mass-sensing resolves dynamic nanoscale mass distributions, Nat. Commun. 6 (2015) 1-8.
59. J. Wang, Analytical electrochemistry, John Wiley & Sons (2006).
60. D. Ahuja, D. Parande, Optical sensors and their applications, J. Sci. Res. and Rev. 1 (2012) 60-68.
61. E. Bakker, E. Pretsch, Potentiometric sensors for trace-level analysis, Trends Analyt. Chem. 24 (2005) 199-207.

62. J. B. Raoof, R. Ojani, M. Kolbadinezhad, Voltammetric sensor for glutathione determination based on ferrocene-modified carbon paste electrode, J. Solid State Electrochem. 13 (2009) 1411-1416.
63. P. Protti Introduction to modern voltammetry and polarographic analysis techniques; fourth ed. Amel electrochemistry (2001).
64. IUPAC Compendium of Chemical Terminology; Sec. ed. 1997.
65. A. J. Bard, L. R. Faulkner. Electrochemical Methods. Fundamentals and applications, Wiley India, (2006).
66. H. H. Qazi, A. B. Mohammad, M. Akram, Recent progress in optical chemical sensors, Sensors 12 (2012) 16522-16556.
67. X. Bai, Y. Lia, Z. Yec, A colorimetric sensor based on thiourea-polyvinyl alcohol microspheres for the selective recognition of Hg^{2+} and Cu^{2+}, New J. Chem. 40 (2016) 8815-8822.
68. J. R. Ablnani, Principles and applications of fluorescence spectroscopy, Wiley-Blackwell (2007).
69. K. N. Shinde, S. J. Dhoble, H. C. Swart, K. Park, Basic mechanisms of photoluminescence, phosphate phosphors for solid–state lighting, Springer Berlin Heidelberg 174, DOI:10.1007/978-3-642-34312-4-2 (2013).
70. M. Adachi, Y. Nagao, Design of near Infrared dyes based on π–conjugation system extension Theoretical elucidation of framework extended derivatives of perylene chromophore, Chem. Mater. 13 (2001) 662-669.
71. D. F. Swinehart, The Beer Lambert Law, J. Chem. Educ. 39 (1962) 333-335.
72. B. Wardle, Principle and applications of photochemistry, John Wiley & Sons, Chichester (2009).
73. M. Dierksen, S. Grimme, An efficient approach for the calculation of Franck–Condon integrals of large molecules, J. Chem. Phys. 122 (2005) 244101-1-244101-9.
74. F. Santoro, R. Improta, A. Lami, J. Bloino, V. Barone, Effective method to compute Franck-Condon integrals for optical spectra of large molecules in solution, J. Chem. Phys. 126 (2007) 84509.
75. M. Kasha, Characterisation of electronic transitions in complex molecules, Discuss. Faraday Soc. 9 (1950) 14-19.
76. Berlman, Handbook of florescence spectra of aromatic molecules, Elsevier (2012).

77. C. Bhaumik, S. Das, D. Saha, S. Dutta, S. Baitalik, Synthesis, characterization, photophysical, and anion-binding studies of luminescent heteroleptic bis-tridentate Ruthenium(II) complexes based on 2,6-bis(benzimidazole-2-yl)pyridine and 4'-substituted 2,2':6',2'' terpyridine derivatives, Inorg. Chem. 49 (2010) 5049-5062.
78. D. Saha, S. Das, D. Maity, S. Dutta, S. Baitalik, Synthesis, structural characterization, and photophysical, electrochemical, intercomponent energy-transfer, and anion-sensing studies of imidazole 4,5-bis(benzimidazole)-bridged $Os^{II}Os^{II}$ and $Ru^{II}Os^{II}$ bipyridine complexes, Inorg. Chem. 50 (2011) 46-61.
79. R. S. Vadavi, H. Kim, K. M. Lee, T. Kim, J. Lee, Y. S. Lee, M. H. Lee, Turning on MLCT phosphorescence of Iridium(III)-Borane conjugates upon fluoride binding, Organometallics 31 (2012) 31-34.
80. S. K. Kim, J. Yoon, A new fluorescent PET chemosensor for fluoride ions, Chem. Commun. (2002) 770-771.
81. T. Hirano, K. Kikuchi, Y. Urano, T. Higuchi, T. Nagano, Highly Zinc-selective fluorescent sensor molecules suitable for biological applications, J. Am. Chem. Soc. 122 (2000) 12399-12400.
82. K. Kiyose, H. Kojima, Y. Urano, T. Nagano, Development of a ratiometric fluorescent zinc ion probe in near-infrared region, based on tricarbocyanine chromophore, J. Am. Chem. Soc. 128 (2006) 6548-6549.
83. A. P. de Silva, H. Q. N. Gunaratne, T. Gunnlaugsson, A. J. M. Huxley, C. P. McCoy, J. T. Rademacher, T.E. Rice, Signalling recognition events with fluorescent sensors and switches, Chem. Rev. 97 (1997) 1515-1566.
84. K. Rurack, Flipping the light switch "ON" the design of sensor molecules that show cation-induced fluorescence enhancement with heavy and transition metal ions, Spectrochim. Acta Mol. Biomol. Spectrosc. 57 (2001) 2161-2195.
85. Z. Xu, Y. Xiao, X. Qian, J. Cui, D. Cui, Ratiometric and selective fluorescent sensor for Cu(II) based on internal charge transfer (ICT), Org. Lett. 7 (2005) 889-892.
86. M. J. Peng, Y. Guo, X. F. Yang, F. Suzenet, J. Li, C. W Li, Y. W. Duan, Coumarin-hemicyanine conjugates as novel reaction-based sensors for cyanide detection: convenient synthesis and ICT mechanism, RSC Adv. 4 (2014) 19077-19085.
87. Z. Liu, X. Wang, Z. Yang, W. He, Rational design of a dual chemosensor for cyanide anion sensing based on dicyanovinyl-substituted benzofurazan, J. Org. Chem. 76 (2011) 10286-10290.

88. J. H. Chang, Y. M. Choi, Y. K. Shin, A significant fluorescence quenching of anthrylaminobenzocrown ethers by paramagnetic metal cations, Bull. Korean Chem. Soc. 22 (2001) 527-530.
89. S. Das, S. Goswami, K. Aich, K. Ghoshal, C. K. Quah, M. Bhattacharyya, H. K. Fun, ESIPT and CHEF based highly sensitive and selective ratiometric sensor for Al^{3+} with imaging in human blood cells, New J. Chem. 39 (2015) 8582-8587.
90. S. S. Razi, R. Ali, R. C. Gupta, S. K. Dwivedi, G. Sharma, B. Koch, A. Misraa, Phenyl-end-capped-thiophene (P-T type) based ICT fluorescent probe (D-p-A) for detection of Hg^{2+} and Cu^{2+} ions: Live cell imaging and logic operation at molecular level, J. Photochem. Photobiol. A 324 (2016) 106-116.
91. N. J. Turro, Modern molecular photochemistry, University Science Books, Sausalito CA (1991).
92. A. Sharma, S. G. Schulman, Introduction to fluorescence spectroscopy, John Wiley & Sons, Chichester (1999).
93. T. Förster, 10^{th} spiers memorial lecture. Transfer mechanism of electronic excitation, Discuss. Faraday Soc. 27 (1959) 7-17.
94. K. E. Sapsford, L. Berti, I. L. Medintz, Materials for fluorescence resonance energy transfer analysis: beyond traditional donor-acceptor combinations, Angew. Chem. Int. Ed. 45 (2006) 4562-4589.
95. J. F. Zhu, H. Yuan, W. H. Chan, A. W. M. Lee, A FRET fluorescent chemosensor SPAQ for Zn^{2+} based on a dyad bearing spiropyran and 8-aminoquinoline unit, Tetrahedron Lett. 51 (2010) 3550-3554.
96. C. Kaewtong, J. Noiseephum, Y. Uppa, N. Morakot, B. Wanno, T. Tuntulanic, B. Pulpokac, A reversible E_m-FRET rhodamine-based chemosensor for carboxylate anions using a ditopic receptor strategy, New J. Chem. 34 (2010) 1104-1108.
97. D. L. Dexter, A theory of sensitized luminescence in solids, J. Chem. Phys. 21 (1953) 836-850.
98. X. Zhang, Y. Xiao, L. He, Y. Zhang, Through-bond energy transfer cassettes for multicolor encoding, J. Org. Chem. 79 (2014) 6315-6320.
99. N. Kumar, V. Bhalla, M. Kumar, Resonance energy transfer-based fluorescent probes for Hg^{2+},Cu^{2+} and Fe^{2+}/Fe^{3+} ions, Analyst 139 (2014) 543-558.

100. C. Thivierge, J. Han, R. M. Jenkins, K. Burgess, Fluorescent proton sensors based on energy transfer, J. Org. Chem. 76 (2011) 5219-5228.
101. J. S. Wu, J. H. Zhou, P. F. Wang, X. H. Zhang, S. K. Wu, New fluorescent chemosensor based on exciplex signaling mechanism, Org. Lett. 7 (2005) 2133-2136.
102. A. Banerjee, A. Sahana, S. Guha, S. Lohar, I. Hauli, S. K. Mukhopadhyay, J. S. Matalobos, D. Das, Nickel(II)-induced excimer formation of a naphthalene–based fluorescent probe for living cell imaging, Inorg. Chem. 51 (2012) 5699-5704.
103. Y. Wu, J. Wang, F. Zeng, S. Huang, J. Huang, H. Xie, C. Yu, S. Wu, Pyrene derivative emitting red or near-infrared light with monomer/excimer conversion and its application to ratiometric detection of hypochlorite, ACS Appl. Mater. Interfaces 8 (2016) 1511-1519.
104. S. Nishizawa, Y. Kato, N. Teramae, Fluorescence sensing of anions *via* intramolecular excimer formation in a pyrophosphate-induced self-assembly of a pyrene-functionalized guanidinium receptor, J. Am. Chem. Soc. 121 (1999) 9463-9464.
105. A. Manna, D. Sarkar, S. Goswami, C. K. Quah, H. K. Fun, Single excited state intramolecular proton transfer (ESIPT) chemodosimeter based on rhodol for both Hg^{2+} and OCl^- : ratiometric detection with live-cell imaging, RSC Adv. 6 (2016) 57417-57423.
106. Y. Wu, X. Peng, J. Fan, S. Gao, M. Tian, J. Zhao, S. Sun, Fluorescence sensing of anions based on inhibition of excited-state intramolecular proton transfer, J. Org. Chem. 72 (2007) 62-70.
107. J. Mei, N. L. C. Leung, R. T. K. Kwok, J. W. Y. Lam, B. Z. Tang, Aggregation-induced emission: together We Shine, United We Soar, Chem. Rev. 115 (2015) 11718-11940.
108. C. W. Liao, M. R. Rao, S. S. Sun, Structural diversity of new solid-state luminophores based on quinoxaline-b-ketoiminate boron difluoride complexes with remarkable fluorescence switching properties, Chem. Commun. 51 (2015) 2656-2659.
109. J. Mei, Y. Hong, J. W. Lam, A. Qin, Y. Tang, B. Z. Tang, Aggregation-induced emission: The whole is more brilliant than the Parts, Adv. Mater. 26 (2014) 5429-5479.
110. X. Ma, R. Sun, J. Cheng, J. Liu, F. Gou, H. Xiang, X. Zhou, Fluorescence aggregation-caused quenching versus aggregation induced emission: A visual teaching technology for undergraduate chemistry students, J. Chem. Educ. 93 (2016) 345-350.

111. Y. T. Wu, M. Y. Kuo, Y. T. Chang, C. C. Shin, T. C. Wu, C. C. Tai, T. H. Cheng, W. S. Liu, Synthesis, structure and photophysical properties of highly substituted 8,8a-dihydrocyclopenta[a]indenes, Angew. Chem. Int. Ed. 47 (2008) 9891-9894.
112. T. Anand, G. Sivaraman, P. Anandh, D. Chellappa, S. Govindarajan, Colorimetric and turn-on fluorescence detection of Ag(I) ion, Tetrahedron Lett. 55 (2014) 671-675.
113. J. S. Wu, W. M. Liu, X. Q. Zhuang, F. Wang, P. F. Wang, S. L. Tao, X. H. Zhang, S. K. Wu, S. T. Lee, Fluorescence turn on of coumarin derivatives by metal cations: A new signaling mechanism based on C=N isomerization, Org. Lett. 9 (2007) 33-36.
114. S. Saha, A. Ghosh, P. Mahato, S. Mishra, S. K. Mishra, E. Suresh, S. Das, A. Das, Specific recognition and sensing of CN^- in sodium cyanide solution, Org. Lett. 12 (2010) 3406-3409.
115. B. B. Shi, P. Zhang, T. B. Yao, Q. Lin, Y. M. Zhang, Highly selective fluorescent sensing for CN^- in water: utilization of the supramolecular self-assembly, Chem. Commun. 49 (2013) 7812-7814.
116. P. B. Pati, Organic chemodosimeter for cyanide: A nucleophilic approach, Sens. Actuators, B 222 (2016) 374-390.
117. S. Goswami, A. Manna, S. Paul, A. K. Das, K. Aich, P. K. Nandi, Resonance-assisted hydrogen bonding induced nucleophilic addition to hamper ESIPT: ratiometric detection of cyanide in aqueous media, Chem. Commun. 49 (2013) 2912-2914.
118. X. Lv, J. Liu, Y. L. Liu, Y. Zhao, M. L. Chen, P. Wang, W. Guo, Rhodafluor-based chromo- and fluorogenic probe for cyanide anion, Sens. Actuators, B 158 (2011) 405-410.
119. C. H. Lee, H. J. Yoon, J. S. Shim, W. D. Jang, A boradiazaindacene-based turn-on fluorescent probe for cyanide detection in aqueous media, Chem. Eur. J. 18 (2012) 4513-4516.
120. W. Chen, Z. Zhang, X. Li, H. Agren, J. Su, Highly sensitive detection of low-level water content in organic solvents and cyanide in aqueous media using novel solvatochromic AIEE fluorophores, RSC Adv. 5 (2015) 12191-12201.
121. S. Park, H. J. Kim, Highly activated Michael acceptor by an intramolecular hydrogen bond as a fluorescence turn-on probe for cyanide, Chem. Commun. 46 (2010) 9197-9199.

122. J. L. Liu, Y. Liu, Q. Liu, C. Y. Li, L. N. Sun, F. Y. Li, Iridium(III) complex-coated Nanosystem for ratiometric upconversion luminescence bioimaging of cyanide anions, J. Am. Chem. Soc. 133 (2011) 15276-15279.
123. Q. J. Zhang, Y. Cai, W. J. Qu, G. Y. Gao, Q. Lin, H. Yao, Y. M. Zhang, T. B. Wei, A facile colorimetric and fluorescent cyanide chemosensor: utilization of the nucleophilic addition induced by resonance-assisted hydrogen bond, Tetrahedron 71 (2015) 857-862.
124. R. Ali, S. S. Razi, P. Srivastava, A. Misra, Tetrasubstituted imidazole core containing ESIPT fluorescent chemodosimeter for selective detection of cyanide in different medium, Sens. Actuators, B 221 (2015) 1236-1247.
125. H. J. Kim, K. C. Ko, J. H. Lee, J. Y. Lee, J. S. Kim, KCN sensor: unique chromogenic and 'turn-on' fluorescent chemodosimeter: rapid response and high selectivity, Chem. Commun. 47 (2011) 2886-2888.
126. X. H. Huang, X. G. Gu, G. X. Zhang, D. Q. Zhang, A highly selective fluorescence turn-on detection of cyanide based on the aggregation of tetraphenylethylene molecules induced by chemical reaction, Chem. Commun. 48 (2012) 12195-12197.
127. Y. K. Yang, J. Tae, Acridinium salt based fluorescent and colorimetric chemosensor for the detection of cyanide in water, Org. Lett. 8 (2006) 5721-5724.
128. J. Ren, W. Zhu, H. Tian, A highly sensitive and selective chemosensor for cyanide, Talanta 75 (2008) 760-764.
129. H. Y. Xia, J. G. Li, G. Zou, Q. J. Zhang, C. Jia, A highly sensitive and reusable cyanide anion sensor based on spiropyran functionalized polydiacetylene vesicular receptors, J. Mater. Chem. A 1 (2013) 10713-10719.
130. R. Guliyev, S. Ozturk, E. Sahin, E. U. Akkaya, Expanded bodipy dyes: anion sensing using a bodipy analog with an additional difluoroboron bridge, Org. Lett. 14 (2012) 1528-1531.
131. T. Matsumoto, C. R. Wade, F. P. Gabbaı, Synthesis and lewis acidic behavior of a cationic 9-thia-10-boraanthracene, Organometallics 29 (2010) 5490-5495.
132. G. Qian, X. Li, Z. Y. Wang, Visible and near-infrared chemosensor for colorimetric and ratiometric detection of cyanide, J. Mater. Chem. 19 (2009) 522-530.
133. J. H. Lee, A. R. Jeong, I. S. Shin, H. J. Kim, J. I. Hong, Fluorescence turn-on sensor for cyanide based on a cobalt(II)-coumarinylsalen complex, Org. Lett. 12 (2010) 764-767

134. Q. Zou, X. Li, J. Zhang, J. Zhou, B. Sun, H. Tian, Unsymmetrical diarylethenes as molecular keypad locks with tunable photochromism and fluorescence *via* Cu^{2+} and CN^{-} coordinations, Chem. Commun. 48 (2012) 2095-2097.
135. M. R. Ajayakumar, P. Mukhopadhyay, Single-electron transfer driven cyanide sensing: A new multimodal approach, Org. Lett. 12 (2010) 2646-2649.
136. M. R. Ajayakumar, K. Mandal, K. Rawat, D. Asthana, R. Pandey, A. Sharma, S. Yadav, S. Ghosh, P. Mukhopadhyay, Single electron transfer-driven multi-dimensional signal read-out function of TCNQ as an "Off-the-Shelf" detector for cyanide, ACS Appl. Mater. Interfaces 5 (2013) 6996-7000.
137. X. Lou, D. Ou, Q. Li, Z. Li, An indirect approach for anion detection: the displacement strategy and its application, Chem. Commun. 48 (2012) 8462-8477.
138. A. Bencini1, V. Lippolis, Metal-based optical chemosensors for CN^{-} detection Environ. Sci. Pollut. Res. DOI 10.1007/s11356-016-7419-1.
139. M. Shahid, S. S. Razi, P. Srivastava, R. Ali, B. Maiti, A. Misra A useful scaffold based on acenaphthene exhibiting Cu^{2+} induced excimer fluorescence and sensing cyanide *via* Cu^{2+} displacement approach, Tetrahedron 68 (2012) 9076-9084.
140. H. S. Jung, J. H. Han, Z. H. Hwan, C. Kang, J. S. Kim, K. H. Jung, K. H. Lee Efficient Coumarin-Cu(II) ensamble-based cyanide sensing chemodosimeter. Org. Lett. 13:5056-5059. DOI:10.1021/ol2018856.
141. K. P. Divya, S. Sreejith, B. Balakrishna, P. Jayamurthy, P. Anees, A. Ghosh, Zn^{2+}-specific fluorescent molecular probe for the selective detection of endogenous cyanide in biorelevant samples, Chem. Commun. 46 (2010) 6069-6071.
142. A. Aviram, Molecules for memory, logic, and amplification J. Am. Chem. Soc. 110 (1988) 5687-5692.
143. A. P. de Silva, H. Q. N. Gunaratne, C. P. McCoy, A molecular photoionic AND gate based on fluorescent signalling. Nature 364 (1993) 42-44.
144. A. P. de Silva, H. Q. N. Gunaratne, C. P. McCoy, Molecular photoionic AND logic gates with bright fluorescence and "off-on" digital action, J. Am. Chem. Soc. 119 (1997) 7891-7892.
145. A. Credi, V. Balzani, S. J. Langford, J. F. Stoddart, A. Credi, V. Balzani, S. J. Langford, J. Stoddart, Logic operations at the molecular level: An XOR gate based on a molecular machine, J. Am. Chem. Soc. 119 (1997) 2679-2681.

146. A. P. de Silva, N. D. McClenaghan, Proof-of-principle of molecular-scale arithmetic, J. Am. Chem. Soc. 122 (2000) 3965-3966.

147. A. Kumar, P. S. Pandey, Steroidal 1,2,3-triazole-based sensors for Hg^{2+} ion and their logic gate behavior, Tetrahedron Lett. 50 (2009) 5842-5845.

148. S. H. Lee, J. Y. Kim, S. K. Kim, J. H. Lee, J. S. Kim, Pyrene-appended calix[4]crowned logic gates involving normal and reverse PET: NOR, XNOR and INHIBIT, Tetrahedron 60 (2004) 5171-5176.

149. H. J. Jung, N. Singh, D. Y. Lee, D. O. Jang, Single sensor for multiple analytes: chromogenic detection of I^- and fluorescent detection of Fe^{3+}, Tetrahedron Lett. 50 (2009) 5555-5558.

150. Y. Liu, M. Li, Q. Zhao, H. Wu, K. Huang, F. Li, Phosphorescent iridium(III) complex with an N-O ligand as a Hg^{2+} selective chemodosimeter and logic gate, Inorg. Chem. 50 (2011) 5969-5977.

CHAPTER 2

Hydrogen Bonding Based Cyanide Sensor

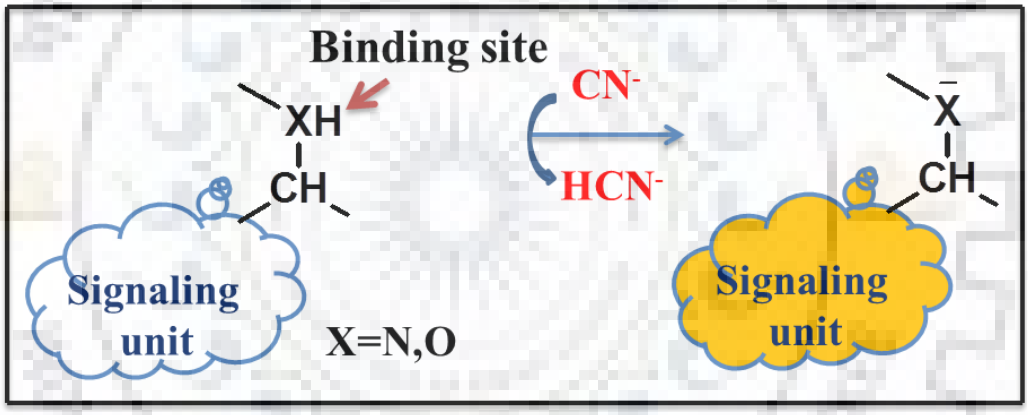

2.1 INTRODUCTION

In analogy to metal ions, anions play a leading role in chemical, biological and environmental processes due to its structural features and reactivity [1-6]. Anions can easily interact with receptor molecules and form a stable complex, so the sensing and recognition properties of anions have great attention to the micro environment [7-8]. Among contrasting anions CN^- is extremely toxic and it has strong binding affinity with the active site of cytochrome a3, this process disrupting the electron-transport chain in mitochondria, thus decreased oxidative metabolism [9-10] and leads to cell death. It increases the Ca^{2+} concentration within the cell by which the level of reactive oxygen species (ROS) increases, thus inhibit antioxidant defense systems [11-12]. CN^- could be easily absorbed *via* the gastrointestinal tract, lungs and skin and causing convulsion, vomiting and loss of consciousness [13-15]. CN^- is enormously toxic for mammals; even moderately lesser amounts (0.5-3.5 mg/kg of body weight) are disastrous to human beings [16]. It has widespread industrial applications including electroplating, gold mining, textile, and metallurgy, plastic and paper industries [17]. The WHO has set a determined tolerant level of CN^- limit (1.9 μM) in drinking water [18]. Therefore, the development of selective and effective CN^- sensors is essential.

There are several experimental techniques, such as electrochemical methods [19], chromatography [20] flow injection analysis [21] and atomic absorption spectrometry [22] for CN^- sensing. However, most of these methods are costly, time consuming, require sophisticated equipment and trained operators. In contrast, colorimetric methods have many advantages like low cost, high selectivity and easily detect target ions with the naked eye [23-28]. Among the various intelligent a strategy in designing cyanide sensors, the deprotonation approach is used which causes changes in their absorption properties. Anion sensors such as amides [29], thiourea [30-31], pyrrole [32] and hydroxyl [23] containing subunits having acidic proton recognize CN^- *via* hydrogen-bonding interactions or deprotonation.

Generally proton based receptor have two functional units: the reaction site (responsible for interaction with the analyte) and a signalizing unit (provide an optical signal indicating the presence of analyte). On the basis of this idea firstly we synthesized four Nobel salicyladehyde (containing p-nitro azo moieties) and chromone based receptors due to its biological importance and also its ability to form

charge transfer complexes. Heteroatom form a strong intramolecular hydrogen bond with hydroxyl and an immine group in nonpolar solvents, resultant H-bonded proton shows the large low-field in ^{1}H NMR (> 13 ppm) and induce charge transfer upon deprotonation with CN^{-}, thus it induce colorimetric sensing properties of the receptor site. The choice of the objects of research was based on the fact that, in comparison with the parent compounds have an extended conjugation system and contains substituent with stronger electron withdrawing $-NO_2$ (B1/B2) and -C=O group (B3/B4) which provide the ability to charge delocalization. The ionic interaction of CN^{-} with hydroxyl -OH group (B1/B2) and amidic -NH group (B3/B4) affects the ICT efficiency of receptor and induces naked-eye color detection. The -C=N and -C=O chelating groups have high binding affinity towards transition metal ions, therefore receptor B3/B4 shows selectivity towards Cu^{2+} and Ni^{2+} metal ions. Generally CN^{-} has a strong affinity towards Cu^{2+}/Ni^{2+} and the photophysical properties of receptors are change *via* displacement approach. In this case, the presence of metal ions (Cu^{2+}/Ni^{2+}) doesn't effect on sensing mechanism (deprotonation phenomenon), it enhance the sensitivity of receptors towards CN^{-}.

2.2 EXPERIMENTAL SECTION

2.2.1 Materials and Instrumentation

All reagents for the synthesis work were brought from Sigma-Aldrich. Anions that are used for experiments were taken in the form of their tetrabutylammonium salts. A solvent used for the preparation of solutions dried with the help of drying agent $CaCl_2$ and distilled under reduced pressure then stored on Molecular sieve. PerkinElmer FT-IR 1000 spectrophotometer were used for IR spectra with the help of KBr solid film. Elemental analysis for carbon, hydrogen, nitrogen and sulfur was carried out using a vireo MICRO V3.1.1 CHNS (analytical functional testing). Absorption spectra were recorded on Specord S600 PC double beam spectrophotometer with quartz cuvette of path length 1 cm. JEOL 400 MHz spectrophotometer was used for ^{1}H, ^{13}C NMR and for titration by applying tetramethylsilane (TMS) as an internal standard. Density Functional Theory (DFT) method was implemented in the gas phase by Gaussian 09 W program, using a B3LYP/6-31G basis set.

2.2.2 General Procedure for UV-vis Spectrophotometer Experiments

The stock solution (1 mM) of receptor B1/B2 in ACN and B3/B4 in DMSO was prepared and used for all spectroscopic studies after appropriate dilution. The salts of each anions F^-, Cl^-, Br^-, I^-, CN^-, SCN^-, AcO^-, N_3^-, CO_3^-, AsO_2^-, PO_4^-, SO_4^-, $H_2PO_4^-$, HPO_4^{2-} (10 mM), were prepared in water solutions. The absorption spectra were recorded upon the addition of salts (10 eq.) keeping with the concentration of receptor 25 μM and 20 μM for B3/B4 in all experiments. The antagonism experiment was carried out with various anions with CN^- in the ratio of 1:2. Benesi-Hilderbrand Plot [33] was used for calculation of the binding constant, involving plotting the inverse of the changes in its absorbance against the inverse of the CN^- concentration means $1/(A-A_0)$ versus $1/[CN^-]^n$, where n is the stoichiometry. For ^{1}H NMR titrations, receptor and CN^- were prepared in DMSO d_6 and $CDCl_3$.

2.2.3 Synthesis and Characterization of Receptors B1 and B2

Compound B1 and B2 were synthesized by condensation between reported dye A [34] (1 mmol) with respected amine (2-amino-Picoline & furfurylamine) (1 mmol) by using DCM as solvent (Scheme 2.1), stirred 1 h. After completing the reaction mixture (thin layer chromatography monitored) ppt was filtered and washed with methanol. The dark red colored compound was obtained with 70% yield.

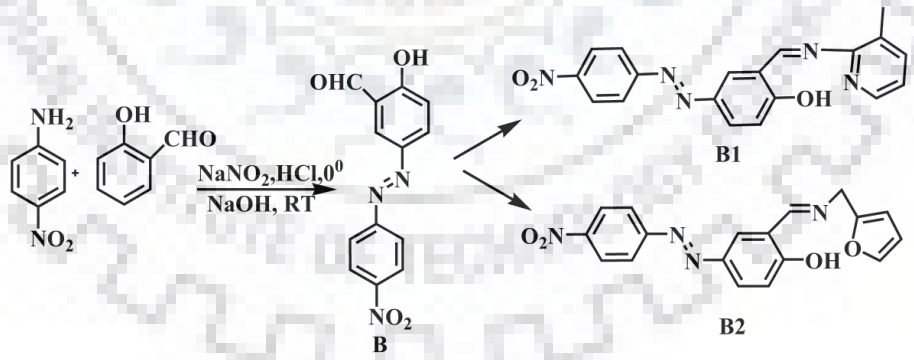

Scheme: 2.1 Synthesis of receptors B1 and B2.

B1: (3-methylpyridin-2-yl) iminomethyl-((4nitrophenyl) diazenyl) phenol

Anal. Calc. ($C_{19}H_{15}N_5O_3$) : C-63.15, H-4.18, N-19.38, O-13.29; Found : C-63.48, H-4.20, N-19.53; IR (KBr, υ/cm^{-1}) : 3438 (-OH), 1570 (-C=N); ^{1}H NMR ($CDCl_3$, 400 MHz, δ/ppm) : 14.79 (s, 1H), 9.59 (s, 1H), 8.38 (d, 2H), 8.23 (s, 1H), 8.11 (d, 1H), 8.01 (d, 2H), 7.65 (d,

1H), 7.20 (t, 1H), 7.16 (d, H), 2.51 (s, 3H); ^{13}C NMR ($CDCl_3$, 100 MHz, δ/ppm) : 167.5, 162.7, 155.9, 154.4, 148.3, 146.6, 145.3, 139.8, 131.5, 128.3, 127.7, 124.8 (2C), 123.2 (2C), 119.1, 118.6, 100.0, 31.0

B2: (furan-2-yl methyl) iminomethyl-4-((4nitrophenyl) diazenyl) phenol

Anal. Calc. ($C_{18}H_{14}N_4O_4$) : C-61.71, H-4.03, N-15.99, O-18.27; Found : C-59.73, H-3.96, N-15.54; IR (KBr, υ/cm-^{1}) : 3461 (-OH), 1576 (-C=N); ^{1}H NMR ($CDCl_3$, 400 MHz, δ/ppm) : 14.20 (s, 1H), 8.86 (s, 1H), 8.41 (d, 2H), 8.22 (s, 1H), 8.01 (d, 3H), 7.69 (s, 1H), 6.95 (d, 1H), 6.49 (t, 2H), 4.91 (s, 2H); ^{13}C NMR ($CDCl_3$, 100 MHz, δ/ppm) : 171.1, 167.3, 156.1, 150.7, 148.2, 143.8, 143.7, 133.1, 127.3, 125.7 (2C), 123.5 (2C), 121.3, 117.5, 111.1, 108.8, 51.9.

2.2.4 Synthesis and Characterization of Receptors B3 and B4

The synthetic method of B3/B4 is validated in Scheme 2.2. An ethanolic solution of 3-formyl chromone derivatives (1 mmol), (which was synthesised by previously reported literature [35-36]) and acylhydrazone (1 mmol) was mixed & refluxed. After completion of the reaction mixture (thin layer chromatography monitored), white colored ppt was obtained with 80% yield.

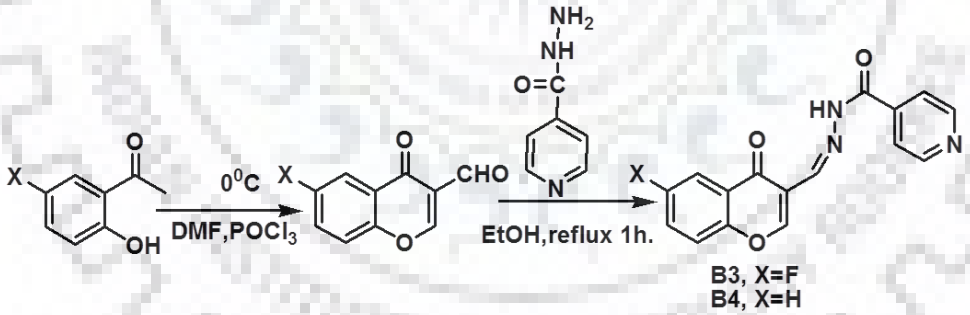

Scheme: 2.2 Synthesis of receptors B3 and B4.

B3: ((6-fluoro-4-oxo-4H-cromen-3-yl)methylene) isonicotinohydrazide

Anal. calc. ($C_{16}H_{10}FN_3O_3$) : C-61.74, H-3.24, N-13.5, O-15.42; Found : C- 61.95, H-3.12, N-13.63; IR (KBr, υ/cm^{-1}) : 3415 (-NH), 3018 (H-C=N), 1708 (N-C=O), 1647 (-C=O), 1611 (-C=N); ^{1}H NMR (DMSO d_6, 400 MHz, δ/ppm) : 12.19 (s, 1H), 8.91 (s, 1H), 8.80 (d, 2H) 8.64 (s, 1H), 7.92-7.77 (m, 5H); ^{13}C NMR (DMSO d_6, 100 MHz, δ/ppm) : 175.0, 162.0, 161.1, 158.6, 155.7, 152.9, 150.9 (2C), 147.6, 141.9, 140.8, 125.2, 122.2 (2C), 118.1, 110.5.

B4: N-((4-oxo-4H-cromen-3yl)methylene)isonicotinohydrazide

Anal. calc. ($C_{16}H_{11}N_3O_3$) : C-65.53, H-3.78, N-14.33, O-16.37; Found : C- 65.77, H-3.78, N-14.48; IR (KBr, υ/cm^{-1}) 3250 (-NH), 3040 (H-C=N), 1690 (-N-C=O), 1632 (-C=O), 1530 (-C=N); ^{1}H NMR (DMSO d_6, 400 MHz, δ/ppm) : 12.18 (s, 1H), 8.88 (s, 1H), 8.80 (d, 2H), 8.65 (s, 1H), 8.15 (d, 1H), 7.90-7.84 (m, 3H), 7.75 (d, 1H), 7.57 (t, H); ^{13}C NMR (DMSO d_6, 100 MHz, δ/ppm) : 175.6, 162.0, 156.3, 155.7, 151.4, 151.0 (2C), 142.2, 140.9, 135.2, 126.8, 125.8, 122.0 (2C), 119.4, 118.7.

2.3 RESULTS AND DISCUSSION

2.3.1 Sensing Studies of Receptors B1 and B2

2.3.1.1 UV-vis Spectral Response of B1 and B2

The naked-eye sensing behavior of B1/B2 with different anions was observed, which was further confirmed by absorption spectra in water-acetonitrile solution (1:9 v/v, pH-7.4 HEPES buffer). Receptor B1 shows high energy charge transfer band (due to π-π* transition) at 371 nm along with a broad shoulder band 473 nm (due to n- π*). Similarly B2 shows two high energy bands at 271 nm, 377 nm and a broad low energy band at 458 nm. Upon interaction with different anions, both B1/B2 shows relatively high affinity for CN^-, small extent of AcO^- and exhibit the immediate color response (red with CN^- and light pink with AcO^-). The electronic transition band centered at 371 nm decreased with a red shift of 170 nm to appear at 540 nm with CN^- and at 550 nm with AcO^-. Other tested anions failed to show any change in the optoelectronic behavior of B1/B2 (Fig. 2.1). This sensation, behavior could be explained on the basis of basicity and hydrogen bonding ability of the anions in aq. medium. The order of basicity of the anions is as follows- $CN^- > AcO^- > F^- > H_2PO_4^- > Cl^- > Br^-$ and the ability of hydrogen bonding (on the basis of electronegativity) is expected to be in the order of $F^- > AcO^- > CN^-$, so in water the hydration energy of F^- is higher and not able to deprotonate the phenolic proton of receptor, only CN^- and AcO^- easily deprotonate the phenolic proton than other anions in aq. medium.

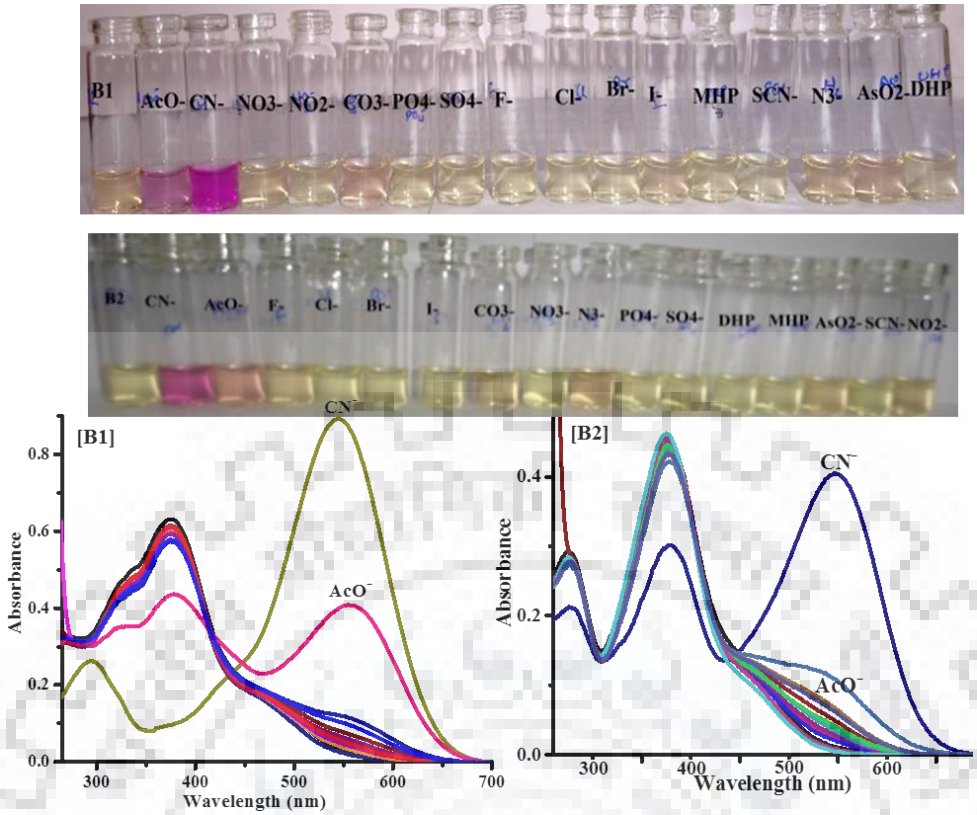

Fig. 2.1 Absorption spectra of B1/B2 with different anions and naked eye detection of CN^- in H_2O-ACN (1:9 v/v, pH-7.4 HEPES buffer).

An interference study was performed by UV-vis. absorption spectra. In case of CN^-, other tested anions (20 eq.) didn't interfere, but in case of AcO^- only CN^- interferes due to higher basic character (Fig. 2.2). This result suggests that both receptors could be a better sensor for CN^- than AcO^- in the presence of the other competing anions.

To further examine the absorption titration to understand the binding affinity of receptors with the CN^- and AcO^-. Upon gradual addition of CN^- (0-10 eq.), original absorption band decreases slowly and a band of 540 nm was increased to an isosbestic point at 434/428 nm with B1/B2 respectively, this shown that more than one intermediate was present in the reaction medium. The saturation limit was achieved with 15 eq. of CN^- with B1 and 40 eq. of CN^- with B2 (Fig. 2.3). Titration experiments were also carried out with AcO^-. This result shows that there is a small change occurring with B1 and almost no observable changes detected with B2 due to weaker basicity of acetate ion than cyanide ion and steric effects are the main cause of the selectivity of CN^- over AcO^-. Generally deprotonations/hydrogen bonds affects the electronic properties of the receptor, which results a new charge-transfer band between CN^- and basic -OH proton attached to the electron

deficient nitro group. The delocalization of π electrons is improved due to deprotonation process which reduce the energy of the p–p transition and a new absorption band at 540 nm was appeared that resultant the formation of the red color from light yellow color.

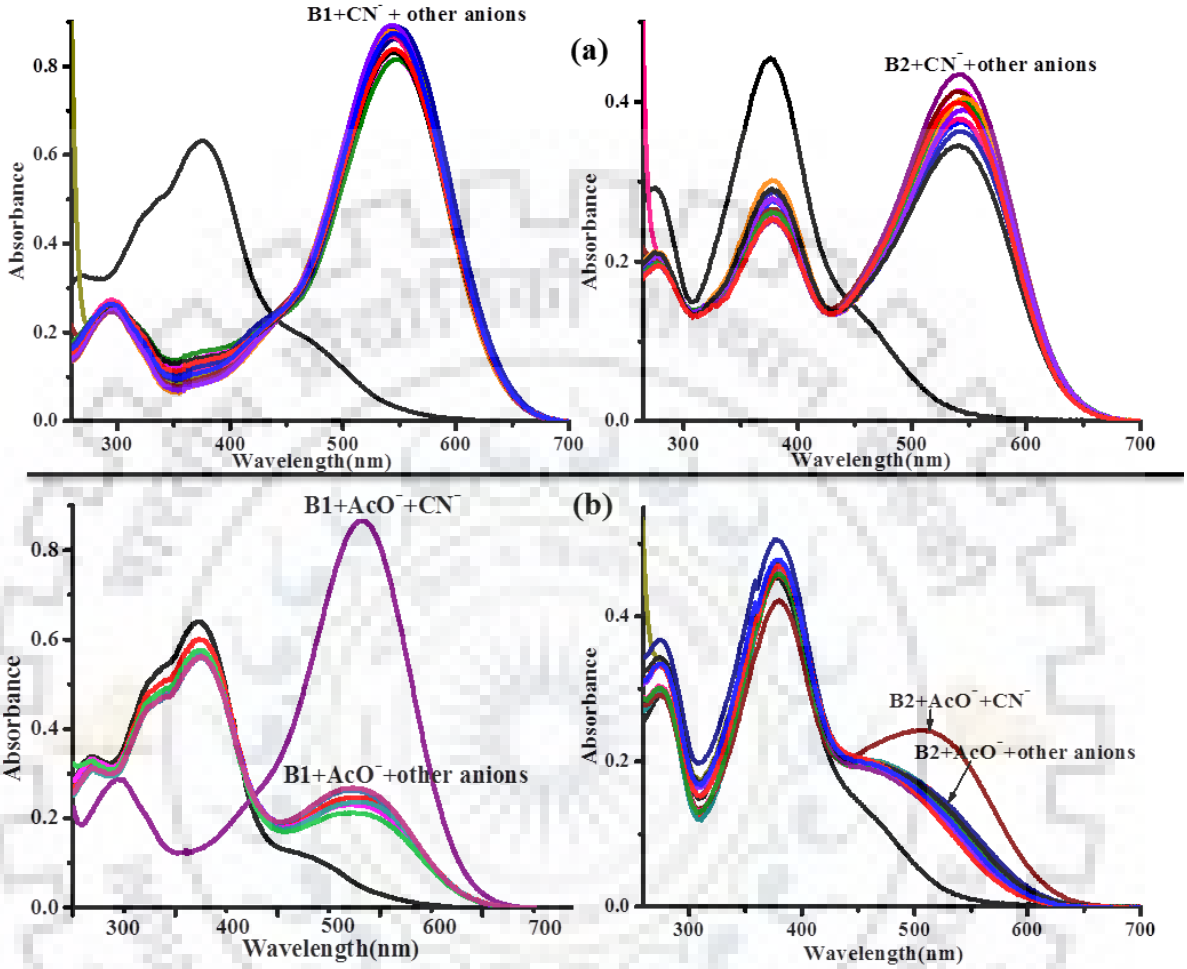

Fig. 2.2 Interference studies by absorption spectra of B1/B2; (a) CN^- (b) AcO^- with different anions (20 eq.) in H_2O-ACN (1:9 v/v, pH-7.4 HEPES buffer).

The Job plot (Inset of Fig. 2.3) shows a 1:1 binding interaction. The binding constant was calculated by Benesi-Hildebrand equation, which shows a good linear within the range of ($1.0\text{-}1.0 \times 10^5$), as explored by previously reported receptor for CN^-. The binding constant calculations were also performed with AcO^- (Fig. 2.4, Table: 2.1).

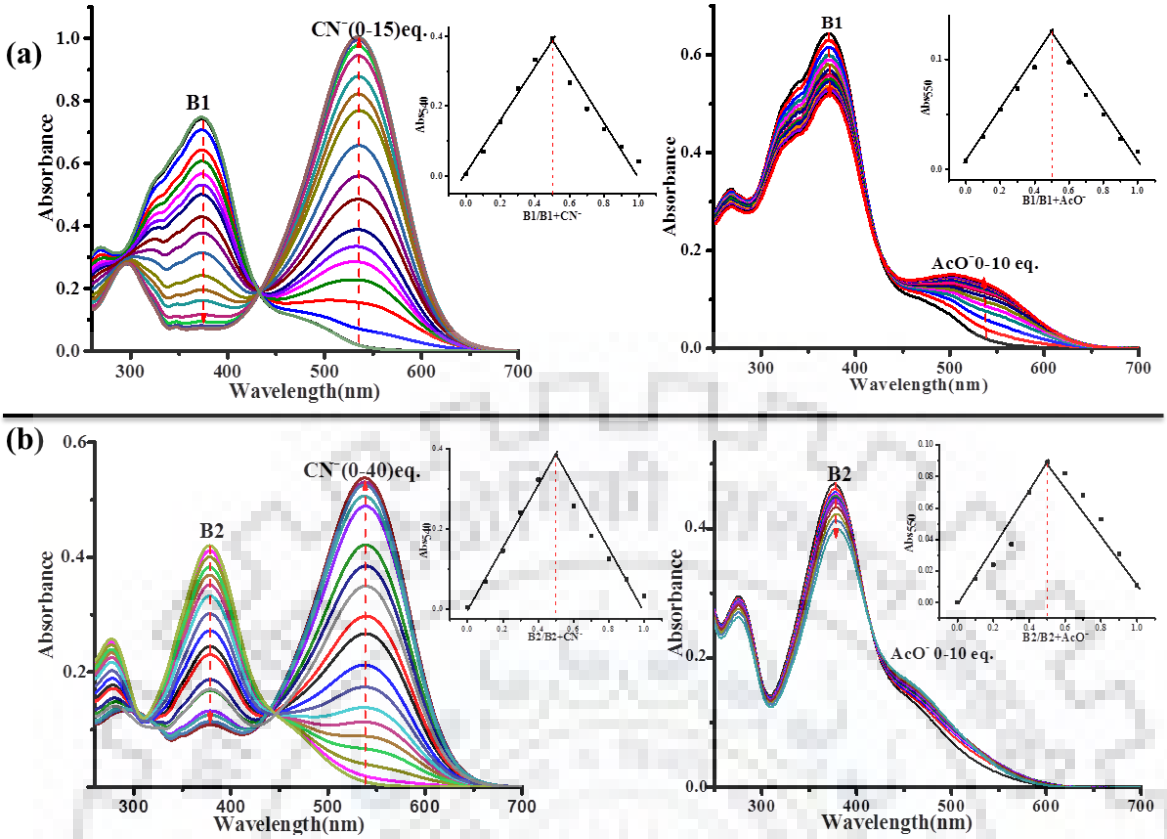

Fig. 2.3 Absorption titration spectra upon addition of CN^- & AcO^-; (a) B1 (b) B2; Inset: Jobs plot in H_2O-ACN (1:9 v/v, pH-7.4 HEPES buffer).

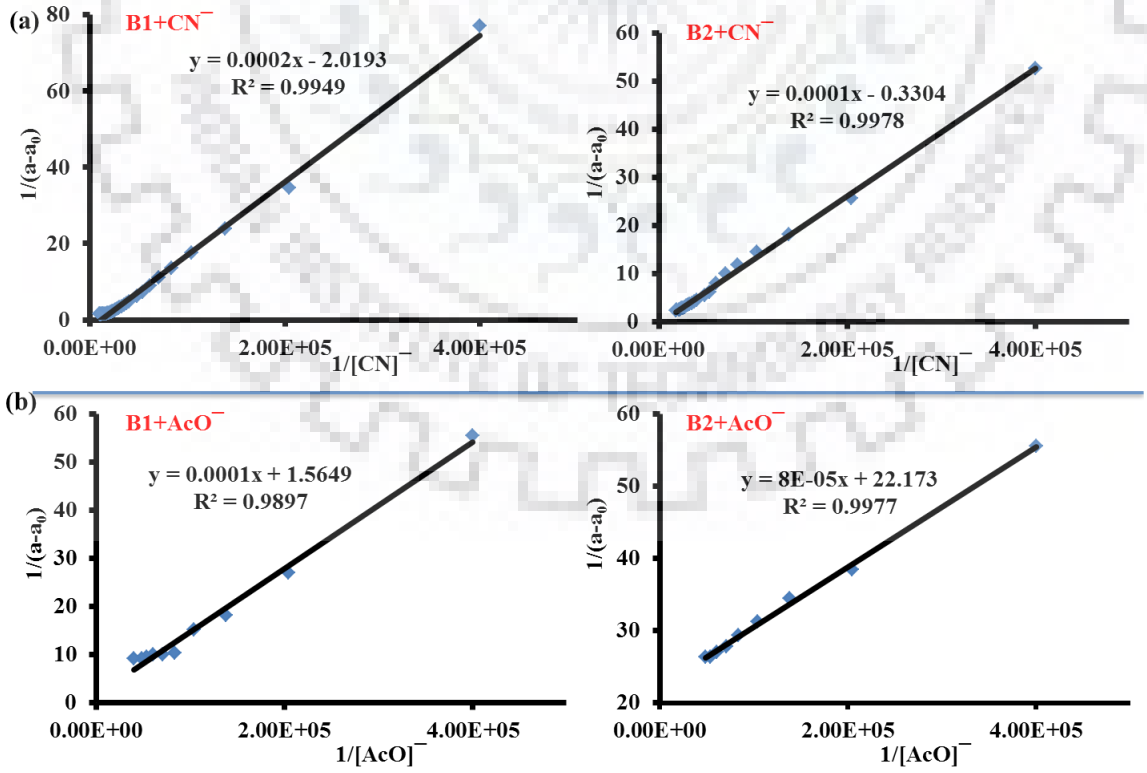

Fig. 2.4 Benesi-Hilderbrand plot for binding of CN^- & AcO^- with B1/B2.

The pH dependence of B1/B2 was monitored by absorption spectroscopy at different pH values from 3 to 10. This result indicated that between 6-7.5 pH range both receptors was stable (Fig. 2.5 a). The recognition of rapid response with CN^- is significant for the receptor in its practical application. To understand the chemical reaction between B1/B2 with CN^- has been performed to changes in the absorption signals at one minute interval time. We find out that the reaction was completed within 1-2 min (Fig. 2.5 b).

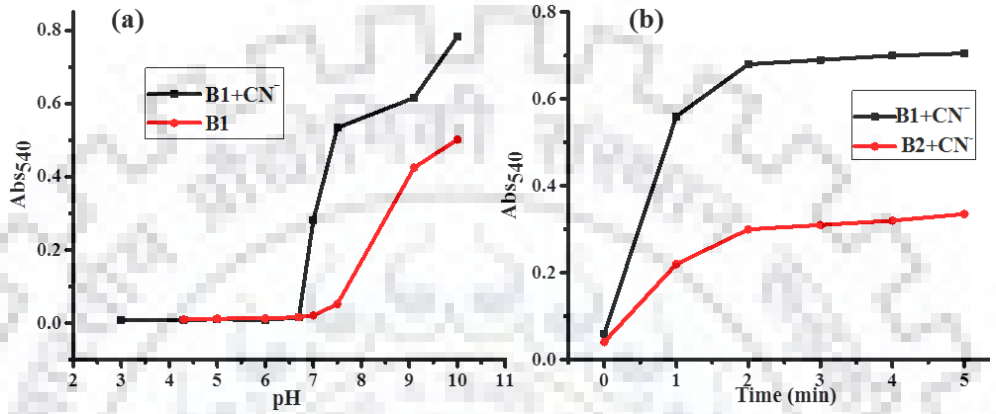

Fig. 2.5 (a) pH dependent (b) Time-dependent absorption intensity of B1/B2 with 5 eq. CN^- in H_2O-ACN (1:9 v/v, pH-7.4 HEPES buffer).

The minimum concentration of receptor B1/B2 for CN^- and AcO^- was calculated as perilously reported method (3σ/slope), where σ is the standard deviation of the blank solution; S is the slope of the calibration curve and it was found to below the standard level of WHO (1.9 μM) in drinking water as shown in Table 2.1 & Fig. 2.6.

Table: 2.1 Determination of binding constant and limit of detection.

Ligand	Binding constant	Slope	SD	LOD
$B1+CN^-$	1.054×10^4	8845.91	0.00141	0.478 μM
$B1+AcO^-$	1.181×10^3	504.74	0.00141	8.38 μM
$B2+CN^-$	2.5×10^3	8199.97	0.00455	1.66μM
$B2+AcO^-$	2.67×10^2	1007.72	0.00455	13.39 μM

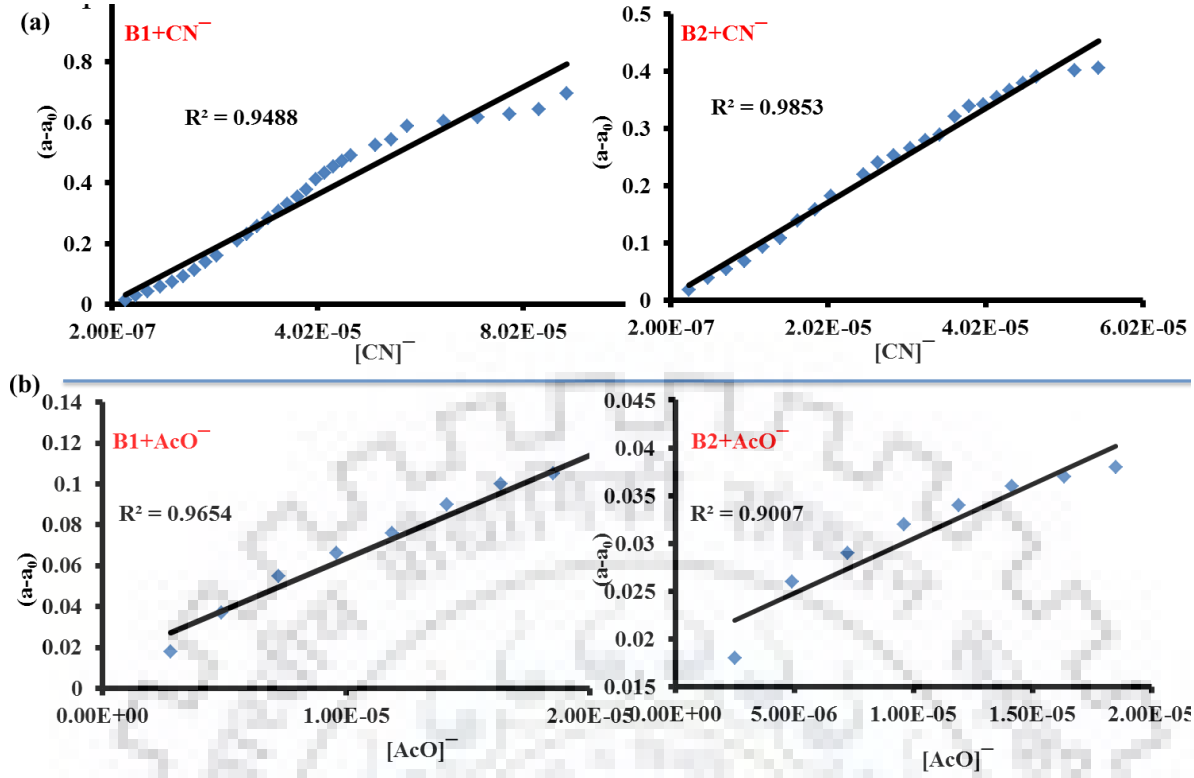

Fig. 2.6 Calibration Plot for the binding of CN^- (a) & AcO^- (b) with B1/B2.

To examine the reversibility of B1/B2 toward CN^- in a mixture of H_2O-ACN (1:9 v/v, pH-7.4 HEPES buffer) solution, 1 eq. hydrochloride acid (HCl) was added, color changes from red to yellow and a peak of 540 nm was completely disappeared and regenerate the free sensors. Repeat this experiment several times with the sequential alternative addition of CN^- and HCl (Fig. 2.7). These results indicate that B1/B2 could be easily recyclable with a proper reagent such as HCl.

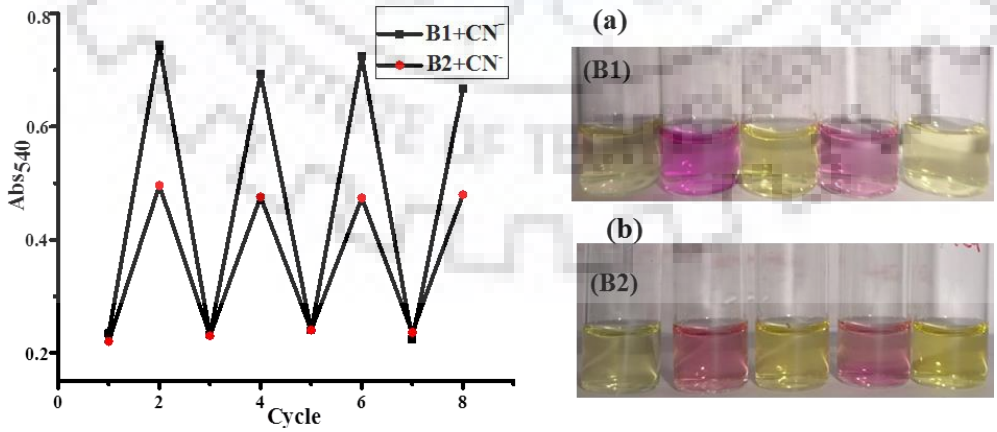

Fig. 2.7 Reversibility of B1/B2 color varies upon an alternate addition of CN^- and HCl.

2.3.1.2 To Proof the Probable Mechanism of B1/B2 with CN^-

The photochemical and photophysical incidence of B1/B2 with CN^- was assumed to undergo the deprotonation of the hydroxyl group. This assumption was supported by ^1H NMR titration spectra (Fig. 2.8). When 1 eq. of CN^- was added to B1/B2, the proton signal of -OH at 14.74/14.2 (s, 1H) ppm had completely disappeared and the other aromatic ring proton which involves in delocalization chemically small up-field shifts. This showed that the deprotonated negative charge of hydroxyl group was shielded to aromatic protons as shown in Scheme 2.3, which was further supported by basic titration of B1/B2 (Fig. 2.9).

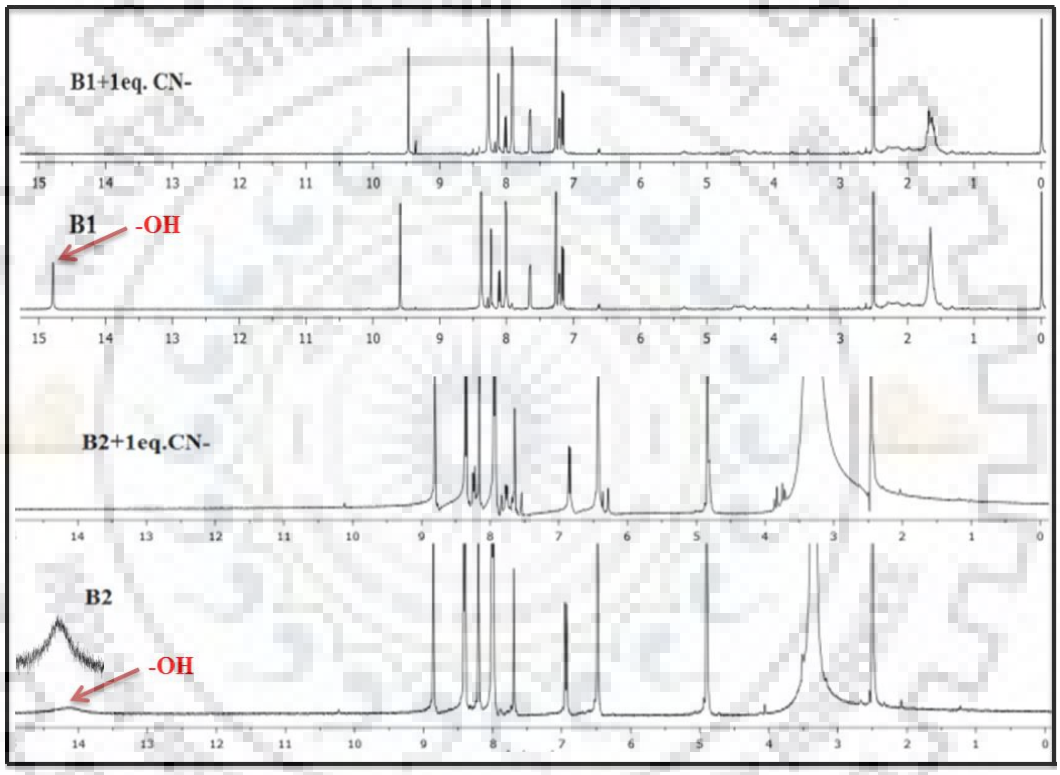

Fig: 2.8 Stacked ^1H NMR titration of B1 ($CDCl_3$) & B2 (DMSO d_6) with CN^-.

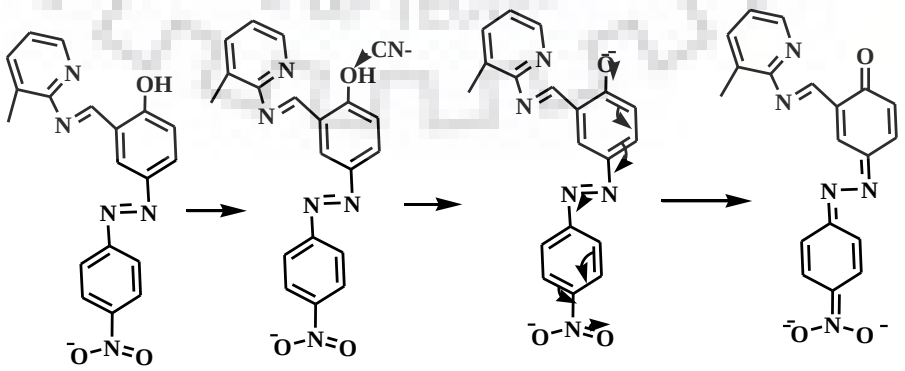

Scheme: 2.3 Proposed sensing mechanism of B1with CN^-.

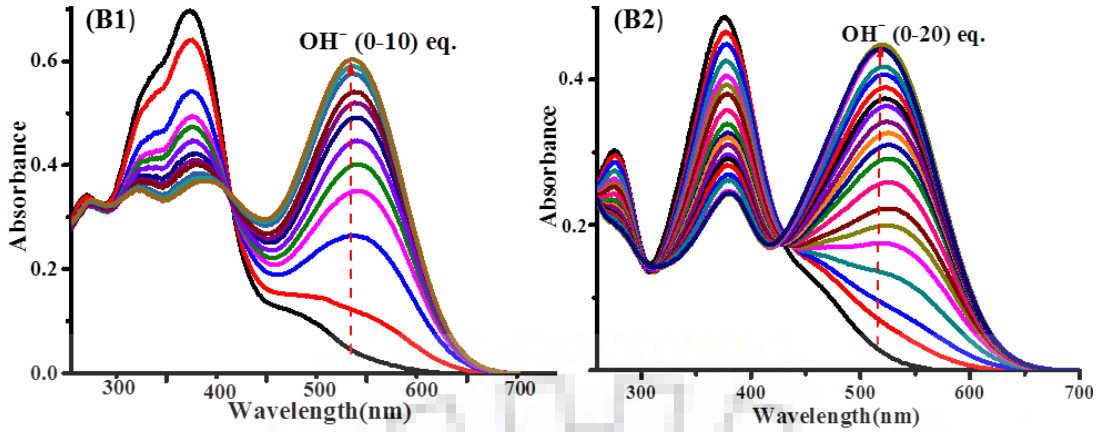

Fig. 2.9 Absorption titration spectra of B1/B2 with NaOH solution in H_2O-ACN (1:9 v/v, pH-7.4 HEPES buffer).

2.3.1.3 Dipstick Test of B1/B2

It is an easy-to-use paper strip method for detection of CN^-. Firstly, we have prepared 1 mM solution of B1/B2 in ACN, and then the strips of Whatman filter paper immersed in it and dried. Now test strips were exposed in different concentration of CN^-. The color of paper strips changed immediately (Fig. 2.10).

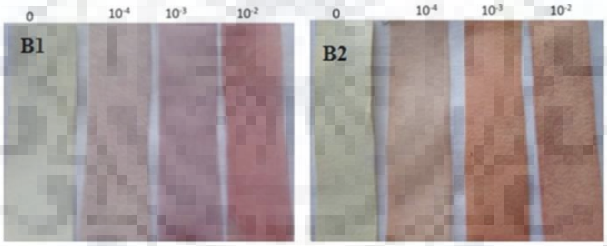

Fig. 2.10 Response of B1/B2 with coated paper strips in different concentrations (0 to 0.01 M) of CN^-.

2.3.1.4 Water Sample Analysis

As characterized above, B1/B2 was colorimetric receptors for CN^- with high selectivity, sensitivity, stability and reversible response. So it had varied applications for detection of CN^- in different water sample. We collected water samples from industrial waste, sewage, river and tap water from IIT Roorkee campus and nearby the Roorkee town area. The insoluble materials which were present in the water, removed through a 0.22 mm membrane filter paper (3 times) and then analyzed directly under the suitable conditions. These water samples were used as a solvent component with ACN (1:9) in spite of milipore water, then the solution was spiked with known concentrations of CN^- (25 µM). Now we

performed the whole experiments and the concentration of CN^- was calculated from the calibration curve. The experimental result has been tabulated in Table 2.2.

Table: 2.2 Analytical results of CN^- detection in different water samples.

Sample	Added [CN^-] (μM)	UV-Vis [CN^-] (μM)	Recovery %
Industrial waste	25	30.3	99.73
Sewage water	25	28.2	100.2
River water	25	25.5	100.8
Tap water	25	25.03	99.88

2.3.1.5 Comparative Studies of B1/B2

The sensing properties of receptors B1/B2 were compared with some highly sensitive and easily synthesized reported receptor for CN^- and AcO^- by colorimetric method (Table 2.3).

Table: 2.3 Comparison of some reported receptors by deprotonation colorimetric method for CN^- with the present work.

Previously literatures	Solvent	Sensing ions	LOD	Binding constant M^{-1}
New J. Chem. 38 (2014) 5769-5776 (ref. 23)	MeOH-H_2O (2:1)	CN^-	105×10^{-6}	1.7×10^2
J. Fluorine Chem. 175 (2015) 180-184 (ref. 24)	ACN-H_2O (1:9)	F^- CN^-	1.5×10^{-6} $1.9\text{-}5.2\times10^{-6}$	4.6×10^4 5.5×10^4
Sens. Actuators, B 202 (2014) 645-655 (ref. 37)	DMSO-H_2O (8:2)	CN^- AcO^-	60×10^{-6} 140×10^{-6}	3.2×10^3 1×10^3
Tetrahedron Lett. 52 (2011) 6919-6922 (ref. 38)	ACN-DMSO-H_2O (93:1:6)	CN^-	$0\text{-}1.9\times10^{-6}$	2.3×10^3
Sens. Actuators, B 204 (2014) 125-135 (ref. 39)	DMSO-H_2O (95:5)	CN^- AcO^-	3×10^{-6} (N1) 1×10^{-6} (N1)	7.52 7.07
B1/B2	ACN-H_2O (1:9)	CN^-	0.478×10^{-6} 1.66×10^{-6}	1.0×10^4 (B1) 2.5×10^4 (B2)

2.3.2 Sensing Studies of Receptors B3 and B4

2.3.2.1 Anion Sensing Without Metal Ions: Colorimetry and Spectrophotometry

The receptors were insoluble in water and protic solvents, so the supramolecular interface with tested anions such as F^-, Cl^-, Br^-, I^-, CN^-, N_3^-, SCN^-, AcO^-, AsO_2^-, CO_3^{2-}, NO_3^-, PO_4^{2-}, SO_4^{2-}, $H_2PO_4^-$ and HPO_4^{2-} (as tetrabutylammonium salts) were examined in H_2O-DMSO (1:9 v/v, pH-7.4 HEPES buffer). As shown in Fig. 2.11, the absorption band of B3/B4 (λ_{max} - 316/311 nm) shifted towards bathochromic region with emergence of a new band (λ_{max} - 470/464 nm, $\Delta\lambda$ = 154/153 nm) as one solution changed from colorless to yellow only with CN^-. The high charge separation between donor and acceptor unit, subsequently causes tremendous delocalization of electron into the isoniazid unit.

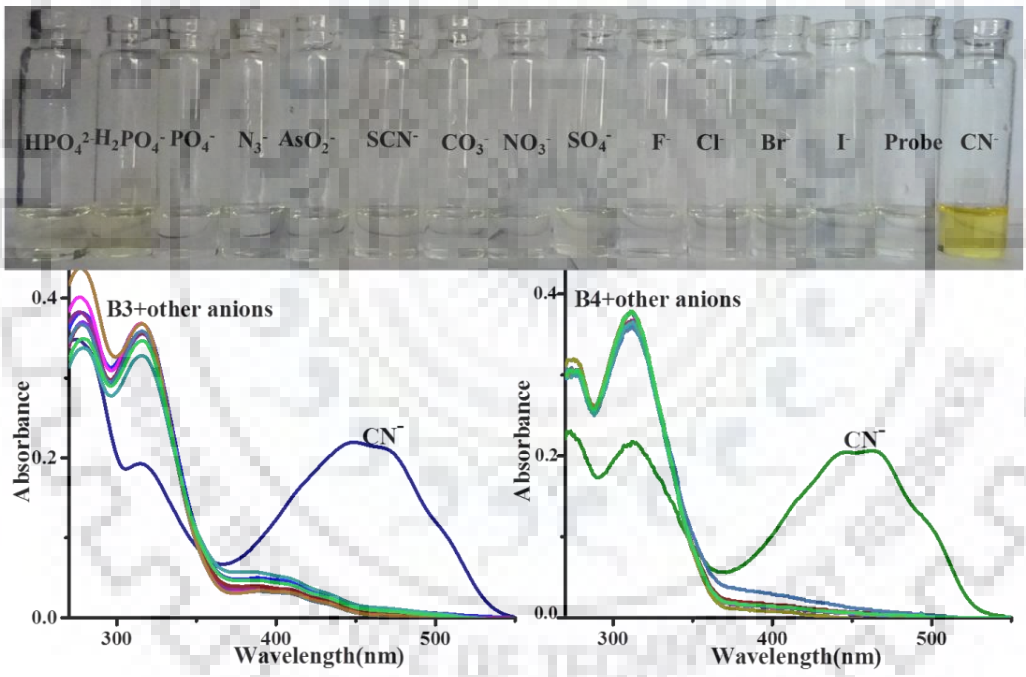

Fig. 2.11 Interaction of B3/B4 with 5 eq. of different anions in H_2O-DMSO (1:9 v/v, pH-7.4 HEPES buffer).

The discriminating sensing ability of receptor towards CN^- can be revealed through anions basicity (pKa value) and hydrogen bonding ability (hydration energy). In pure DMSO AcO^-, F^- and $H_2PO_4^-$ display deleterious interference, which was removed by using 10% H_2O-DMSO binary solution. By increasing the water content the effect of interfering anions is completely avoided through hydrogen-bonding. CN^- has less hydration energy (ΔH_{hyd} = -67 kJ mol^{-1}) as parallel to other competing anions like F^-

(ΔH_{hyd} = -505 kJ mol^{-1}), AcO^- (ΔH_{hyd} = -375 $kJmol^{-1}$) and $H_2PO_4^-$ (ΔH_{hyd} = -260 $kJmol^{-1}$), which block its interaction with the receptor in aqueous medium. Further, the pKa values for HF, CH_3COOH, H_3PO_4 and HCN in water are 3.17, 4.76, 2.12 and 9.21 respectively, which indicates that CN^- is a stronger base than other competing anions in aqueous medium [40-41]

Furthermore, the red shift in the absorption band of the receptor suggested that the intramolecular charge transfer (ICT) transition occurred with by deprotonation phenomenon (Bhattacharya's suggestion [42-43]). To determine the ICT, property of B3 and B3-CN^-, illustrate the change in absorption spectra in both non-polar (DCM) and polar solvents (ACN, DMSO, MeOH). Polar solvents relaxed the ICT excited state by dipole relaxation. This result suggested that free receptor is solvent independents; the excited state and ground state has an almost identical dipole moment and weak charge transfer, while the receptor-CN^- complex displayed stronger solvent dependence. This emphasizes that the dipole moment between ground and excited state was moderately high charge transfer generated by electronic excitation as shown in Fig. 2.12 a and Table: 2.4. For Interference study, B3 was tested with 10 eq. of other competing anions in presence of 5 equiv. of CN^-. The result showed that these anions didn't affect the absorption spectra of the receptor-CN^- system (Fig. 2.12 b).

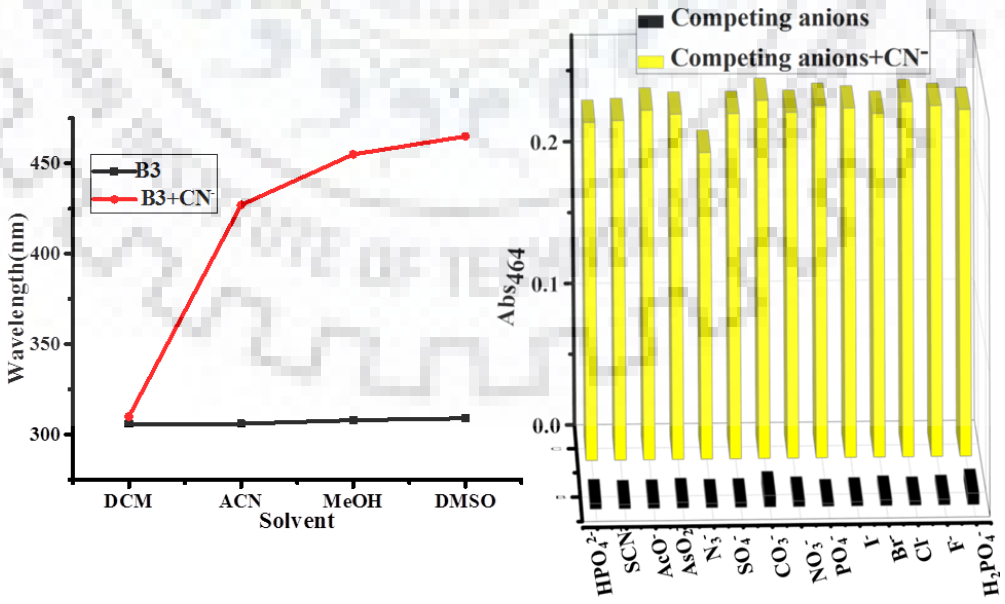

Fig. 2.12 (a) Solvatochromic studies of B3 with CN^- with different solvent (b) competition studies of B3-CN^- with 10 eq. of different anions.

Table: 2.4 Solvatochromic studies of B3 with CN^- in different polar solvents.

Solvent	λ_{abs} of B3	λ_{abs} of B3-CN^-
DCM	306	310
ACN	306	427
DMSO	308	455
MeOH	310	465

The binding affinities of receptors B3/B4 were determined by titration experiment with the sequential addition of CN^- (Fig. 2.13). In absorption titration the peak at 316/311 nm steadily decreases and temporarily a new peak concentrated at 470/464 nm increasingly with a clear isosbestic point at 353/349 nm, designated an interconversion into single distinct chemical species throughout the titration progression upon addition of CN^-. The binding approach between CN^- and B3/B4 was resolved over and done with Job's plot, which displays a 1:1 binding interaction (Inset of Fig. 2.13).

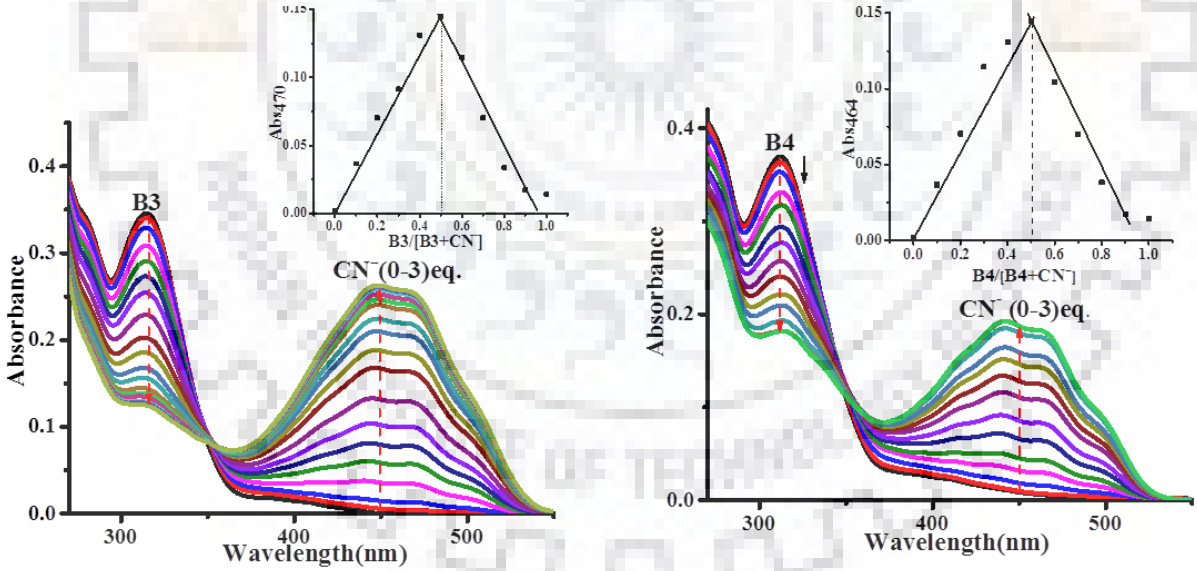

Fig. 2.13 Absorption titration spectra of B3/B4 upon addition 0-3 eq. CN^-; Inset: Jobs plot shows 1:1 in H_2O-DMSO (1:9 v/v, pH-7.4 HEPES buffer).

The values of association constants were calculated by using Benesi-Hildebrand equation and found to be $3.84\times10^4/2.96\times10^4$ M^{-1} (Fig. 2.14 a). The detection limit was calculated by (3σ/slope) and found to be 0.76/0.68 μM (Table: 2.5, Fig. 2.14 b).

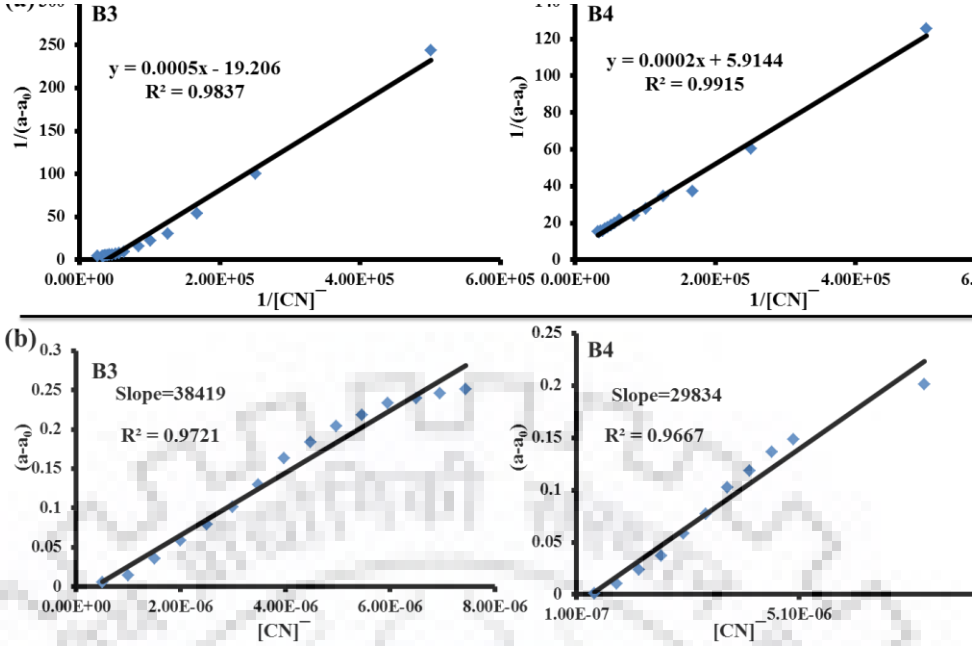

Fig. 2.14 (a) Benesi-Hilderbrand Plot (b) Limit of detection for the binding of CN^- with B3/B4.

To observe the recyclability of B3 with CN^- in a mixture of H_2O-DMSO (1:9 v/v) solution, 2 eq. HCl was added, the color changed from yellow to colorless and 470 nm peak entirely disappeared with redevelopment of free receptor (Fig. 2.15 a). The color variation was almost changeable with alternative addition of HCl and CN^-. This result further promoted the detection of CN^- by deprotonation mechanism.

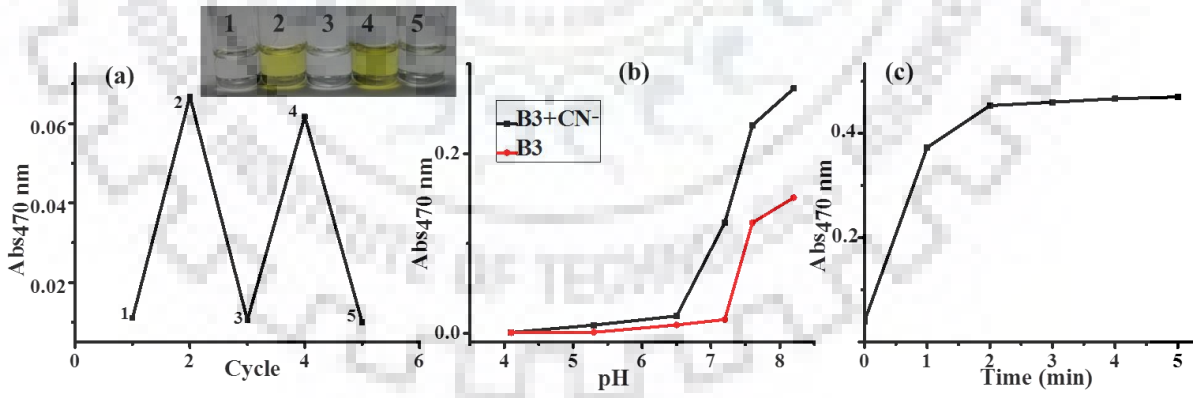

Fig. 2.15 (a) Reversibility study (b) pH dependent (c) Time-dependent absorption intensity of B3 with 5 equiv. CN^- in H_2O-DMSO (1:9 v/v, pH- 7.4 HEPES buffer).

The pH dependency of B3 and CN^- complex was examined at different pH values (4-8.3) at 470 nm. As shown in Fig. 2.15 b, the B3 and B3-CN^- complex is almost stable between 4.0-6.5 pH values, but above 6.5 pH values, the absorbance increases dynamically. The selectivity of CN^- decreased pointedly under acidic conditions and

gave increased absorbance under basic conditions due to protonation-deprotonation of the -NH group. This signifies that B3 and CN^- detection was stable at neutral pH. The appreciation of quick reaction with CN^- is noteworthy for the receptor in its hands-on application. The kinetic result showed that the reaction is accomplished within 2 min (Fig. 2.15 c).

2.3.2.2 Anion Sensing in Presence of Metal Ions: Colorimetry and Spectrophotometry

Since B3/B4 have a hetero-atom binding position, so its selectivity towards different cations (Ba^{2+}, Sn^{2+}, Pb^{2+}, Mn^{2+}, Ni^{2+}, Fe^{2+}, Cu^{2+}, Co^{2+}, Ag^{+}, Zn^{2+}, Cd^{2+}, Hg^{+}, Hg^{2+}) has been examined through absorption spectra. B3 shows a charge transfer band at 355 nm with Ni^{2+} and 440 nm with Cu^{2+} (Fig. 2.16 a). Upon gradual addition of Cu^{2+}/Ni^{2+} into the receptor B3, a clear isosbestic point appeared at 347/333 nm with 2:1/1:1 binding stoichiometry respectively (inset of Fig. 2.16 b, c).

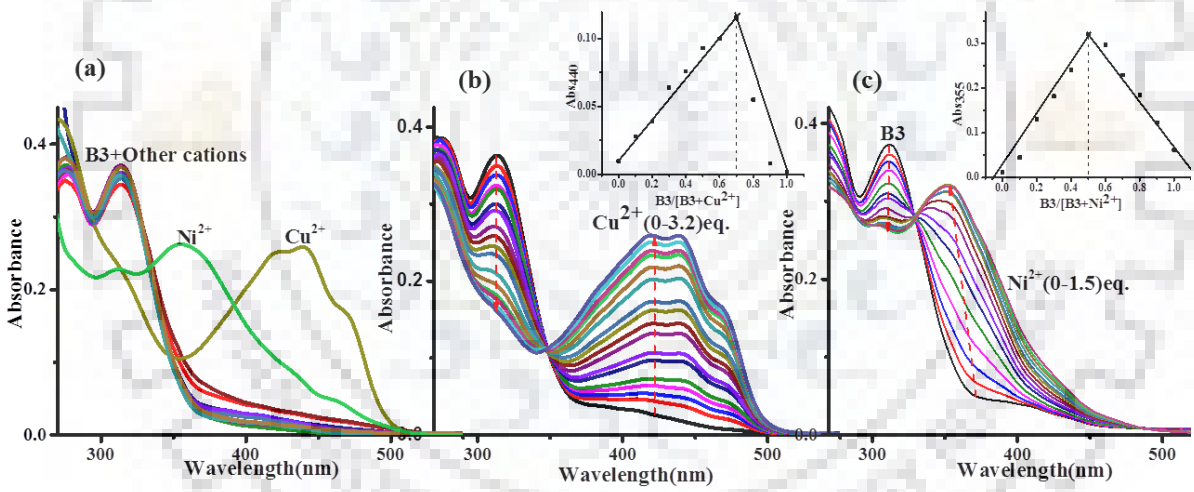

Fig. 2.16 (a) Interaction of B3 upon 5 eq. of metal (b) Absorption titration spectra of B3 upon addition of Cu^{2+} (Inset: Jobs plot shows 1:2) (c) Ni^{2+} (Inset: Jobs plot shows 1:1) in H_2O-DMSO (1:9 v/v, pH-7.4 HEPES buffer).

The selectivity of CN^- in presence of Cu^{2+}/Ni^{2+} was analyzed by absorption spectra. Results showed that only CN^- was selective in the presence of both metal ions (Fig. 2.17). Upon sequential addition of CN^- to B3-Cu^{2+} complex (0.5 eq.), shifting occurs in peak from 440 nm to 464 nm with a clear isosbestic point at 360 nm. Similarly, in presence of Ni^{2+} (1eq.) the absorption band at 355 nm decreases with a concomitant increase of 464 nm band with a clear coexistent point at 385 nm. Both absorption titrations showed an analogous pattern as

in the absence of metal ions, the only difference in saturation point. The saturation limits were attained with 2 eq. of CN^- in presence of Cu^{2+} and 1.5 eq. with Ni^{2+}.

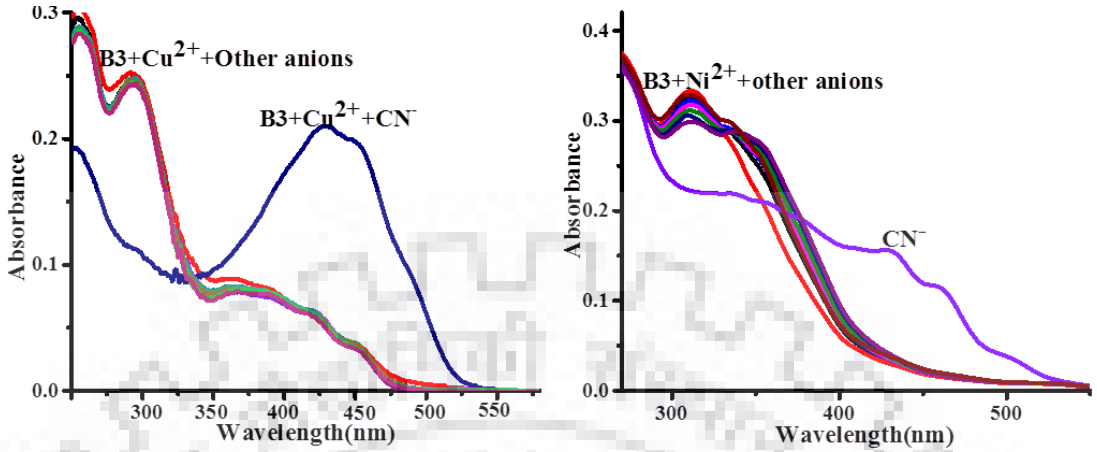

Fig. 2.17 Interaction of B3-Cu^{2+} & B3-Ni^{2+} complex with 5 eq. of different anions in H_2O-DMSO (1:9 v/v, pH-7.4 HEPES buffer).

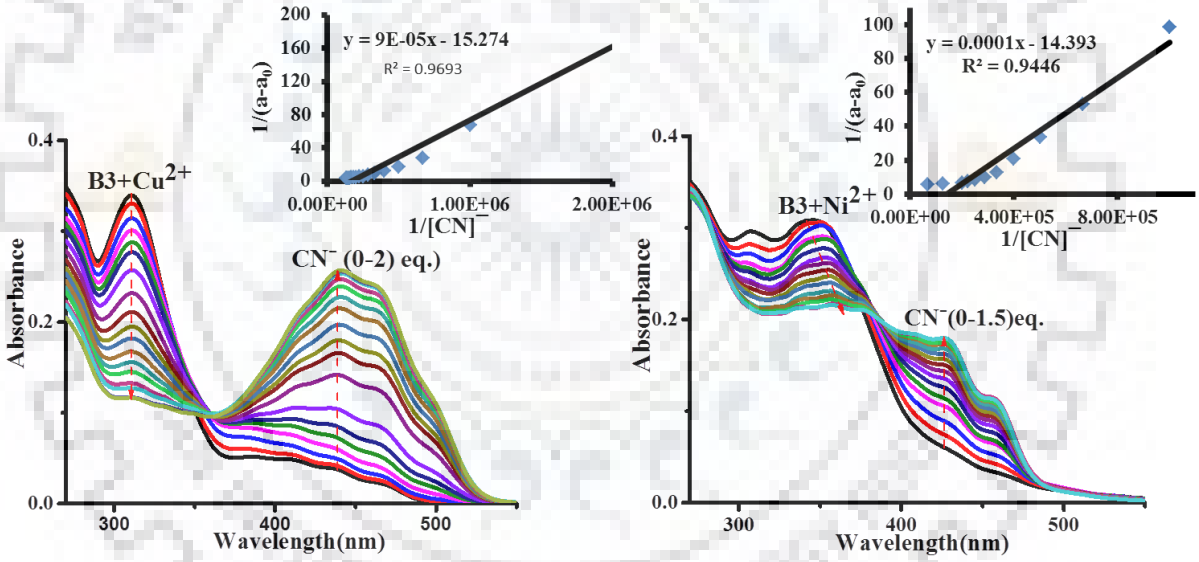

Fig. 2.18 Absorption titration spectra of B3-Cu^{2+} complex & B3-Ni^{2+} complex upon addition of CN^-; Inset: B.H. plot in H_2O-DMSO (1:9 v/v, pH-7.4 HEPES buffer).

The binding constant of B3 for CN^- in presence of Cu^{2+}/Ni^{2+} was found to be 1.7×10^5 M^{-1}/1.44×10^5 M^{-1} (inset of Fig. 2.18) with 3.58/6.37 μM detection limit (Fig. 2.19, Table: 2.5). The higher binding constant than that in free receptor (3.83×10^4 M^{-1}) proved that -NH proton of metal complexes is somewhat more acidic than free receptor due to electron withdrawing character of metal ions, thus metal complexes can turn as a superior H-bonded donor moiety for CN^-.

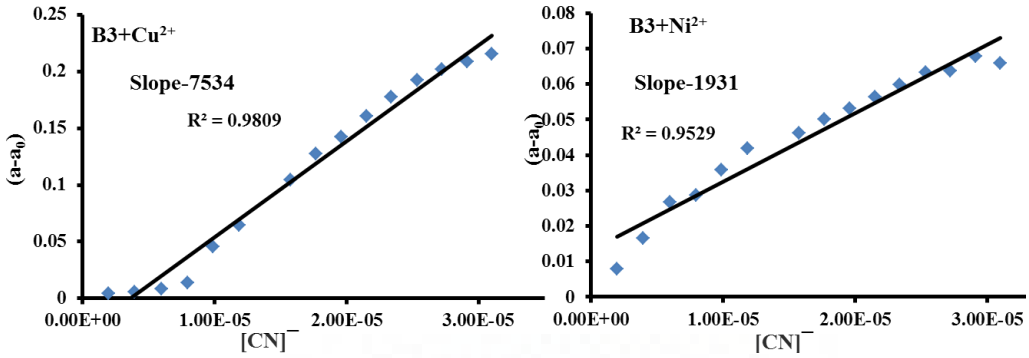

Fig. 2.19 Calibration curve for the binding of CN^- with B3-Cu^{2+} & B3-Ni^{2+} complex.

Table: 2.5 Determination of limit of detection.

CN^- complex	SD	Slope CN^-
B3	0.0097	38419
B4	0.00675	29834
B3+Cu^{2+}	0.009	7534
B3+Ni^{2+}	0.0041	1931.8

2.3.2.3 Nature of Interaction of B3 with CN^-

To analyse host-guest interaction between CN^- and receptor, ^{1}H NMR titration was executed in the absence and presence of CN^-. B3 has singlets at 10.19 and 8.90 ppm corresponding to -NH and HC=N proton, whereas the aromatic protons appeared in the region of 8.80-7.77 ppm. Upon slow addition of CN^-, the -NH proton disappeared in B3. In addition, no extra peak was generated within the range of 4-5 ppm, which designates prohibiting of the nucleophilic attack *via* CN^- (Fig. 2.20).

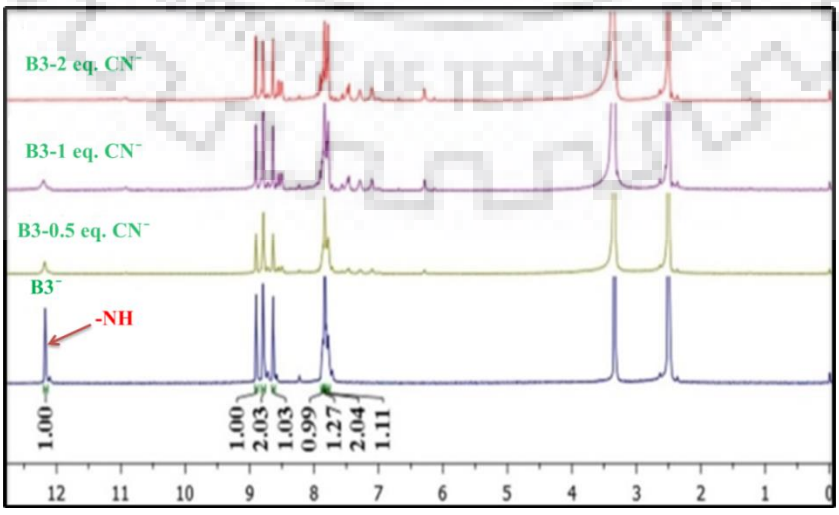

Fig. 2.20 Stacked ^{1}H NMR titration of B3 in DMSO d_6.

The interaction between CN^- and B3 was also confirmed by infrared spectra which shows the stretching vibration peaks at 3415 cm^{-1} (-NH), 3018 cm^{-1} (H-C=N), 1708 cm^{-1} (-C=O), 1647 cm^{-1} (N-C=O) and 1611 cm^{-1} (-C=N). Upon interaction with CN^- the -NH peak disappeared with a slight shifting of other peaks. It validates that CN^- binds with -NH protons (Fig. 2.21).

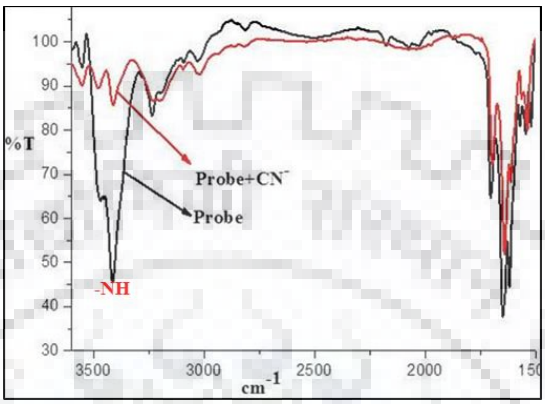

Fig. 2.21 IR spectra of B3 and B3-CN^-.

The binding procedures of CN^- with B3 was also supported by advanced computational DFT calculation in the gas phase by Gaussian 09 W program, using a B3LYP/6-311+G (d, p) basis set [44]. There is hydrogen bonding exchanges between isoniazid –C=O and -NH group (2.356 Å) in the gas phase. The optimized structures of B3-CN^- openly designated that CN^- reduces the exchange of hydrogen bonding, which can be proved that CN^- interaction with the acidic hydrogen. Furthermore, the HOMO/LUMO energy gap between B3 and CN^- are smaller (ΔE = 3.015 eV) in comparison to B3 (ΔE = 4.025 eV), which are also suggested by the bathochromic shift due to ICT transition upon deprotonation of -NH by CN^- (Fig. 2.22).

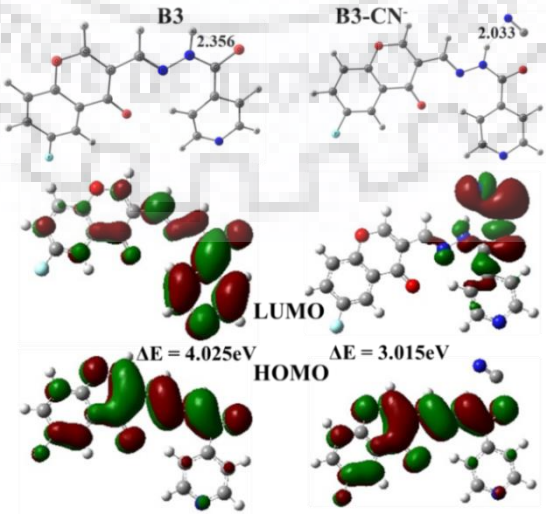

Fig. 2.22 Optimized structure and HOMO/LUMO energy band gap of B3 & B3-CN^-.

To further prove deprotonation is the possible sensing mechanism (even in the presence of Cu^{2+}/Ni^{2+}), interaction between B3, B3-Cu^{2+} complex and B3-Ni^{2+} complex were titrated with TBAOH instead of CN^{-}. An analogous UV-vis spectral change observed as addition of CN^{-}, which proved deprotonation phenomenon (Fig. 2.23).

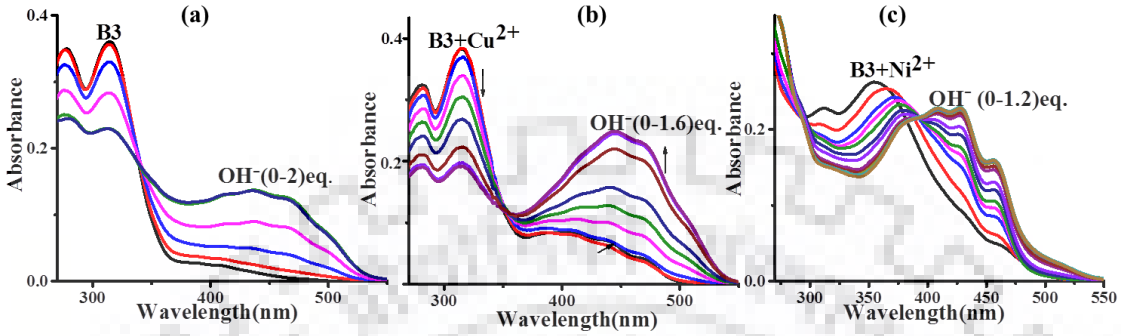

Fig. 2.23 Absorption titration spectra of (a) B3 (b) B3-Cu^{2+} (c) B3-Ni^{2+} with TBAOH in H_2O-DMSO (1:9 v/v, pH-7.4 HEPES buffer).

It comes out to be clear that hydrogen-bonding exchange is essential for anion binding sites. Shape, charge and mixed solvent system were also exceptionally significant between the guests-host interactions. ^{1}H NMR titration, IR spectroscopy, -OH titration and DFT calculation were provided enlightening picture of the real host-guest interaction. All results showed that the mechanism proceeds *via* deprotonation which affects intramolecular charge transfer (ICT) transition. Thus, based on all the spectroscopic experiments, the suggested binding mode of receptor with CN^{-} was shown in Scheme 2.4.

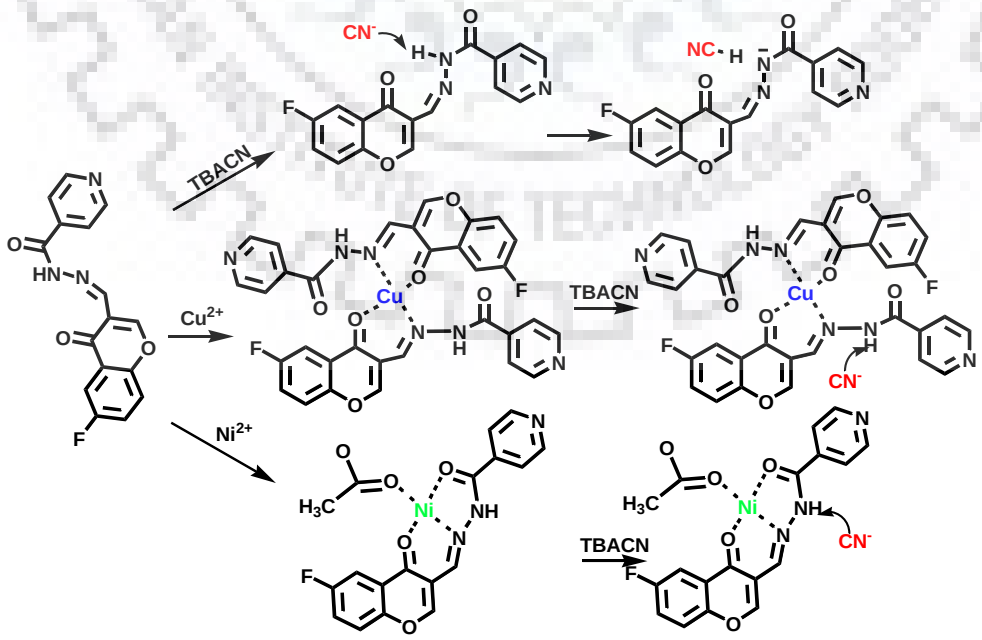

Scheme: 2.4 Suggested sensing mechanism of B3 with CN^{-}.

2.3.2.4 Analysis of CN^- in Water Samples

The receptor had widespread application for CN^- determination in different wastewater testers, which was composed of River Ganga of Haridwar, Roorkee and tap water of Roorkee. The insoluble materials were removed by 0.22 mm membrane filter paper. A known amount of CN^- (20 μM) was spiked in water samples. These water analytes were used as a solvent constituent with DMSO (10%). Table 2.6 shows the results were investigated by direct absorption study.

Table: 2.6 Analytical results of CN^- detection in water samples.

Sample	Added [CN^-] (μM) added	By Absorption spectra [CN^-][a] (μM)	Recovery%
Roorkee Tap water	20	19.8±0.5	99%
Haridwar water	20	19.7±0.2	98.5%
Roorkee water	20	19.96±0.7	100.5%

[a]Mean value ± standard deviation (triplicate measurement).

2.3.2.5 Application as Logic Gate

Based on the reversibility of B3-CN^- and H^+ ion with consequent changes in its absorption intensity at 470 nm, we have applied our system as a molecular switch, which perform on Boolean logic operations. In order to explain the design of the logic gate, we assign logic 0 and 1 to the inputs and outputs. The four probable (0, 0), (1, 0), (0, 1) and (1, 1) input combinations were shown in (Fig. 2.24). It has been detected that both the input signals: in the absence or presence of CN^- & H^+ (CN^-, H^+ = 1 or CN^-, H^+ = 0) no output signals were achieved, while in the presence of CN^- only an

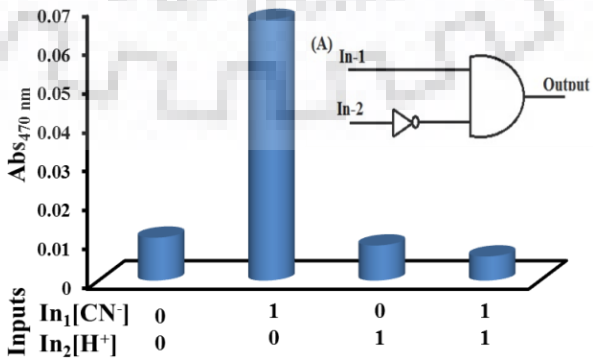

Fig. 2.24 Changes in the absorption intensity at 470 nm (B3) under four different input conditions; Inset: INHIBIT logic diagram.

input signal (CN^- = 1, H^+ = 0), absorption maxima at 470 nm was observed as the output signal but inverse of that (CN^- = 0, H^+ = 1) bring about no output signal. Thus, the logic circuit integrating the truth table with two inputs as CN^- (In_1) and H^+ (In_2), B3 has the ability to reveal INHIBIT job *via* absorption output. In fact, it exemplifies an AND logic gate with an inverter [45] in its input.

2.3.2.6 Comparative Studies of B3/B4

The sensing property of B3 was related to some easily synthesized reported receptors (containing -NH moiety) for CN^- by colorimetric method (Table 2.7). The data showed that B3 is highly selective for CN^- with high binding constant.

Table: 2.7 Comparison of the proposed receptors with previously reported literatures (containing -NH group) by colorimetric method for CN^-.

Previously literatures	**Selectivity**	**Solvent System**	**Binding Constant (M^{-1})**
Tetrahedron Lett. 54 (2013) 5612-5615 (ref. 31)	F^-, AcO^-	ACN	1.22×10^4, 2.59×10^4
Anal. Methods 5 (2013) 6401-6410 (ref. 46)	F^-, AcO^-	DMSO	4.30×10^3, 3.80×10^3 (S1) 2.26×10^4, 2.13×10^4 (S2)
RSC Adv. 6 (2016) 16586-16597 (ref. 47)	CN^-, S^{2-}	H_2O-DMSO (1:9)	4.20×10^3, 1.20×10^3
Anal. Chim. Acta. 663 (2010) 77-84 (ref. 28)	F^-, CN^-	DMSO	-------
Sens. Actuators, B 231 (2016) 768-778 (ref. 48)	F^-, CN^-	H_2O-DMF (1:1)	5.53×10^5, 8.27×10^4 (R-Cu comp.) 7.58×10^5, 9.87×10^4 (R-Co comp.) 2.60×10^6, 9.04×10^4 (R-Ni comp.) 7.13×10^4 (R-Zn comp.)
Sens. Actuators, B 202 (2014) 645-655 (ref. 39)	CN^- AcO^-	DMSO	7.52, 7.07 (N1) 8.52, 7.86 (N2)
Dalton Trans. 45 (2016) 1166-1175 (ref. 49)	F^-, CN^-	ACN-DMSO (5:95)	1.17×10^4, 4.9×10^4 (R) 1.37×10^5, 1.19×10^4 (R-Cu comp.)
This work	CN^-	H_2O-DMSO (1:9)	3.83×10^4 (B3) 1.72×10^5 (Cu complex) 2.80×10^5 (Ni complex)

2.4 CONCLUSION

In summary, firstly we developed simple azo linked salicyladehyde based Schiff base colorimetric receptor B1/B2 which is highly selective for CN^- and small extent for AcO^- with the distinct color changes, from light yellow to red. Further developed a simple -NH containing Schiff base B3/B4, which accentuates the detection of CN^- *via* deprotonation of the -NH group in the presence of anions and renders the appreciation due to the shift of the charge transfer band. However, selectivity and sensitivity for CN^- increased in the presence of Cu^{2+} and Ni^{2+} due to its coordinating aptitude with receptor and increased the acidity, which stimulates the deprotonation of the –NH group. The binding constant and 1:1 stoichiometry of all receptor with CN^- were calculated from B.H. and Job's plot. In contrast, selectivity for CN^- over other anions was explained by the basicity of anion in aq. medium. There were some advantages associated to receptor such as (i) inexpensive and simple synthesis, (ii) displaying high sensitivity for CN^- over other coexistent anion instead of in the presence of some metal ions and (iii) a practical application by paper strip test kit and water sample analysis.

References

1. D. Chen, R. J. Letcher, L. T. Gauthier, S. G. Chu, R. M. Crindle, D. Potter, Novel methoxylated polybrominated diphenoxybenzene congeners and possible sources in herring gull eggs from the Laurentian Great Lakes of North, America. Environ. Sci. Technol. 45 (2011) 9523-9530.
2. Y. Ding, T. Li, W. Zhu, Y. Xie, Highly selective colorimetric sensing of cyanide based on formation of dipyrrin adducts, Org. Biomol. Chem. 10 (2012) 4201-4207.
3. J. J. Park, Y. Kim, C. Kim, J. Kang, Naked eye detection of fluoride and pyrophosphate with an anion receptor utilizing anthracene and nitrophenyl group as signaling group, Tetrahedron Lett. 5 (2012) 2759-2763.
4. E. J. Song, H. Kim, I. H. Hwang, K. B. Kim, A. R. Kim, I. Noh, C. Kim, A single fluorescent chemosensor for multiple target ions: Recognition of Zn^{2+} in 100% aqueous solution and F^{-} in organic solvent, Sens. Actuators, B 195 (2014) 36-43.
5. A. P. de Silva, D. B. Fox, A. J. M. Huxley, T. S. Moody, Combining luminescence, coordination and electron transfer for signalling purposes, Coord. Chem. Rev. 205 (2000) 41-57.
6. M. Dutta, D. Das, Recent developments in fluorescent sensors for trace-level determination of toxic-metal ions, Trends Anal. Chem. 32 (2012) 113-132.
7. J. Yoon, S. K. Kim, N. J. Singh, K. S. Kim, Imidazolium receptors for the recognition of anions, Chem. Soc. Rev. 35 (2006) 355-360.
8. J. W. Steed, A modular approach to anion binding podands: adaptability in design and synthesis leads to adaptability in properties, Chem. Commun. 25 (2006) 2637-2649.
9. M. A. Holland, L. M. Kozlowski, Clinical features and management of cyanide poisoning, Clin. Pharm. 5 (1986) 737-741.
10. F. J. Baud, Cyanide: critical issues in diagnosis and treatment, Toxicology 26 (2007) 191-201.
11. J. D Johnson, T. L Meisenheimer, G. E. Isom, Cyanide-induced neurotoxicity: role of neuronal calcium, Toxicol Appl. Pharmacol. 84 (1986) 464-469.
12. B. K. Ardent, J. L. Borowitz, G. E. Isom, Brain lipid peroxidation and antioxidant protectant mechanisms following acute cyanide intoxication, Toxicological 56 (1989) 147-154.
13. K. W. Kulig, Cyanide Toxicity; U.S. Department of Health and Human Services: Atlanta, GA, 1991.

14. S. I. Baskin, T. G. Brewer, Cyanide poisoning, in medical aspects of chemical and biological warfare, Washington, DC (1997) 271-286.
15. C. Baird, M. Cann, Environmental Chemistry, 5th Edition, Freeman, New York, 2005.
16. X. Huang, X. Gu, G. Zhang, D. Zhang, A highly selective fluorescence turn-on detection of cyanide based on the aggregation of tetraphenylethylene molecules induced by chemical reaction, Chem. Commun. 48 (2012) 12195-12197.
17. R. Koenig, Environmental Disasters. Wildlife Deaths Are a Grim Wake-Up Call in Eastern Europe, Sci. 287 (2000) 1737-1738.
18. Guidelines for Drinking-Water Quality, World Health Organization, Geneva, 2 (1996).
19. A. Abbaspour, M. Asadi, A. Ghaffarinejad, E. Safaei, A selective modified carbon paste electrode for determination of cyanide using tetra-3,4 pyridinoporp hyrazinatocobalt (II), Talanta 66 (2005) 931-936.
20. J. S. Raul, A. Geraut, L. Berthelon, B. Ludes, Determination of blood cyanide by HPLC-MS, J. Anal. Toxicol. 26 (2002) 144-148.
21. S. Dadfarnia, A. M. H. Shabani, F. Tamadon, M. Rezaei, Indirect determination of free cyanide in water and industrial wastewater by flow injection-atomic absorption spectrometry, Microchim. Acta 158 (2007) 159-163.
22. M. Noroozifar, M. K. Motlagh, S. N. Hosseini, Flow injection analysis-flame atomic absorption spectrometry system for indirect determination of cyanide using cadmium carbonate as a new solid-phase reactor, Anal. Chim. Acta 528 (2005) 269-273.
23. Y. J. Na, G. J. Park, H. Y. Jo, S. A. Lee, C. Kim, A colorimetric chemosensor based on a Schiff base for highly selective sensing of cyanide in aqueous solution: the influence of solvents, New J. Chem. 38 (2014) 5769-5776.
24. D. Udhayakumari, S. Velmathi, M. S. Boobalan, Novel chemosensor for multiple target anions: The detection of F^- and CN^- ion *via* different approach, J. Fluorine Chem. 175 (2015) 180-184.
25. S. Saha, A. Ghosh, P. Mahato, S. Mishra, S. K. Mishra, E. Suresh, S. Das, A. Das, Specific recognition and sensing of CN^- in sodium cyanide solution, Org. Lett. 12 (2010) 3406-3409.
26. A. Mouradzadegun, F. Abadast, An improved organic/inorganic solid receptor for colorimetric cyanide-chemosensing in water: Towards new mechanism aspects, simplistic use and portability, Chem. Commun. 50 (2014) 15983-15986.

27. X. Zhang, S. Chen, S. Jin, X. Lu, L. Li, X. Chen, Q. Shu, Naphthalene based lab-on-a-molecule for the highly selective and sensitive detection of CN^- and Ag^+ in aqueous solution, Sens. Actuators, B 237 (2016) 367-372.
28. V. Kumar, M. P. Kaushik, A. K. Srivastava, A. Pratap, V. Thiruvenkatam, T. N. Guru Row, Thiourea based novel chromogenic sensor for selective detection of fluoride and cyanide anions in organic and aqueous media, Anal. Chim. Acta 663 (2010) 77-84.
29. S. S. Sun, A. J. Lees, Anion recognition through hydrogen bonding: a simple, yet highly sensitive, luminescent metal-complex receptor, Chem. Commun. 17 (2000) 1687-1688.
30. G. Vinithra, S. Suganya, S. Velmathi, Naked eye sensing of anions using thiourea based chemosensors with real time application, Tetrahedron Lett. 54 (2013) 5612-5615.
31. A. Misra, M. Shahid, P. Dwivedi, An efficient thiourea-based colorimetric chemosensor for naked-eye recognition of fluoride and acetate anions: UV-vis and ^1H NMR studies, Talanta 80 (2009) 532-538.
32. M. K. Chahal, M. Sankar, Porphyrin chemodosimeters: synthesis, electrochemical redox properties and selective 'naked-eye' detection of cyanide ions, RSC Adv. 5 (2015) 99028-99036.
33. H. A. Benesi, J. H. Hildebrand, A spectrophotometric investigation of the interaction of iodine with aromatic hydrocarbons, J. Am. Chem. Soc. 71 (1947) 2703-2707.
34. S. S. Razi, R. Ali, P. Srivastava, M. Shahid, A. Misra, An azo based colorimetric probe for the detection of cysteine and lysine amino acids and its real application in human blood plasma, RSC Adv. 4 (2014) 16999-17007.
35. P. A. Nikitina, L. G. Kuz'mina , V. P. Perevalov, I. I. Tkach, Synthesis and study of prototropic tautomerism of 2-(3-chromenyl)-1-hydroxyimidazolee, Tetrahedron 69 (2013) 3249-3256.
36. K. M. Khan, N. Ambreen, U. R. Mughal, S. Jalil, S. Perveen, M. I. Choudhary, 3-Formylchromones: potential antiinflammatory agents, Eur. J. Med. Chem. 45 (2010) 4058-4064.
37. G. R. You, G. J. Park, S. A. Lee, Y. W. Choi, Y. S. Kim, A single chemosensor for multiple target anions: The simultaneous detection of CN^- and OAc^- in aqueous media, Sens. Actuators, B 202 (2014) 645-655.
38. D. Y. Lee, N. Singh, A. Satyender, D. O. Jang, An azo dye-coupled tripodal chromogenic sensor for cyanide, Tetrahedron Lett. 52 (2011) 6919-6922.
39. V. K. Gupta, A. K. Singh, N. Gupta, Colorimetric sensor for cyanide and acetate ion using novel biologically active hydrazones, Sens. Actuators, B 204 (2014) 125-135.

40. S. Mardanya, S. Karmakar, D. Mondal, S. Baitalik, An imidazolyl-pyreno-imidazole conjugate as a cyanide sensor and a set–reset memorized sequential logic device, Dalton Trans. 44 (2015) 15994-16012
41. H. J. Mo, Y. Shen, B. H. Ye, Selective recognition of cyanide anion *via* formation of multipoint NH and phenyl CH hydrogen bonding with acyclic ruthenium bipyridine imidazole receptors in water, Inorg. Chem. 51 (2012) 7174-7184.
42. N. Kumari, S. Jha, S. Bhattacharya, Colorimetric probes based on anthraimidazolediones for selective sensing of fluoride and cyanide ion *via* intramolecular charge transfer, J. Org. Chem. 76 (2011) 8215-8222.
43. L. Li, F. Liu, H. Li, Selective fluorescent probes based on C-N isomerization and intramolecular charge transfer (ICT) for zinc ions in aqueous solution, Spectrochim. Acta, Part A 79 (2011) 1688-1692.
44. M. J. Frisch, G. W. Trucks, H. B. Schlegel, G. E. Scuseria, M. A. Robb, J. R. Cheeseman, J. A. Montgomery, J. T. Vreven, K. N. Kudin, J. C. Burant, J. M. Millam, S. S. Iyengar, J. Tomasi, V. Barone, B. Mennucci, M. Cossi, G. Scalmani, N. Rega, G.A. Petersson, H. Nakatsuji, M. Hada, M. Ehara, K. Toyota, R. Fukuda, J. Hasegawa, M. Ishida, T. Nakajima, Y. Honda, O. Kitao, H. Nakai, M. Klene, X. Li, J. E. Knox, H. P. Hratchian, J. B. Cross, V. Bakken, C. Adamo, J. Jarmillo, R. Gomperts, R. E. Stratmann, O. Yazyev, A. J. Austin, R. Cammi, C. Pomelli, J. W. Ochterski, P. Y. Ayala, K. Morokuma, G. A. Voth, P. Salvador, J. J. Dannenberg, V. G. Zakrzewski, S. Dapprich, A. D. Daniels, M. C. Strain, O. Farkas, D. K. Malick, A. D. Rabuck, K. Raghavachari, J. B. Foresman, J. V. Ortiz, Q. Cui, G. Baboul, S. Clifford, J. Cioslowski, B. B. Stefanov, G. Liu, Liashenko, P. Piskorz, I. Komaromi, R. L. Martin, D. J. Fox, T. Keith, M. A. Al-Laham, C. Y. Peng, A. Nanayakkara, M. Challacombe, P.M.W. Gill, B. Johnson, W. Chen, M. W. Wong, C. Gonzalez, J. A. Pople, Gaussian, 03, Revision D.01, Gaussian, Inc., Wallingford CT (2004).
45. M. K. Chahal, M. Sankar, 1,8-Naphthyridinic fluorescent 'turn-on' and 'turnoff' chemosensors for detection of F^- and Hg^{2+} ions mimicking INHIBIT molecular logic behavior, Anal. Methods 7 (2015) 4552-4559.
46. M. S. Kumar, S. Loganathan, A. Kumar, A. Sreekanth, Highly selective fluorogenic anion chemosensors: naked-eye detection of F^- and AcO^- ions in natural water using a test strip, Anal. Methods 5 (2013) 6401-6410.
47. K. Y. Ryu, J. J. Lee, J. A. Kim, D. Y. Park, C. Kim, Colorimetric chemosensor for multiple targets, Cu^{2+}, CN^- and S^{2-}, RSC Adv. 6 (2016) 16586-16597.

48. C. Parthibana, S. Ciattinib, L. Chelazzib, K .P. Elango, Colorimetric sensing of anions by Cu(II), Co(II), Ni(II) and Zn(II) complexes of naphthoquinone-imidazole hybrid-Influence of complex formation on selectivity and sensing medium, Sens. Actuators, B 231 (2016) 768-778.
49. A. Sarkar, S. Bhattacharyya, A. Mukherjee, Colorimetric detection of fluoride ions by anthraimidazoledione based sensors in the presence of Cu (II) ions, Dalton Trans. 45 (2016) 1166-1175.

CHAPTER 3

Metal Complexation Based Cyanide Sensor

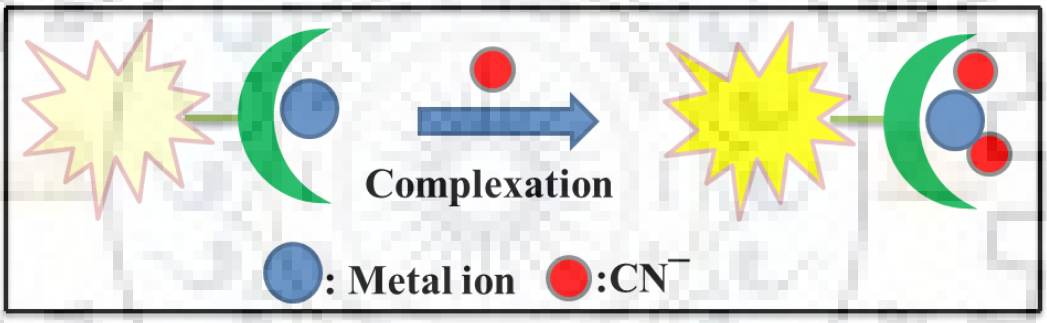

3.1 INTRODUCTION

CN^- is used in numerous industrial applications, containing electroplating, polymer synthesis, mining and metallurgy [1-2]. For illustration, CN^- percolation is a vital extraction procedure for the resourceful regaining of gold from composite ores and also used in the separation of gold, copper and silver from platinum [3]. Regrettably, chronic CN^- revelation induces pain, irritation, nervous damage and critical CN^- poisoning can be lethal due to disruption of the mitochondrial electron transport chain by interrelating with cytochrome c oxidase, thus causes cellular asphyxilation [4-5]. The environmental contagion of CN^- occurs through industrial progressions on accidental workplace disclosure and very harmful as a result of criminal, suicidal and terroristic events. Moreover, CN^- poisoning in domestic fires occurs *via* combustion of melamine, polyurethanes and other plastics can be lethal well formerly victims have breathed in toxic levels of CO, thus the dreadful concentration of CN^- within the blood of fire victims has been suggested to be between 23-26 mM [6-8].

Optical chemosensors clasp much application for the rapid and simple selective recognition of many analysts together with CN^-. The contemporary state of skill of colorimetric and fluorimetric approaches for CN^- have been technologically advanced over the past few years by using the reaction-based (chemodosimetric) nucleophilic attack of CN^-, either an electrophilic carbon [9-12] or a boron center [13-14] along with hydrogen bonding interactions [15-17], single-electron transfer reaction [18-19] and quantum dots technology [20-21]. Other approaches were involved metal complexes as receptors for CN^- sensing, due to greater binding affinity of CN^- with transition metal ions, in which the mechanism of sensing involves a direct CN^--metal relations. They are characterized by two methods: (i) CN^- transfer the metal ion from the metal-ligand complex and forms stable metal cyanide adduct (displacement approach) and (ii) CN^- act together with a metal ion complex *via* advantage of the immediate effect of back donation and electron pair donation (complexation approach). The coordination ability are implicate addition with Ru^{2+}-pyridine [22], Co^{2+}-complex [23], Ni^{2+}/Zn^{2+}porphyrin [24-25] and Cu^{2+}-complex [26-28]. Further, most of the CN^- sensors drives 1:1 binding mode with non-metal probes (nucleophilic and hydrogen bonding interaction). The 1:2 binding mode, however, does diligently look like nature's binding or recognition methods similar to protein-metal ion and

antigen-antibody binding [29]. We supposed that 1:2 binding mode between a metal complex and CN^- would be responsible for a useful sensing mechanism. Additionally, the high ligand field splitting, subsequent from CN^- coordination also brings high-to-low spin variation, frequently leads to noticeable variation in the UV-vis spectra. Finally, the emission properties of complexes containing fluorescent moieties are frequently turned by CN^- coordination *via* binding to transition metal ions as exogenous coligands and able to strongly affect their electronic states, thus change the emission properties. All the above features make an applicable device for CN^- optical sensing *via* transition metal complexes.

However, as concerns the 'metal displacement approach' [30-34] has been earlier design for the recognition of CN^- (fluorescent ''turn-on''). In our preceding report, we report Cu and Ag displacement method for CN^- detection on chromone based receptor [35-36]. Till date few numbers of metal coordination approaches have been reported for CN^-, generally based on Co^{2+} complex [23]. From this perception, we report a novel 4-hydroxy-6-methyl-chromenone based molecular receptor 2a, which is selective for Co^{2+} and subsequent complex for CN^- with a high binding constant, positive response time and respectable detection limit.

3.2 EXPERIMENTAL SECTION

3.2.1 Chemical and Instrumentation

All reagents and solvents for experimental work were taken from Sigma-Aldrich. DMF solvent was dried with the help of $CaCl_2$ as drying agent. CHNS (carbon, hydrogen, nitrogen, sulfur) elemental analysis was supported by using a vireo MICROV3.1.1. IR spectra were recorded with Perkin Elmer FT-IR 1000 spectrophotometer (KBr solid film). Specord S600 Thermo-Scientific PC double beam spectrophotometer used for absorption spectra with quartz cuvette of path length 1 cm. Horiba RF-5301PC was used for emission spectra with the standard quartz cell of path length 3 cm. The NMR spectra were recorded in JEOL 400 MHz spectrophotometer. The Cyclic Voltammograms were noted down with a CHI760E Electro analyser, three-electrode cell with glassy carbon as the working electrode, $Hg/HgCl_2$ as the reference electrode, Pt wire as the counter electrode and 0.1 M tetrabutylammonium hexafluorophosphate (nBu_4NPF_6) was used as the supporting electrolyte on 0.1V s^{-1} scan rate.

3.2.2 Synthesis and Characterization of Receptors 2a and 2b

2a and 2b were synthesized as shown in Scheme 3.1. 1 mmol methanolic solution of 1 (3-acetyl-4-hydroxy-6-methylcuomerin, synthesised by formerly reported literature) [37-38] and coupling component (2-aminopicoline and napthylamine) mixed and refluxed. After completion of the reaction obtained ppt was filtered. The whitish yellow colored compound was achieved with 68% yield.

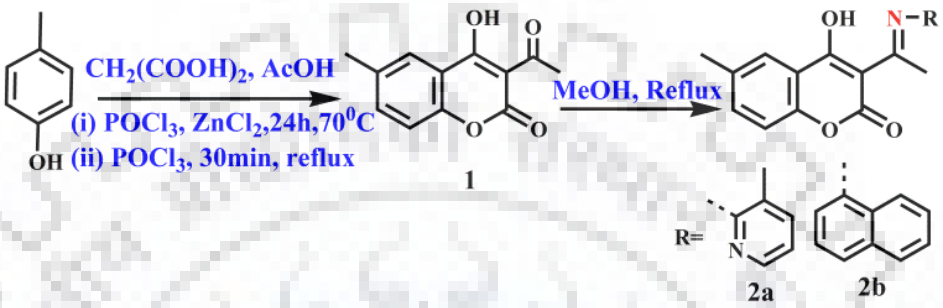

Scheme: 3.1 Synthesis of receptors 2a and 2b.

1: 3-acetyl-4-hydroxy-6-methyl-2H-chromen-2-one

Anal. Calc. ($C_{12}H_{10}O_4$) : C-66.05, H-4.42, O-29.33; Found : C-66.40, H-4.29; ^{1}H NMR ($CDCl_3$, 400 MHz, δ/ppm) : 17.74 (s, 1H), 7.84 (s, 1H), 7.49 (d, 1H), 7.20 (d, 1H), 2.78 (s, 3H), 2.43 (s, 3H); ^{13}C NMR ($CDCl_3$, 100 MHz, δ/ppm) : 206.2, 178.8, 160.4, 153.0, 137.4, 134.4, 125.1, 116.9, 115.0, 101.5, 30.2, 20.9.

2a: 4-hydroxy-6-methyl-3-(1-(3methylpyridin-2-ylimino)ethyl)-2H-chromen-2one

Anal. Calc. ($C_{18}H_{16}N_2O_3$) : C-70.12, H-5.23, N-9.09, O-15.57; Found : C-69.47, H-5.29, N-8.87; IR (KBr, υ/cm^{-1}); 3431 (-OH), 1699 (-C=O), 1631 (-C=N); ^{1}H NMR (DMSO d_6, 400 MHz, δ/ppm) : 15.83 (s, 1H) 8.42 (d, 1H), 7.90 (d, 1H), 7.82 (s, 1H), 7.51 (d, 1H), 7.41-7.38 (m, 1H), 7.22 (d, 1H) 2.75 (s, 3H), 2.38 (s, 6H); ^{13}C NMR ($CDCl_3$, 100 MHz, δ/ppm) : 182.5, 177.2, 162.5, 152.1, 149.5, 146.6, 139.9, 135.6, 133.4, 127.9, 125.9, 123.0, 119.7, 116.6, 99.3, 21.4, 20.8, 17.7; APCI-MS m/z (m+H) = 309.3 (calcd-309.12).

2b: 4-hydroxy-6-methyl-3-(1-napthalene-1-ylimino)ethyl)-2H-chrome-2-one

Anal. Calc. ($C_{22}H_{17}NO_3$) : C-76.95, H-4.99, N-4.08, O-13.98; Found : C-76.97, H-5.09, N-4.17**;** ^{1}H NMR ($CDCl_3$, 400 MHz, δ/ppm) : 15.88 (s, 1H), 7.97-7.88 (m, 4H), 7.61-7.54 (m, 3H), 7.39 (t, 2H), 7.17 (d, 1H), 2.62 (s, 3H), 2.43 (s, 3H); ^{13}C NMR ($CDCl_3$, 100 MHz,

δ/ppm) : 182.5, 177.6, 162.8, 152.2, 135.5, 134.3, 133.5, 132.8, 129.1, 129.0, 128.7, 127.9, 127.3, 125.9, 125.3, 123.8, 122.2, 119.8, 116.6, 98.4, 21.1, 20.9.

3.3 RESULTS AND DISCUSSION

3.3.1 Optical Response of 2a as Primary Sensor for Co^{2+} Ion

Considering partial water solubility, the spectral properties of 2a was measured H_2O-DMF ((1:9 v/v, pH-7.4 HEPES buffer) mixture. The newly produced ligand 2a exhibited a characteristic band at 344 nm in absorption spectra (20 μM) with an emission maximum at 431 nm (λ_{ext} - 350 nm, 5 μM). To estimate the selectivity of 2a, it was treated with various tested metal ions such as Mg^{2+}, Ca^{2+}, Al^{3+}, Pb^{2+}, Sn^{2+}, Cr^{3+}, Mn^{2+}, Fe^{2+}, Co^{2+}, Ni^{2+}, Cu^{2+}, Ag^{+}, Zn^{2+}, Cd^{2+}, Hg^{+} and Hg^{2+}. Interestingly, the receptor 2a was found to be extremely sensitive and selective towards Co^{2+} with shifting in absorption band at 332 nm and induced a substantial quenching in its fluorescence spectra. The competitive study was also executed to confirm the selectivity of2a with Co^{2+} in the presence of other interfering metal ions. The result displays that there was no interference of other tested metal ions concerning the selection of Co^{2+} (Fig. 3.1).

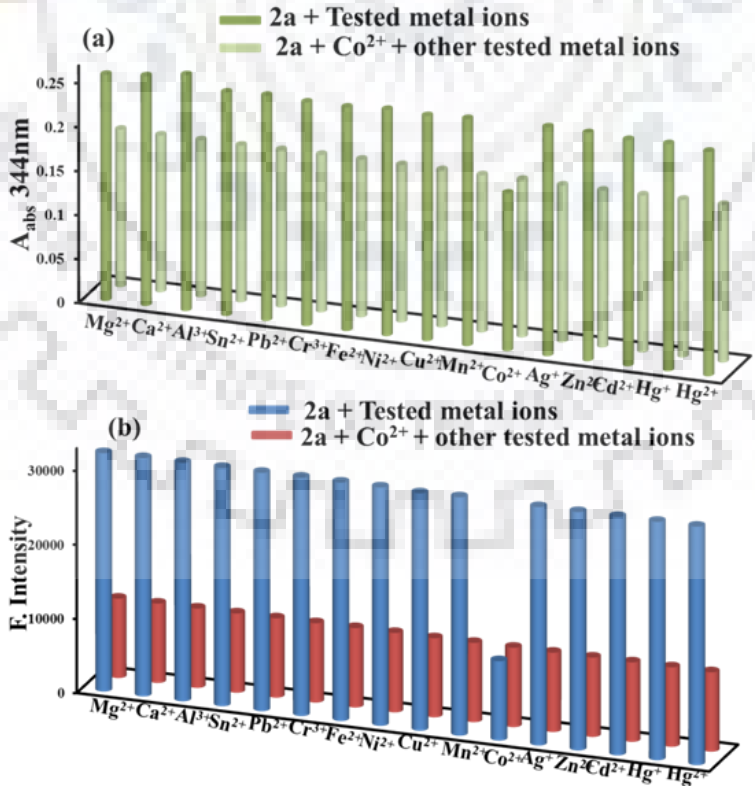

Fig. 3.1 Interaction of 2a with 10 eq. of metal ion; (a) Absorption spectra (b) Emission spectra in H_2O-DMF (1:9 v/v, pH-7.4 HEPES buffer).

The pH dependent potential discrimination of 2a and cobalt complex was resolute by emission behavior. The solution of 2a was prepared in DMF solvent due to low solubility in water. 0.5 M HCl and 1 M NaOH was used for pH adjustment. Receptor 2a was stable at 4-8 pH range and below pH 4.0 and above pH 8.0 decreased marginally due to protonation and deprotonation of -OH group. Similarly the cobalt complex was stable at 4-9 pH (Fig. 3.2 a). At high pH value, -OH will compete with receptor to bind cobalt, which influenced the detection. This proved the utility of 2a and cobalt complex as a sensor under physiological pH conditions. The effect of water content on the sensitivity of 2a-Co^{2+} complex has been studied by fluorescence spectra. It have been diminished the sensitivity of Co^{2+} on increasing the content of water up to 10% (Fig. 3.2 b).

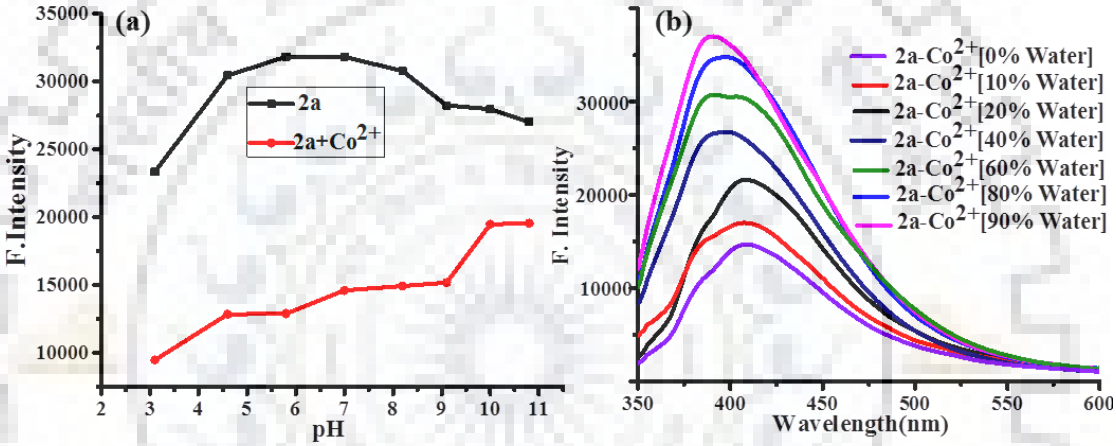

Fig. 3.2 Effect of pH (a) and water content (b) on emission intensity of 2a-Co^{2+} complex.

In order to estimate the binding affinity of 2a, absorption and emission titration experiment was accompanied with Co^{2+}. Upon gradual addition of Co^{2+} (0-2 eq.), the band at 344 nm shifted towards the blue region at 332 nm with clear co-existent point at 303 nm (Fig. 3.3 a). Job's Plot analysis reveals the 2:1 stoichiometry between the receptor-Co^{2+} complexation (Fig. 3.3 b). Similarly the emission maxima constantly decreased with the gradual addition of Co^{2+} (0-2.2 eq.), which signifying the conversion of un-complex species to complex species (Fig. 3.4 a). The Benesi-Hildebrand [39] plot displays a very good linearity (R^2_{abs} = 0.9914 and R^2_{em} = 0.9900), which intensely supported 2:1 binding mode between receptor and Co^{2+} by plotting between $[1/Co^{2+}]^{1/2}$ and $1/(A_0\text{-}A)$ or $1/(F_0\text{-}F)$. In addition the binding constant was calculated from the intercept/slope, which obtained as $K_{abs}= 1.34 \times 10^2\ M^{-1/2}$ and $K_{em}= 2.1 \times 10^2\ M^{-1/2}$ (Fig. 3.4 b). The detection limit was intended by (3σ/slope) and found to be 1.9 μM (Fig. 3.5).

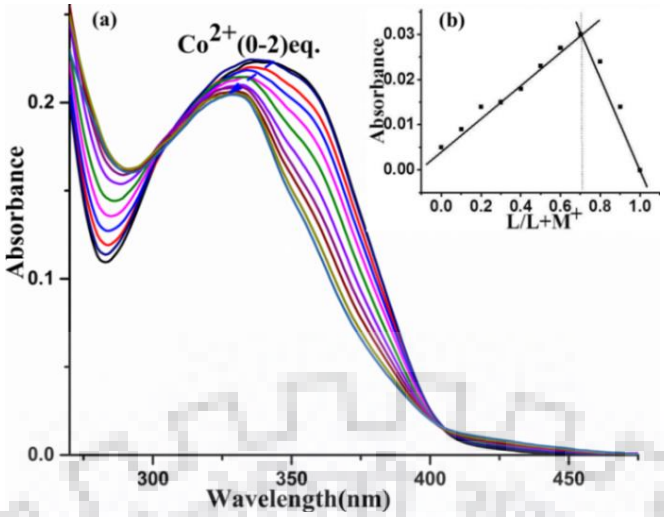

Fig. 3.3 (a) Absorption titration spectra (b) Jobs plot of 2a upon addition of Co^{2+} in H_2O-DMF (1:9 v/v, pH-7.4 HEPES buffer).

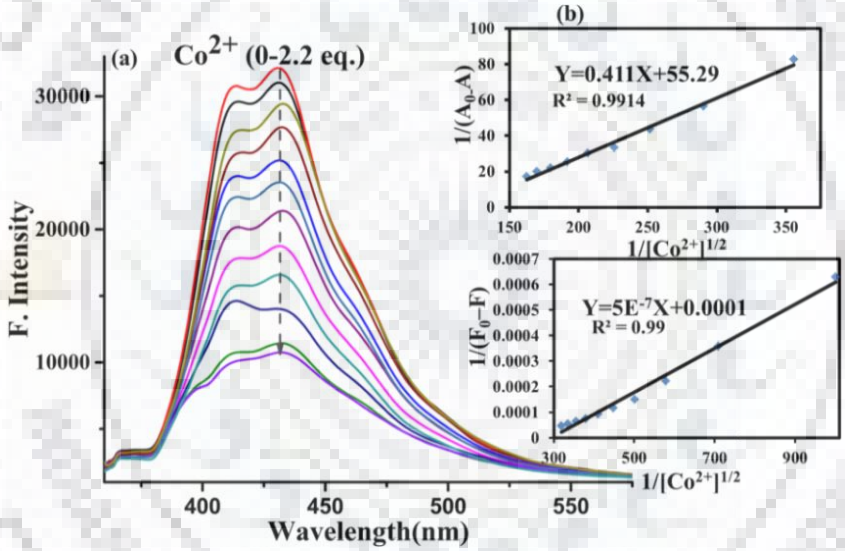

Fig. 3.4 (a) Emission titration spectra (b) Benesi-Hilderbrand Plot for the binding constant of 2a upon addition of Co^{2+} in H_2O-DMF (1:9 v/v, pH-7.4 HEPES buffer).

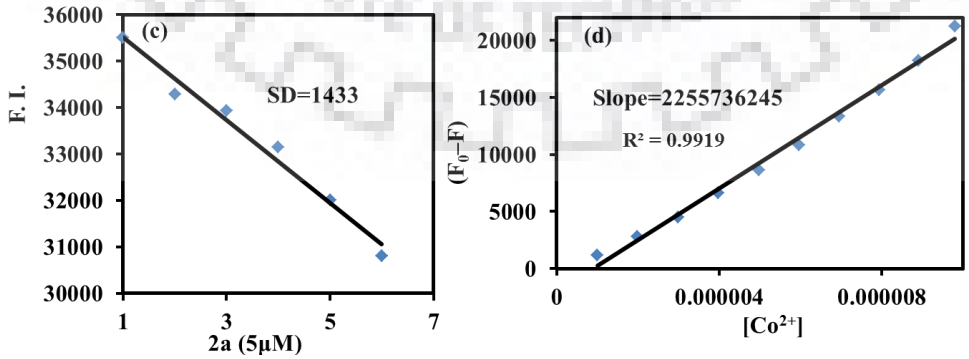

Fig. 3.5 (a) Calibration sensitivity of 2a (b) Calibration curve of Co^{2+} in H_2O-DMF (1:9 v/v, pH-7.4 HEPES buffer).

3.3.2 Optical Responses of 2a-Co^{2+} Complex as Secondary Sensor for CN^- Ion

Generally, Co^{2+} can form 4-6 coordinated complexes. Conversely, one cobalt atom binds with two receptors and shows 4 coordination numbers in this case. Explicitly, there are still two axial coordination sites are vacant. Apparently, the structural feature makes a prospect of availability of CN^- coordination of axial position due to the strong binding ability of CN^- to Co^{2+}. The sensing ability of 2a-Co^{2+} complex was examined in H_2O-DMF (1:9 v/v, pH-7.4 HEPES buffer) with several tested anions and found with a substantial variation in the optical properties individually with CN^-. The absorbance spectra of 2a-Co^{2+} complex with CN^- shows two new peak at 289 nm, 274 nm with blue shift in 332 nm to 314 nm and remains constant with other anions including F^-, Cl^-, Br^-, I^-, N_3^-, AcO^-, AsO_2^-, CO_3^{2-}, SO_4^{2-} and HPO_4^{2-}, except EDTA (Fig. 3.6 a). Even though the absorbance of 2a-Co^{2+} is modulated with CN^-, under the similar situations a significant high fluorescence enhancement was observed at 431 nm on comparison to 2a, thus signifying that CN^- coordinates to 2a-Co^{2+} center. In fact, among various tested anion, only EDTA can bind with Co^{2+} from 2a-Co^{2+} complex and release 2a, signifying the strong coordination interaction with Co^{2+} (Fig. 3.6 b).

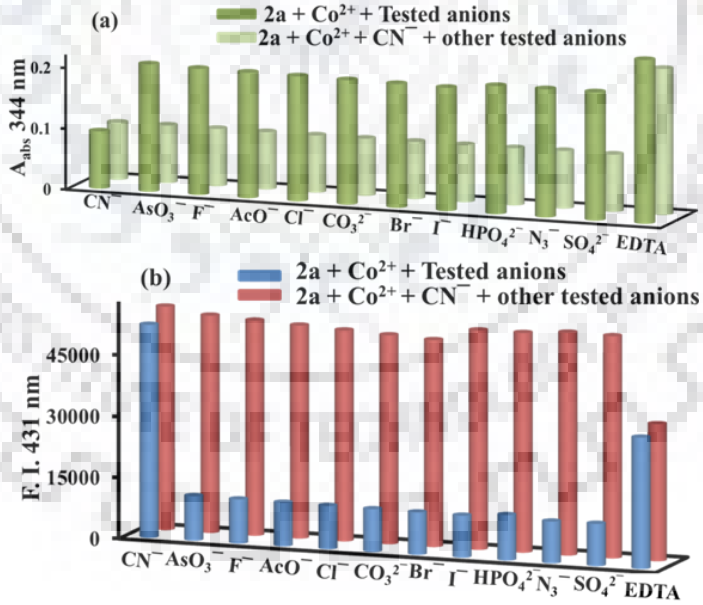

Fig. 3.6 Interaction of 2a-Co^{2+} complex with 20 eq. of anions; (a) Absorption spectra (b) Emission spectra in H_2O-DMF (1:9 v/v, pH-7.4 HEPES buffer).

The binding affinity of 2a-Co^{2+} complex with CN^- was predictable by carrying out titration experiment. Upon progressive addition of CN^- (0-1.4 eq.), the molar absorptive band at 332 nm increasingly shifted towards blue region with

hyperchromic shift at 314 nm. Further addition of CN^- (1.5-3.0 eq.), two new peaks generated at 289 and 274 nm with hyperchromic shift and a clear isosbestic point at 324 nm was appeared (Fig. 3.7). Thus the first CN^- axially coordinated to metal complex and from less stable square pyramidal state. Such structural variation would be responsible for second CN^- as a guest on the opposite face and formed stable hexa-coordinated state.

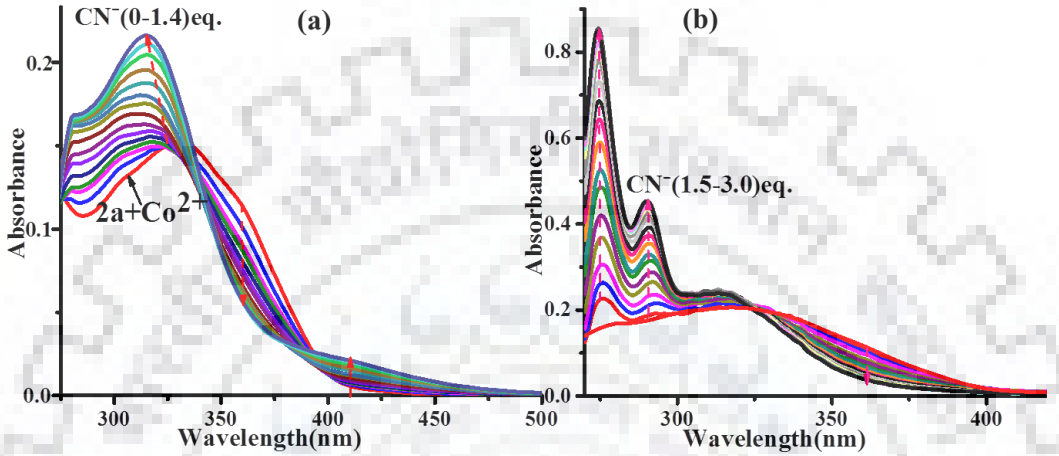

Fig. 3.7 Absorption titration spectra of 2a-Co^{2+} complex upon addition of CN^-; (a) 0-1.4 eq (b) 1.5-3.0 eq. in H_2O-DMF (1:9 v/v, pH-7.4 HEPES buffer).

Similarly the emission titration of 2a-Co^{2+} complex when recorded upon incremental addition of CN^-, the weak emission band at 431 nm was intensely enhanced and saturate with 2.6 eq. of CN^- (Fig. 3.8 a). The exceeding results disclose a probable sensing mechanism for the emission turn-on reaction of CN^- with 2a-Co^{2+} complex. In absence of CN^-, 2a-Co^{2+} complex show a weak fluorescence due to PET (photo-induced electron transfer) quenching process between the chromone and the coordinated Co^{2+} metal ion [26-28]. Upon axial coordination of CN^- would modify the energy level of 2a-Co^{2+} complex, consequently inhibit the PET quenching, thus notable a significant fluorescence enhancement. The reaction time of 2a-Co^{2+} complex was examined with 2 eq. of CN^- and observed the emission spectral changes (431 nm) at regular time interval. The kinetic result displayed that there is no fluorescence enhancement after 40 second, thus the reaction is accomplished within 40 second (Fig. 3.8 b). Job's Plot study discloses the 1:2 binding stoichiometry between the 2a-Co^{2+} complex and CN^- (Fig. 3.8 c).

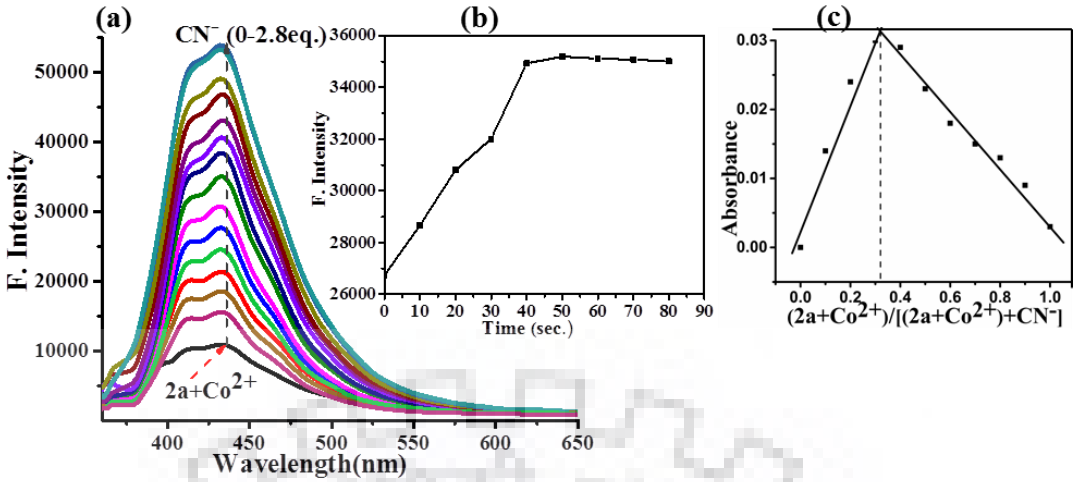

Fig. 3.8 (a) Emission titration spectra (b) Kinetic study (c) Jobs plot between 2a-Co^{2+} complex and CN^- in H_2O-DMF (1:9 v/v, pH-7.4 HEPES buffer).

The binding constants were intended by using B.H. equation and found to be K_{1ab} = 3.3 × 10^4 M^{-1}, K_{2ab} = 8.55 × 10^3 M^{-1} (Fig. 3.9 a, b) and K_{em} = 7.51 × 10^{10} M^{-2} (Fig. 3.9 c).

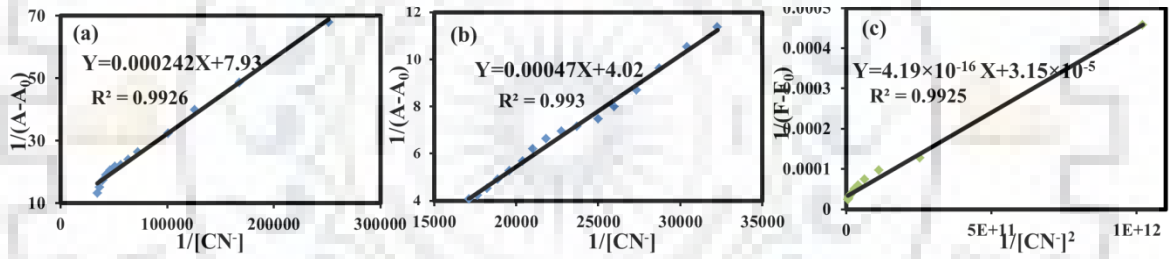

Fig. 3.9 Benesi-Hilderbrand Plot for the binding constant of 2a-Co^{2+} complex towards CN^- absorbance spectra; (a) (0-1.4) eq. CN^- (b) (1.4-3.0) eq. CN^-& (c) emission spectra.

Limit of detection (LOD) was estimated by (3σ/m) where, *σ* illustrates the standard deviation for the blank solution of 2a-Co^{2+} and *m* calibration sensitivity for CN^- and found to be 0.12 μM (Fig. 3.10).

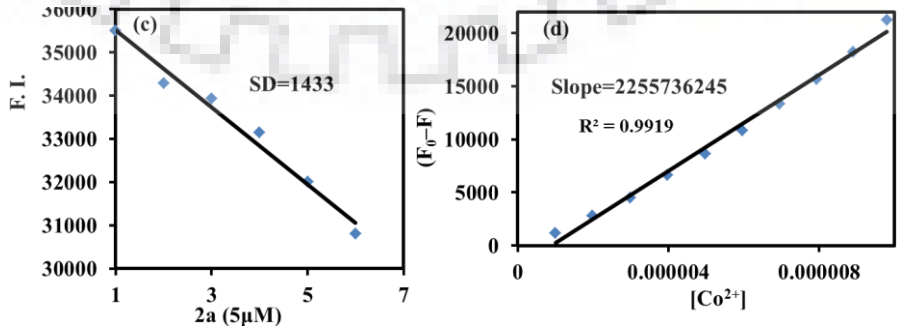

Fig. 3.10 (a) Calibration curve for 2a-Co^{2+} complex (b) Calibration sensitivity for CN^- in H_2O-DMF (1:9 v/v, pH-7.4 HEPES buffer).

3.3.3 Possible Binding Interaction of receptor 2a with Co^{2+}

We have examined the ^1H NMR spectra of 2a with Co^{2+} and found that the hydroxyl group (δ = 15.83 ppm) is totally disappeared, accompanied by a downfield shift of aromatic proton, since the cationic species induces a diamagnetic deshielding due to the complexation process (Fig. 3.11). This result demonstrated that Co^{2+} bind with deprotonated oxygen and immine nitrogen, not with carbonyl oxygen and pyrimidine nitrogen atom.

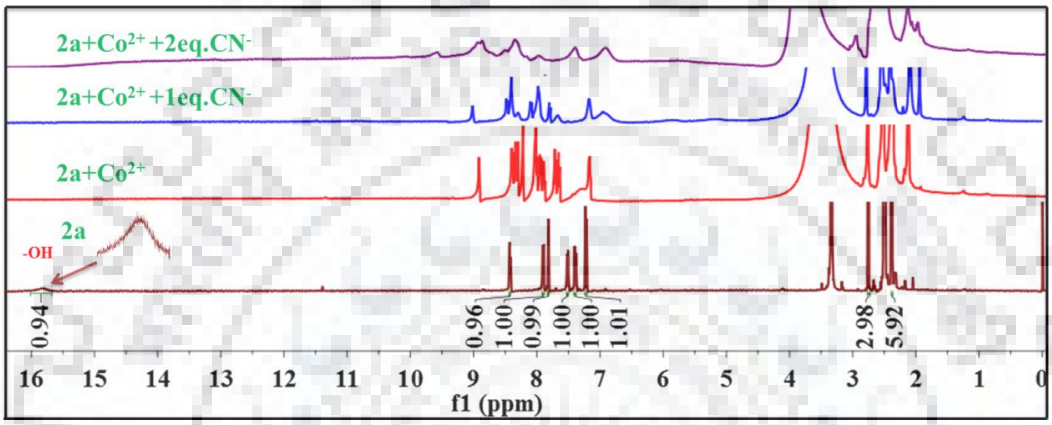

Fig. 3.11 ^1H NMR spectra of 2a-Co^{2+} complex and 2a-Co^{2+}-CN^- complex.

Further the FT-IR spectrum of 2a shown the characteristic stretching absorption at 3431 cm^{-1} (-OH), 1699 cm^{-1} (C=O) and 1631 (C=N) cm^{-1}. Upon interaction with Co^{2+}, the band at 1631 cm^{-1} shifted to 1561 cm^{-1} with the disappearance of band 3431 cm^{-1}. No substantial change was detected at 1699 cm^{-1} (Fig. 3.12).

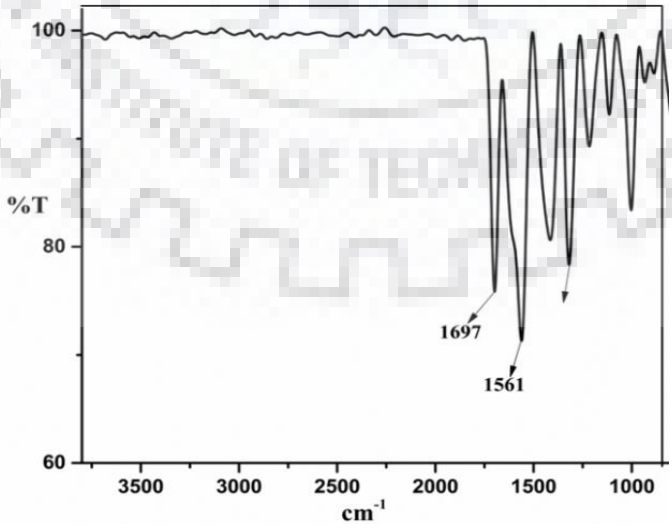

Fig. 3.12 IR spectrum of 2a-Co^{2+} complex.

The mass spectrum of 2a-Co^{2+} complex shown a 2:1 binding mode *via* coordination bond, which exhibited a peak at m/z 674.2 (cald- 674.15) results to [(2×2a)+Co^{2+}-2H+H] (Fig. 3.13).

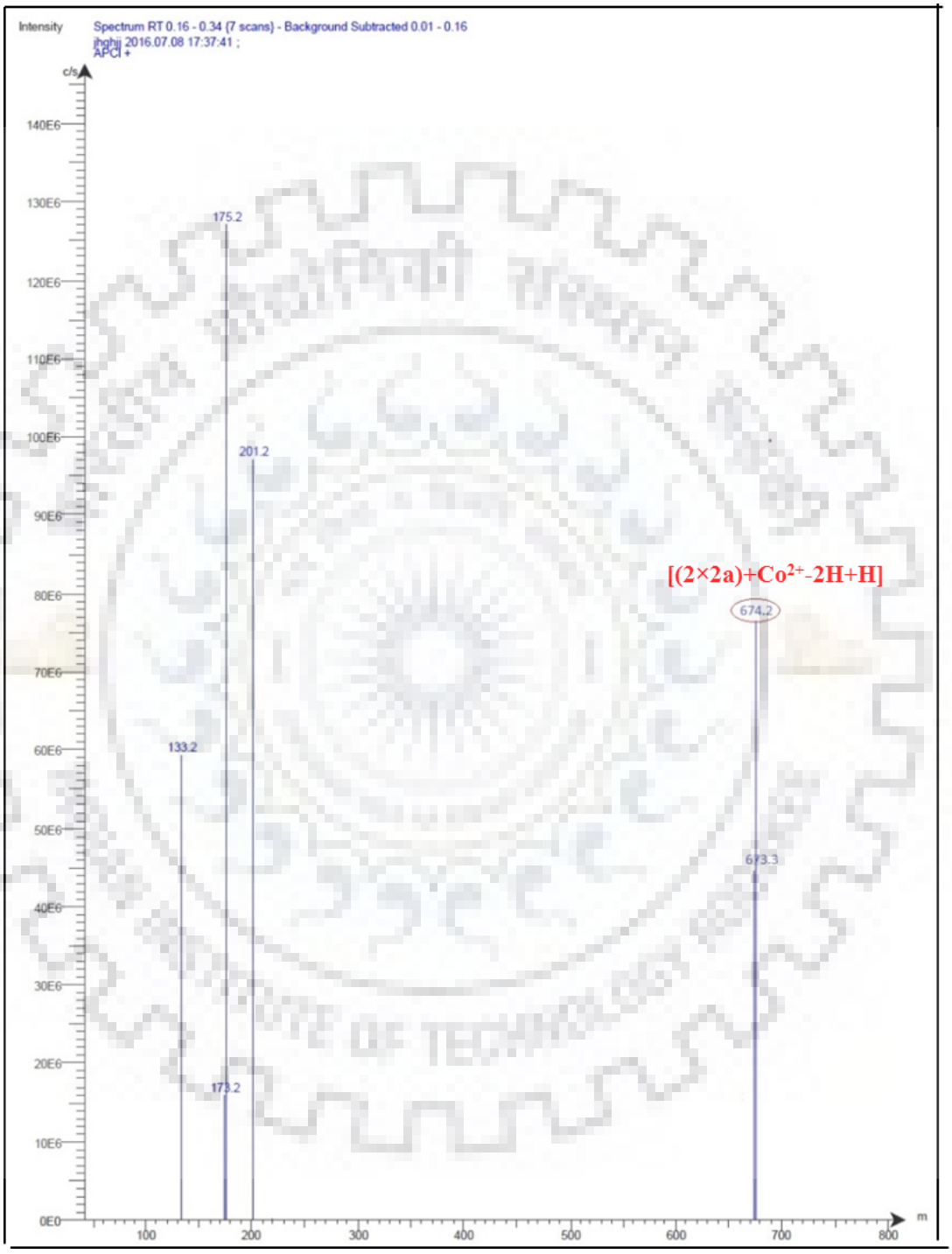

Fig. 3.13 Mass spectrum of 2a-Co^{2+} complex.

To confirm the participation of adjacent pyridinium nitrogen in the complexation process with Co^{2+}, a control study was also performed with 2b in which pyridinium

nitrogen is absent. Absorbance and emission titration experiment of 2b with Co^{2+} displayed similar result as 2a Therefore, it can be determined that pyridinium nitrogen doesn't take part in the complexation process (Fig. 3.14).

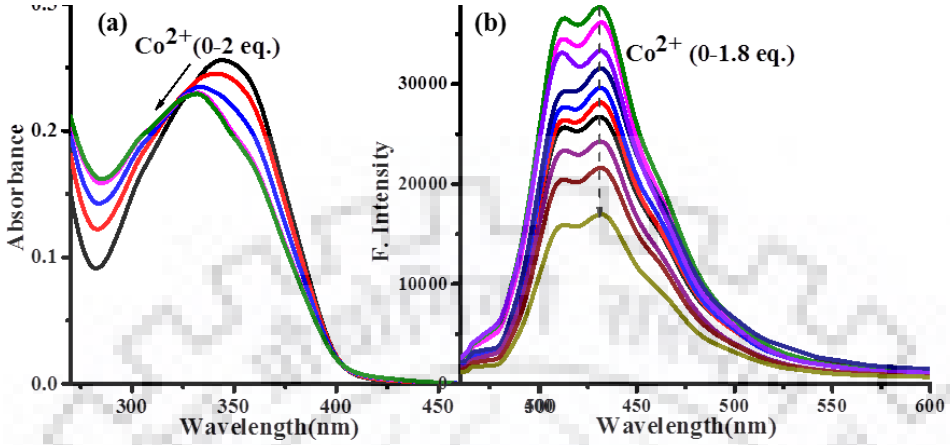

Fig. 3.14 (a) Absorption titration spectra (b) Emission titration spectra of 2b upon addition of Co^{2+} in H_2O-DMF (1:9 v/v, pH-7.4 HEPES buffer).

3.3.4 Possible Binding Interaction of 2a-Co^{2+} Complex with CN^-

Additionally, the ^1H NMR spectra of 2a-Co^{2+} complex also displayed broadening of all peak upon interaction with CN^- due to conversion of paramagnetic hexa-coordinate state from square planner state (Fig. 3.11). Upon interaction with CN^- with 2a-Co^{2+} complex, band at 1697 and 1561 cm^{-1} shifted to 1685 and 1552 cm^{-1} with generation of new peak at 2217 cm^{-1} which is characteristic stretching absorption peak to CN^- in the FT-IR spectrum (Fig. 3.15).

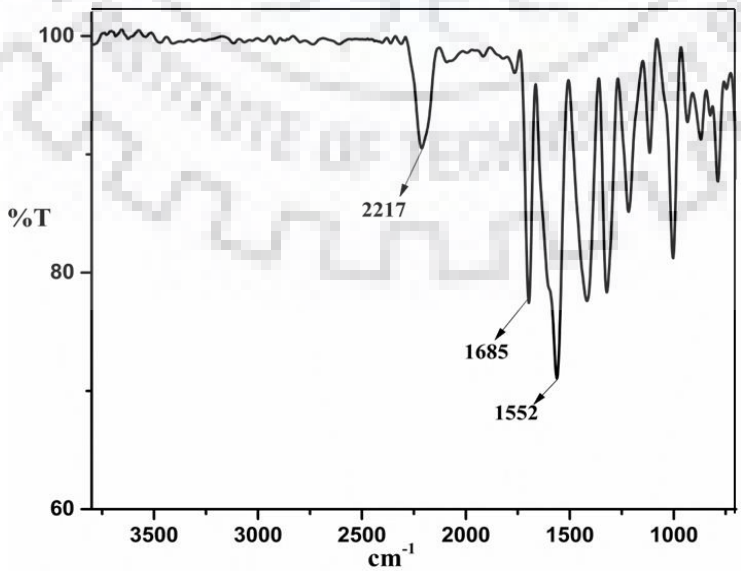

Fig. 3.15 IR spectrum of 2a-Co^{2+}-CN^- complex.

Moreover, the mass spectrum of 2a-Co^{2+} complex with CN^{-} shown a 1:2 binding coordination, which displayed a peak at m/z 725.2 (cald-725.16) corresponding to [(2×2a)+Co^{2+}-2H+2CN] (Fig. 3.16). Therefore, we can determine that the binding of Co^{2+} is very tight with 2a and avoids adverse absorption and emission changes of 2a due to de-metalation.

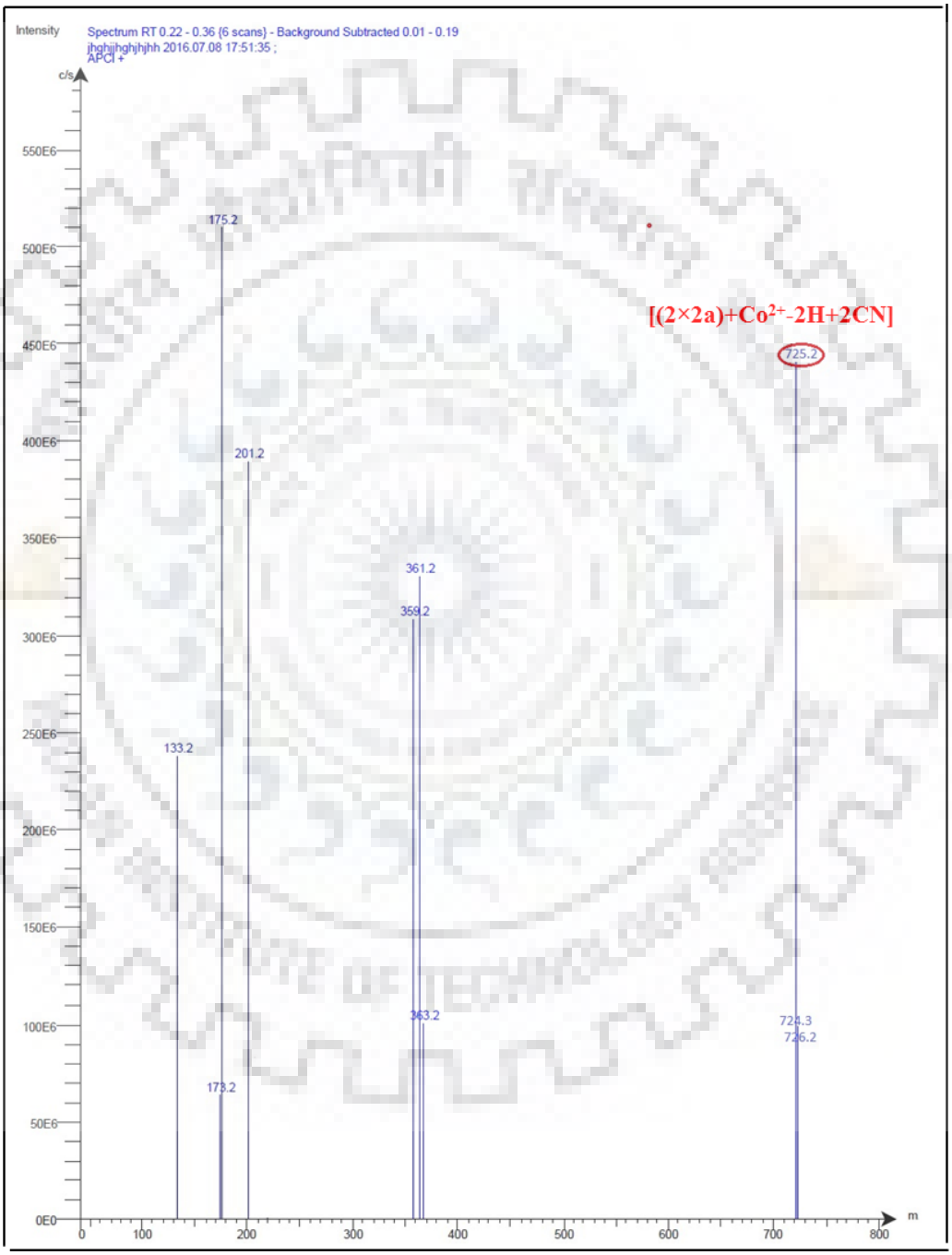

Fig. 3.16 Mass spectrum of 2a-Co^{2+}-CN^{-} complex.

3.3.5 Electrochemical Studies

However, the electrochemical study of 2a is significance, which would be accountable for the suggested binding interaction of Co^{2+} and CN^{-}. It can be seen that without Co^{2+}, there is no formation of redox peak in 2a (red line), on the other hand, the presence of Co^{2+}, the conductivity of the electrode increases and can be described as that the complex has electrochemically active Co^{2+} and functional groups of 2a (magenta line). After addition of CN^{-}, it is possible to observe a new peak at -0.218 V signifying the incidence of new oxidized species and increases the current which can be explained that the electrochemical metallic center is highly liable to interact with CN^{-} (electron donors) *via* coordination bond $Co^{2+}\leftarrow CN^{-}$ (Fig. 3.17). A probable clarification for the sensor reaction is based on the fact that the cobalt, nickel and iron type transition elements form stable complexes with CN^{-} due to formation of d–p bonds by using their d orbital, moreover coordinated ligation σ of $M\leftarrow CN^{-}$ [40].

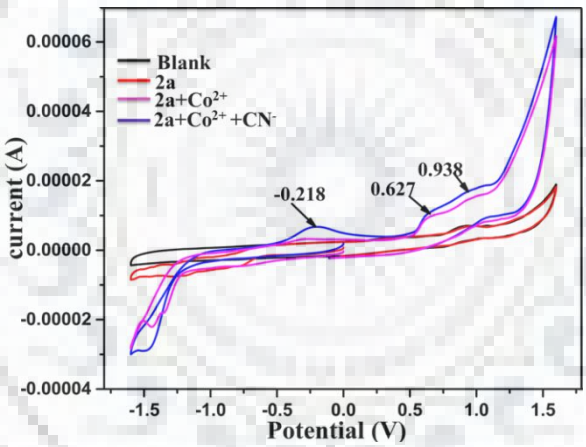

Fig. 3.17 Cyclic Voltammograms of 2a with Co^{2+} and CN^{-} in H_2O-DMF (1:9 v/v, pH-7.4 HEPES buffer).

All the exceeding results reveal a possible sensing mechanism for Co^{2+} and CN^{-} as shown in Scheme 3.2.

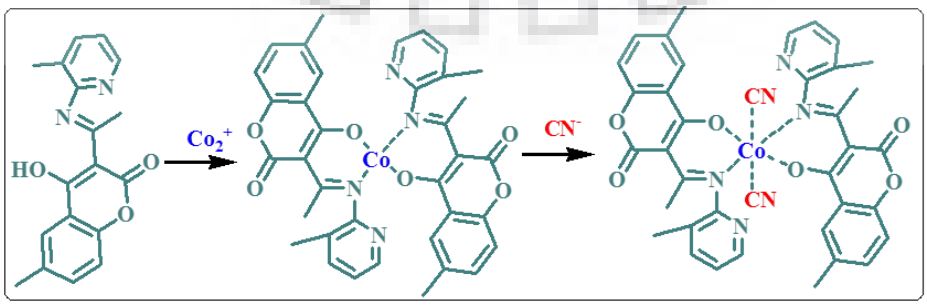

Scheme: 3.2 Suggested sensing mechanism of 2a with Co^{2+} and 2a-Co^{2+} complex with CN^{-}.

3.3.6 Real Sample Analysis of CN^-

For a practical study of 2a-Co^{2+} complex was executed in real water sample for CN^- by spiking a known CN^- concentration in deionized water, river water of Roorkee and tap water. Firstly the unsolvable materials of water samples were discarded by 0.22 mm membrane filter paper and spiked CN^- analyte at the optimum contact time and pH conditions. These prepared water samples were used as a solvent component with DMF (10%). The results are shown in terms of % recovery for CN^- (Table 3.1). The regaining values reveal the potential of 2a-Co^{2+} complex as detection of concerned ion (CN^-) in real samples.

Table: 3.1 Recovery analysis of spiked CN^- concentration in different water samples.

Spiked Conc. (μM)	Deionized water		River water		Tap water	
	Found (μM)	Recovery[a] (%)	Found (μM)	Recovery[a] (%)	Found (μM)	Recovery[a] (%)
0.00	0.01		0.06		0.02	
10	10.00	100 ± 1.2	10.16	101.6 ±2.4	10.05	100.5 ±3.8
20	19.98	99.9 ± 2.1	20.26	101.3 ±3.1	20.08	100.4 ±1.9

[a]Mean value ± standard deviation (triplicate measurements)

3.3.7 Optical Logic Circuit Devices

In direction to execute the logic setups, the presence and absence of Co^{2+} and CN^- were deliberated as input 1 and 0 respectively on emission mode. In the prevailing system, the fluorescence intensity at 431 nm is consigned as the "ON" state (output = 1), while the weak fluorescence intensity as the "OFF" state (output = 0). For threshold value 70% maximum fluorescence intensity of 2a (21000 au) has been taken [41-42]. The fluorescence intensity beyond the threshold level is documented in the presence (1, 1) and absence (0, 0) of both inputs. These results simply form the IMPLICATION logic gate. The working principle of the IMPLICATION logic gate is outlined in Fig. 3.18.

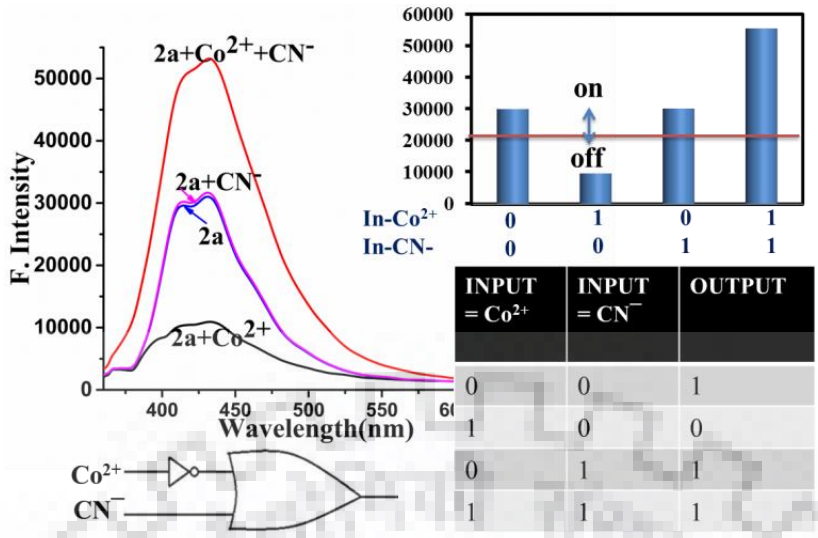

INPUT = Co^{2+}	INPUT = CN^-	OUTPUT
0	0	1
1	0	0
0	1	1
1	1	1

Fig. 3.18 Alteration in emission spectra and output intensities (bar chart) of 2a with Co^{2+} and CN^- as chemical inputs; Truth table designates IMPLICATION logic gate.

3.3.8 Application as Antimicrobial Studies of 2a and 2a-Co^{2+} complex

Antibacterial activity of 2a and 2a-Co^{2+} complex were premeditated *via* disk diffusion method against Gram +ve *Brevibacillus brevis*, *Staphylococcus aureos* and Gram -ve *Pseudomonas diminuta* bacterial strains. The sterilized petri dish of agar plates was equipped by using nutrient agar and kept at 37ºC. The platinum wire loop was used for inoculation process. The disk (prepared by Whatman filter paper, 4 mm diameter) was dipped in a solution of DMF, 2a and 2a-Co^{2+} complex solution and dried. Kept disk on bacterial growth plate and measured inhibition zone after 24 h. A clear inhibition zone was observed even at lower concentrations (MIC: 1.5 mg mL^{-1}) due to heterocycle moiety, while the inhibition zone of 2a-Co^{2+} complex are high due to metal activity (Fig. 3.19). Similarly antifungal activity of 2a and 2a-Co^{2+} complex was examined against *Bipolaris oryzae* (MTCC3717) strains by using the agar well diffusion method [43-44] on potato dextrose agar (PDA) medium. The mycelium of test fungi was inoculated in the middle of petri plates. Now made 6 mm wells in each plate with the help of sterile cork borer. After inoculation, the plates were suitably enclosed, labelled and kept at 37 °C for 3 days and monitored the % inhibition growth with reference (Table 3.2).

Table: 3.2 List of bacterial strains used for antimicrobial activity test.

Con. (μg L^{-1})	Microorganism	Type	% inhibition with reference
1.5, 2a	*Staphylococcus aureos*	Gram positive bacteria	67
1.5, 2a-Co^{2+}	*Staphylococcus aureos*	Gram positive bacteria	74
1.5, 2a	*Brevibacillus brevis*	Gram positive bacteria	92
1.5, 2a-Co^{2+}	*Brevibacillus brevis*	Gram positive bacteria	98
1.5, 2a	*Pseudomonas diminuta*	Gram negative bacteria	94
1.5, 2a-Co^{2+}	*Pseudomonas diminuta*	Gram negative bacteria	97
1.5, 2a	*Bipolaris oryzae*	Fungal strain	31
1.5, 2a-Co^{2+}	*Bipolaris oryzae*	Fungal strain	40

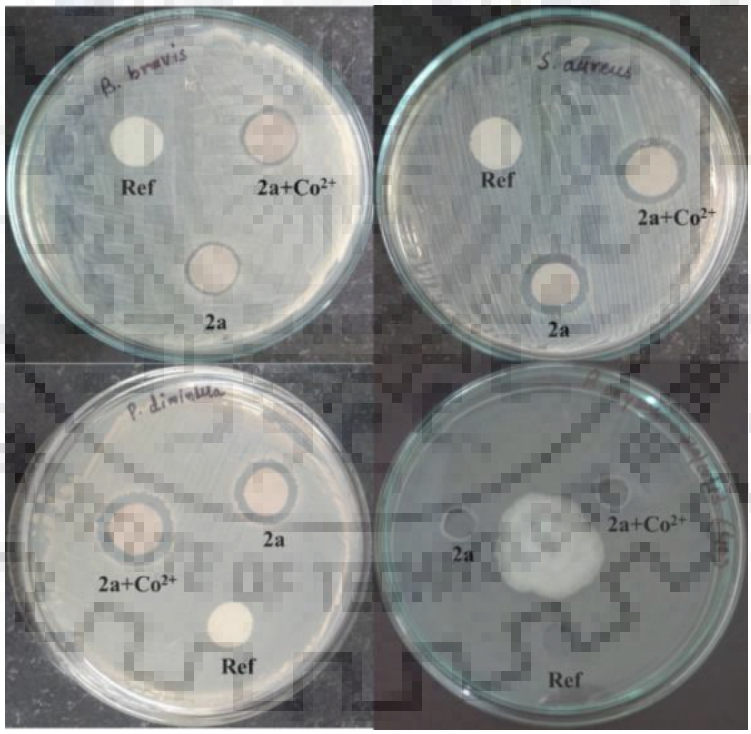

Fig. 3.19 Antimicrobial activity of 2a and 2a-Co^{2+} complex against *B. brevis, S. aureos, P. diminuta* bacterial strain and *B. oryzae* fungal species.

3.3.9 Comparative Studies

Some metal-coordinated CN^{-} chemosensors have been synthesized by several metals with various groups as shown in Table 3.3. An analysis of all chemosensors in

terms of their stoichiometry, binding constant and LOD, it has been noticed that our receptor has high binding constant and low LOD with 1:2 stoichiometry.

Table: 3.3 Comparison of some reported complexation based CN^- sensors to present work.

Previous literature	Metal-complex	Stoichiometry	Binding Constant	LOD
Org. Lett. 12 (2010) 764-767 (ref. 23)	Coumarinylsalen based Co (II) Complex	1:2	$K_1= 10^7\ M^{-1}$ $K_2= 4\times10^5\ M^{-1}$	
Chem. Commun. 51 (2015) 7486-748 (ref. 24)	Porphyrin based Ni (II) Complex	1:2	$2.4\times10^4\ M^{-1}$ $6.8\times10^4 M^{-1}$	
Sens. Actuators, 237 (2016) 470-478 (ref. 26)	Calix-naph-based Cu (II) Complex	1:2	$4.6\times10^8\ M^{-2}$	0.34 μM
Chem. Commun. 48 (2012) 2095-2097 (ref. 27)	Diarylethenes based Cu (II) Complex	1:1		0.225 μM
J. Mater. Chem. 22 (2012) 1747-1750 (ref. 28)	Rhodamine based Cu II) Complex	1:2		0.14 μM
Inorg. Chem. 48 (2009) 1272-1274 (ref. 45)	Corrinoids based Co (II)Complex	1:1	$1.2\times10^5 M^{-1}$	10 μM
Present work	Chromene-py based Co (II) Complex	1:2	$7.51\times10^{10} M^{-2}$	0.12 μM

3.4 CONCLUSION

Novel chromone moiety based receptor 2a was synthesized, which is especially selective for Co^{2+} in 2:1 binding mode. Further the *in-situ* complex is able to distinguish for CN^- in the presence of other co-existing ions with 1:2 binding mode and 0.12 μM LOD. The system applied as logic gates at 431 nm by emission spectrum. Further 2a and 2a-Co^{2+} complex were found to be active towards some bacterial and fungal strains.

References

1. G. Liu, W. Cai, L. Kong, G. Duan, Y. Li, J. Wang, Z. Cheng, Trace detection of cyanide based on SERS effect of Ag Nano plate-built hollow microsphere arrays, J. Hazard. Mater. 248 (2013) 435-441.
2. M. A. Acheampong, R. J. W. Meulepasa, P. N. L. Lens, Removal of heavy metals and cyanide from gold mine wastewater, J. Chem. Technol. Biotechnol. 85 (2010) 590-613.
3. J. O. Marsden, C. I. House, Littleton, CO, The Chemistry of Gold Extraction; 2006.
4. F. J. Baud, Cyanide: critical issues in diagnosis and treatment, Toxicology 26 (2007) 191-201.
5. H. B. Leavesley, L. Li, K. Prabhakaran, J. L. Browitz, G. E. Isom, Interaction of cyanide and nitric oxide with cytochrome c oxidase: implications for acute cyanide toxicity, Toxicol. Sci. 101 (2008) 101-111.
6. U. S. Food and Drug Administration (FDA): FDA News Release, 2006; ht tp://www.fda.gov/NewsEvents/Newsroom/ Press Announcements/2006/ucm 108807.html (accessed April 2012).
7. S. I. Baskin, T. G. Brewer, Cyanide poisoning, in medical aspects of chemical and biological warfare, Washington, DC (1997) 271-286.
8. R. A. Greenfield, B. R. Brown, J. B. Hutchins, J. J. Iandolo, R. Jackson, L. N. Slater, M. S. Bronze, Microbiological, biological, and chemical weapons of warfare and terrorism, Am. J. Med. Sci. 323 (2002) 326-340.
9. J. Jo, A. Olasz, C. H. Chen, D. Lee, Interdigitated hydrogen bonds: electrophile activation for covalent capture and fluorescence turn-on detection of cyanide, J. Am. Chem. Soc. 135 (2013) 3620-3632.
10. M. Shahid, A. Misra, A simple and sensitive intramolecular charge transfer fluorescent probes to detect CN^- in aqueous media and living cells, Anal. Methods 5 (2013) 434-437.
11. L. Yuan, W. Lin, Y. Yang, J. Song, J. Wang, Rational design of a highly reactive; ratiometric fluorescent probe for cyanide, Org. Lett. 13 (2011) 3730-3733.
12. N. Maurya, A. K. Singh, "Turn-on" fluorescence chemodosimeter for CN^- by activated Michael acceptor possessing different polar substituents: reduced ICT-based signal transduction, Sens. Actuators, B 245 (2017) 74-80.

13. A. Dwivedi, P. Rajakannu, M. Ravikanth, meso-Salicylaldehyde substituted BODIPY as a chemodosimetric sensor for cyanide anions, Dalton Trans. 44 (2015) 4054-4062.
14. C. Chakraborty, M. K. Bera, P. Samanta, S. Malik, Selective detection of cyanide by a polyfluorenebased organoboron fluorescent chemodosimeter, New J. Chem. 37 (2013) 3222-3228.
15. K. Y. Ryu, J. J. Lee, J. A. Kim, D. Y. Park, C. Kim, Colorimetric chemosensor for multiple targets, Cu^{2+}, CN^{-} and S^{2-}, RSC Adv. 6 (2016) 16586-16597.
16. J. H. Hu, J. B. Li, J. Qi, Y. Sun, Selective colorimetric and ''turn-on'' fluorimetric detection of cyanide using an acylhydrazone sensor in aqueous media, New J. Chem. 39 (2015) 4041-4046.
17. A. Kumar, H. S. Kim, A pyrenesulfonyl-imidazolium derivative as a selective cyanide ion sensor in aqueous media, New J. Chem. 39 (2015) 2935-2942.
18. M. R. Ajayakumar, P. Mukhopadhyay, Single-electron transfer driven cyanide sensing: a new multimodal approach, Org. Lett. 12 (2010) 2646-2649.
19. M. R. Ajayakumar, K. Mandal, K. Rawat, D. Asthana, R. Pandey, A. Sharma, S. Yadav, S. Ghosh, P. Mukhopadhyay, Single electron transfer-driven multi-dimensional signal read-out function of TCNQ as an "off-the-shelf" detector for cyanide, Appl. Mater. Interfaces, 5 (2013) 6996-7000.
20. C. R. Maldonado, A. T. Varela, A. C. Jones, J. C. M. Rivas, A turn on fluorescence sensor for cyanide from mechanochemical reactions between quantum dots and copper complexes, Chem. Commun. 47 (2011) 11700-11702.
21. A. T. Varela, E. I. Stevenson, J. A. G. Gasion, D. T. F. Dryden, J. C. M. Rivas, Selective turn-on fluorescence detection of cyanide in water using hydrophobic CdSe quantum dots, Chem. Commun. 17 (2008) 1998-2000.
22. C. F. Chow, M. H. W. Lam, W. Y. Wong, A hetero-bimetallic ruthenium(II)-copper(II) donor-acceptor complex as a chemodosimetric ensemble for selective cyanide detection, Inorg. Chem. 43 (2004) 8387-8393.
23. J. H. Lee, A. R. Jeong, I. S. Shin, H. J. Kim, J. I. Hong, Fluorescence turn-on sensor for cyanide based on a cobalt (II)-coumarinylsalen complex, Org. Lett. 12 (2010) 764-767.
24. K. I. Hong, H. Yoon, W. D. Jang, A triazole-bearing picket fence type nickel porphyrin as a cyanide selective allosteric host, Chem. Commun. 51 (2015) 7486-7488.

25. J. L. Worlinsky, S. Halepas, C. Brückner, PEGylated meso-arylporpholactone metal complexes as optical cyanide sensors in water, Org. Biomol. Chem. 12 (2014) 3991-4001.
26. M. Shahid, H. M. Chawla, P. Bhatia, A calix[4]arene based turn off/turn on molecular receptor for Cu^{2+} and CN^{-} ions in aqueous medium, Sens. Actuators, B 237 (2016) 470-478.
27. Q. Zou, X. Li, J. Zhang, J. Zhou, B. Sun, H. Tian, Unsymmetrical diarylethenes as molecular keypad locks with tunable photochromism and fluorescence *via* Cu^{2+} and CN^{-}, Chem. Commun. 48 (2012) 2095-2097.
28. Y. Liu, X. Lv, Y. Zhao, J. Liu, Y. Q. Sun, P. Wang, W. Guo, A Cu (II)-based chemosensing ensemble bearing Rhodamine B fluorophore for fluorescence turn-on detection of cyanide, J. Mater. Chem. 22 (2012) 1747-1750.
29. J. Emerit, C. Beaumont, F. Trivin, Iron metabolism, free radicals and oxidative injury, Biomed. Pharmacother. 55 (2001) 333-339.
30. S. Y. Chung, S. W. Nam, J. Lim, S. Park, J. Yoon, A highly selective cyanide sensing in water via fluorescence change and its application to *in-vivo* imaging, Chem. Commun. 20 (2009) 2866-2868.
31. H. S. Jung, P. S. Kwon, J. W. Lee, J. Kim, C. S. Hong, J. W. Kim, S. Yan, J. Y. Lee, J. H. Lee, T. Joo, J. S. Kim, Coumarin-derived Cu^{2+} selective fluorescence sensor: synthesis, mechanisms and applications in living cells, J. Am. Chem. Soc. 131 (2009) 2008-2012.
32. K. H. Jung, K. H. Lee, Efficient ensemble system based on the copper binding motif for highly sensitive and selective detection of cyanide ions in 100% aqueous solutions by fluorescent and colorimetric changes, Anal. Chem. 87 (2015) 9308-9314.
33. C. H. Tung, Q. Z. Yang, A colorimetric and fluorometric dual-modal chemosensor for cyanide in water, Sens. Actuators, B 168 (2012) 14-19.
34. L. Tang, M. Cai, A highly selective and sensitive fluorescent sensor for Cu^{2+} and its complex for successive sensing of cyanide *via* Cu^{2+} displacement approach, Sens. Actuators, B 173 (2012) 862-867.
35. N. Maurya, S. Bhardwaj, A. K. Singh, Selective colorimetric and fluorescence 'turn-on' sensor for Ag^{+} and *in-situ* sensing of CN^{-} (off-on-off) *via* displacement approach, Mater. Sci. Eng., C 74 (2017) 55-61.

36. S. Bhardwaj, N. Maurya, A. K. Singh, R. Varshney, P. Roy, Promising ESIPT-based fluorescence sensor for Cu^{2+} and CN^{-} ions: investigation towards logic gate behaviour, anticancer activities and bioimaging application, RSC Adv. 6 (2016) 102096-102101.
37. G. S. Al, E. Abdullah, R. Gogary, Synthesis and photooxygenation of fluro[3,2-c] coumarin derivatives as antibacterial and DNA intercalating agent, Chin. J. Chem. 30 (2012) 316-320.
38. M. M. Heravi, S. Khaghaninejad, M. Mostofi, Peckmann reaction in the synthesis of coumarin derivatives, Adv. Heterocycl Chem. 112 (2014) 1-50.
39. H. A. Benesi, J. H. Hildebrand, A spectrophotometric investigation of the interaction of iodine with aromatic hydrocarbons, J. Am. Chem. Soc. 71 (1947) 2703-2707.
40. E. C. Figueira, L. C. S. Neres, M. R. S. Ruy, G. F. Troianod, M. D. P. T. Sotomayor, Development of a biomimetic sensor for selective identification of cyanide, Anal. Methods 8 (2016) 6353-6360.
41. A. Misra, P. Srivastava, M. Shahid, Fluorescent probe mimicking multiple logic gates and a molecular keypad lock upon interaction with Hg^{2+} and bovine serum albumin, Analyst 137 (2012) 3470-3478.
42. P. Srivastava, S. S. Razi, R. Ali, R. C. Gupta, S. S. Yadav, G. Narayan, A. Misra, Selective naked-eye detection of Hg^{2+} through an efficient turn-on photoinduced electron transfer fluorescent probe and its real applications, Anal. Chem. 86 (2014) 8693-8699.
43. W. H. Hegazy, Synthesis of organometallic-based biologically active compounds: *in-vitro* antibacterial and antifungal of asymmetric ferrocene-derived Schiff-bases chelates, Int. Res. J. Pure Appl. Chem. 2 (2012) 170-182.
44. M. Balouirin, M. Sadiki, S. K. Ibnsouda, Methods for *in-vitro* evaluating antimicrobial activity: A review JPA 6 (2016) 71-79.
45. C. M. Croisé, F. Zelder, Side chains of cobalt corrinoids control the sensitivity and selectivity in the colorimetric detection of cyanide, Inorg. Chem. 48 (2009) 1272-1274.

CHAPTER 4

Nucleophilic Addition Based Cyanide Sensor

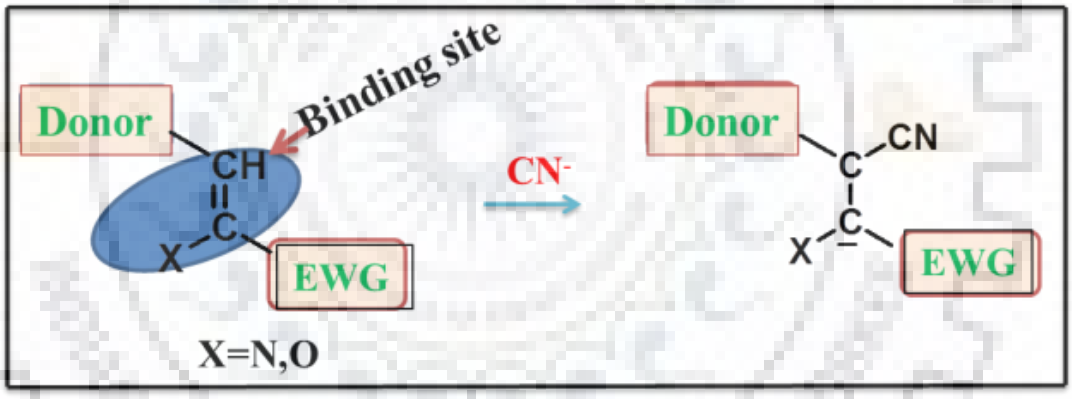

4.1 INTRODUCTION

Many anions such as sulfate, phosphate and carboxylate are vital for biological functions [1-2], while CN^- is exceptionally hazardous. CN^- salts are extensively employed in the enormous organic synthesis, electroplating, gold extraction, metallurgy, paper industries etc. [3-4]. Conversely, this relates severe hazardous leaking into the environment. CN^- is actual inhibitor for the non-metallo enzymes and metallo enzymes [5-6]. The harmful mechanism is interrelated to their strong binding affinity with haem units of cytochrome c oxidase, thus interrupting the electron transport chain of mitochondria and causes cellular asphyxiation [7-8]. CN^- increases Ca^{2+} concentration within the cell, consequently, increases the level of ROS (reactive oxygen species), which obstruct antioxidant defense system [9-10]. The disastrous concentration of CN^- among the blood of fire fatalities has been recommended to be between 23-26 mM [11-12]. The lower limit of CN^- in drinking water is 1.9 μM, as recognized by World Health Organization [13]. Hence, the development of selective and effective receptor is essential for CN^- detection.

A number of devices have been used to discriminate CN^- through various investigation techniques. Amongst these, the colorimetric and fluorimetric techniques are most attractive methodology and innovative attentions for CN^- sensors, which consent the optical recognition *via* color variation without resorting to the consumption of instruments [14-19]. CN^- sensitive molecular receptors, recognized by the nucleophilic addition reaction (on activated carbon-heteroatom/carbon double bond [20-27], CdSe quantum dots [28-29], boron derivatives [30-31]), a stable metal CN^- complex (displacement analyse) [32-35] and hydrogen bonding interaction with proton donating receptors [36-37]. However, the hydrogen bonding method has poor selectivity and suffers from $H_2PO_4^-$, AcO^- and F^- interference anions [38-39]. Other receptor for CN^- are based on strong coordination ability with transition metal, such as Cu (II) [40-43], Co (II) [44-45], Zn/Ni (II) [46-47] complex, but they only accessible an indirect way for CN^- detection.

Consequently, when pick out a receptor for the objective anions, the geometry and shape should be sensibly accountable and the finest counterpart with receptor to get high selectivity. Due to excellent nucleophilicity of CN^-, chemodosimeter have materialized way in the research area of momentous significance. The

chemodosimetric methodology includes the use of a precise irreversible chemical response instigated by the analyte that are combined with spectral or color variation. The nucleophilic addition on α-β unsaturated C=O group by CN^- of a suppressed chromophore with formation of adduct having different emission/absorption spectra. The productivity of reaction rate can pointedly be enhanced by electron-withdrawing substituent which stabilizes the negative charge of adduct. Additionally the electron donating groups present on donor site appropriate for ICT (intramolecular charge transfer). Recently, reaction-based receptor between the nucleophilic CN^- and attuned electrophilic center are used, which assist the design of appreciation system for analyte-specific reaction and interference reduction in solvent system. For the CN^- specific reaction, pyrylium [14], oxazines [48], dicyanovinyl [24, 49], salicylaldehyde and tri-fluoroacetamide derivatives [50-51] are used previously. The C-O bond of spiropyran shows individual color change upon reaction with ionic species is feasible, unusual for CN^- sensing in addition their electrical and optical memory devices. An exposure of light, the closed SP (spiropyran) form converts itself into open MC (merocyanine) form, which can be abused to bind for CN^- due to the development of negative charge and alters the spectral variation [52-54].

In this work, 2-methoxy naphthalene unit is selected as a donor site for L1 and L2. To efficiently influence of ICT process, sensibly placed different electron-withdrawing substituents (-C=O, -COOH and -CN groups) at α-carbon of unsaturated -C=C group, which operate as an internal activating group for CN^- attack. Further, we designed indoline-chromone based compound L3/L4, (due to its biological importance) as a green-emitting receptors toward CN^-, in which the indoline group act as reaction site and chromone as signalizing unit. As the C-2 atom of indoline is an effective and easily combine object for the nucleophilic attack of CN^- and the intramolecular conformational variations will alter the ICT (intramolecular charge transfer) transition, prompting a significant change in emission, absorption, NMR spectra and redox property of receptors. Moreover the synthesized receptor shows antimicrobial activity.

4.2 EXPERIMENTAL SECTION

4.2.1 Chemical and Instrumentation

All reagents and solvents for experimental work were taken from Sigma-Aldrich. DMF and ACN solvents were dried with the help of $CaCl_2$ as drying agent and then stored on molecular sieve after distillation process (under reduced pressure). CHNS

(carbon, hydrogen, nitrogen, sulfur) elemental analysis was supported by using a vireo MICROV3.1.1. IR spectra were recorded with Perkin Elmer FT-IR 1000 spectrophotometer (KBr as solid film). Specord S600 Thermo-Scientific PC double beam spectrophotometer (path length 1 cm) used for absorption spectra and Horiba RF-5301PC (path length 3 cm) used for emission spectra with standard quartz cell. The NMR spectra were recorded in JEOL 400 MHz spectrophotometer by applying tetra-methyl-silane (TMS) as an internal standard. The Cyclic Voltammograms were noted down with a CHI760E Electro analyser three-electrode cell with glassy carbon as the working electrode, $Hg/HgCl_2$ as the reference electrode, Pt wire as the counter electrode and 0.1 M tetrabutylammonium hexafluorophosphate (nBu_4NPF_6) was used as the supporting electrolyte on 0.1V s^{-1} scan rate. Quantum chemistry computation (DFT) was instigated in the Gaussian 09 W program in the gas phase by applying **a** B3LYP/6-31G basis set.

4.2.2 General Procedure for Experiments

1 mM stock solution of receptors were prepared and used for all spectroscopic studies after proper dilution. The absorption spectroscopy was monitored by keeping the receptor concentration at 20 μM, while 5 μM used for emission spectroscopy. The interference investigation was carried out with different co-existing anions with CN^- in 2:1 ratio. The rate constant was calculated under pseudo first-order reaction condition. The slope corresponding to rate constant by a plot between ln $[(A_{max} - A_t) / A_{max}]$, against time t ($A_{max}$ = absorbance at the end of the reaction and A_t = absorbance at time t) [55]. The minimum concentration (LOD) was calculated by the perilously reported method (3σ/slope), where σ is the standard deviation of the blank solution; S is the slope of the calibration curve [36-37]. For electrochemical study, distilled DMF and ACN has been used as solvent and nBu_4NPF_6 as supporting electrolyte on which receptors were dispersed (1 mM) and scan for potential peak (0.1 V s^{-1}, range -2.0 to +2.0 V). Further check the variation in potential peak of L-CN^- complex.

4.2.3 Synthesis and Characterization of Receptors L1 and L2

The synthetic procedure of L1/L2 is authenticated in Scheme 4.1. 1 mmol ethanolic solution of 2-methoxy-1-napthaldehyde and coupling component (1-3

indandione, cyanoacetic acid) was mixed with 2 drops of piperdine base and refluxed (knowengeal condensation). After completion of the reaction mixture (thin layer chromatography monitored) ppt was filtered. Brown color compounds were achieved with 78% yield.

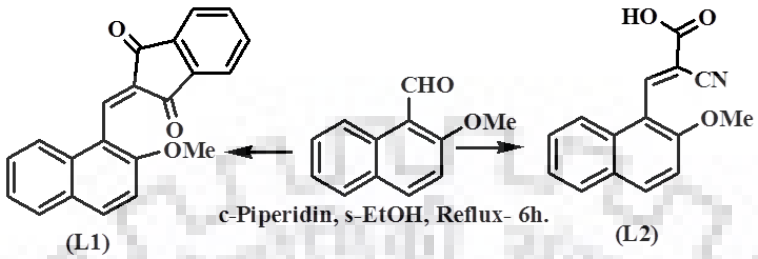

Scheme: 4.1 Synthesis of receptors L1 and L2

L1: 2-((2-methoxynaphthalene-1-yl) methylene)-2H-indene-1-3dione

Anal. Calc. ($C_{21}H_{14}O_3$) : C-80.24, H-4.49, O-15.27; Found : C-80.14, H-4.69; IR (KBr, υ/cm^{-1}) : 2932 (-HC=C-), 1728 (-C=O), 1689 (-C=O); ^{1}H NMR ($CDCl_3$, 400 MHz, δ/ppm) : 8.41 (s, 1H), 8.05 (d, 1H), 7.97 (d, 1H), 7.90 (d, 1H), 7.82-7.73 (m, 4H), 7.47 (t, 1H) 7.38 (t, 1H), 7.32 (d, 1H), 3.95 (s, 3H); ^{13}C NMR ($CDCl_3$, 100 MHz, δ/ppm) : 190.0, 188.1, 157.3, 142.9, 140.7, 138.8, 135.4, 135.1, 133.4, 132.6, 132.4, 128.8, 128.6, 127.6, 124.5, 124.1, 123.7, 123.4, 116.4, 112.4, 56.4; APCI-MS m/z (m+H) = 315.3 (calcd-315.10).

L2: 2-cyano-3-(2-methoxynaphthalene-1-yl) acrylic acid

Anal. Calc. ($C_{15}H_{11}NO_3$) : C-71.14, H-4.38, N-5.53, O-18.95; Found : C-71.04, H-4.29, N-5.48; IR (KBr, υ/cm^{-1}) : 3527 (-OH), 2881 (-HC=C-), 2153 (-CN), 1785 (-C=O); ^{1}H NMR ($CDCl_3$, 400 MHz, δ/ppm) : 13.45 (s, 1H), 8.33 (s, 1H), 8.03 (d, 1H), 7.84 (d, 1H), 7.71 (d, 1H), 7.61 (t, 1H), 7.45 (t, 1H), 7.32 (d, 1H), 4.08 (s, 3H); ^{13}C NMR ($CDCl_3$, 100 MHz, δ/ppm) : 175.8, 157.3, 155.3, 135.8, 131.7, 129.2, 129.0, 128.4, 125.0, 122.6, 114.4, 113.4, 112.5, 88.9, 55.9; APCI-MS m/z (m+H) = 254.2 (calcd-254.08).

4.2.4 Synthesis and Characterization of Receptors L3 and L4

Spiropyran derivative L3 and L4 were achieved by using as previously reported method (Scheme 4.2). The ethanolic solution of 1-Methyl-2,3,3-trimethyl-3H-indolium (1 mmol) and coupling component (3-formyl chromene derivatives, 1 mmol)

was mixed and stirred at room temperature. After completion of the reaction mixture, ppt was filtered with 72% yield. Further receptors L3 and L4 were characterized *via* spectroscopically to confirm the data.

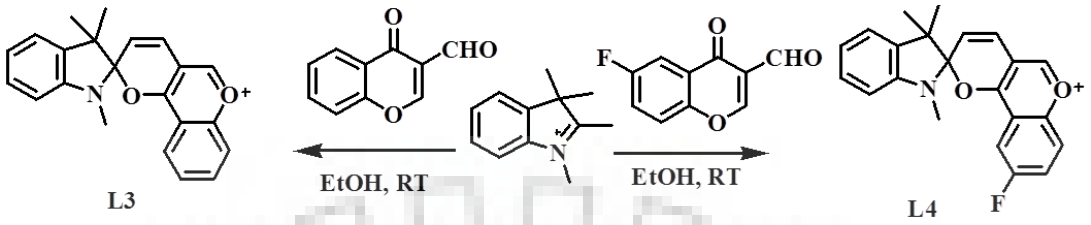

Scheme: 4.2 Synthesis of receptors L3 and L4

L3: 1,3,3-trimethylspiro[indoline-2,2'-pyrano[3,2-c]chromen]-6-ium

Anal. calc. ($C_{22}H_{20}NO_2$) : C-79.97, H-6.10, N-4.24, O-9.68; Found **:** C-79.89, H-6.12, N-4.22; IR (KBr, υ/cm^{-1}) : 1653 (-C=O); ^{1}H NMR ($CDCl_3$, 400 MHz, δ/ppm) **:** 10.28 (s, 1H), 8.86 (d, 1H), 8.56 (d, 1H), 8.27 (d, 1H), 7.78 (t, 1H), 7.62-7.58 (m, 5H), 7.52 (t, 1H), 4.40 (s, 3H), 2.36 (s, 6H); ^{13}C NMR ($CDCl_3$+DMSO d_6, 100 MHz, δ/ppm) : 183.5, 175.9, 165.2, 155.2, 148.0, 143.1, 141.2, 135.0, 130.2, 129.5, 126.8, 126.0, 123.9, 122.8, 118.6 (2C), 114.8, 113.8, 52.7, 35.3, 26.2 (2C); APCI-MS m/z (m) = 330.1 (calcd-330.15).

L4: 9'fluoro-1,3,3-trimethylspiro[indoline-2,2'-pyrano[3,2-c]chromen]-6-ium

Anal. calc. ($C_{22}H_{19}NO_2F$) : C-75.84, H-5.50, N-4.02, O-9.18, F-5.45; Found : C-75.64, H-5.49, N-4.08; IR (KBr, υ/cm^{-1}) : 1660 (-C=O); ^{1}H NMR (DMSO d_6, 400 MHz, δ/ppm) : 9.41 (s, 1H), 8.52 (d, 1H), 8.24 (d, 1H), 8.03-7.88 (m, 5H), 7.70 (s, 2H), 4.12 (s, 3H), 1.85 (s, 6H); ^{13}C NMR (DMSO d_6, 100 MHz, δ/ppm) : 181.7, 174.5, 164.8, 160.4, 158.0, 151.0, 145.1, 143.1, 141.3, 129.1, 128.6, 124.5, 122.4, 121.3, 117.1, 114.9, 114.2, 110.0, 51.6, 33.9, 24.8 (2C); APCI-MS m/z (m) = 348.1 (calcd-348.14).

4.3 RESULTS AND DISCUSSION

4.3.1 Sensing Studies of Receptors L1 and L2

4.3.1.1 Spectroscopic Sensing Properties of L1 and L2

The UV-vis spectra of L1 and L2 displays low energy band at 437, 387 nm, with high energy band at 342, 339 nm due to π-π^* and intra molecular charge transfer (ICT)

transition from 2-methoxynaphthalene donor moiety to electron deficient acceptor moiety. The ICT transition of L1 shows more (437 nm) red shifted value comparable to that of the L2 (387 nm), signifying that -CN and -COOH group is a stronger electron withdrawing group than -C=O, as expected which declines the electron-donating aptitude of 2-methoxy naphthalene unit. The yellow color solution decolorizes upon addition of CN^{-}. The blue shift phenomenon occurs by nucleophilic addition of CN^{-} to the receptors, which gradually lay off the ICT transition and relatively a new band appeared at low wavelength as a product of addition reaction and the colorless solution detected in the visual recognition experiment, as expected (Fig. 4.1).

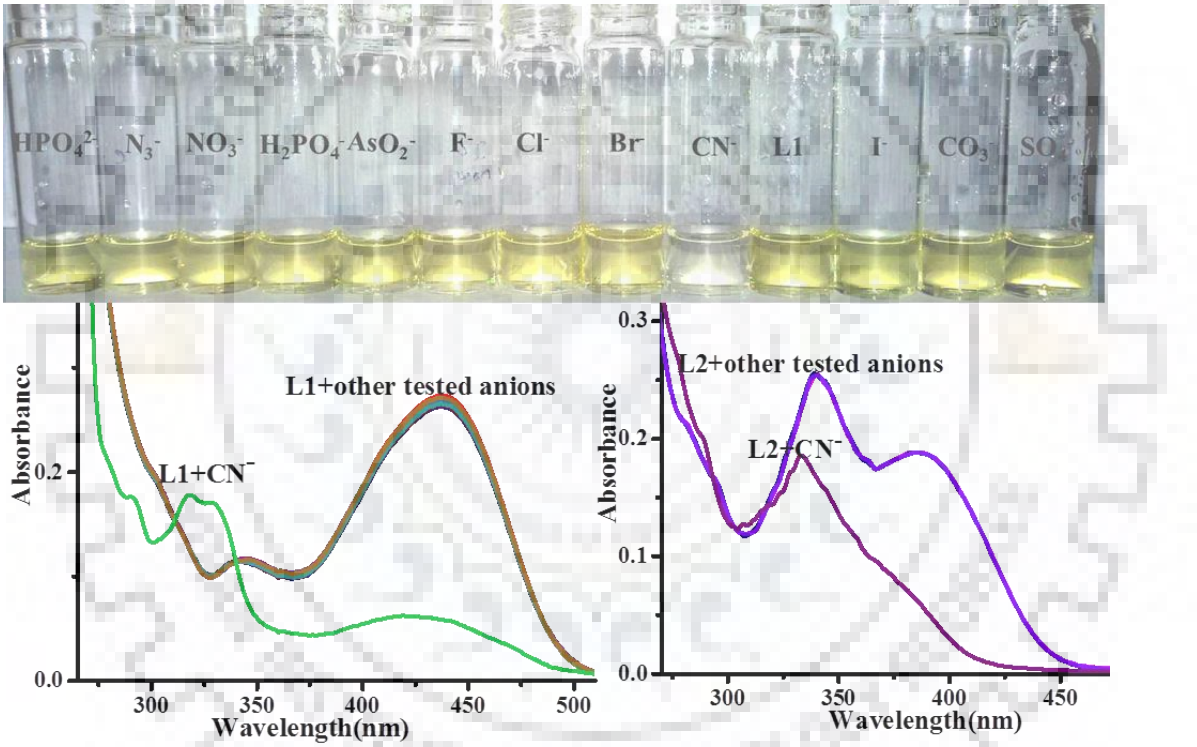

Fig. 4.1 Interaction of L1/L2 upon 2 eq. of anions by absorption spectra in H_2O-DMF (9:1 v/v, pH-7.4 HEPES buffer).

To determine the sensitivity of L1 and L2 in the existence of other competing anions, an interference experiment was executed. Fig. 4.2 visibly approves the high-class CN^{-} sensing aptitude even in the presence of all co-existing anions in the same solution phase. Amongst all anions only CN^{-} perturbs the electronic performance of L1 and L2 to a substantial range in comparison to other anions such as F^{-}, CI^{-}, Br^{-}, I^{-}, N_3^{-}, SCN^{-}, AcO^{-}, AsO_2^{-}, CO_3^{2-}, NO_3^{-}, PO_4^{2-}, SO_4^{2-}, $H_2PO_4^{-}$, and HPO_4^{2-} (tetrabutylammonium salts).

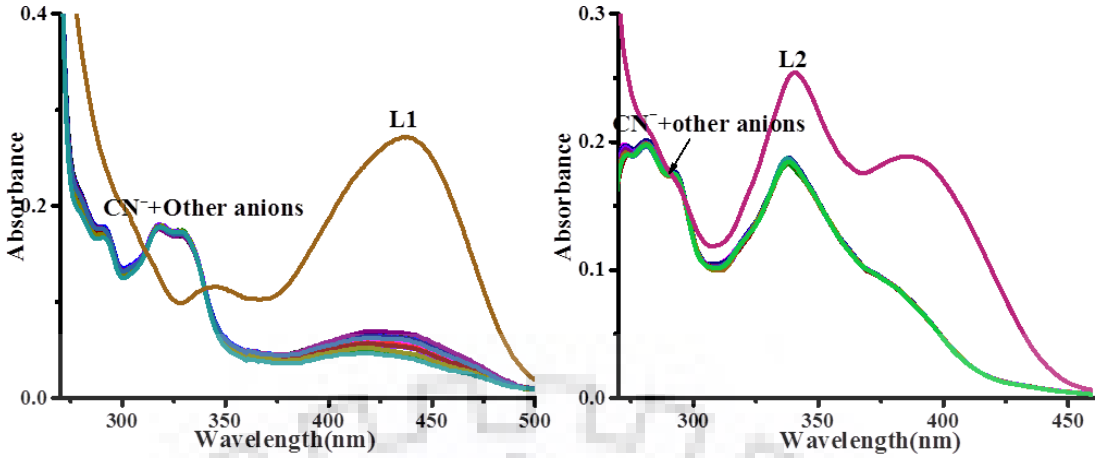

Fig. 4.2 Interference studies by absorption spectra of L1/L2-CN^- with different anions (10 eq.) in H_2O-DMF (9:1 v/v, pH-7.4 HEPES buffer).

To estimate the discriminating nature of L1 and L2, studied the absorption spectral variations upon addition of different eq. of CN^-. The result shows that the low energy band decreases with a clear isosbestic point at 340, 313 in L1 and 326 nm in the case of L2 respectively, which clearly indicates their conversion into the different species. Further, L1 required higher quantities of CN^- than L2 for complete bleaching of reaction. Since, -CN and -COOH moiety are a higher electron withdrawing group than -C=O so increases the rate of nucleophilic addition on -C=C bond. This was further supported by the kinetics response of L1 and L2 with CN^-. 2.2 equiv. of CN^- were reacted with L1 in 30 sec, whereas 1.6 equiv. of CN^- were essential for L2 within 10 sec, to complete the bleaching action (Fig. 4.3).

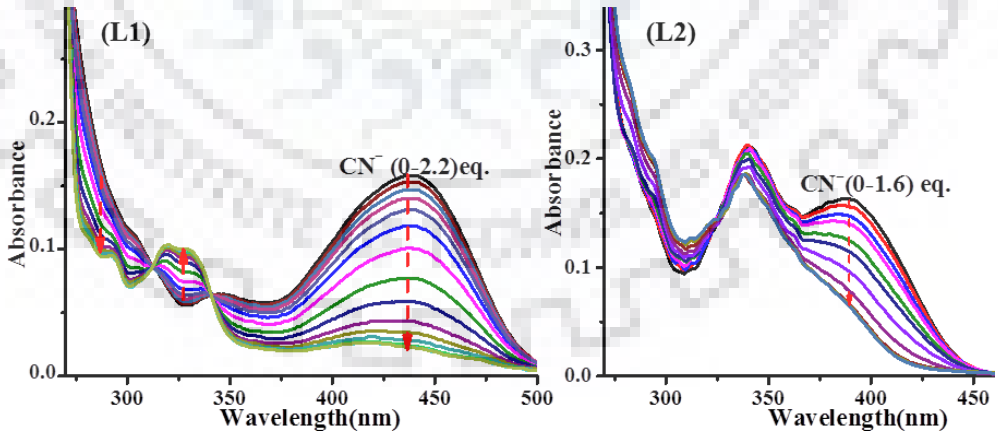

Fig. 4.3 Absorption titration spectra of L1/L2 upon addition of CN^- in H_2O-DMF (9:1 v/v, pH-7.4 HEPES buffer).

The rate constant for L1 and L2 was calculated by pseudo first-order reaction condition and found to be 0.025 s^{-1} and 0.029 s^{-1} respectively (Fig. 4.4). As we know that greater the

electron withdrawing power of substituent close to the C-atom at α-position, more will be the polarization of C=C bond (higher will be the positive charge at β positon), subsequent easier the nucleophilic addition of CN^- and foremost the greater value of rate constant. The complexation between L-CN^- was proved by Job's plot which corroborated the 1:1 binding stoichiometry (Fig. 4.5).

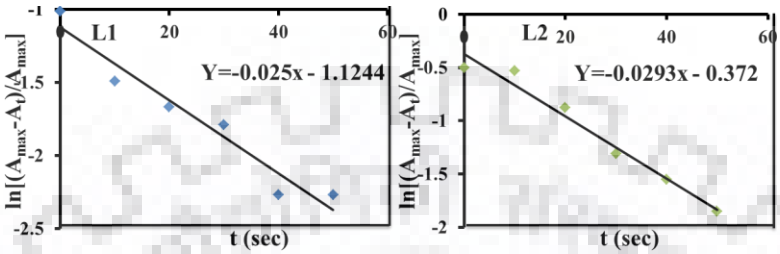

Fig. 4.4 Kinetic responds of L1/L2 with CN^- interaction.

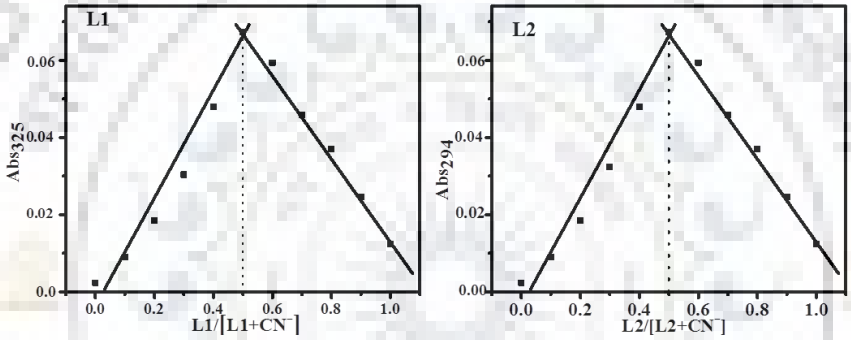

Fig. 4.5 Jobs plot of L1/L2 with CN^- in H_2O-DMF (9:1 v/v, pH-7.4 HEPES buffer).

The emission spectra of L1 shows a weak ICT emission band at 425 nm (λ_{ext} = 310 nm), while L2 displays at 410 nm (λ_{ext} = 340 nm). It is apparent from Fig. 4.6 that the emission intensity of both receptors was intensely enhanced upon addition of CN^-. No significant changes were observed with other co-existing anions.

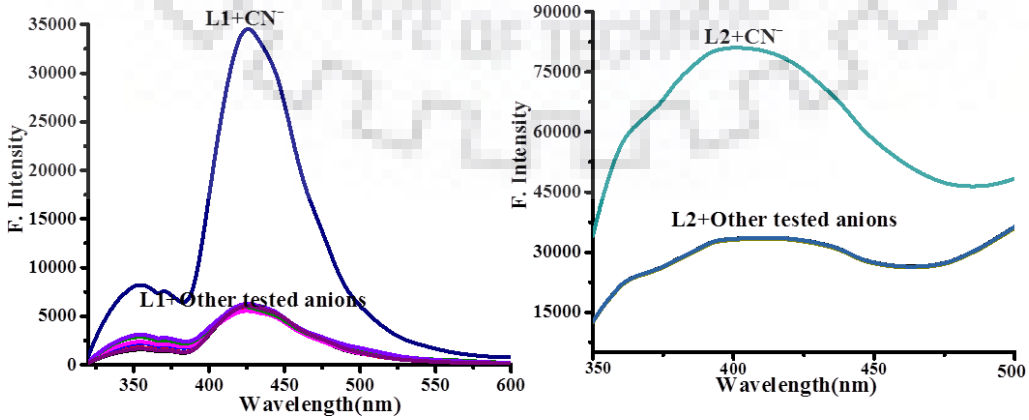

Fig. 4.6 Interaction of L1/L2 upon 2 eq. of anions by emission spectra in H_2O-DMF (9:1 v/v, pH-7.4 HEPES buffer).

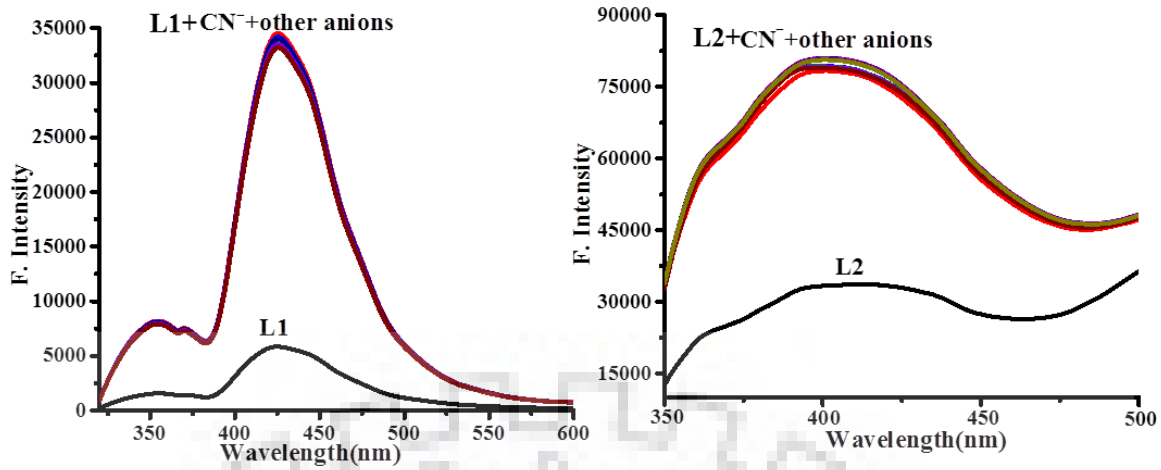

Fig. 4.7 Interference spectra of L1-CN^- and L2-CN^- with different anions (10 eq.) by emission spectra in H_2O-DMF (9:1 v/v, pH-7.4 HEPES buffer).

Further, interference study also recommends high selectivity of L1 and L2 for CN^- (Fig. 4.7). The emission titration spectra showed that the saturation point was achieved with 1.5 eq. and 1.1 eq. of CN^- in L1 and L2 respectively, which further shows high reactivity of L2 (Fig. 4.8). The minimum concentration (LOD) of L1 and L2 with CN^- has been found to be 1.2 nm and 1.15 nm, which are much lower than the WHO standard level (Fig. 4.9).

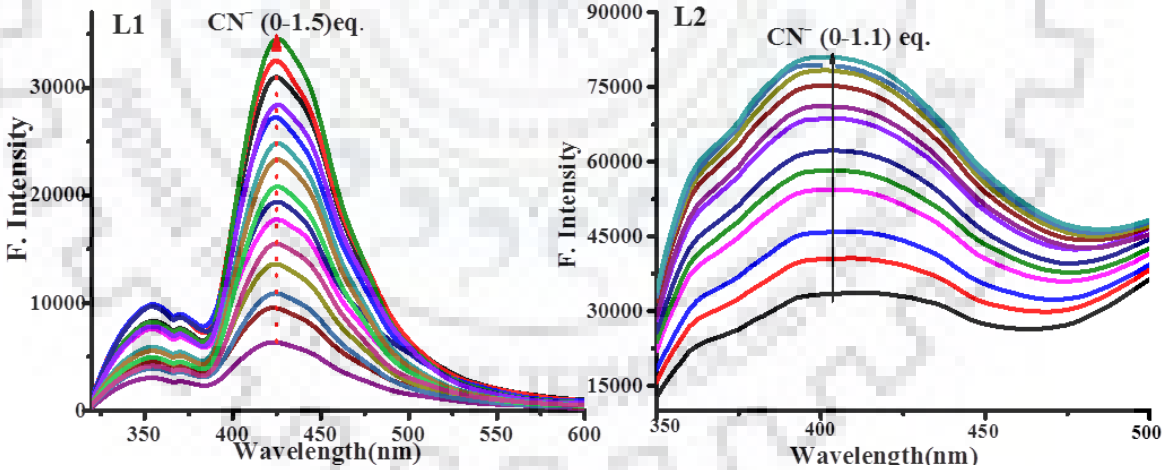

Fig. 4.8 Emission titration spectra of L1/L2 upon addition of CN^- in H_2O-DMF (9:1 v/v, pH-7.4 HEPES buffer).

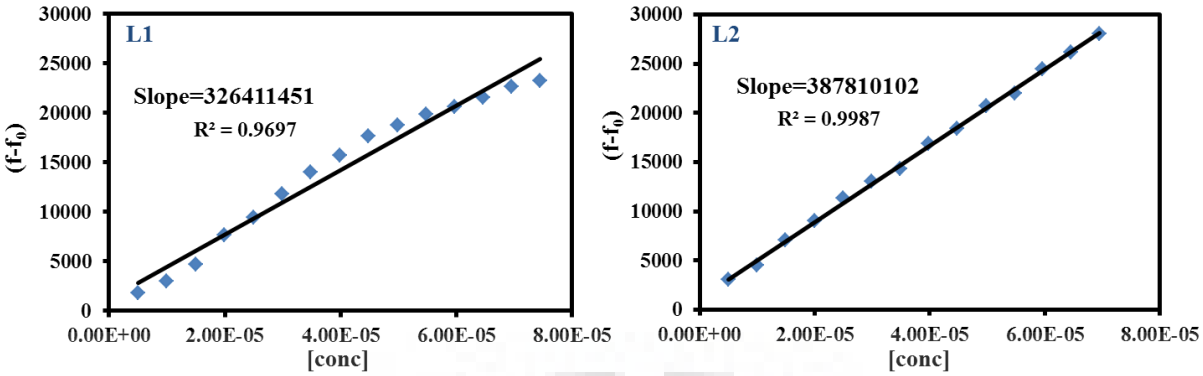

Fig. 4.9 Calibration curve of L1 and L2 for the binding of CN^-.

4.3.1.2 Possible Binding Interaction of L1/L2 with CN^-

The specified recognition mechanism of L-CN^- was investigated by the binding interaction was confirmed by FTIR spectroscopy upon comparison between L and L-CN^- adduct (1:1), disappearance of -CH peak 2932 and 2881 cm^{-1} with the generation of a new peak at 2181 and 2178 cm^{-1} in L1 and L2 respectively, which designates to CN^- vibration peak (Fig. 4.10).

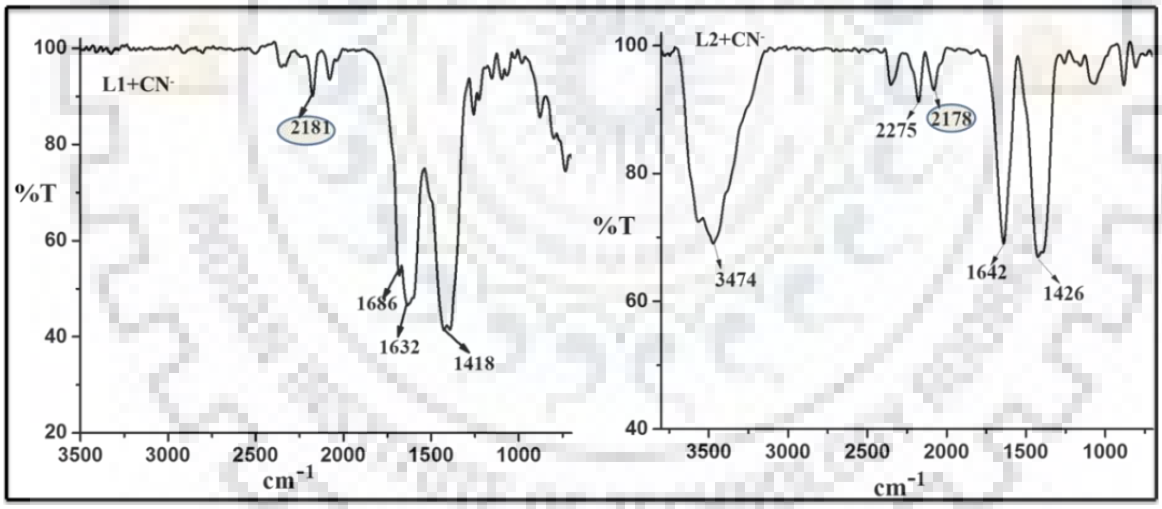

Fig. 4.10 IR spectra of L1-CN^-/L2-CN^- complex.

Further, in ^{1}H NMR titration spectroscopy in which the resonance signal at 8.41 and 8.33 ppm were recognized to the vinylic proton (β position), which disappeared in the CN^-- adduct, with generation of a new signal at 4.82 and 4.51 ppm in L1 and L2 respectively. All aromatic protons shifted to upfield region due to the development of negative charge on the molecules. Similarly, in ^{13}C NMR spectra, the vinylic α-β carbon of L1 and L2 appeared at 133, 157 and 88, 155 ppm. respectively, which were

shifted to 44, 33 ppm in case of L1 and 45, 23 ppm in case of L2 and generation of new peaks at 115 ppm, 116 ppm corresponding to CN^{-} carbons (Fig. 4.11).

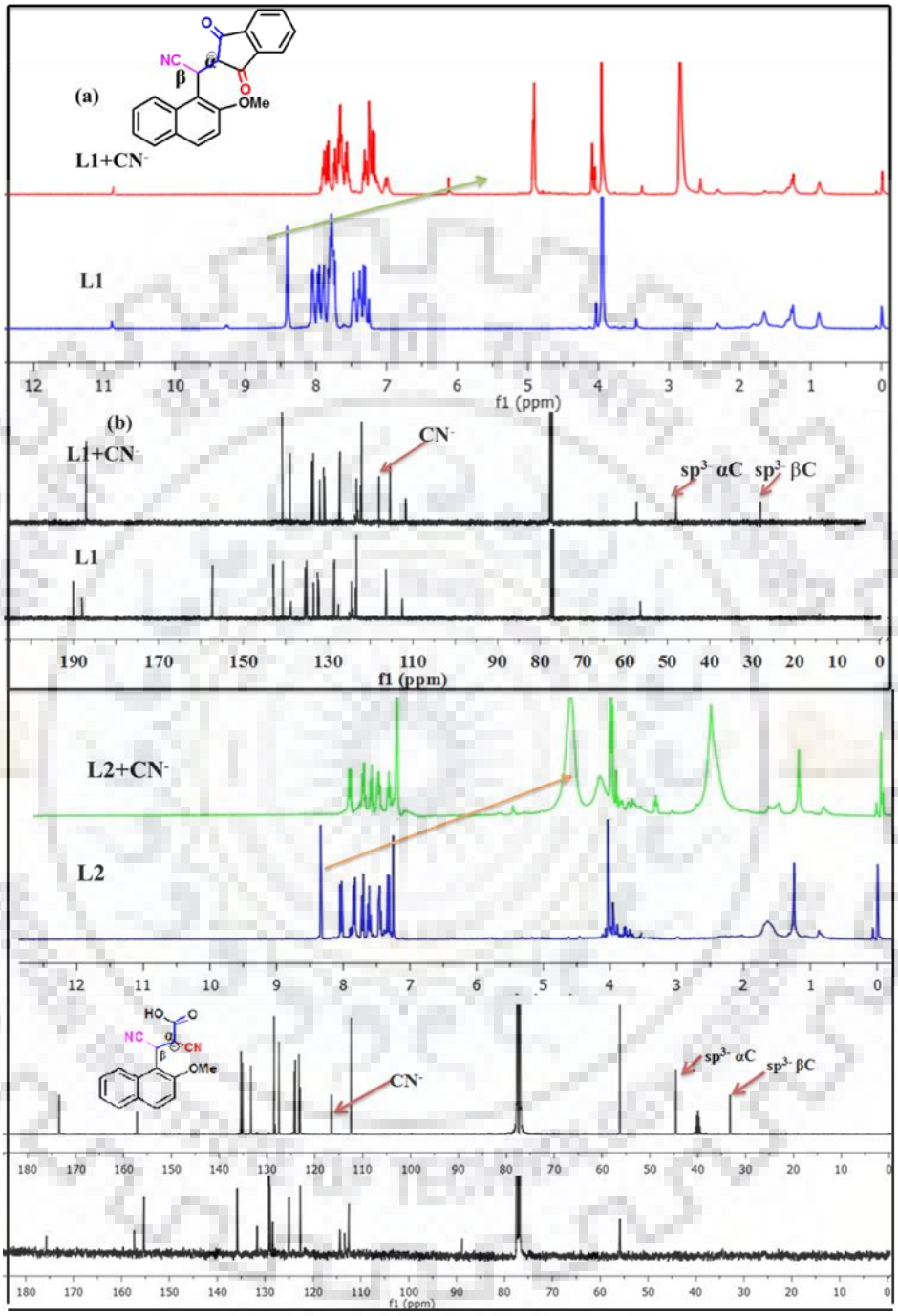

Fig. 4.11 (a) ^{1}H NMR spectra (b) ^{13}C NMR spectra of L & L-CN^{-} in $CDCl_3$ solvent.

The product L-CN^{-} was further investigated by mass spectral analyses. The m/z ion peak was detected at 315.3 and 254.2 which is equivalent to $[L1+H]^{+}$ and $[L2+H]^{+}$. The ion peak at m/z 341.1 and 280.1 confirmed the formation of $[L1+CN^{-}+H]^{-}$ and $[L2+CN^{-}+H]^{-}$ adduct (Fig. 4.12). All the above results reveal the conversion of sp^2 to sp^3 hybridized C with

the nucleophilic addition at β position of -C=C double bond after the formation of cyanide adduct.

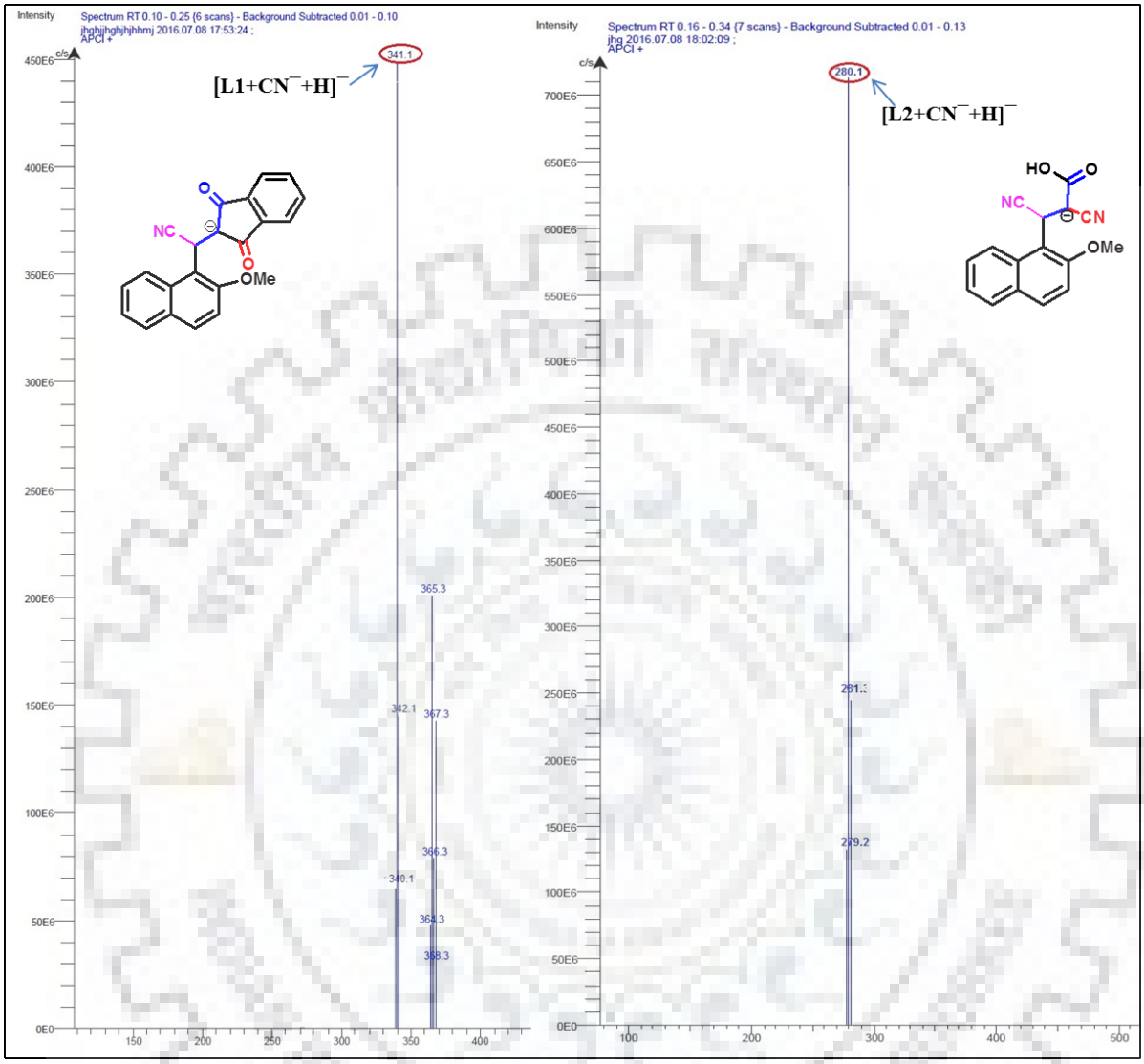

Fig. 4.12 Mass spectra of L1-CN^- and L2-CN^- adduct.

The 1-4 nucleophilic addition of CN^- was further supported by quantum chemical calculations (DFT) by using Gaussian 03 suits of database employing basis sets B3LYP/6-31G [56]. Receptors L1 and L2 were nearly planar, which delivered effectual p-conjugation and hence preferred the ICT transition from the 2-methoxy naphthalene moiety to attach substituent. Upon interaction with CN^-, the planar geometry goes through noticeable twist, which interrupted the p-conjugation and leads to decreased ICT transition with a blue shift in the absorption spectra. Fig. 4.13 represents the frontier molecular orbitals of L and L-CN^- complex. In case of HOMO the electron density resides on 2-methoxy naphthalene moiety, while in LUMO it is

located on acceptor arm, which establish charge transfer interface between donor-acceptor systems of dosimeters. However, the electronic dispersal in L-CN^- was relatively different from L. In case of the L-CN^- adduct, there is a disruption in the p-conjugation by which electron density resides on acceptor moiety in HOMO, which supported the anionic adduct formation. Moreover, the feasible adducts L-CN^- advised the change in bond distance from 1.357/1.364 to 1.514/1.538 Å. This result suggested that the addition of CN^- changed sp^2 hybridized -C=C bond to sp^3 -C-C bond.

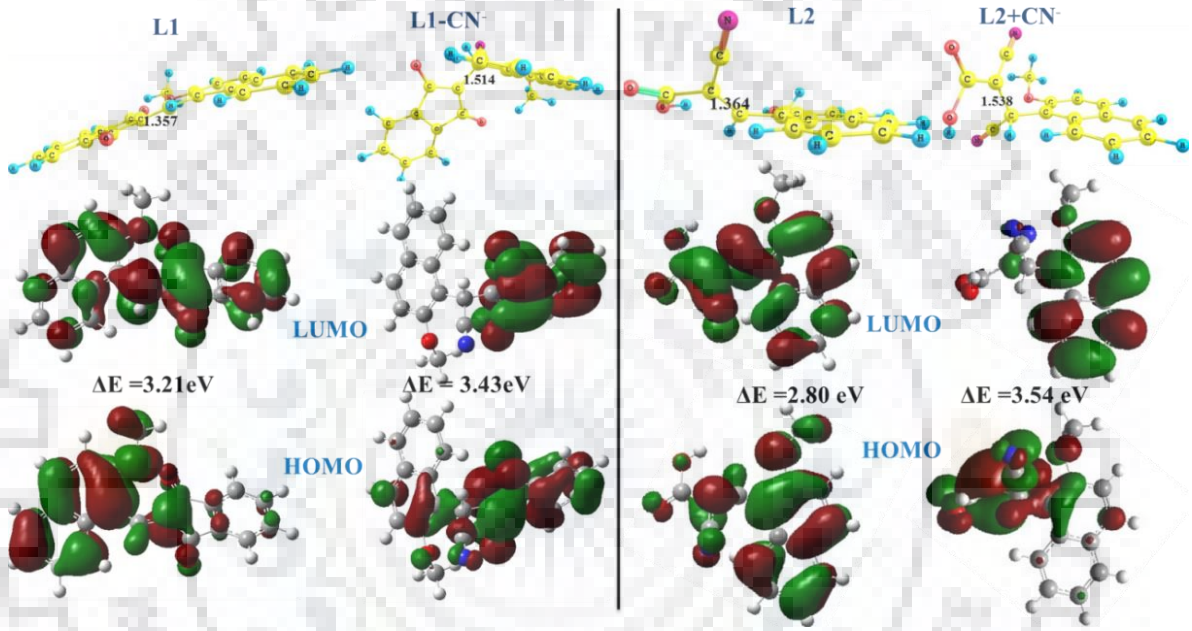

Fig. 4.13 DFT optimized structure and HOMO-LUMO energy band gap of L1/L2 and L1-CN^-/L2-CN^- adduct.

4.3.1.3 Electrochemical Studies of L1/L2 with CN^-

However, the electrochemical study of L is important, which would be responsible for the suggested sensing mechanism of CN^-. L1 and L2 displayed reversible reduction potentials at -1.40 and -1.33 V without any oxidation potential signifying that L is electron deficient. L2 has relatively less reduction potential due to the presence of strong electron withdrawing moiety (-CN, -COOH), which decreases more electron density from naphthalene moiety, subsequently easy to reduce and consequential lower E_{pc} value [16]. Upon sequential addition of CN^-, reduction peak is shifted towards positive potentials designating that the electro-reduction of naphthalene moiety becomes more and more informal (Fig. 4.14). The Michael

addition of CN^- terminates the intra molecular charge transition, which reduces the electron density on the naphthalene moiety and therefore makes easier electron reduction relatively [17].

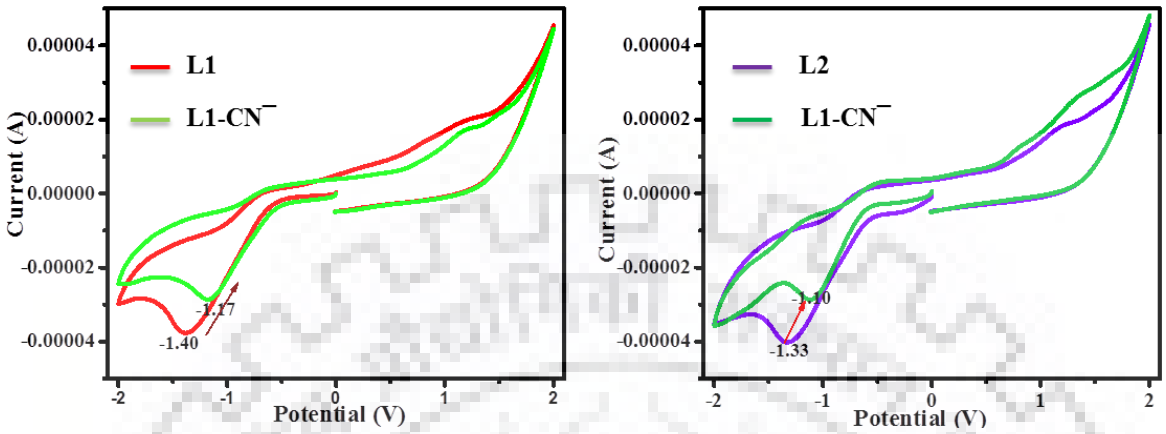

Fig. 4.14 Cyclic Voltammograms of L1/L2 with CN^- in H_2O-DMF (9:1 v/v, pH-7.4 HEPES buffer).

4.3.1.4 Dip Stick Test of L1

Encouraged by the auspicious sensing features of the receptors L1 and L2, we equipped paper test strips to examine their hands-on application. The paper strips were prepared by dipping in a DMF solution of the L1 (1 mM) and then expose to air for drying. Further the prepared strips were immersed in different concentration of CN^- solutions; the strips displayed a remarkable, easily viewed color change. Having seen the confirmation of the test strips to discriminate CN^- in solution phase, also a primary attempt was done in the solid state by simply grinding method with CN^-. To our amusement, L1 displays a drastic color variation from yellow to colorless within a few minutes (Fig. 4.15).

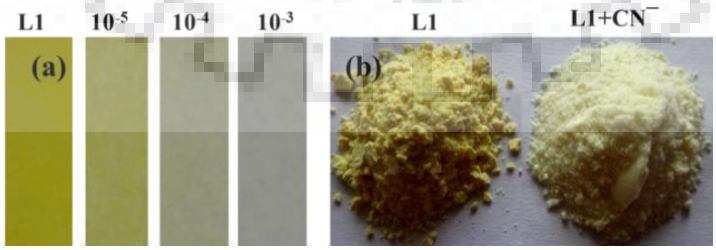

Fig. 4.15 Color change of L1 in (a) solution phase by coated paper strips with different concentrations (10^{-5} to 10^{-3} M) of CN^- (b) solid state.

4.3.1.5 Comparative Studies of L1/L2

Some Michael type CN^- chemodosimeter have been synthesized by various group as given in Table 4.1. On investigation of all chemodosimeter in terms of their solvent system, LOD and reaction time, it has been detected that our receptors have very low LOD with fast response time and can apply in aqueous medium.

Table: 4.1 Comparison of some reported Michael based CN^- receptors with present work.

Previous literature	Solvent system	LOD	Reaction time
Tetrahedron Lett. 55 (2014) 1052-1056 (ref. 21)	H_2O	0.2 μM	50-60 min.
Sens. Actuators, B 221 (2015) 1441-1448 (ref. 16)	H_2O-ACN (4:1, v/v)	0.14-0.49 μM	--
Org. Lett. 13 (2011) 3730-3733 (ref. 25)	ACN	0.328 μM	60 sec.
Dyes Pigm. 95 (2012) 168-173 (ref. 57)	ACN	0.18 μM	60 sec.
New J. Chem. 39 (2015) 7211-7218 (ref. 58)	H_2O	0.75 μM	8 min.
Spectrochim. Acta Part A, 138 (2015) 164-168. (ref. 59)	DMSO-H_2O (95:5, v/v)	0.51 μM	5 h
Org. Lett. 14 (2012) 130-133 (ref. 60)	THF	2.28 μM	30 min.
Sens. Actuators, B 221 (2015) 463-469 (ref. 61)	ACN	74 μM	---
Chem. Commun. 46 (2010) 9197–9199 (ref. 62)	ACN	1.7 μM	9 h
This work	H_2O-DMF (9:1, v/v)	1.15-1.2 nm	10-30 sec.

4.3.2 Sensing Studies of Receptor L4

4.3.2.1 Naked Eye Detection and Photochromic Properties of L4

The produced spiropyran ligand L4 was assessed for photochromic properties by using absorption and emission spectroscopy at room temperature. The effect of water content and pH has been deliberate by emission spectra on the sensitivity of L4. The

result shows that above 50% water content diminished the sensitivity of receptor (Fig. 4.16 a). The pH adjustment was done by using 0.5 M HCl and 1 M NaOH. L4 was stable at 4-9.4 pH range, below pH 6.8 decreased marginally, which may be because of merocyanine forms in acidic medium through protonation of oxygen atom of the phenolic ring (Fig. 4.16 b). From above result displays the compatibility of L4 in H_2O-ACN system in the biological pH range, thus all analytical studies were accomplished in H_2O-ACN (1:1 v/v, pH-7.4, HEPES buffer).

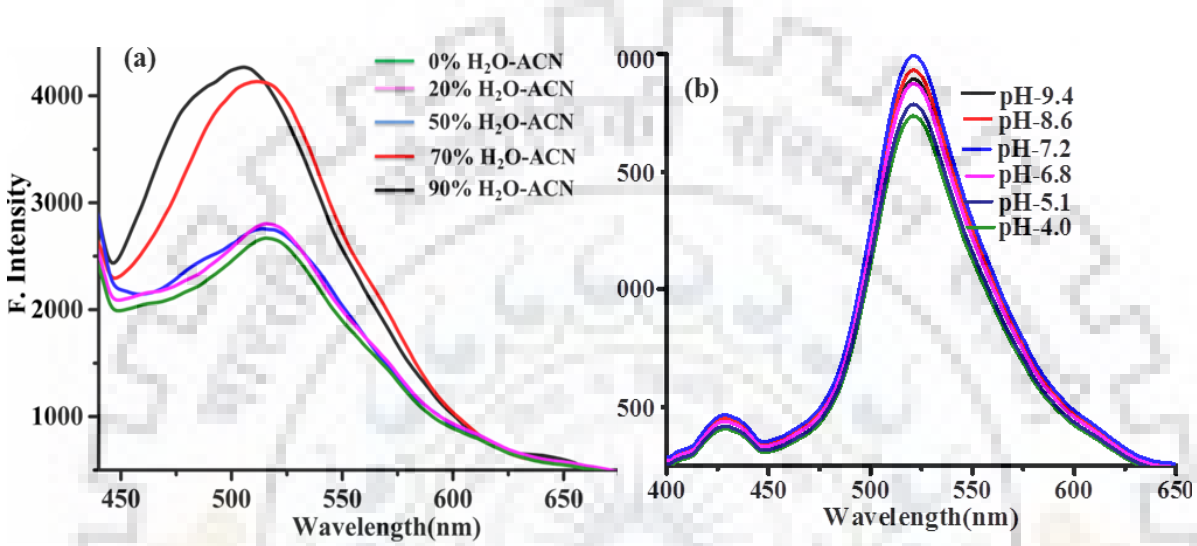

Fig. 4.16 Variations in emission properties of L4 with consequences; (a) amount of water (b) pH.

The closed form of L3/L4 (20 mM) shows a high energy band at 242 nm and 381 nm due to π-π*, n-π* transition along with a broad shoulder at 477 nm, additionally exhibited weak emission intensity at 520 nm (λ_{ext} - 395 nm, 5 μM). A sequence of anionic ions (more or less nucleophilic properties) such as F^-, Cl^-, Br^-, I^-, CN^-, N_3^-, SCN^-, AcO^-, AsO_2^-, CO_3^{2-}, NO_3^-, PO_4^{2-}, SO_4^{2-}, $H_2PO_4^-$ and HPO_4^{2-} (n-Bu_4N^+ salts) were carefully chosen as interference ions. The molar absorptivity of high energy band at 242 nm increased and 381 nm decreases with increasing low energy band at 471 nm pointedly only with CN^- and alters the light green solution to yellow solution. Similarly the emission intensity centered at 520 nm enhanced with non-fluorescent in fluorescent green color (Fig. 4.17 green bars). To conclude the sensitivity of L4 in the presence of other competing anions, an interference experiment was accomplished. In addition, the CN^- convinced the absorption spectral shift and emission enhancement was not pointedly affected by incidence of other competing anions in the CN^- solution (Fig. 4.17 yellow bars).

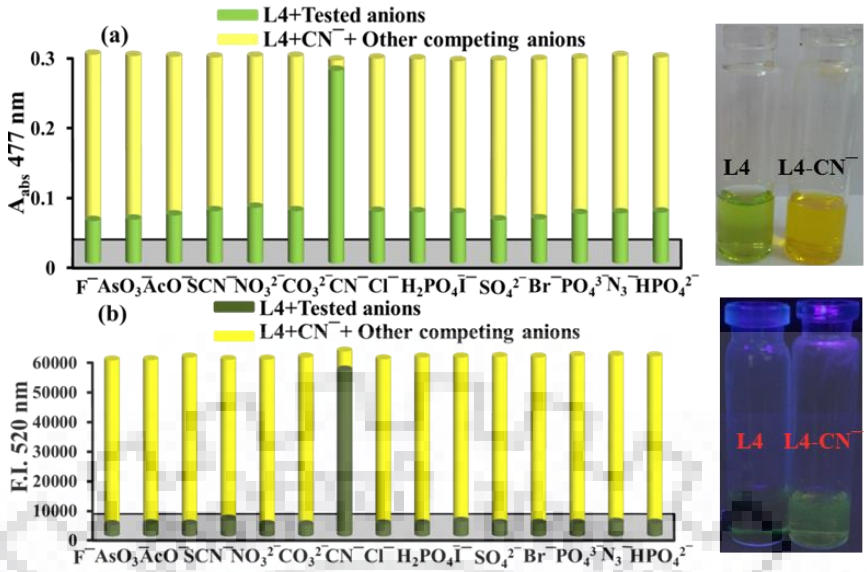

Fig. 4.17 Interaction of L4 with 20 eq. of anions; (a) Absorption (b) Emission spectra in H_2O-ACN (1:1 v/v, pH-7.4 HEPES buffer).

To recognize the binding affinity of L4 with CN^-, absorption and emission titration studies were executed. Upon sequential addition of CN^- (0-1.5 eq.) to the solution of L4, the absorption band centered at 381 nm reduced gradually and bands at 242 and 471 nm increased sequentially with formation of two isosbestic points at 274 and 434 nm. This proposed the feasible survival of more than one species in environment i.e., molecular isomerization of SP form to MC form, then nucleophilic attack of CN^- (Fig. 4.18 a).

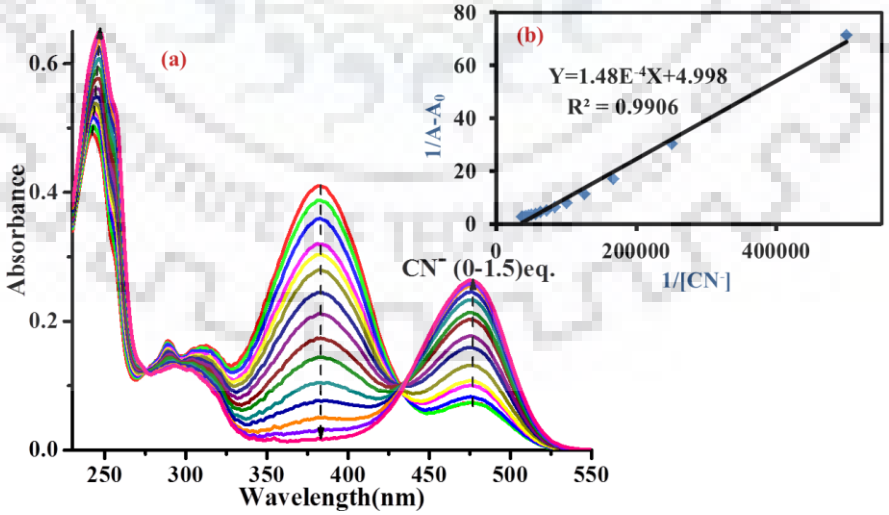

Fig. 4.18 (a) Absorption titration spectra (b) Benesi-Hilderbrand Plot of L4 with CN^- in H_2O-ACN (1:1 v/v, pH-7.4 HEPES buffer).

Correspondingly, the emission titration spectra show a gradual increase in intensity (at 520 nm) due to reduction in ICT transition from chromone unit to indoline unit (Fig. 4.19 a). Job's plot study dependably shown 1:1 binding stoichiometry for the interface between L4 and CN^- (Fig. 4.20 a), for which the binding constants were predictable by the B-H method and were found to be $K_{abs} = 3.38 \times 10^4\ M^{-1}$ and $K_{em} = 9.97 \times 10^4\ M^{-1}$ (Fig. 4.18 b, 4.19 b).

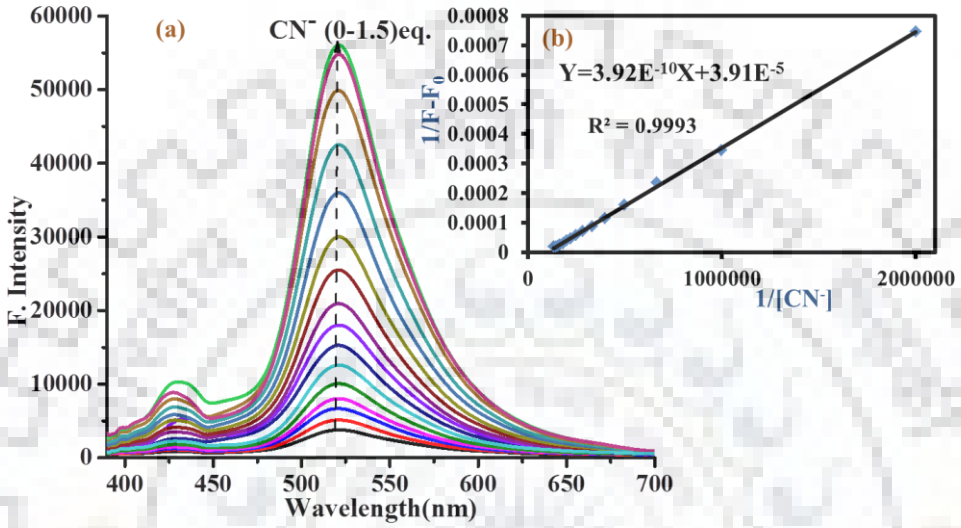

Fig. 4.19 (a) Emission titration spectra (c) Benesi-Hilderbrand Plot of L4 with CN^- in H_2O-ACN (1:1 v/v, pH-7.4 HEPES buffer).

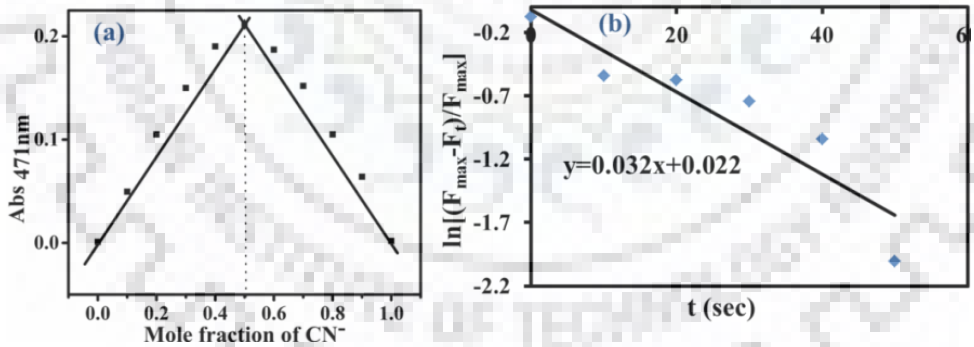

Fig. 4.20 (a) Jobs plot (b) Kinetic response of L4 with CN^-.

The rate constant between L4 and CN^- interaction was obtained to be 0.022 S^{-1} (Fig. 4.20 b) and detection limit has been found to be 57.9 nm, which is much below the standard level of WHO (1.9 μM, Fig. 4.21).

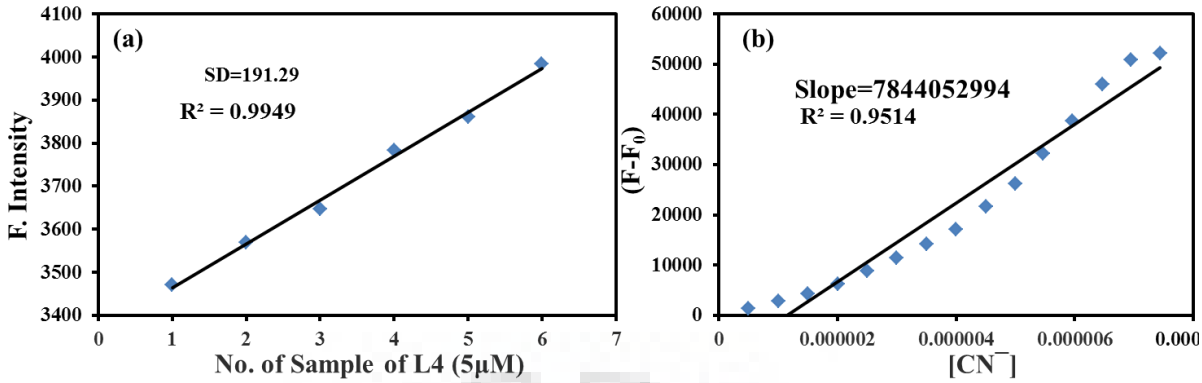

Fig. 4.21 (a) Calibration curve (b) Calibration sensitivity of L4 for the binding of CN^-.

4.3.2.2 Possible Sensing Mechanism of L4 with CN^-

The specified recognition mechanism of L4-CN^- was investigated by the binding interaction was confirmed by FT-IR spectra, which shows a new peak at 2256 cm^{-1} in L4-CN^- adduct, which defines to CN^- vibration peak (Fig. 4.22).

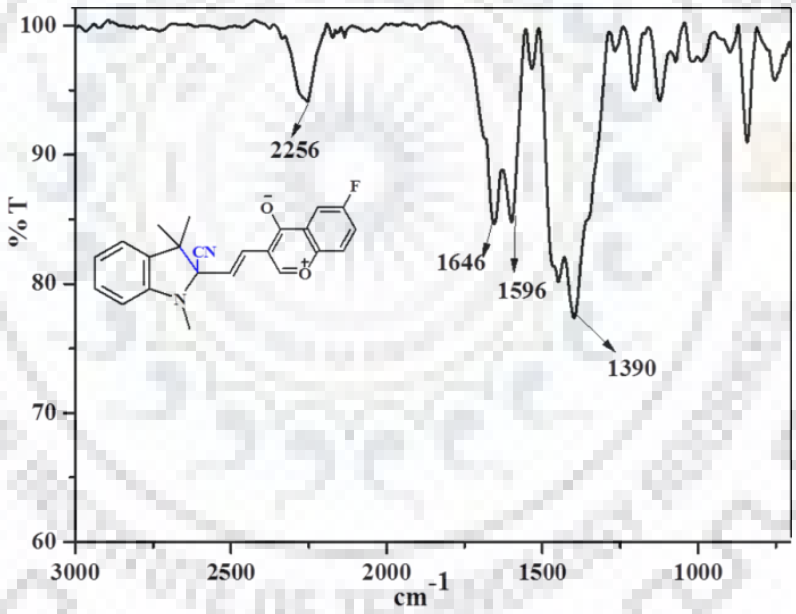

Fig. 4.22 IR spectrum of L4-CN^- adduct.

Moreover the NMR spectra noticeably reveal the complexation of open form of L4 with CN^-. The appearance of a new set of peaks (upfield region) with addition of CN^- specifies that ring opening of SP form and formed MC form as an intermediate. The H_5 proton goes to deshielded and all other aromatic protons go to upfield region, validate that CN^- attached to the spirocarbon which developed a negative charge on carbonyl oxygen atom [53], thus upfield shift in aromatic proton was observed (Fig. 4.23 a). Similarly, in ^{13}C NMR spectra, new set of peaks appeared after addition of

CN^- as conversion of MC form. After some time some peaks disappeared with generation of new peak at 113 nm, corresponding to CN^- carbon (Fig. 4.23 b).

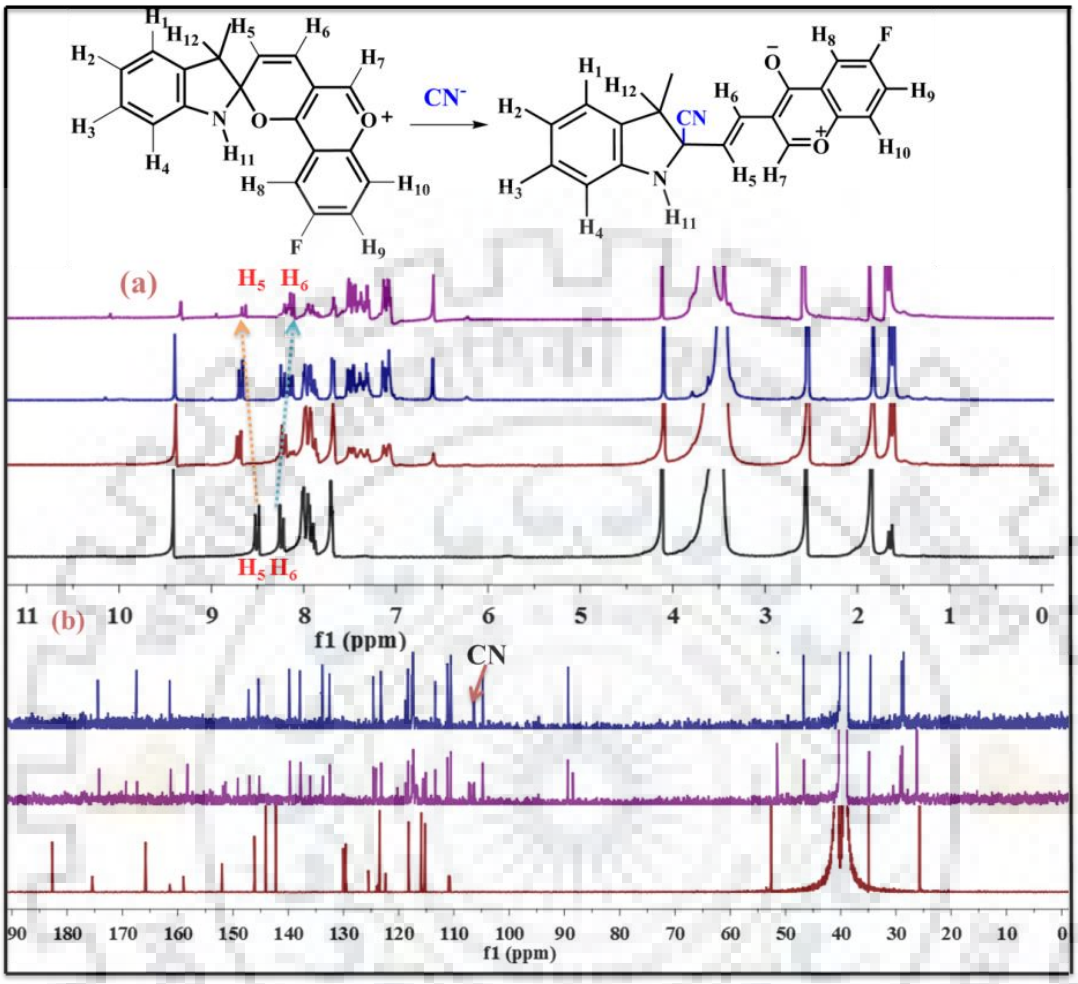

Fig. 4.23 ^{1}H NMR and ^{13}C spectra of L4 with CN^- in DMSO d_6.

The adduct L4-CN^- was further examined *via* mass spectral analyses. The m/z ion peak was detected at 375.2 (calc.-375.15) which is corresponding to [L4+CN^-+H] adduct (Fig. 4.24). All the exceeding results reveal the nucleophilic attack of CN^- on carbon atom of indoline moiety.

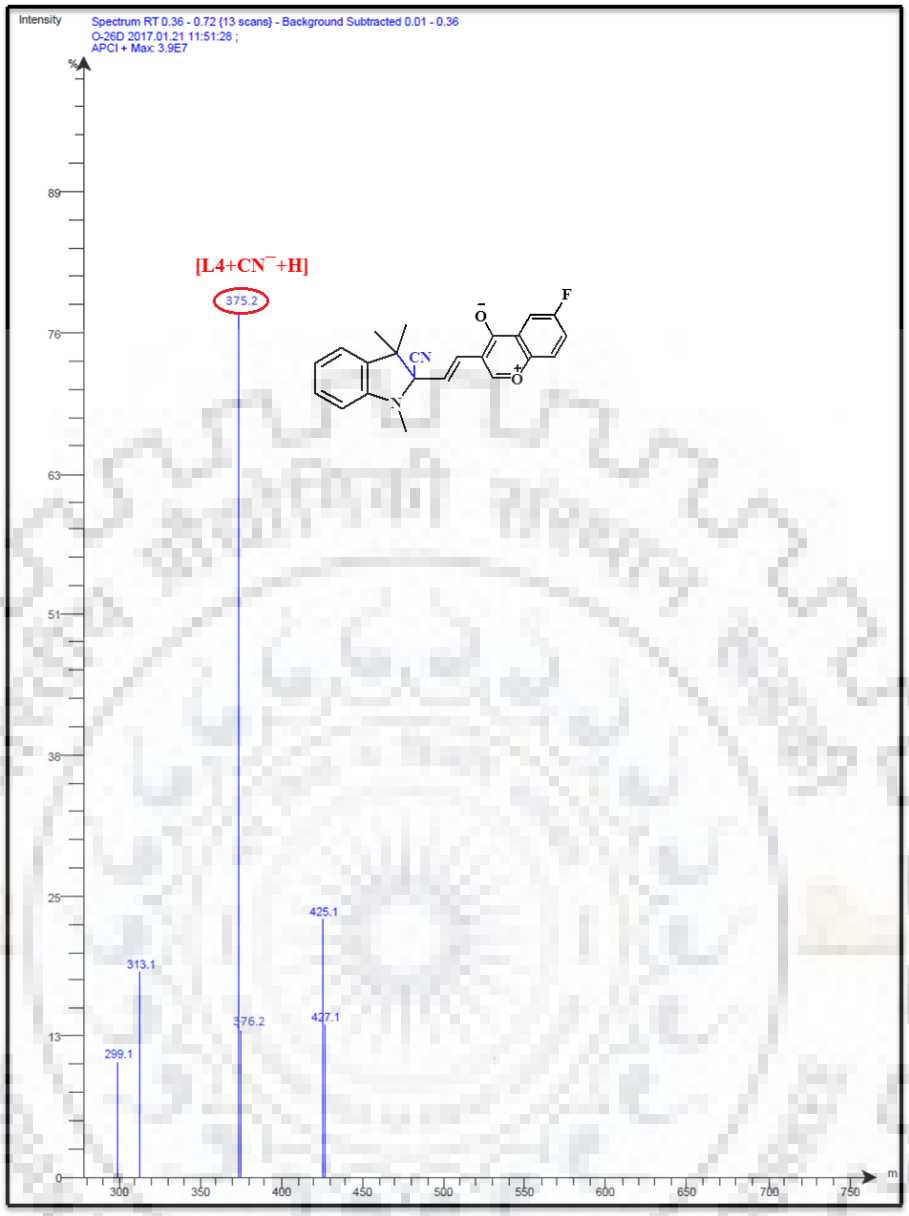

Fig. 4.24 Mass spectrum of L4-CN^- adduct.

The ring opening of L4 upon CN^- interaction was further proved by quantum chemical calculations. Fig. 4.25 signifies the frontier molecular orbitals of L4 and L4-CN^- complex. In case of L4, the electron density of HOMO residing in chromone unit, whereas in LUMO it is residing on whole moiety. However, the electronic dispersal in open form and CN^- complex are relatively different from close form of L4. The electron density of open form is dispersed over the whole moiety therefore; the absorption band can be ascribed to the ICT transition from chromone to indoline moiety. In addition, of CN^-, the electrons in HOMO orbitals mainly reside on indoline moiety while in LUMO concentrated on chromone unit which supported the change in ICT transition. The HOMO-LUMO energy gap (ΔE = 3.1 eV) for the ring

opening process of L4 was detected to be lower than the energy gap of the closed form of L4 (ΔE = 3.81 eV) and L4-CN adduct (ΔE = 3.22 eV). This result specified the ring opening of L4 is simply adaptable at room temperature with CN^- and supported a bathochromic shift in absorption spectra [56] (Fig. 4.25).

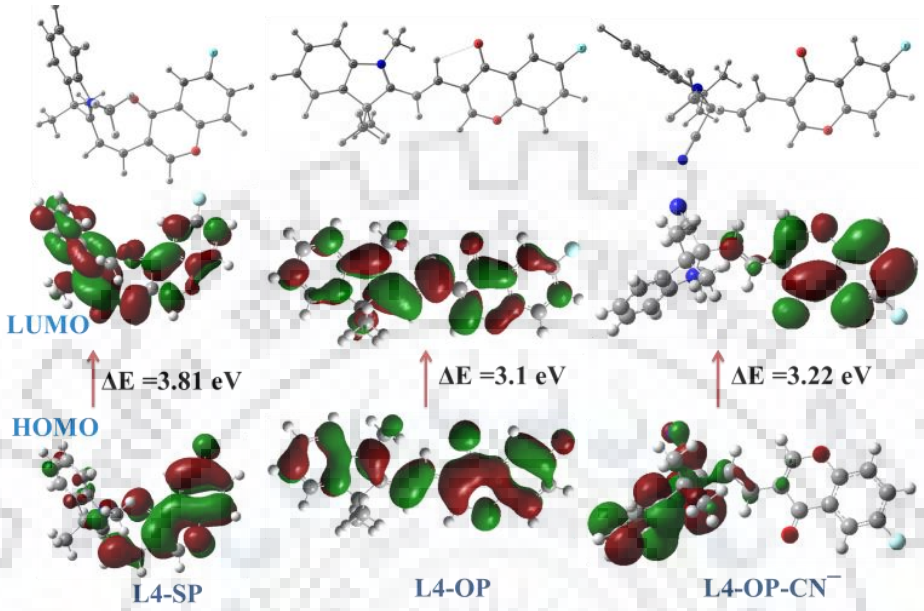

Fig. 4.25 DFT optimized structure and HOMO-LUMO energy band gap of L4 and L4-CN^-.

4.3.2.3 Electrochemical Studies of L4 with CN^-

Conversely, the proposed sensing mechanism of CN^- with L4 (ring opening) was further proved by electrochemical study. A reversible and irreversible reduction peak was detected in L4 at -1.21 & -0.578 V accompanying to the reduction of chromone unit. Oxidation of SP is described by irreversible oxidation of the indoline moiety at 0.27, 1.04 V. Upon addition of CN^- both the reduction and oxidation peaks were shifted concerning to positive potentials defining the easy reduction of L4. Moreover a new reduction peak appeared at -1.39 V; propose the new chemical species produced on attacking to reacting site (Fig. 4.26). It is significant that conflicting to the effects accessible in this report, neither depletion in the oxidation nor the presence of other oxidation peaks suggests the electrochemical ring-opening of the spiropyran structure after reduction of chromone oxygen [53].

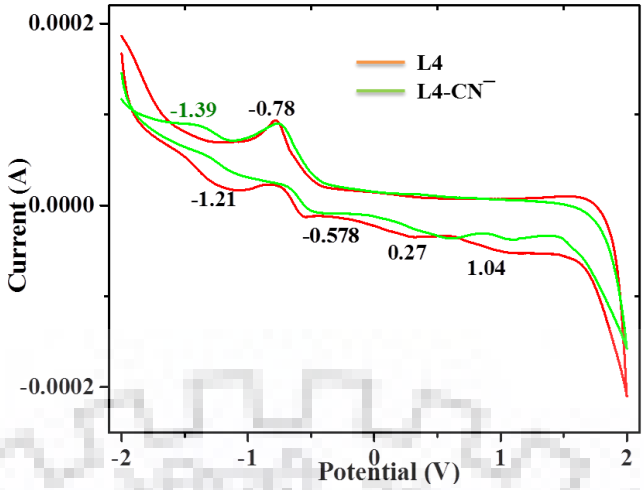

Fig. 4.26 Cyclic Voltammograms of L4 & L4-CN^- adduct in H_2O-ACN (1:1 v/v, pH-7.4 HEPES buffer).

4.3.2.4 Practical Application of L4

Encouraged by the promising sensing ability of L4, observe the hands-on application *via* paper test strip method. The strips were prepared in L4 solution (20 μM) and dried by air exposing. Moreover the dried strips were submerged in altered concentration of CN^- solutions; the strips exhibited significant and easily observed color changes. To distinguish CN^- also a primary attempt was done by a simple grinding method (solid state). The result shows alteration in color (colorless to yellow) within a few minutes (Fig. 4.27).

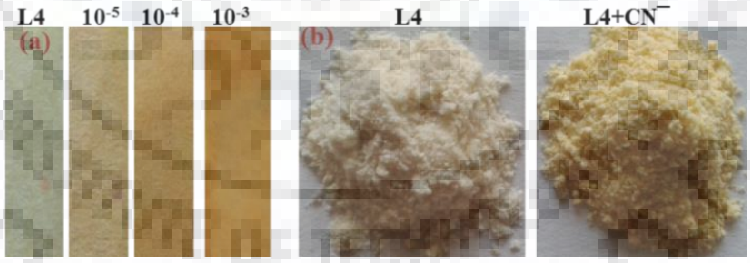

Fig. 4.27 Color variation of L4 in (a) solution phase by coated paper strips with different concentrations (10^{-5} to 10^{-3} M) of CN^- (b) solid state.

4.3.2.5 Antimicrobial Studies of L4 & L4-CN^- Adduct

Antibacterial activities of L4 and L4-CN^- adduct (1:1 stoichiometry) were studied *via* the disk diffusion method in contradiction of gram +ve *Brevibacillus brevis* & *Staphylococcus aureos* bacterial strains. The sterilized Petri dish of agar plates was equipped by using nutrient agar and kept at 37ºC. The platinum wire loop

was used for inoculation process. The disk (prepared by Whatman filter paper, 4 mm diameter) was dipped in a solution of ACN, L4 and L4-CN^- adduct (20 μM) solution and dried. Kept disk on bacterial growth plate and measured inhibition zone after 24 h. A clear inhibition zone was observed even at lower concentrations of L4 (MIC: 1.5 mg mL^{-1}) due to heterocycle pyran moiety, while CN^- adduct has not shown any antibacterial activity due to pyran ring opening (Fig. 4.28 a, b). Similarly the antifungal activity was also tested against *Bipolaris oryzae* (MTCC3717) strain *via* well diffusion method. Now 4 mm diameter well was made with sterile cork borer, then loaded ACN (as a control), L4 and L4-CN adduct solution. Further the plates were properly covered, labelled and stored at 37°C for 48 h and measured inhibition zone (Fig. 4.28 C, Table 4.2). The result shows weak Antifungal activities towards *Bipolaris oryzae*.

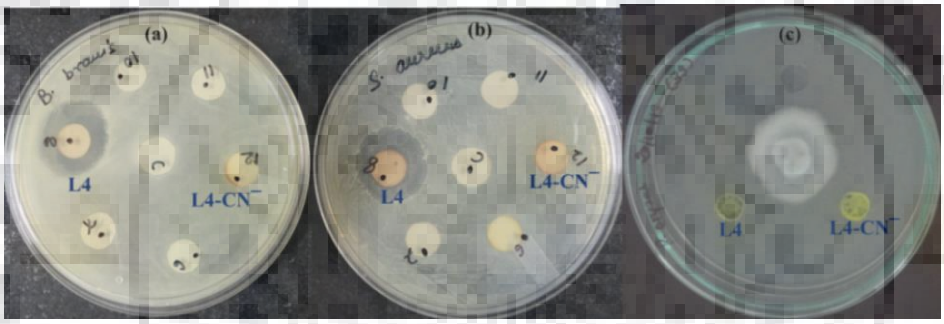

Fig. 4.28 Antimicrobial activity of L4 and L4-CN^- complex against *Brevibacillus brevis*, *Staphylococcus aureos* bacteria (20 μM, no. 8 & 12 respectively) and *Bipolaris oryzae* fungal species (1 mM).

Table: 4.2 List of bacterial strains used for antimicrobial activity test.

Con. (μg L^{-1})	**Microorganism**	**Type**	**% inhibition with reference**
L4	*Brevibacillus brevis*	Gram positive bacteria	92
L4-CN^-	*Brevibacillus brevis*	Gram positive bacteria	7
L4	*Staphylococcus aureos*	Gram positive bacteria	95
L4-CN^-	*Staphylococcus aureos*	Gram positive bacteria	9
L4	*Bipolaris oryzae*	Fungal strain	33
L4-CN^-	*Bipolaris oryzae*	Fungal strain	11

4.3.2.6 Comparative Studies of L4

Some 1-Methyl-2,3,3-trimethyl-3H-indolium based CN^- chemodosimeter have been synthesized by several aldehydes as given in Table 4.3. On analysis of all receptors in terms of the LOD, it has been perceived that our receptor has very low LOD.

Table: 4.3 Comparison of some reported 1-Methyl-2,3,3-trimethyl-3H-indolium based CN^- receptors with the present work.

Previous literature	Chemodosimeter	LOD (μM)
RSC Adv. 5 (2015) 24274-24280 (ref. 63)	Pyridine-carboxaldehyde based	1.5
RSC Adv. 4 (2014) 19077-19085 (ref. 64)	Ethyl-8-formoxyl-7-hydroxy coumarin-3-carboxylate based	14.2
Analyst 137 (2012) 5581-5585 (ref. 65)	4-Nitrosalysaldehyde based	0.4
Sens. Actuators, B 203 (2014) 382-387. (ref. 66)	9-Anthracene-carboxaldehyde based	0.059
Talanta 148 (2016) 229-236 (ref. 67)	Carbazole-3-carbaldehyde based	0.408
Chem. Commun. 47 (2011) 12843-12845 (ref. 68)	Diethyl-aminocoumarin-aldehyde based	0.6
RSC Adv. 4 (2014) 8295-8299 (ref. 69)	Phenothiazine-2-carbaldehyde based	0.0667
Sens. Actuators, B 237 (2016) 856-864. (ref. 53)	4-Nitrophenylazo-benzaldehyde based	0.64, 0.14
This work	6-Fluoro-3-formyl chromene based	0.0579

4.4 CONCLUSION

In conclusion, firstly we demonstrate two simple and selective naphthalene based chemodosimeter, which sense CN^- in an aqueous medium with low detection limit (1-1.2 nM). The sensing mechanism implicates Michael addition of CN^- at

electron deficient -C=C bond, ascribed to decrease in ICT due to stable adduct formation, which reduces the electron density on naphthalene moiety and subsequently electron reduction relatively becomes easier. Similarly, we validate two simple and selective spiropyran based chemodosimeter, which selective for CN^- with low detection limits (57.9 nM). The sensing mechanism involves the nucleophilic addition of CN^- *via* ring opening, attributed to reduction of ICT transition of chromone unit and emission enhancement occur. The reduction of electron density on chromone moiety makes easier reduction. Further L4 shows admirable antibacterial activities towards *B. brevis, S. aureos* strains and antifungal activities with *B. oryzae* strain.

References

1. P. D. Beer. P. A. Gale, Anion Recognition and Sensing, Angew. Chem., Int. Ed. 40 (2001) 486-516.
2. J. Yoon, S. K. Kim, N. J. Singh, K. S. Kim, Imidazolium receptors for the recognition of anions, Chem. Soc. Rev. 35 (2006) 355-360.
3. G. Liu, W. Cai, L. Kong, G. Duan, Y. Li, J. Wang, Z. Cheng, Trace detection of cyanide based on SERS effect of Ag Nano plate-built hollow microsphere arrays, J. Hazard. Mater. 248 (2013) 435-441.
4. M. A. Acheampong, R. J. W. Meulepasa, P. N. L. Lens, Removal of heavy metals and cyanide from gold mine wastewater, J. Chem. Technol. Biotechnol. 85 (2010) 590-613.
5. K. W. Kulig, Cyanide Toxicity; U.S. Department of Health and Human Services: Atlanta, GA, 1991.
6. Z. Xu, X. Chen, H. N. Kim, Yoon, Sensors for the optical detection of cyanide ion, J. Chem. Soc. Rev. 39 (2010) 127-137.
7. F. J. Baud, Cyanide: critical issues in diagnosis and treatment, Toxicology, 26 (2007) 191-201.
8. H. B. Leavesley, L. Li, K. Prabhakaran, J. L. Browitz, G. E. Isom, Interaction of cyanide and nitric oxide with cytochrome c oxidase: implications for acute cyanide toxicity, Toxicol. Sci. 101 (2008) 101-111.
9. J. D. Johnson, T. L. Meisenheimer, G. E. Isom, Cyanide-induced neurotoxicity: role of neuronal calcium, Toxicol. Appl. Pharmacol. 84 (1986) 464-469
10. B. K. Ardent, J. L. Borowitz, G. E. Isom, Brain lipid peroxidation and antioxidant protectant mechanisms following acute cyanide intoxication, Toxicological 56 (1989) 147-154.
11. S. I. Baskin, T. G. Brewer, Cyanide poisoning, in medical aspects of chemical and biological warfare, Washington, DC (1997) 271-286.
12. R. A. Greenfield, B. R. Brown, J. B. Hutchins, J. J. Iandolo, R. Jackson, L. N. Slater, M. S. Bronze, Microbiological, biological, and chemical weapons of warfare and terrorism, Am. J. Med. Sci. 323 (2002) 326-340.
13. World Health Organisation, Guidelines for Drinking-Water Quality, World Health Organisation, Geneva, Switzerland (1996).

14. A. Mouradzadegun, F. Abadast, An improved organic/inorganic solid receptor for colorimetric cyanide-chemosensing in water: Towards new mechanism aspects, simplistic use and portability, Chem. Commun. 50 (2014) 15983-15986.
15. C. Zhoua, M. Suna, C. Yana, Q. Yanga, Y. Lia, Y. Song, A new colorimetric and fluorescent chemodosimeter for fast detection of cyanide, Sens. Actuators, B 203 (2014) 382-387.
16. Jayasudha, R. Manivannan, K. P. Elango, Simple colorimetric chemodosimeters for selective sensing of cyanide ion in aqueous solution *via* termination of ICT transition by Michael addition, Sens. Actuators, B 221 (2015) 1441-1448.
17. R. Manivannan, K. P. Elango, Structure–reactivity correlation in selective colorimetric detection of cyanide in solid, organic and aqueous phases using quinone based chemodosimeters, New J. Chem. 40 (2016) 1554-1563.
18. K. Y. Chen, W. C. Lin, A simple 7-azaindole-based ratiometric fluorescent sensor for detection of cyanide in aqueous media, Dyes Pigm. 123 (2015) 1-7.
19. B. Garg, L. Yan, T. Bisht, C. Zhu, Y. C. Ling, A phenothiazine-based colorimetric chemodosimeter for the rapid detection of cyanide anions in organic and aqueous media, RSC Adv. 4 (2014) 36344-36349.
20. J. Jo, A. Olasz, C. H. Chen, D. Lee, Interdigitated hydrogen bonds: Electrophile activation for covalent capture and fluorescence turn-on detection of cyanide, J. Am. Chem. Soc. 135 (2013) 3620-3632.
21. S. S. Razi, R. Ali, P. Srivastava, A. Misra, A selective quinolone-derived fluorescent chemodosimeter to detect cyanide in aqueous medium, Tetrahedron Lett. 55 (2014) 1052-1056.
22. R. Ali, S. S. Razi, P. Srivastava, A. Misra, Tetrasubstituted imidazole core containing ESIPT fluorescent chemodosimeter for selective detection of cyanide in different medium, Sens. Actuators, B 221 (2015) 1236-1247.
23. H. M. Chawla, M. Shahid, D. S. Black, N. Kumar, A new calix [4] arene based molecular probe for selective and sensitive detection of CN^- ions in aqueous media, New J. Chem. 38 (2014) 2763-2765.
24. M. K. Chahal, M. Sankar, Porphyrin chemodosimeters: synthesis, electrochemical redox properties and selective 'naked-eye' detection of cyanide ions, RSC Adv. 5 (2015) 99028-99036.
25. L. Yuan, W. Lin, Y. Yang, J. Song, J. Wang, Rational design of a highly reactive; ratiometric fluorescent probe for cyanide, Org. Lett. 13 (2011) 3730-3733.

26. C. Y. Kim, S. Park, H. J. Kim, Indocyanine based dual optical probe for cyanide in HEPES buffer, Dyes Pigm. 130 (2016) 251-255.
27. S. Y. Na, H. J. Kim, Azo dye-based colorimetric chemodosimeter for the rapid and selective sensing of cyanide in aqueous solvent, Tetrahedron Lett. 56 (2015) 493-495.
28. C. R. Maldonado, A. T. Varela, A. C. Jonesa, J. C. M. Rivas, A turn-on fluorescence sensor for cyanide from mechanochemical reactions between quantum dots and copper complexes, Chem. Commun. 47 (2011) 11700-11702.
29. A. T. Varela, E. I. Stevenson, J. A. G. Gasion, D. T. F. Dryden, J. C. M. Rivas, Selective turn-on fluorescence detection of cyanide in water using hydrophobic CdSe quantum dots, Chem. Commun. 17 (2008) 1998-2000.
30. A. Dvivedi, P. Rajakannu, M. Ravikanth, meso-Salicylaldehyde substituted BODIPY as a chemodosimetric sensor for cyanide anions, Dalton Trans. 44 (2015) 4054-4062.
31. C. Chakraborty, M. K. Bera, P. Samanta, S. Malik, Selective detection of cyanide by a polyfluorene-based organoboron fluorescent chemodosimeter, New J. Chem. 37 (2013) 3222-3228.
32. I. Takashima, A. Kanegae, M. Sugimoto, A. Ojida, Aza-crown-ether-appended xanthene: Selective ratiometric fluorescent probe for silver (I) ion based on arene-metal ion interaction, Inorg. Chem. 53 (2014) 7080-7082.
33. H. M. Chawla, M. Shahid, L. S. Arora, B. Uttam, Synthesis and evaluation of a tri-armed molecular receptor for recognition of mercury and cyanide, toxicants http://dx.doi.org /10.1080/ 10610278.2016.1175567.
34. L. Tang, M. Cai, A highly selective and sensitive fluorescent sensor for Cu^{2+} and its complex for successive sensing of cyanide *via* Cu^{2+} displacement approach, Sens. Actuators, B 173 (2012) 862-867.
35. S. Bhardwaj, N. Maurya, A. K. Singh, R. Varshney, P. Roy, Promising ESIPT-based fluorescence sensor for Cu^{2+} and CN^{-} ions: investigation towards logic gate behavior, anticancer activities and bioimaging application, RSC Adv. 6 (2016) 102096-102101.
36. N. Maurya, S. Bhardwaj, A. K. Singh, Selective and sensitive colorimetric sensor for CN^{-} in the absence and presence of metal ions (Cu^{2+}/Ni^{2+}): mimicking logic gate behavior, RSC Adv. 6 (2016) 71543-71549.
37. S. Bhardwaj, A. K. Singh, Visual & reversible sensing of cyanide in real samples by an effective ratiometric colorimetric probe & logic gate application, J. Hazard. Mater. 296 (2015) 54-60.

38. N. Maurya, S. Bhardwaj, A. K. Singh, A modest colorimetric chemosensor for investigation of CN^- in semi-aqueous environment with high selectivity and sensitivity, Sens. Actuators, B 229 (2016) 483-491.
39. N. Yadav, A. K. Singh, Dual anion colorimetric and fluorometric sensing of arsenite and cyanide ions, RSC Adv. 6 (2016) 100136-100144.
40. M. Shahid, H. M. Chawla, P. Bhatia, A calix [4]arene based turn off/turn on molecular receptor for Cu^{2+} and CN^- ions in aqueous medium, Sens. Actuators, B 237 (2016) 470-478.
41. Q. Zou, X. Li, J. Zhang, J. Zhou, B. Sun, H. Tian, Unsymmetrical diarylethenes as molecular keypad locks with tunable photochromism and fluorescence via Cu^{2+} and CN^- coordination, Chem. Commun. 48 (2012) 2095-2097.
42. M. Shahid, S. S. Razi, P. Srivastava, R. Ali, B. Maiti, A. Misra, A useful scaffold based on acenaphthene exhibiting Cu^{2+} induced excimer fluorescence and sensing cyanide via Cu^{2+} displacement approach, Tetrahedron 68 (2012) 9076-9084.
43. N. Maurya, S. Bhardwaj, A. K. Singh, Selective colorimetric and fluorescence 'turn-on' sensor for Ag^+ and *in-situ* sensing of CN^- (Off–On-Off) *via* displacement approach, Mater. Sci. Eng., C 74 (2017) 55-61.
44. J. H. Lee, A. R. Jeong, I. S. Shin, H. J. Kim, J. I. Hong, Fluorescence turn-on sensor for cyanide based on a cobalt (II) coumarinylsalen complex, Org. Lett. 12 (2010) 764-767.
45. C. M. Croisé, F. Zelder, Side chains of cobalt corrinoids control the sensitivity and selectivity in the colorimetric detection of cyanide, Inorg. Chem. 48 (2009) 1272-12741.
46. K. I. Hong, H. Yoon, W. D. Jang, A triazole-bearing picket fence type nickel porphyrin as a cyanide selective allosteric host, Chem. Commun. 51 (2015) 7486-7488.
47. R. Kumar, N. Chaudhri, M. Sankar, Ratiometric and colorimetric "naked eye" selective detection of CN^- ions by electron deficient Ni(II) porphyrins and their reversibility studies, Dalton Trans. 44 (2015) 9149-9157.
48. M. Tomasulo, S. Sortino, A. J. P. White, F. M. Raymo, Chromogenic oxazines for cyanide detection, J. Org. Chem. 71 (2006) 744-753.
49. M. Shahid, A. Misra, A simple and sensitive intramolecular charge transfer fluorescent probe to detect CN^- in aqueous media and living cells, Anal. Methods 5 (2013) 434-437.
50. H. T. Niu, D. Su, X. Jiang, W. Yang, Z. Yin, J. He, J. P. Cheng, A simple yet highly selective colorimetric sensor for cyanide anion in an aqueous environment, Org. Biomol. Chem. 6 (2008) 3038-3040.

51. R. Sukato, N. Sangpetch, T. Palaga, S. Jantrac, V. Vchirawongkwin, C. Jongwohanc, M. Sukwattanasinittd, S. Wacharasindhud, New turn-on fluorescent and colorimetric probe for cyanide detection based on BODIPY-salicylaldehyde and its application in cell imaging, J. Hazard. Mater. 314 (2016) 277-285.
52. S. Yagi, K. Maeda, H. Nakazumi, Photochromic properties of cationic merocyanine dyes thermal stability of the spiropyran form produced by irradiation with visible light, J. Mater. Chem. 9 (1999) 2991-2997.
53. K. Prakash, P. R. Sahoo, S. Kumar, A substituted spiropyran for highly sensitive and selective colorimetric detection of cyanide ions, Sens. Actuators, B 237 (2016) 856-864.
54. Y. Prostota, P. J. Coelho, Cationic 3H-indolium dyes by ring-opening of benzo [1,3], Dyes Pigm. 98 (2013) 93-99.
55. R. K. Konidena, K. R. J. Thomas, Selective naked-eye cyanide detection in aqueous media using a carbazole-derived fluorescent dye, RSC Adv. 4 (2014) 22902-22910.
56. M. J. Frisch, G. W. Trucks, H. B. Schlegel, G. E. Scuseria, M. A. Robb, J. R. Cheeseman, J. A. Montgomery, J. T. Vreven, K. N. Kudin, J. C. Burant, J. M. Millam, S. S. Iyengar, J. Tomasi, V. Barone, B. Mennucci, M. Cossi, G. Scalmani, N. Rega, G.A. Petersson, H. Nakatsuji, M. Hada, M. Ehara, K. Toyota, R. Fukuda, J. Hasegawa, M. Ishida, T. Nakajima, Y. Honda, O. Kitao, H. Nakai, M. Klene, X. Li, J. E. Knox, H. P. Hratchian, J. B. Cross, V. Bakken, C. Adamo, J. Jarmillo, R. Gomperts, R. E. Stratmann, O. Yazyev, A. J. Austin, R. Cammi, C. Pomelli, J. W. Ochterski, P. Y. Ayala, K. Morokuma, G. A. Voth, P. Salvador, J. J. Dannenberg, V. G. Zakrzewski, S. Dapprich, A. D. Daniels, M. C. Strain, O. Farkas, D. K. Malick, A. D. Rabuck, K. Raghavachari, J. B. Foresman, J. V. Ortiz, Q. Cui, G. Baboul, S. Clifford, J. Cioslowski, B. B. Stefanov, G. Liu, Liashenko, P. Piskorz, I. Komaromi, R. L. Martin, D. J. Fox, T. Keith, M. A. Al-Laham, C. Y. Peng, A. Nanayakkara, M. Challacombe, P. M. W. Gill, B. Johnson, W. Chen, M. W. Wong, C. Gonzalez, J. A. Pople, Gaussian, 03, Revision D.01, Gaussian, Inc., Wallingford, CT (2004).
57. X. Zhou, X. Lv, J. Hao, D. Liu, W. Guo, Coumarine indanedione conjugate as a doubly activated Michael addition type probe for the colorimetric and ratiometric fluorescent detection of cyanide, Dyes Pigm. 95 (2012) 168-173.
58. L. Wang, L. Zhu, D. Cao, A colorimetric probe based on diketopyrrolopyrrole and tert-butyl cyanoacetate for cyanide detection, New J. Chem. 39 (2015) 7211-7218.

59. Y. Xu, X. Dai, B. X. Zhao, A coumarin-indole based colorimetric and ‘‘turn on’’ fluorescent probe for cyanide, Spectrochim. Acta, A 138 (2015) 164-168.
60. M. Dong, Y. Peng, Y. M. Dong, N. Tang, Y. W. Wang, A Selective colorimetric and fluorescent chemodosimeter for relay recognition of fluoride and cyanide anions based on 1,10-Binaphthyl scaffold, Org. Lett. 14 (2012) 130-133.
61. Y. Shan, Z. Liu, D. Cao, G. Liu, R. Guan, N. Sun, C. Wang, K. Wang, Coumarinic chalcone derivatives as chemosensors for cyanide anions and copper ions, Sens. Actuators, B 221 (2015) 463-469.
62. S. Park, H. J. Kim, Highly activated Michael acceptor by an intramolecular hydrogen bond as a fluorescence turn-on probe for cyanide, Chem. Commun. 46 (2010) 9197-9199.
63. A. K. Mahapatra, K. Maiti, R. Maji, S. K. Manna, S. Mondal, S. S. Ali, S. Manna, Ratiometric fluorescent and chromogenic chemodosimeter for cyanide detection in water and its application in bioimaging, RSC Adv. 5 (2015) 24274-24280.
64. M. J. Peng, Y. Guo, X. F. Yang, F. Suzenet, J. Li, C.W. Lia, Y. W. Duan, Coumarin-hemicyanine conjugates as novel reaction-based sensors for cyanide detection: convenient synthesis and ICT mechanism, RSC Adv. 4 (2014) 19077-19085.
65. S. Zhu, M. Li, L. Sheng, P. Chen, Y. Zhang, S. X. A. Zhang, A spirooxazine derivative as a highly sensitive cyanide sensor by means of UV-visible difference spectroscopy, Analyst 137 (2012) 5581-5585.
66. C. Zhou, M. Sun, C. Yan, Q. Yang, Y. Lia, Y. Song, A new colorimetric and fluorescent chemodosimeter for fast detection of cyanide, Sens. Actuators, B 203 (2014) 382-387.
67. S. Wang, X. Fei, J. Guo, Q. Yang, Y. Li, Y. Song, A novel reaction based colorimetric and ratiometric fluorescent sensor for cyanide anion with a large emission shift and high selectivity, Talanta 148 (2016) 229-236.
68. X. Lv, J. Liu, Y. Liu, Y. Zhao, Y. Q. Sun, P. Wang, W. Guo, Ratiometric fluorescence detection of cyanide based on a hybrid coumarin-hemicyanine dye: the large emission shift and the high selectivity, Chem. Commun. 47 (2011) 12843-128.
69. M. Sun, S. Wang, Q. Yang, X. Fei, Y. Li, Y. Li, A new colorimetric fluorescent sensor for ratiometric detection of cyanide in solution, test strips and in cells, RSC Adv. 4 (2014) 8295-8299.

CHAPTER 5

Metal Displacement Based Cyanide Sensor (Indirect Approach)

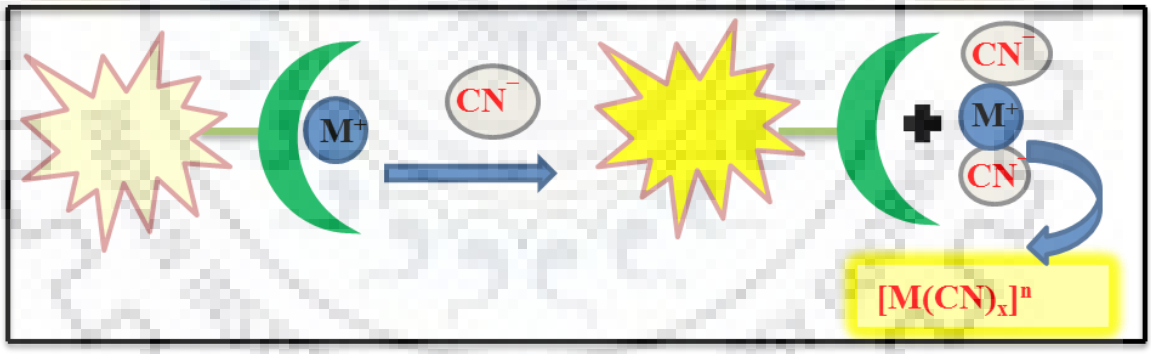

5.1 INTRODUCTION

The design of synthetic receptors for selective recognition of biologically essential cations and anions is an emerging area of research in supramolecular chemistry due to the vital roles played by these species in biological, chemical and environmental processes [1]. Cu^{2+} serves as an essential supplement for life by constituting the active part in various enzymes, counting cytochrome c oxidase, superoxide dismutase and tyrosinase [2]. Contradictory, casual overloading of Cu^{2+} can encourage severe neurodegenerative disorders like as Parkinson's disease, Alzheimer's and prion diseases [3-4]. Likewise CN^- is functional in numerous industrial relevance, such as herbicides, electroplating, metallurgy, polymer-production & mining, also applicative in the scrutiny of copper, silver, and gold from platinum [5-6]. The key extraction step for the proficient recapture of gold from complex ores causes CN^- leaching and presence of acids causes liberation of HCN gas from cyanide salts [3]. Sadly, leaching of CN^- to environment claims intensely detrimental to the living entities because of its inhibitory action on cytochrome oxidase. It disrupts mitochondrial electron transport chain by interacting tightly with the heme unit at the active site of cytochrome a3, resulting the inhibition of cellular respiration called hypoxia [7]. The appalling concentration of CN^- within the blood of fire victims has been recommended to be between 23-26 mM [8-9]. So, the advancement in the field of selective recognition of Cu^{2+} and CN^- is highly desirable.

Subsequently, swift methods that privilege acute *in-situ* recognition with great selectivity have precise promise for medical point-of-care as well as environmental online monitoring. Unlike certain analytical techniques, such as atomic absorption spectrometry, chromatography, and electrochemical methods [10-12], optical detections (*via* fluorescence or colorimetric changes) achieve these qualities and are the valuable techniques with great sensitivity and immense simplicity [13-15]. Development of aggregates emit based chemosensor in aqueous medium has prompted much concern in recent years. Tang's *et al* in 2001 reported "aggregation induced emission enhancement" (AIEE) phenomenon, which is precisely opposite to the aggregation caused quenching (ACQ) effect [16]. Since, AIEE luminogens properties have been intensively deliberate, containing variations of proposed mechanisms and potential applications such as bio/chemosensors organic light-emitting diodes (OLEDs) [17], two-photon absorption (2PA) [18], materials and drug delivery [19].

Due to the optical properties, chromones drag attention in the fluorescence sensing towards biologically important cations and anions on a molecular level. Chromone derivatives practice an important constituent of pharmacophores, naturally occurring biologically active molecules, ubiquitously found in the synthetic as well as natural origin [20-21]. These phytochemicals own a broad spectrum of biological activities due to their well-known antioxidant properties, which stem from their skill to counteract active forms of oxygen and to block the free radical scavenger [22]. They display a remarkable domain of biochemical and pharmacological actions such as antibacterial, antifungal, anticancer, antimalarial, topoisomerase I inhibitor, antidepressant and monoamine oxidase inhibitors properties [23-26]. Some of the chromone derivatives have been figure out for *in-vitro* antiviral activities counter to human immunodeficiency virus (HIV) and Simian immunodeficiency virus (SIV) [27-28].

While numerous brilliant optical sensors have been stated in the literature; still some advances in sensing application in aqueous environment are required. The low water solubility of most sensing receptors is the main reason to minimise the sensitivity during sensing applications in real samples. In order to overcome this problem and to improve sensing activities of organic compounds, fluorescent organic nanoparticles have been developed as an innovative method to enhance the sensing in water [29-31]. The organic nanoparticles are defined as colloidal particles composed of organic compound ranging in diameter from 10 nm to 1mm. These organic nanoparticles can be prepared by various methods like as; procedure based on emulsification, Nano-precipitation and by drying process.

Here we reported some novel cromone based fluorophores due to the optical properties for Cu^{2+} and CN^{-}. Further; we envisioned that aggregates of chromone derivative in the aqueous medium form as organic nanoparticles. These organic nanoparticles mimic as an extremely selective and immensely sensitive fluorogenic 'turn off' sensor toward Cu^{2+}. Interestingly, *in-situ* formed Chromone-Cu^{2+} ensemble complex exhibited remarkably selective fluorogenic 'Turn ON' recognition towards CN^{-} in aqueous solution. Moreover, we applied this sensing system as logic gate behavior as well as antimicrobial activity, proposed their auspicious prospect in biological and environmental science

5.2 EXPERIMENTAL SECTION

5.2.1 Chemical and Instrumentation

All chemicals and solvents (MeOH, EtOH) were perched from Sigma-Aldrich. Both solvent were distilled under reduced pressure ($CaCl_2$ as drying) and stored on molecular sieve. The elemental analysis (for CHNS) was supported by using vireo MICROV3.1.1 instrument. For UV-vis spectra, Specord S600 Thermo-Scientific PC double beam spectrophotometer (path length 1 cm) and for fluorescence spectra Horiba RF-5301PC (path length 3 cm) used with standard quartz cell. The NMR spectra were documented in JEOL 400 MHz spectrophotometer by using TMS as an internal standard. The size and topographical analysis of developed S3-FONs were examined *via* field emission scanning electron microscopy (FESEM). FESEM analysis was performed with on FEI Quanta 200F scanning electron microscope functioning at 5 kV. Confocal Laser Scanning Microscope (LSM 780, Carl Zeiss, and Germany) was used for cell imaging applications. CHI760E Electro analyser three-electrode cell with glassy carbon as working electrode, $Hg/HgCl_2$ as reference electrode, Pt wire as counter electrode and 0.1 M tetrabutylammonium hexafluorophosphate (nBu_4NPF_6) as supporting electrolyte were used for electrochemical study. HeLa (human cervical adenocarcinoma) cell lines were purchased from National Centre for Cell Sciences (NCCS), Pune, India. The cell lines were preserved in Dulbecco's Modified Eagle Medium (DMEM) accompanied with 10% heat inactivated fetal bovine serum and 1% antibiotic mix (100 U/ml of penicillin and 100 µg/ml streptomycin) at 37 ℃ in CO_2 incubator.

5.2.2 General Procedure for Experiments

The absorption spectra were examined by keeping the receptor concentration at 20 µM, while 5 µM used for emission spectra. The antagonism study used different interfering anions with CN^- in 4:1 ratio. The detection limit (LOD) was intended by perilously reported method ($3\sigma/S$) [32-33], where σ is the standard deviation of the blank solution and S is the slope of the calibration curve. For Cyclic Voltammetry, distilled solvent and nBu_4NPF_6 has been used on which S1 was dispersed (1 mM, scan rate 0.1 V s^{-1} and potential range -2.0 to +2.0 V). Further titrate receptor S1 with 1 mM solution of Cu^{2+} & CN^- and observed the change in potential.

5.2.3 Synthesis and Characterization of Receptors (S1-S4)

For synthesis of S1 & S4 the ethanolic solution of 3-formyl chromone (1 mmol) and corresponding amine (1 mmol) was mixed and refluxed. After completion of the reaction, a yellow colored precipitate was formed within 40 minutes. The incorporation of solvent pointed out *in-situ* nucleophilic substitution reaction took place *via* solvent, which was confirmed by replacement of solvent system with methanol and found a methoxy group integrated S2 & S3 with 80% Yield.

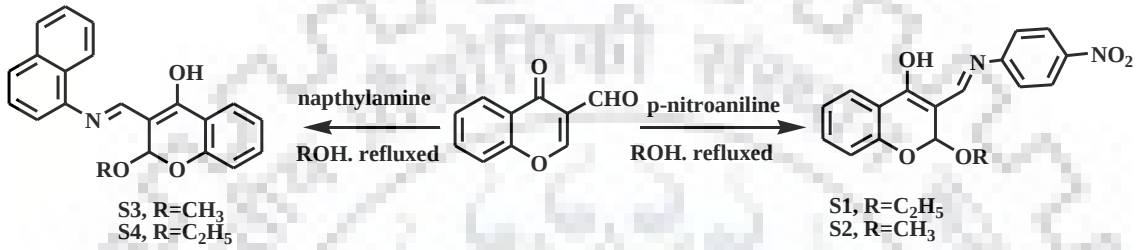

Scheme: 5.1 Synthesis of receptors S1-S4.

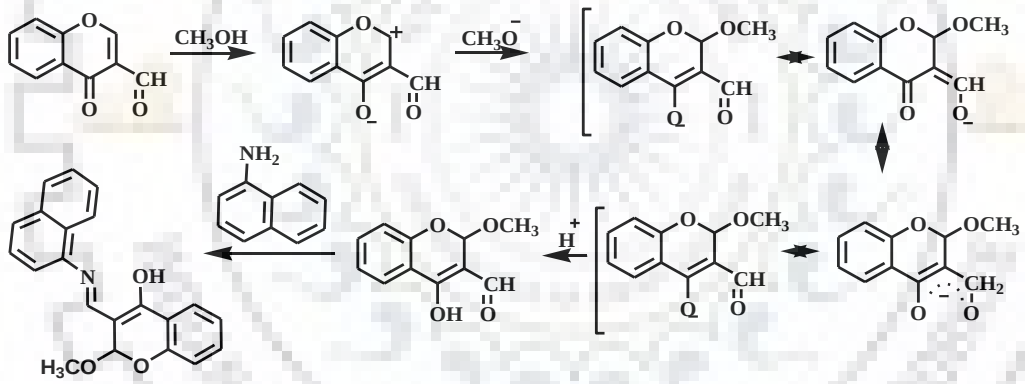

Scheme: 5.2 Mechanistic investigation of *in-situ* nucleophilic substitution at 2-position of reactant *via* methoxide ion (3-formylchromone) to form S3.

S1: (2-ethoxy-3-((p-nitrophenyl-1-ylimino)methyl)-2H-chromen-4-ol)

Anal. Cal. ($C_{18}H_{16}N_2O_5$): C-63.52, H-4.74, N-8.23, O-23.51; Found : C-63.54, H-4.73, N-8.23; ^{1}H NMR ($CDCl_3$, 400 MHz, δ/ppm) : 12.18 (d, 1H), 8.24 (d, 2H), 7.96 (d, 1H), 7.50 (t, 2H), 7.17 (d, 2H), 7.12 (t, 1H), 7.03 (d, 1H), 5.81 (s, 1H), 3.95-3.89 (m, 1H), 3.76-3.70 (m, 1H), 1.22 (t, 3H); ^{13}C NMR ($CDCl_3$, 100 MHz, δ/ppm) : 182.7, 162.0, 156.3, 141.9, 140.0, 135.2, 126.7 (2C), 122.6, 122.4, 118.3, 116.3, 112.7, 106.3 (2C), 101.4, 55.7, 15.4; APCI-MS m/z (m+H) = 341.2 (calcd-341.11).

S2: **(2-methoxy-3-((p-nitrophenyl-1-ylimino)methyl)-2H-chromen-4-ol)**

Anal. Cal. ($C_{17}H_{14}N_2O_5$) : C-62.57, H-4.32, N-8.59, O-24.52; Found: C-62.61, H-4.29, N-8.62; ^{1}H NMR (DMSO d_6, 400 MHz, δ/ppm) : 11.79 (d, 1H), 8.24 (d, 2H), 8.20 (d, 1H), 7.85 (d, 1H), 7.61-7.54 (m, 3H), 7.18-7.10 (m, 2H), 5.85 (s, 1H), 3.40 (s, 3H); ^{13}C NMR (DMSO d_6, 100 MHz, δ/ppm) : 181.4, 156.2, 146.3, 143.9, 143.0, 135.7, 126.3, 126.2, 122.9, 122.7, 118.8, 117.1, 109.1, 106.6, 101.6, 97.5, 55.5; APCI-MS m/z (m+H) = 327.1 (calcd-327.09).

S3: (2-methoxy-3-((naphthalen-1-ylimino)methyl)-2H-chromen-4-ol)

Anal. Cal. ($C_{21}H_{17}NO_3$): C-76.12, H-5.17, N-4.00, O-14.49; Found: C-76.16, H-5.15, N-4.26, ^{1}H NMR (DMSO d_6, 400 MHz, δ/ppm) : 12.98 (d, 1H), 8.37 (d, 1H), 8.03 (d, 1H), 7.98 (d, 1H), 7.89 (d, 1H), 7.73-7.68 (m, 2H), 7.65-7.58 (m, 2H), 7.56-7.51 (m, 2H), 7.15-7.09 (m, 2H), 5.89 (s, 1H), 3.38 (s, 3H); ^{13}C NMR (DMSO d_6, 100 MHz, δ/ppm) : 180.6, 155.4, 146.5, 135.0, 134.6, 133.9, 128.8, 127.1, 126.8, 126.2, 125.7, 124.4, 123.7, 122.6, 122.1, 119.8, 118.1, 111.5, 104.3, 100.9, 54.8.

S4: (2-ethoxy-3-((naphthalen-1-ylimino)methyl)-2H-chromen-4-ol)

Anal. Cal. ($C_{22}H_{19}NO_3$): C-76.50, H-5.54, N-4.06, O-13.90; Found: C-76.52, H-5.52, N-4.08; ^{1}H NMR (DMSO d_6, 400 MHz, δ/ppm) : 13.02 (d, 1H), 8.40 (d, 1H), 8.08 (d, 1H), 8.02 (d, 1H), 7.93 (d, 1H), 7.75 (t, 2H), 7.70-7.64 (m, 2H), 7.60-7.54 (m, 2H), 7.17 (t, 1H), 7.11 (d, 1H), 6.04 (s, 1H), 3.81-3.69 (m, 2H), 1.11 (t, 3H); ^{13}C NMR ($CDCl_3$, 100 MHz, δ/ppm) : 181.8, 156.7, 147.7, 136.2, 135.8, 135.1, 130.0, 128.3, 128.0, 127.4, 126.9, 125.6, 124.9, 123.8, 123.3, 121.0, 119.3, 112.7, 105.5, 102.1, 62.9, 15.2.

5.3 RESULTS AND DISCUSSION

5.3.1 Sensing Studies of Receptor S1

5.3.1.1 AIEE Behavior and Optimization of S1

To examine the AIEE properties of S1 employed MeOH as the decent solvent and water as poor solvent. S1 shows the less molar absorptive band at 382 nm with very low intense emission band (Φ = 0.04) at 456 nm in pure MeOH due to excited

state intramolecular proton transfer (ESIPT) process along with isomerization of C=N bond at the excited state [34]. Clearly, upon altering the water system from methanol (up to 100%), the absorption and emission intensity was enhanced with red shift. The emission band shifted to 503 nm and reaches to the maximum, just about 13 folds (Φ = 0.53) greater than its molecularly discrete species in MeOH, indicates inhibition of ESIPT process and molecules gets aggregates with increasing water content. Thus the specious enhancement in emission was prompted by aggregation, substantiating its AIEE behavior due to the restricted intramolecular motions. The aggregation process could be further assisted due to intermolecular hydrogen bond formation (-N-HO) between adjacent molecules [35-38]. Similarly, in absorption spectra, red shift with large hypochromic shift at 395 nm was observed upon addition of water, due to aggregated process into the molecules, which was further proved by SEM (scanning electron microscopy) images in aqueous mixtures (Fig. 5.1).

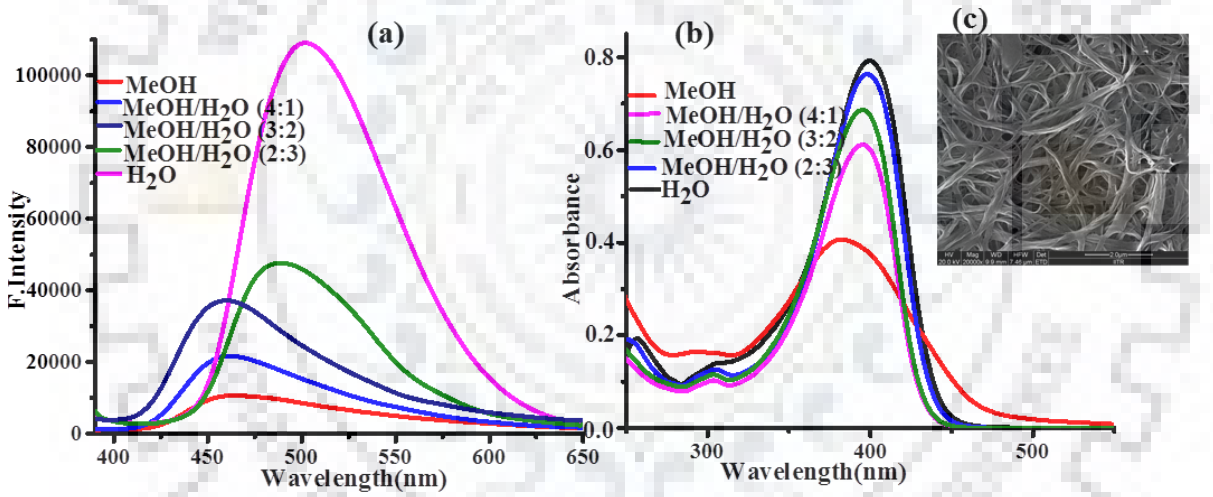

Fig. 5.1 Variations of S1 with consequent amount of water; (a) Emission spectra (b) Absorption spectra (c) SEM image of aggregates on a glass substrate.

The preferred pH was sustained with dilute solutions of hydrochloric acid and sodium hydroxide. Remarkably, the absorption behavior of S1 practically remains constant between 6-9 pH ranges; on the other hand, the emission intensity is stable at 6-8 pH, due to protonation and deprotonation of -OH group (Fig. 5.2). From the above result shows the compatibility of S1 in pure aqueous medium at biological pH range, thus all analytical studies were accomplished in 100% aqueous medium with 7.4 pH HEPES buffer.

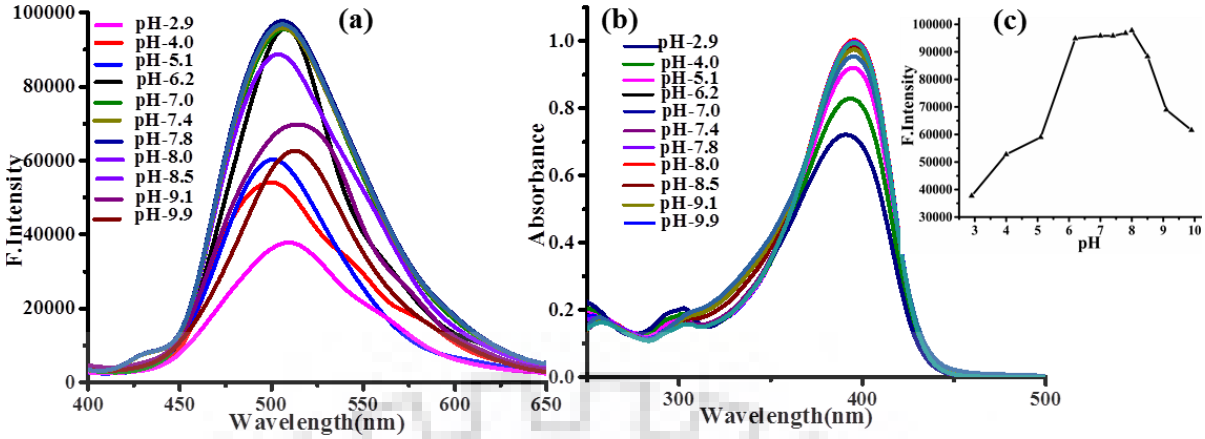

Fig. 5.2 Variations in pH of S1; (a) Emission spectra (b) Absorption spectra (c) pH graph.

5.3.1.2 Optical Responses of S1 as Primary Sensor for Cu^{2+} Ion

The absorption spectrum of S1 showed a low energy band at 395 nm with a shoulder at 302 nm. Furthermore, S1 displayed high emission intensity at 503 nm (λ_{ext} - 390 nm). To estimate the affinity of S1 toward various metal ions (5 eq.) such as Mg^{2+}, Ca^{2+}, Al^{3+}, Pb^{2+}, Sn^{2+}, Cr^{3+}, Mn^{2+}, Fe^{2+}, Co^{2+}, Ni^{2+}, Cu^{2+}, Ag^{+}, Zn^{2+}, Cd^{2+}, Hg^{+} and Hg^{2+} was concluded by emission and absorption spectra. The molar absorptivity of low energy band decreases with slightly blue shift at 389 nm and a new broad band at 257 nm was generated only with Cu^{2+}. In contrast, relative emission was almost quenched (Φ = 0.053). The formed metal complex was dissolved in water, there was no intermolecular H-bond, presenting the interruption of diligently packed aggregates (disaggregates particles) and another reason is the paramagnetic nature of Cu^{2+}, thus quenching occur in emission spectra (Fig. 5.3).

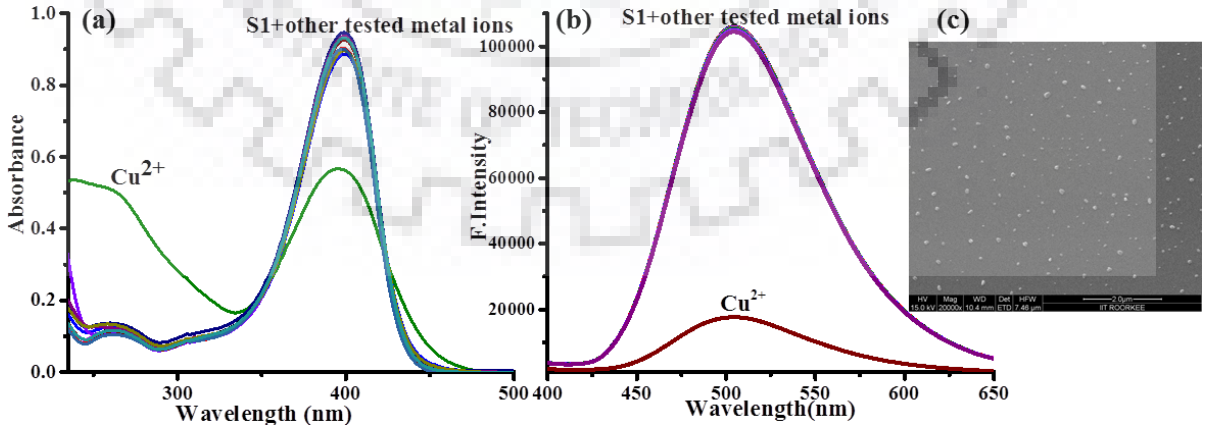

Fig. 5.3 Interaction of S1 with 10 eq. of metal ions; (a) Absorption spectra (b) Emission spectra (c) SEM image of disaggregates of derivative S1-Cu^{2+} complex on a glass substrate in aq. medium (pH-7.4, HEPES buffer).

In the direction of the anti-jamming aptitude of Cu^{2+} selectivity, interference study was supported by excess addition (20 eq.) of other metal ions into the solution of S1-Cu^{2+}. The result shows selectivity of Cu^{2+} was observed over other interferences (Fig. 5.4).

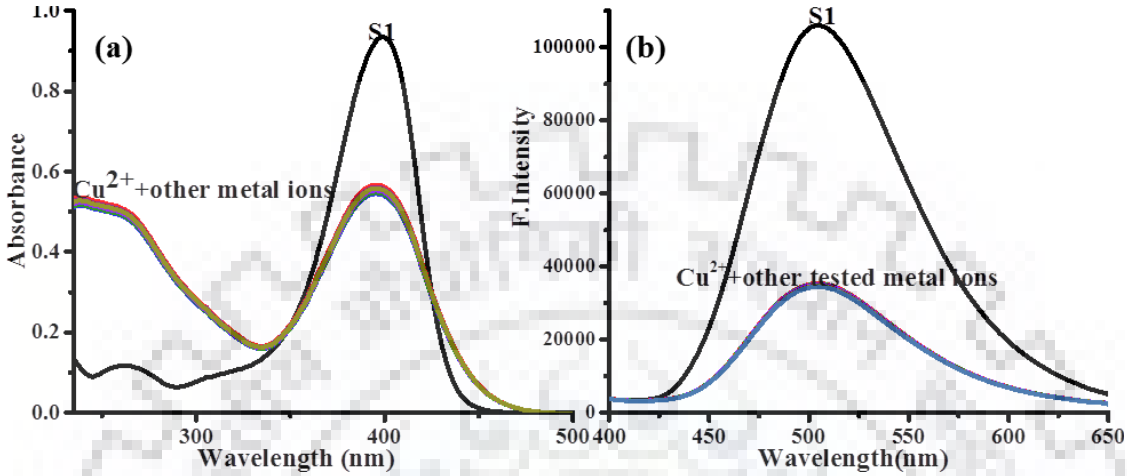

Fig. 5.4 Interference study of S1-Cu^{2+} with other metal ions; (a) Absorption spectra (b) Emission spectra in aq. medium (pH-7.4, HEPES buffer).

Further, to appreciate the binding affinity and stoichiometry between Cu^{2+} and S1, the absorption and emission titration experiments were executed. Upon a consecutive addition of Cu^{2+} (0-3 eq.) into the solution of S1, the molar absorptive band centered, at 395 nm decreases and 257 nm increased with formation of an isosbestic point at 362 nm, signifying transformation without any side equilibria. Correspondingly, fluorescence quenching was observed upon increasing the concentration of Cu^{2+} (Fig. 5.5).

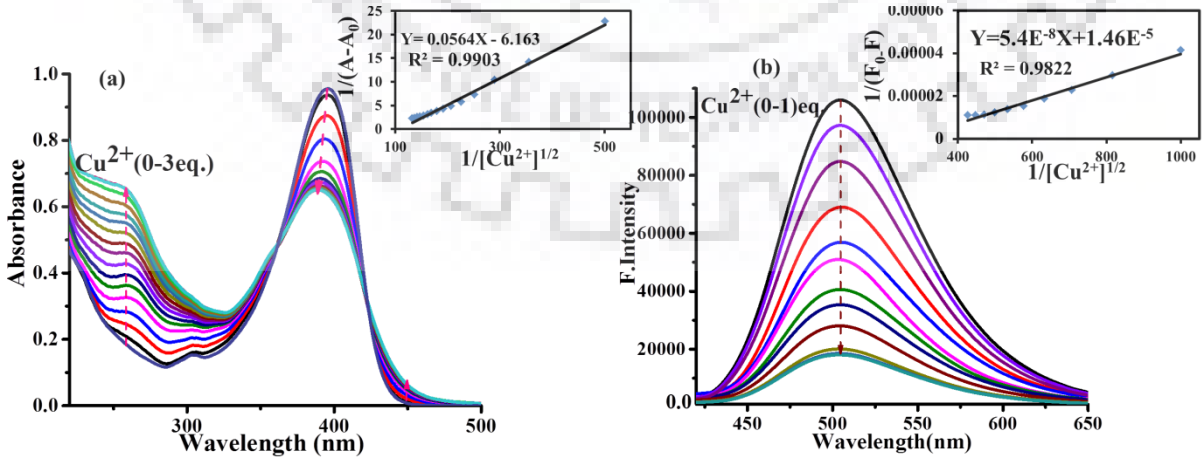

Fig. 5.5 (a) Absorption titration spectra (b) Emission titration spectra; inset: B-H plot of S1 upon addition of Cu^{2+} in aq. medium (pH-7.4, HEPES buffer).

The Benesi-Hildebrand plot [39] shows a very good linearity (R^2_{abs} = 0.9903 and R^2_{em} = 0.9822, inset of Fig. 5.5), which intensely supported 2:1 binding mode between ligand S1 and Cu^{2+} by plotting between $[1/Cu^{2+}]^{1/2}$ and $1/(A_0\text{-}A)$ or $1/(F_0\text{-}F)$. In addition the binding constant was calculated from the intercept/slope, which obtained as $K_{abs} = 1.09 \times 10^2\ M^{-1/2}$ and $K_{em} = 2.69 \times 10^2\ M^{-1/2}$. The reaction time of S1 was observed with 0.5 eq. of Cu^{2+} in emission spectral changes (503 nm) at 30 second time interval. The kinetic result exposed the reaction is accomplished within 60 second (Fig. 5.6 a). Job's plot investigation has shown a 2:1 stoichiometry between S1 and probable Cu^{2+} complex (Fig. 5.6 b).

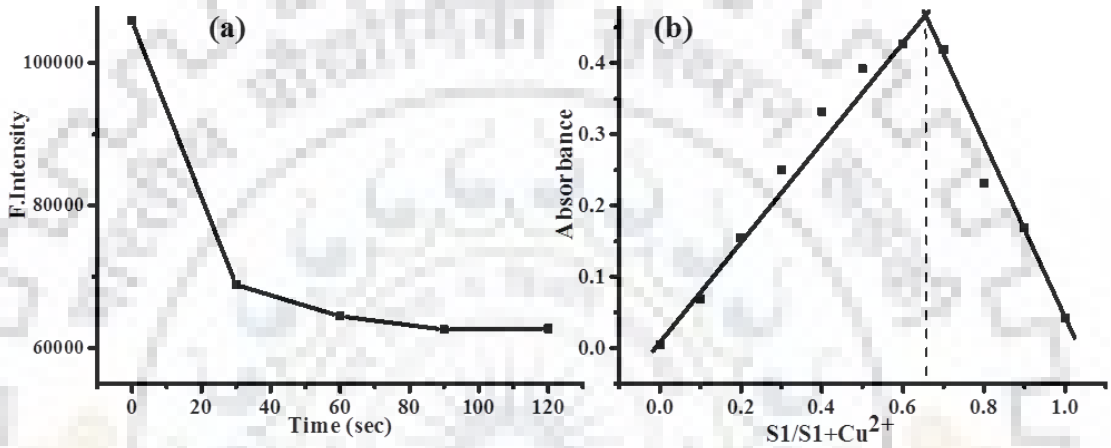

Fig. 5.6 (a) Kinetic study (b) Jobs plot of S1 with Cu^{2+} in aq. medium (pH-7.4, HEPES buffer).

The limit of detection (LOD) was estimated using 3σ/slope and was found to be 1.69 μM (Fig. 5.7), which is below the level of maximum limit (20 μM) of Cu^{2+} in drinking water as set by the U.S. Environmental Protection Agency (EPA). The 2:1 stoichiometry was further confirmed by APCI mass spectroscopy, which shows a peak at m/z = 743.1 (calced-743.12, Fig. 5.8).

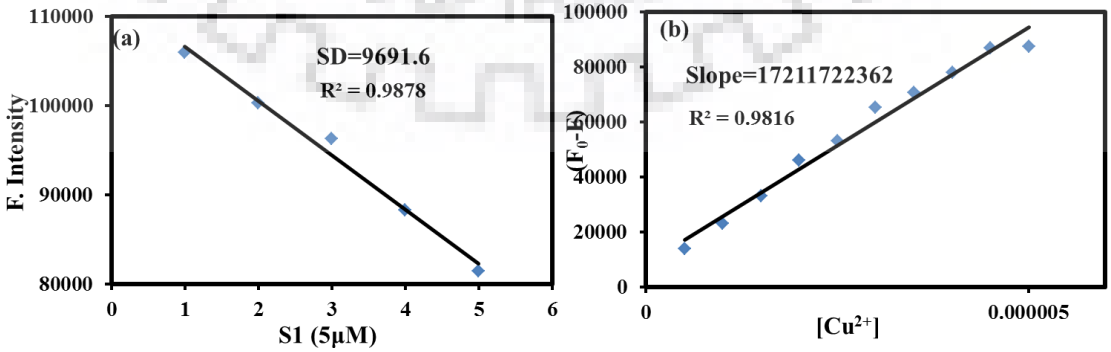

Fig. 5.7 (a) Calibration curve of S1 (b) Calibration sensitivity for Cu^{2+} in aq. medium (pH-7.4, HEPES buffer).

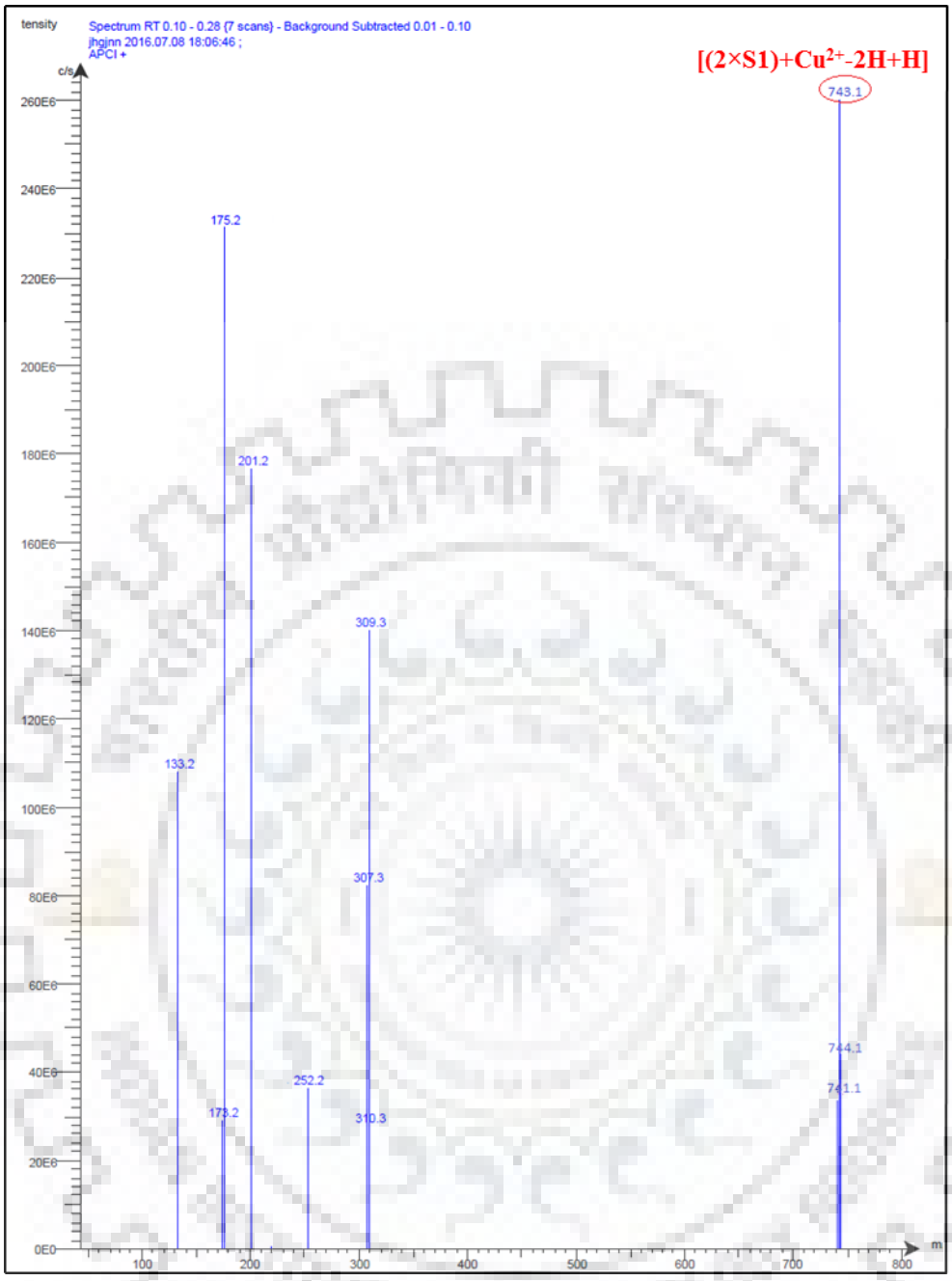

Fig. 5.8 Mass spectrum of S1-Cu^{2+} complex.

5.3.1.3 Optical Responses of S1-Cu^{2+} Complex as Secondary Sensor for CN^- Ion

The renowned interaction of copper with anions such as CN^-, F^-, $H_2PO_4^-$ (metal chelate based) encouraged us to estimate the binding behavior of S1-Cu^{2+} ensemble concerning numerous anions in aqueous medium (pH-7.4, HEPES buffer). Complete restoration of absorbance and emission spectra of the S1 was detected individually with CN^- (Fig. 5.9 a-blue line & 5.9 b-gray line) due to a high binding affinity between copper-cyanide and produce stable $[Cu(CN)x]^{1-x}$ species into the

medium, which results in the aggregation of S1 (Fig. 5.11 a). This result signifies the reverse mode of complexation between S1 and Cu^{2+}. In direction of anti-jamming aptitude of CN^{-} selectivity, an interference studies was performed by the addition of other co-existing anions into the solution of S1-Cu^{2+}. The result shows high selectivity of CN^{-} was observed over other interference anions (Fig. 5.9 a-yellow line & 5.9 b-wine lines).

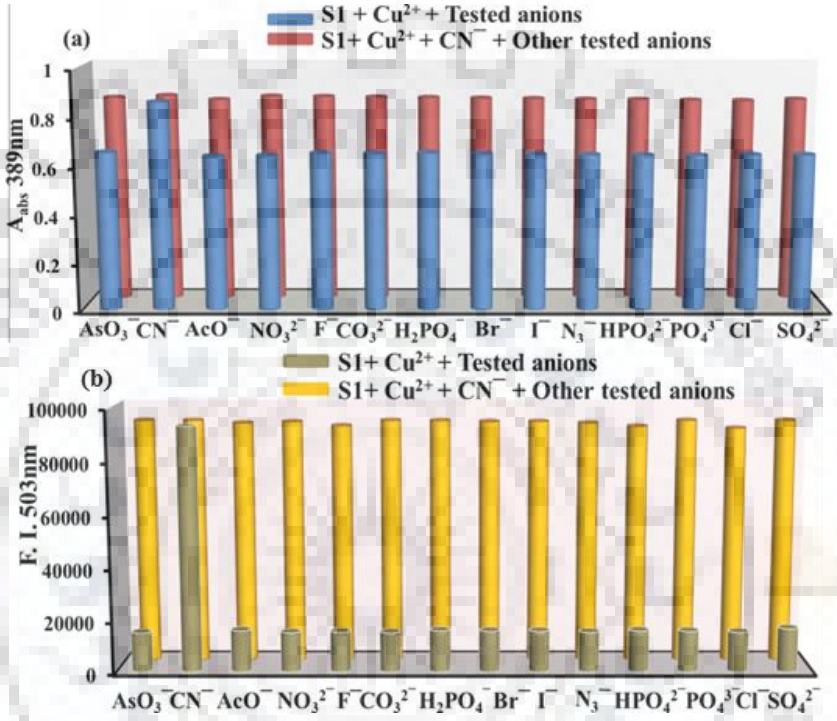

Fig. 5.9 Interaction of S1-Cu^{2+} complex upon 20 eq. of anions; (a) Absorption spectra (b) Emission spectra in aq. medium (pH-7.4, HEPES buffer).

The absorbance and emission titrations of S1-Cu^{2+} complex recorded for the binding affinity of CN^{-} (Fig. 5.10). The B-H plot displayed a very good linearity (R^2_{abs} = 0.9949 and R^2_{em} = 0.9937) with strong binding constant value $K_{abs} = 4.52 \times 10^3\ M^{-1}$ and $K_{em} = 5.23 \times 10^4\ M^{-1}$ (inset of Fig. 5.10). Since, the predictable binding constant of complex concerning S1 and Cu^{2+} was relatively lower than the binding constant of Cu^{2+}-CN^{-}, it is sensible to appreciate the formation of $[Cu(CN)x]^{1-x}$ species in the medium, which modulate both emission and absorption spectra as observed. The reaction kinetics of S1-Cu^{2+} ensemble with 1 eq. of CN^{-} was detected by emission spectral changes (503 nm) at 30 second time interval. The kinetic result reveals the reaction is completed within 90 sec (Fig. 5.11 b). The detection limit was found to be 0.168 μM, which is below the limit of CN^{-} in drinking water set by WHO (1.9 μM), signifying that the S1 is adequately sensitive for practical applications (Fig. 5.12).

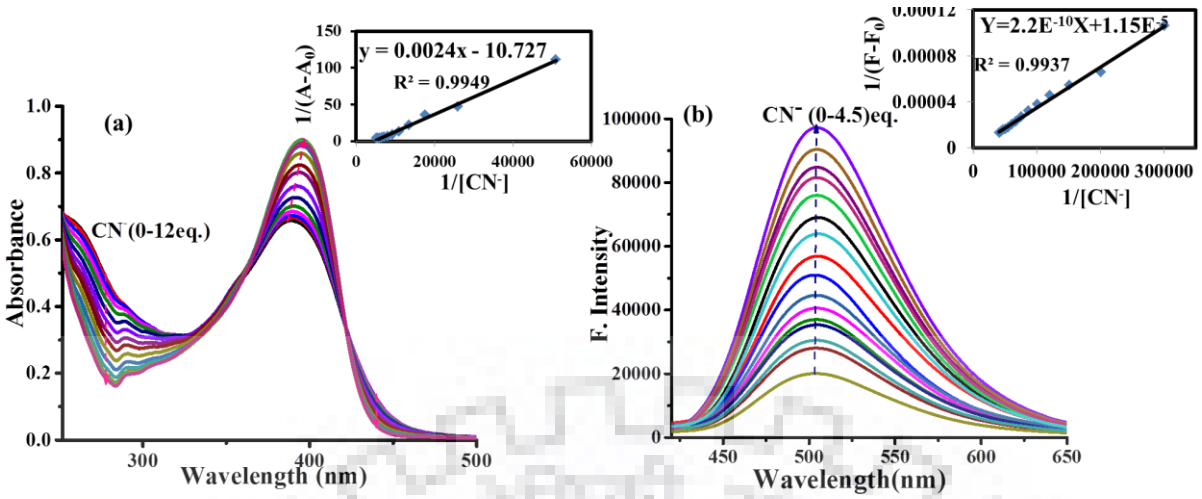

Fig. 5.10 (a) Absorption titration (b) Emission titration; inset: B-H plot of S1-Cu^{2+} complex with addition of CN^{-} in aq. medium (pH-7.4, HEPES buffer).

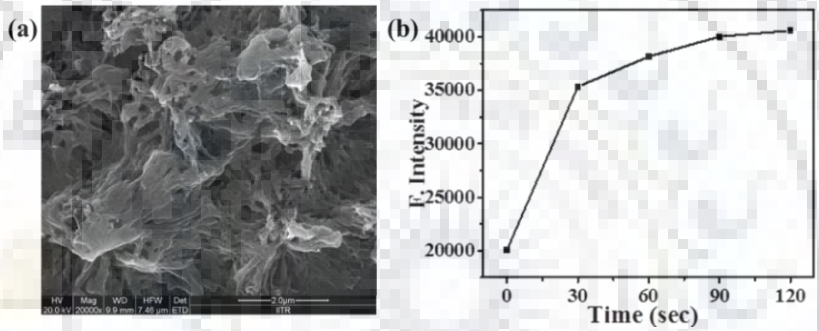

Fig. 5.11 (a) SEM image of aggregates S1-Cu^{2+}-CN^{-} complex (b) Kinetic study of S1-Cu^{2+} complex with CN^{-} in aq. medium (pH-7.4, HEPES buffer).

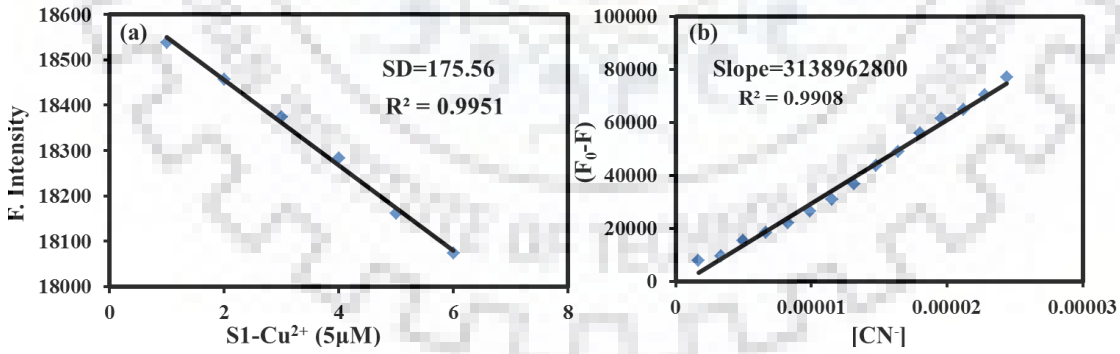

Fig. 5.12 (a) Calibration curve for S1-Cu^{2+} complex (b) Calibration sensitivity for CN^{-} in aq. medium (pH-7.4, HEPES buffer).

5.3.1.4 Electrochemical Studies of S1

Further, the electrochemical study of the S1, S1 with Cu^{2+} and S1-Cu^{2+} with CN^{-} was performed in methanol solution, which is accountable for the suggested

sensing mechanism. The Cyclic Voltammograms of S1 shows one reversible reduction (-0.94 V) peaks and one oxidation peak (1.42 V). After addition of Cu^{2+} solution, shifting observed in reduction peak towards positive potentials (0.17 V) defining that the informal electro-reduction of chromone moiety and generation of a new peak at 0.39 V, demonstrating the presence of a new oxidized species, which can be explained by the electrochemical compound being highly liable to interact with Cu^{2+} *via* coordinate bond. Further addition of 5 eq. of CN^{-} into complex solution, the electrochemical properties have, just like receptor. Thus the reductive electron transfer changed the optical properties due to changes in the electronic structure of the receptor (Fig. 5.13).

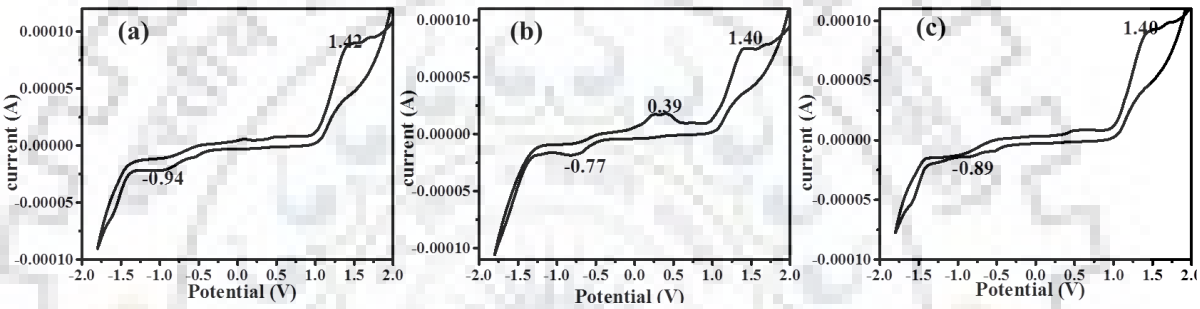

Fig. 5.13 Cyclic Voltammograms of (a) S1 (b) S1-Cu^{2+} complex (c) S1-Cu^{2+}-CN^{-} adduct in aq. medium (pH-7.4, HEPES buffer).

All of the results reveal a potential sensing mechanism for Cu^{2+} and CN^{-}, as shown in Scheme 5.3.

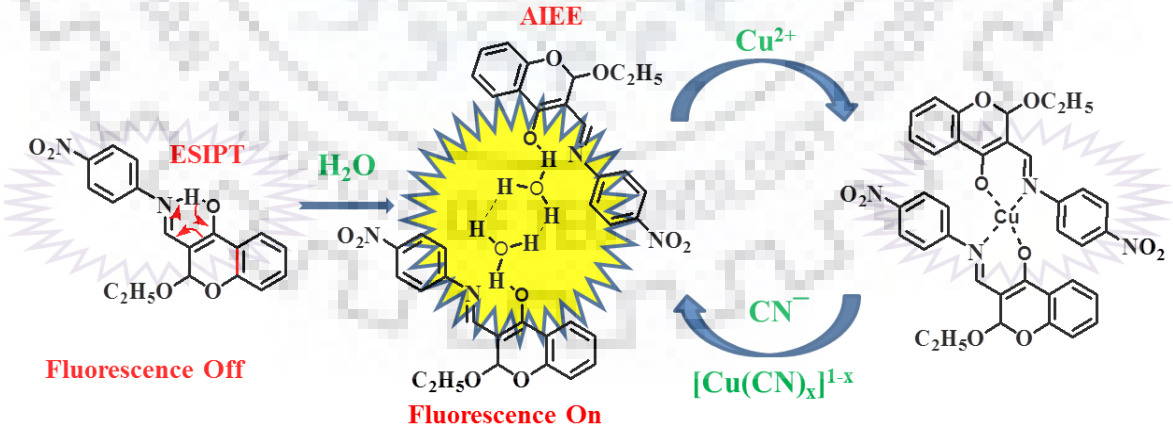

Scheme: 5.3 Reaction mechanism of S1 with Cu^{2+} and CN^{-}.

5.3.1.5 On-Off Switching Activity of S1 and Logic Implication

Based on the reversibility of S1-Cu^{2+} and CN^{-} with subsequent variation in its emission intensity at 503 nm, the consequent system works as a molecular switch at this

emission intensity, which execute on Boolean logic operations. In direction of logic gate design, we assign logic 0 and 1 as inputs and outputs signals. The threshold value has been taken as 70% of maximum output emission intensity at 503 nm and the relative emission intensity above this has been assigned as "1 & ON" state whereas, lower one as "0 & OFF" states correspondingly. The two chemical inputs of Cu^{2+} and CN^{-} were designated correspondingly to Set (S) and Reset (R) inputs. According to truth table (Fig. 5.14 B) when S input is high (1), the system erases and memorizes 0 binary state; conversely, when R input is high (1), the 0 states are written and the 1 state is written and memorized. Thus the reversible and reconfigurable sequences of Set/Reset logic operations in a feedback loop exhibit the memory feature with "write-read-erase-read" functions (Fig. 5.14 D). Fig. 5.14 C describes the bistability behavior, 'ON-OFF' state, of S1 and let slip the non-volatile nature of the memory effect [34].

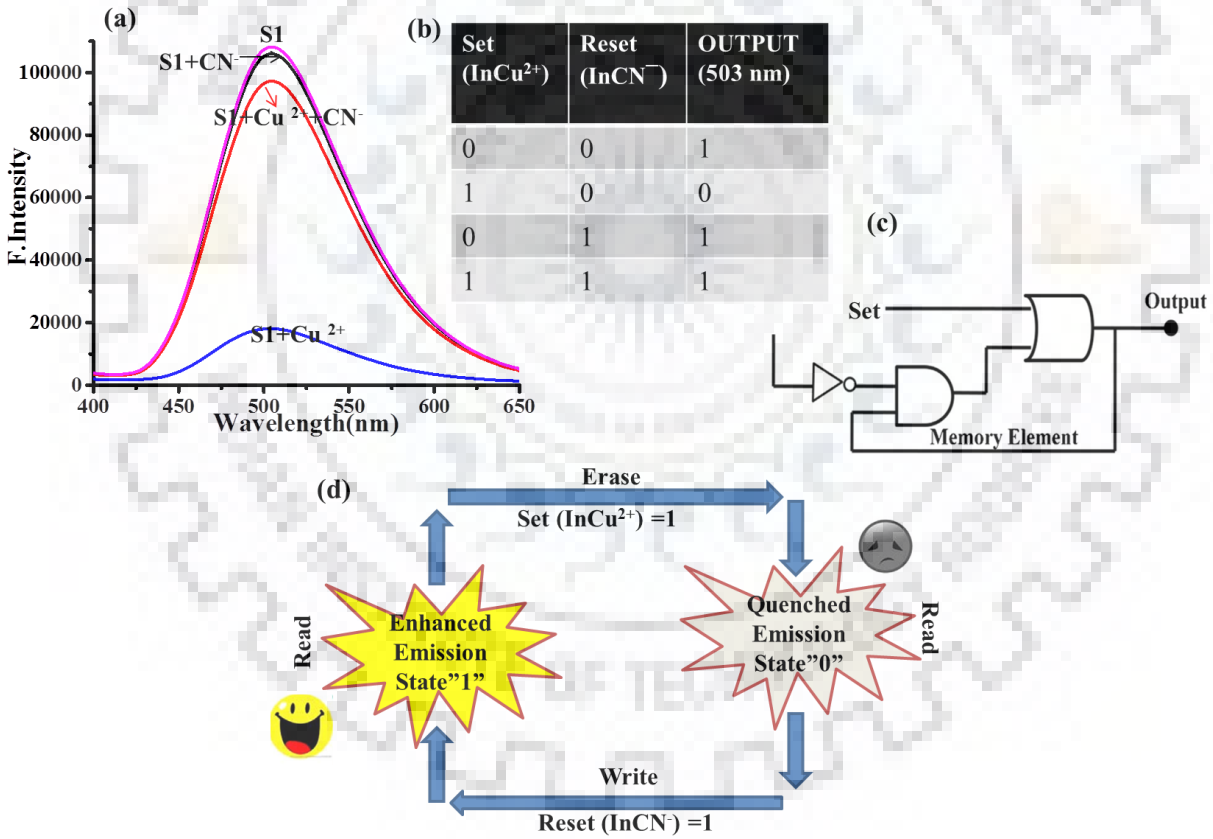

Fig. 5.14 (A) Emission spectra of S1 under four different input conditions (B) Truth table for the sequential logic circuit (C) Memory unit with two inputs and one output (503 nm) (D) A schematic representation of the reversible logic operations for the element possessing 'write-read-erase-read' function.

5.3.1.6 Real Sample Analysis

The practical study of S1 of knowing the concentration of Cu^{2+} and CN^- in real water samples were accomplished by spiking a well-known concentration of Cu^{2+} and CN^- in deionized, tap and river water (the Ganga River). Primarily the water tasters were cleaned to dispose of any particulate suspension continuing to spiking the analyte (Cu^{2+} or CN^-) at optimal pH conditions and interaction time. The results in terms of % recovery for Cu^{2+} and CN^- are displayed in Table 5.1 and 5.2. The retrieval values reveal the potential of S1 and S1-Cu^{2+} association for the recognition of concerned ions in real samples.

Table: 5.1 Recovery analysis of spiked [Cu^{2+}] in different water samples.

Spiked concentration (µM)	Deionized water		Tap water		River water	
	Found (µM)	Recovery[a] (%)	Found (µM)	Recovery[a] (%)	Found (µM)	Recovery[a] (%)
0	0.03		0.08		0.12	
0.2	0.197	98.5 ± 1.7	0.227	135.5 ± 2.4	0.310	155 ± 3.2
0.5	0.516	103 ± 3.1	0.553	110.6 ± 3.3	0.619	123.8 ±3.7

[a]Mean value ± standard deviation (triplicate measurements)

Table: 5.2 Recovery analysis of spiked [CN^-] in different water samples.

Spiked concentration (µM)	Deionized water		Tap water		River water	
	Found (µM)	Recovery[a] (%)	Found (µM)	Recovery[a] (%)	Found (µM)	Recovery[a] (%)
0	0.01		0.03		0.08	
0.2	0.199	99.5 ± 1.4	0.218	109 ± 1.5	0.223	111.5 ± 2.6
2	1.99	99.5 ± 2.1	2.15	107.5 ± 2.9	2.29	114 2.1

[a]Mean value ± standard deviation (triplicate measurements)

5.3.1.7 Antimicrobial Studies of S1 & S1-Cu^{2+} Complex

The antifungal activities were observed against *Rhizoctonia solani* (MTCC 4633) and *Bipolaris oryzae* (MTCC 3717) strains *via* well diffusion method. The fungal mycelium was inoculated in the middle of petri plates having PDA (potato dextrose agar). Now 4 mm diameter well was made with sterile cork borer, then loaded MeOH (as a control), S1 and S1-Cu^{2+} complex. Further the plates were properly covered, labelled and stored at 37 °C for

48 h. A clear inhibition zone (%) was observed with S1 and S1-Cu^{2+} complex as compared to the reference (Table 5.3, Fig. 5.15). The results show antifungal activities towards *Bipolaris oryzae* and *Rhizoctonia solani*. Thus SAR (structure activity relationship) of chromone basis compounds containing an imino group was developed for antimicrobial result. The substitution of the nitro group in the para position of phenyl ring enhanced the inhibitory activity against fungal strains [40-41].

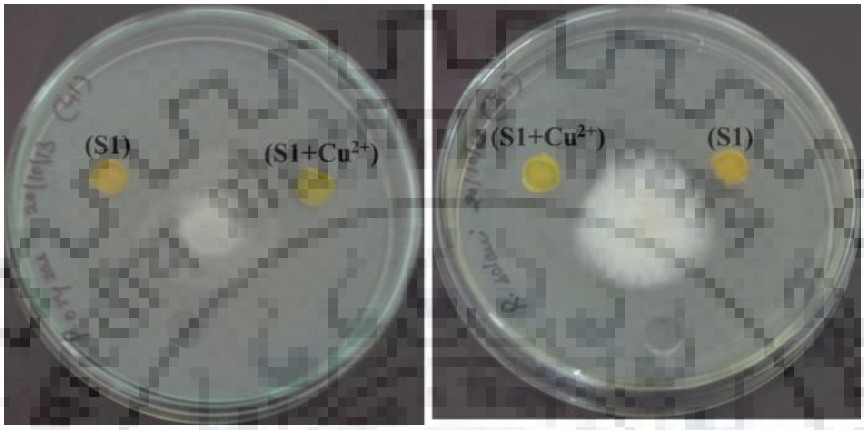

Fig. 5.15 Antifungal activities of S1 and S1-Cu^{2+} complex against *B. oryzae* and *R. solani* fungal species.

Table: 5.3 Inhibition of fungal strains of S1 & S1-Cu^{2+} complex.

Con. (μg mL^{-1})	**Microorganism**	**% Inhibition with ref.***
200 S1	*Bipolaris oryzae*	91
200 S1-Cu^{2+}	*Bipolaris oryzae*	85
200 S1	*Rhizoctonia solani*	66
200 S1-Cu^{2}	*Rhizoctonia solani*	75

5.1.3.8 Comparative Studies

Some Cu^{2+} coordinated CN^{-} receptors (displacement method) have been synthesized by several ligands as shown in Table 5.4. On scrutiny of the entire Cu-complex in terms of their solvent system and LOD, it is observed that our receptor has low LOD and can apply in aqueous medium.

Table: 5.4 Comparison of some reported Cu-complex based CN^- sensors with present work (displacement approach).

Previous literature	Cu-ligand	Solvent system	Detection limit
Chem. Commun. 46 (2010) 8953-8955 (Ref. 42)	2-pyridylmethyl based	ACN- H_2O (95:5)	5 μM
Tetrahedron 66 (2010) 1678-1683 (Ref. 43)	4-bromo-5-nitro-1,8-naphthalimide based	H_2O	2.48 μM, .52 μM
Dalton Trans. 41 (2012) 11413-11418. (Ref. 44)	Triphenylene-triazole based	DMSO	5 μM
Sens. Actuators, B 168 (2012) 14-19 (Ref. 45)	Benzothialzolium-hemicyanine based	H_2O	1.3 μM
Tetrahedron Lett. 50 (2009) 5139-5141 (Ref. 46)	8-aminomethyl-BODIPY based	THF	20 μM
Tetrahedron 68 (2012) 9076-9084 (Ref. 47)	Acenaphthene based	ACN-H_2O (1:4)	1 μM
Bull. Korean Chem. Soc. 32 (2011) 3123-3126 (Ref. 48)	Thiazole based	EtOH-H_2O (1:1)	7.9 ppm
Present work	Chromone based	H_2O	0.168 μM

5.3.2 Sensing Studies of Receptor S3

5.3.2.1 Development of S3-FONs

Development of organic nanoparticles was executed in an aqueous medium by virtue of the production of uniformly sized nanoparticles. The presence of different solvent systems ruined the particle size that's why the receptor exhibited the best sensing action in a pure aqueous medium. The organic nanoparticles were developed by gentle injection of a solution of S3 with water. To assess the effect of water on optical properties of S3, UV-vis and fluorescence spectral studies were performed. The UV-vis absorption spectrum of S3 (10 μM) was recorded in DMF, which show a peak at 397 nm. On altering the solvent system to H_2O the absorption maxima shows a small blue shift at 388 nm with a small decrease in absorbance as exposed in Fig. 5.16 a. The fluorescence emission studies of S3 (1 μM) show two peaks at 461 nm and 487 nm upon altering the solvent system to H_2O, the auto-enhancement in the fluorescence intensity with an evident red shift at 517 nm was recorded. Changes in

emission wavelengths are labelled in Fig. 5.16 b. The formation of uniform size and morphology of nanoparticles of S3 with an average hydrodynamic size of 48 nm was settled *via* FESEM and AFM analysis as shown in Fig. 5.16 c & d.

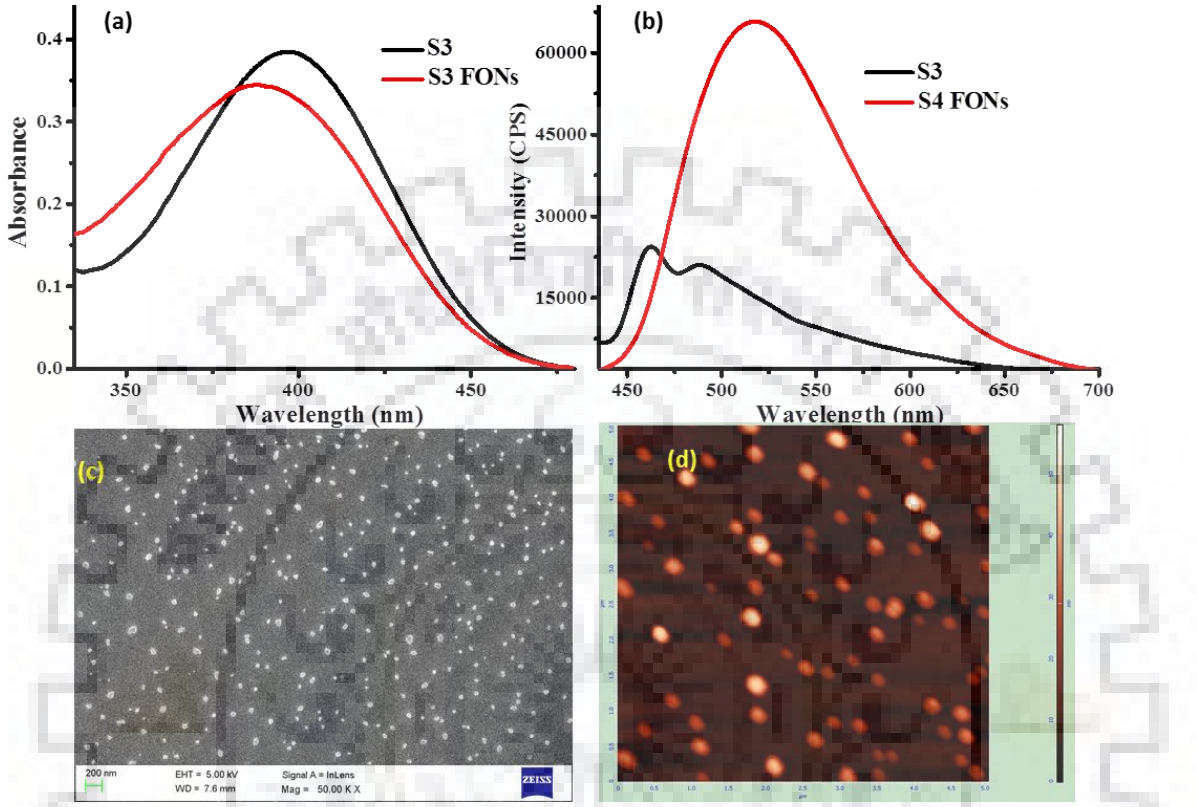

Fig. 5.16 Nanoparticle formation, confirmation *via*; (a) UV-vis absorption spectral change (b) Emission intensity change (c) SEM image showing the distribution of S3-FONs (d) AFM images showing size and distribution of S3-FONs.

5.3.2.2 Spectral Characterizations of S3-FONs

In fluorescence emission measurements, S3 displayed emission at 461 nm and 487 nm in DMF. S3 act as a dual fluorescence emitter due to excited state intramolecular proton transfer (ESIPT) process. In ESIPT processes a proton (amino or hydroxyl) that is linked covalently to an atom X in the ground state of the molecule, immigrates to a neighboring H-bonded atom Y (at distance of < 2 Å) in the excited electronic state, to generate a "phototautomer". Photoexcitation of S3 at 325 nm, leads to rapid transformation from excited states of the enol form (E*) to the excited state of keto form (K*) within the time of picoseconds. Decaying from K* to K originated as an emission band at 487 nm. At ground state level less stable keto form (K) lapses to more stable enol form (E) *via* reverse proton transfer residual molecule at E* that do not sustain ESIPT, causes emission band at 461 nm.

Mechanistic features of ESIPT are shown in Fig. 5.17 a. While changing the solvent system, the fluorescence intensity of S3 increased remarkably with red shift on increasing the fractions of water. Subsequent increment of water in a solvent system quenched the dual emitter property of receptor and in pure aqueous solution a broad single emission band at 517 nm is originated as an indicator of inhibition of the ESIPT process as portrayed in Fig. 5.17 b. S3 molecules form aggregates while their solubility reduced in the solution with greater fractions of water, resulting enrichment of the level of conjugation and florescence emission enhancement (AIE process).

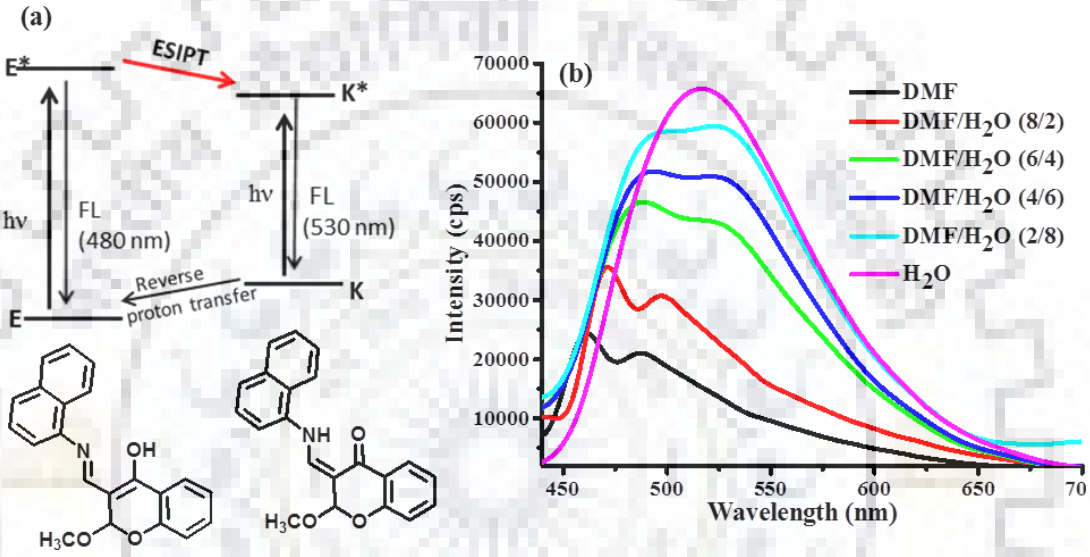

Fig. 5.17 Fluorescence properties; changing from dual emitter to single emitter of S3; (a) ESIPT mechanism followed by S3 in DMF solution (b) Changes in emission properties with subsequent amount of water (formation of Nanoprobe S3-FONs).

Firstly, two monomers of S3 assemble as a dimer *via* hydrogen bonding interactions and act as building blocks for the solid state. These intermolecular hydrogen bonding interactions impede the ESIPT. Receptor S3 forms dimers as precursors of S3-FONs. Formation of S3-FONs results to blue shift in absorption spectra due to the higher hydrophobic effect that leads to π–π stacking interactions. These π-π stacking and hydrogen bond interactions were also supported by ^{1}H NMR spectral studies as presented in Fig. 5.18. ^{1}H NMR spectra of S3-FONs exhibited up field shift in aromatic ring protons as compared to S3, indicates the π-π stacking interactions. S3 displayed a -OH proton signal at 13 ppm, whereas no signal was recorded at 13 ppm in ^{1}H NMR spectra of S3 FONs, this fact supported the hydrogen bonding interaction.

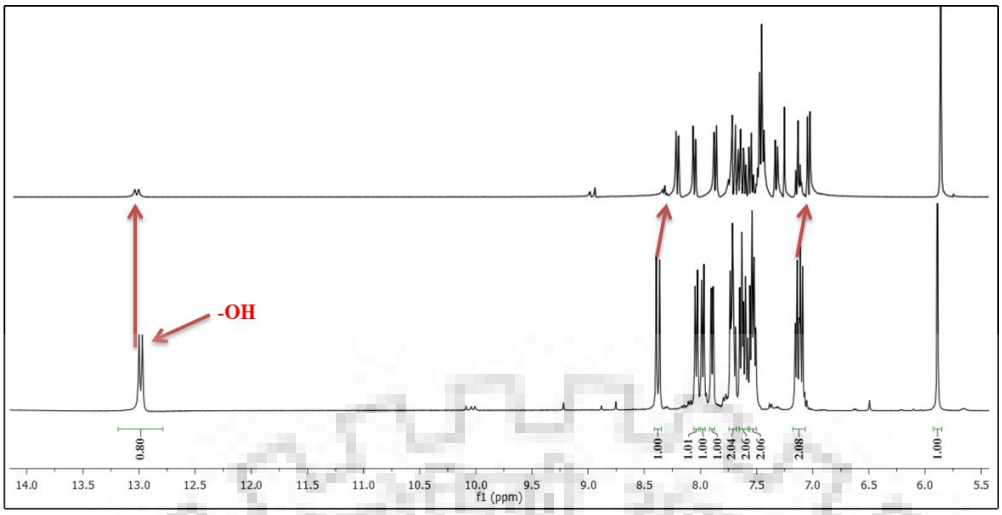

Fig. 5.18 Comparison of ^{1}H NMR spectra of S3 and S3-FONs in DMSO d_6.

The colloidal stability study of the S3-FONs at room temperature was assessed and as Fig. 5.19 states, the S3-FONs are stable at room temperature at least for 12 days.

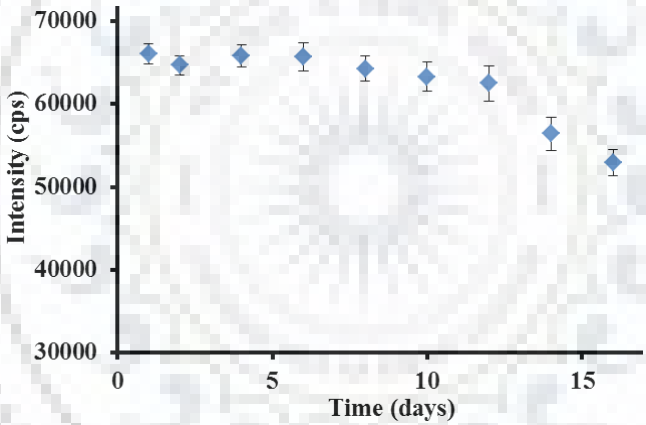

Fig. 5.19 Colloidal stability of S3-FONs in aqueous medium.

5.3.2.3 S3-FONs as Primary Sensor for Cu^{2+} Ion

As prepared S3-FONs provides ample coordination sites for metal ions, ascribed to the existence of lots of immine and hydroxyl binding sites. To discover their possible ions sensing aptitude, we examined the absorption and emission responses of the S3-FONs affected by numerous metal ions. Prior studies of S3-FONs in water with different metal ions (20 equiv.) confess that S3-FONs had a strong affinity towards Cu^{2+}. Addition of Cu^{2+} salt to S3-FONs gives blue shift in absorption spectra and reduced fluorescence intensity in emission spectra presumably because of LMCT-based heavy metal ion phenomena yet the addition of other metal ions, such as Hg^{+}, Hg^{2+}, Fe^{2+}, Mn^{3+}, Cr^{3+}, Zn^{2+}, Pb^{2+}, Mg^{2+}, Co^{2+}, Cd^{2+} Ag^{+} and Ni^{2+} didn't lead to

considerable fluorescence intensity responses. Markedly, the fluorescence intensity at 517 nm almost suppressed upon addition of 10 equiv. of Cu^{2+}, pointing out the complete formation of S3-FONs-Cu assembly (Fig. 5.20).

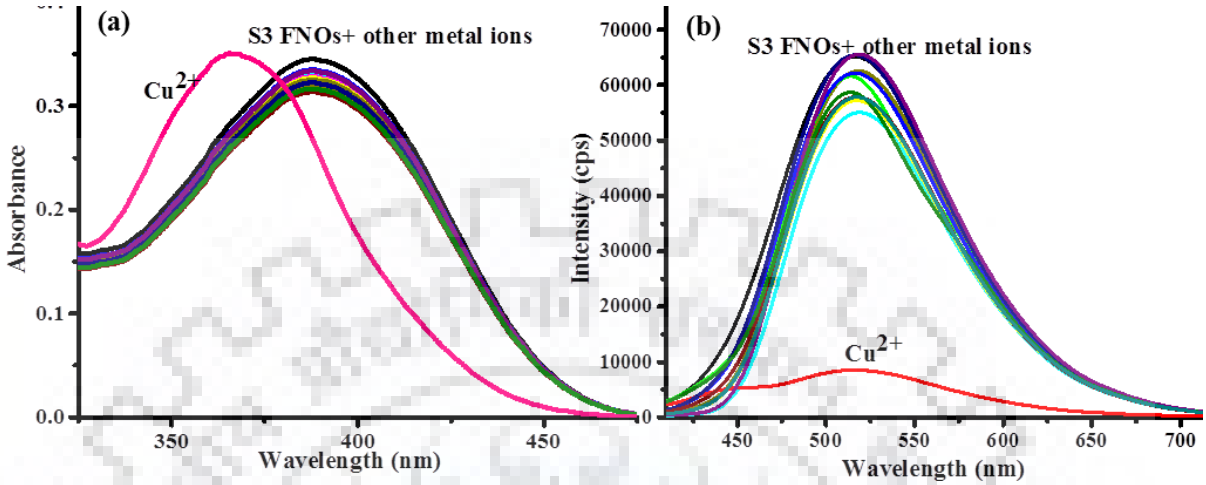

Fig. 5.20 (a) Absorption spectra (b) Emission spectra of S3-FONs in the presence of various metal ions in aq. medium (pH-7.4, HEPES buffer).

Gradual quenching in the fluorescence intensities of S3-FONs treated with a cumulative concentration of Cu^{2+} (Fig. 5.21 a). The prospect of S3-FONs as receptor for sensing Cu^{2+} would rely on recording a quantifiable change in its fluorescence response upon networking with the guest analyte, which follows the Stern-Volmer equation ($I_0/I = 1+K_{sv}[Cu^{2+}]$), Where; I_0 and I are fluorescence intensities of the S3-FONs and S3-FONs treated with Cu^{2+} respectively, K_{sv} is Stern-Volmer constant and $[Cu^{2+}]$ is concentration of Cu^{2+}.

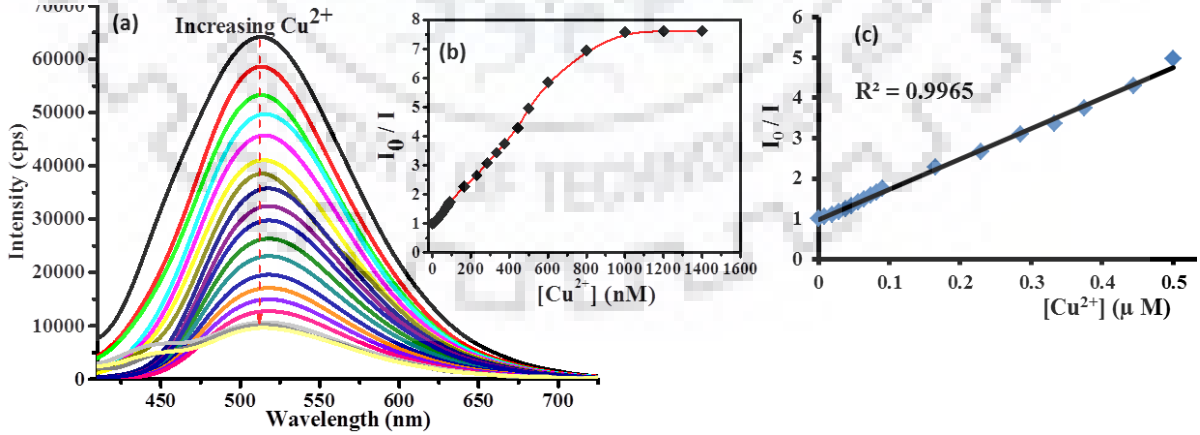

Fig. 5.21 (a) Fluorescence emission intensity quenching of S3-FONs due to interaction of different concentrations of Cu^{2+} (b) Nonlinear S-V quenching profile of S3-FONs with $[Cu^{2+}]$ (c) Linear part of S-V plot in aq. medium (pH-7.4, HEPES buffer).

The linear section of the S-V plot is a key feature for quantitative studies since the slope of linear trend area parallel to the analytical sensitivity for recognizing Cu^{2+}. The linear area of the S-V plot for S3-FONs corresponded to the Cu^{2+} concentration ranging from 10 nM to 500 nM (Fig. 5.21 b, c). The response time between the S3-FONs as a receptor and Cu^{2+} was determined from the kinetic investigation of fluorescence intensity of the solution containing S3-FONs and 10 equiv. of Cu^{2+}. The equilibrium was attained in 10 min, which harmonise to the saturation in the fluorescence intensity (Fig. 5.22 a). Along with the appropriate pH value is of immense importance to investigate the sensing behavior of receptor towards analyte for practical applications. The desired pH was maintained *via* dilute solutions of sodium hydroxide and hydrochloric acid. For S3-FONs, in acidic conditions, at pH 5, small quenching in fluorescence intensity was observed and in basic conditions fluorescence intensity increases slightly after 8 pH. Results indicate the working pH range for S3-FONs is of 6-8 pH value. While the S3-FONs-Cu^{2+} assembly remains almost constant in both acidic and basic conditions at the pH range 4-10 (Fig. 5.22 b). The limit of detection (LOD) for Cu^{2+} was calculated as 12.3 nM.

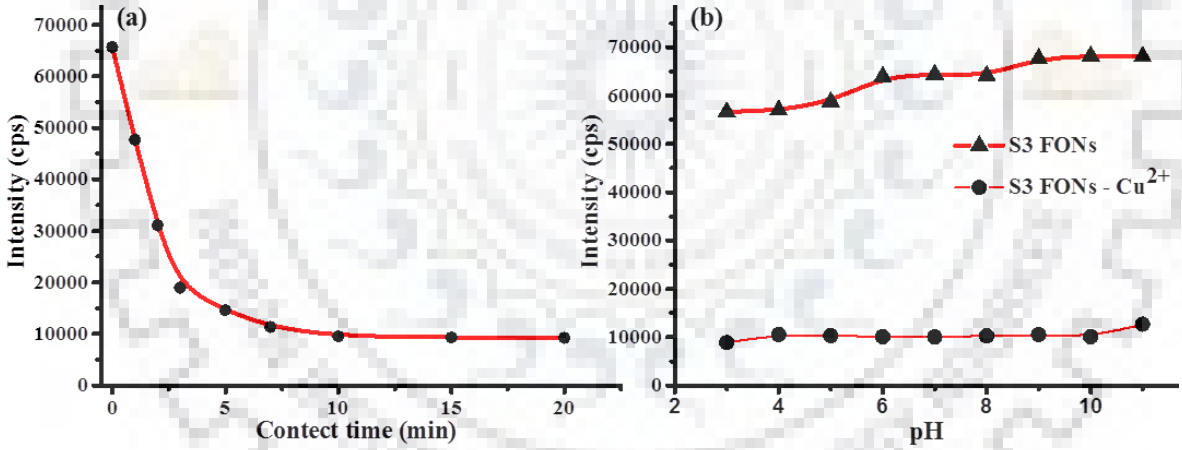

Fig. 5.22 (a) Kinetic study (b) pH study of S3-FONs with Cu^{2+} in aq. medium (pH-7.4, HEPES buffer).

To examine the anti-jamming capacity of S3-FONs towards Cu^{2+}, fluorescence titration of the mixture contains S3-FONs (1.0 µM) and Cu^{2+} (1×10^{-3}) were performed in the presence of 20 equiv. of other competitive metal ions. The results specified that coexistence with competitive metal ions does not cause substantial interferences in Cu^{2+} sensing and S3-FONs reviled strong selectivity towards Cu^{2+} described in Fig. 5.23.

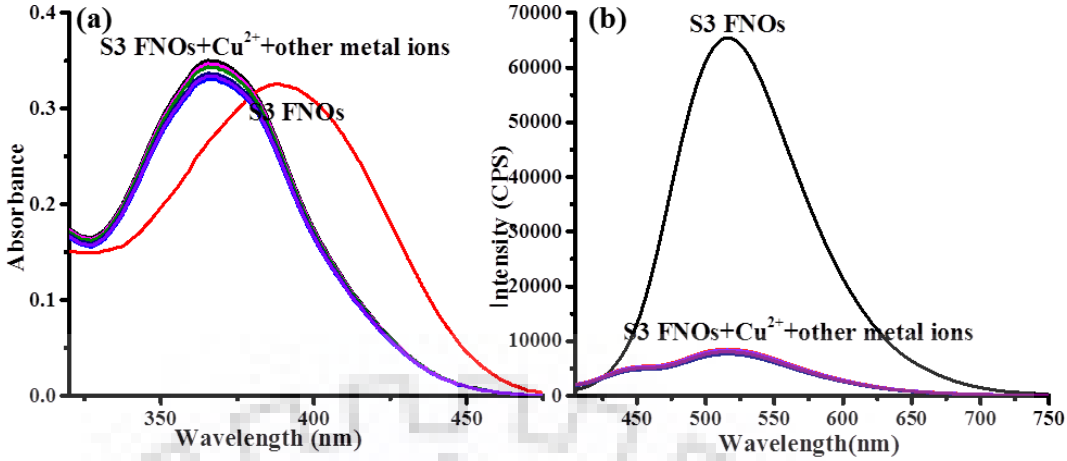

Fig. 5.23 Interference study of S3-FONs-Cu^{2+}; (a) Absorption spectra (b) Emission spectra in aq. medium (pH-7.4, HEPES buffer).

5.3.2.4 S3-FONs-Cu^{2+} Assembly as Secondary Sensor for CN^- Ions

Since S3-FONs recognizes Cu^{2+} selectively, the *in-situ* response of S3-FONs-Cu^{2+} complex towards different anions counting F^-, Cl^-, Br^-, I^-, CN^-, NO_3^-, PO_4^{3-}, HPO_4^{2-} AcO^-, CO_3^{2-}, AsO_2^-, SO_4^{2-}, N_3^- and S^{2-} were subsequently examined. The aqueous solution of S3-FONs-Cu^{2+} complex was treated with 20 equiv. of series of anions. As shown in Fig. 5.24, reaction of CN^- with S3-FONs-Cu^{2+} complex resulted in regaining of absorption wavelength and fluorescence intensity of original S3-FONs.

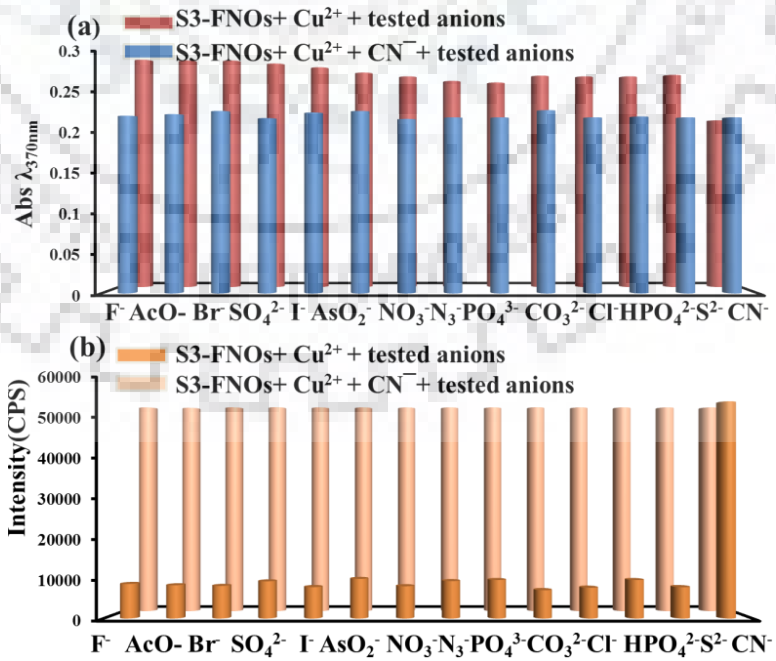

Fig. 5.24 (a) Absorption spectra (b) Emission spectra of S3-FONs-Cu^{2+} with various anions in aq. medium (pH-7.4, HEPES buffer).

By contrast, none of the other anion resulted in nearly no visible disturbance to the original fluorescence spectrum of S3-FONs-Cu^{2+} complex, indicating that it act as a secondary sensor towards CN^-. The anti-jamming studies of S3-FONs-Cu^{2+} complex towards CN^- in the presence of 20 equiv. of other competitive anions stratify the strong selectivity towards CN^-.

The outcomes of the quantitative detection of CN^- are revealed in Fig. 5.25 a. With inclusion of CN^-, the fluorescence intensity at 517 nm gradually developed due to the relatively intense affinity between CN^- and Cu^{2+}. The S-V plot for S3-FONs-Cu^{2+} assembly corresponded to the CN^- shows the good linearity in between 0.2 µM to 2 µM concentrations of CN^- (inset of Fig. 5.25 a). The response time between the S3-FONs-Cu^{2+} assembly for CN^- detection was determined *in-situ* from the kinetic investigation of fluorescence intensity. The equilibrium was attained in 5 min, which harmonise to the saturation in the fluorescence intensity (Fig. 5.25 b). The limit of detection (LOD) for CN^- by S3-FONs-Cu^{2+} assembly was calculated as 21.4 nM. Titration experiment at various concentrations of CN^- reviled sensing ability of the sensing system to nanomolar detection of CN^- in aqueous and biological systems.

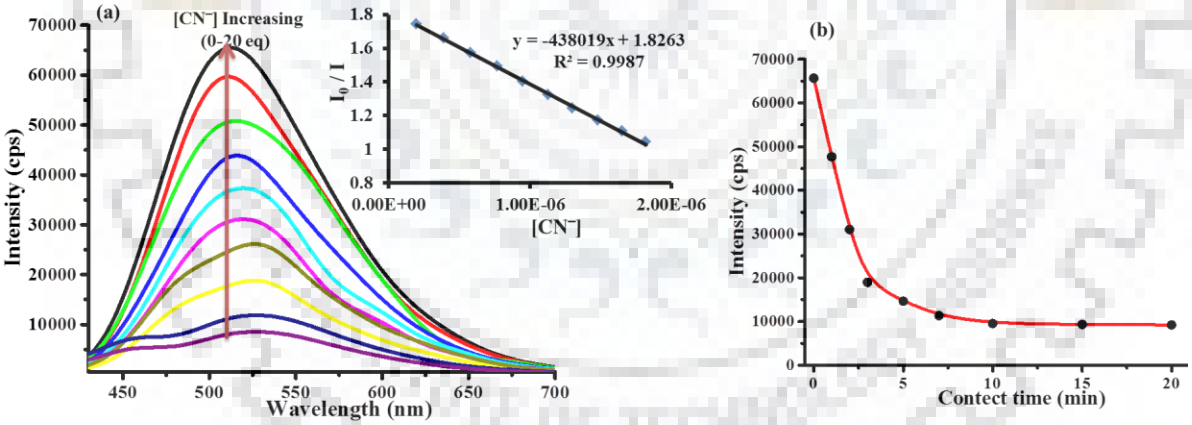

Fig. 5.25 (a) Fluorescence emission intensity quenching; inset: Linear part of the S-V plot ranging from 0.2-2 µM (b) Kinetic study of S3-FONs-Cu^{2+} with CN^- in aq. medium (pH-7.4, HEPES buffer).

5.3.2.5 Quantum Chemistry Computation

The optimized structures of LMCT were calculated by Density Functional Theory (DFT) method using a Gaussian B3LYP function with 6-31G (d, p) for ligand and LANL2DZ for possible complexes. Fig. 5.26 represents the frontier molecular orbitals of S3 and S3-Cu^{2+}

complex. In case of HOMO the electron density is present on naphthalene moiety, while in LUMO it is located on whole receptor, which establishing charge transfer interface between donor-acceptor systems. However, the electronic dispersal in S3-Cu^{2+} was relatively different. In this case it is shifted towards the metal center, which supported the adduct formation and also a ligand to metal charge transfer.

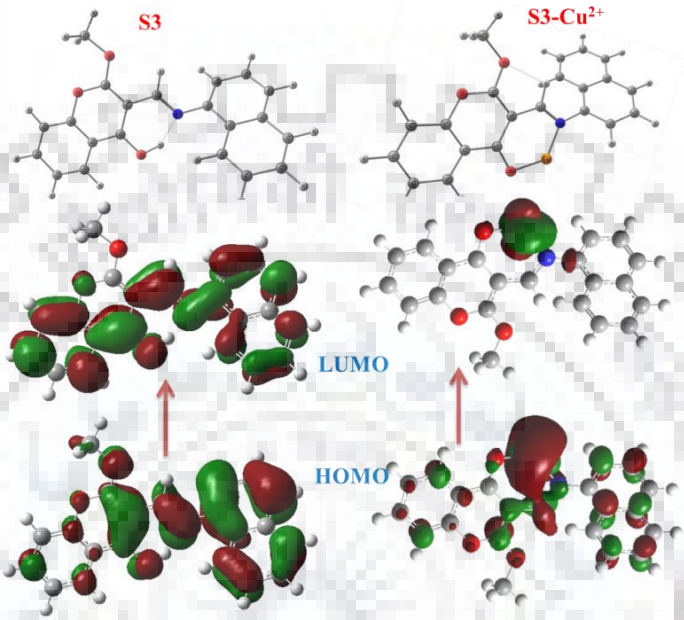

Fig. 5.26 DFT optimized structure of S3 and S3-Cu^{2+} complex.

5.3.2.6 Logic Gate Behavior of S3-FONs

As the Cu^{2+} displacement strategy grounds consequent variations in emission intensity at 517 nm, consequentially the system functioned as a molecular switch at this particular intensity and accomplished the Boolean logic operations. The molecular logic function was implemented with the S3-FONs onwards Cu^{2+} (In-1) along with CN^- (In-2) as per inputs in the emission genre. In current the scheme, the strong emission intensity at 517 nm is defined as ON switch (output-1), whereas the weak emission intensity allotted as the OFF switch (output-0). 30000 CPS is specified as a threshold value of emission intensity. Subsequent addition of Cu^{2+} in S3-FONs solution leads fluorescence intensity quenching lower than the threshold level, however the *in-situ* incubation of 4 equiv. CN^- almost recovered the fluorescence intensity. The strong emission intensity exceeding the threshold level, assigned as a positive output signal was standard in the presence (1, 1) and absence (0, 0) of both inputs and moreover CN^- alone in S3-FONs solution. Thus, simply the addition of Cu^{2+} would produce a negative output signal, simply yielding the IMPLICATION

logic gate. The operational principle of IMPLICATION logic gate is drawn in Fig. 5.27.

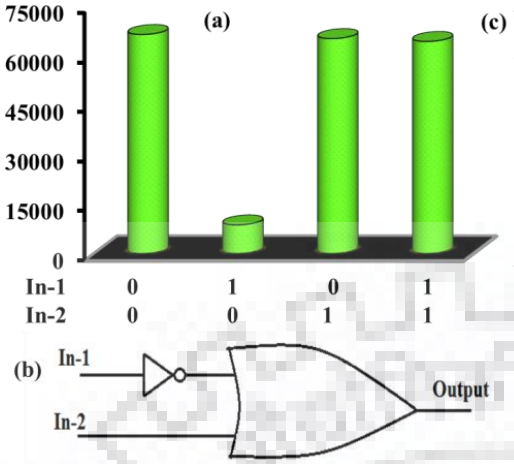

Inputs		Output
Cu^{2+}	CN^-	IMPLICATION
0	0	1
1	0	0
0	1	1
1	1	1

Fig. 5.27 Arrangement of the IMPLICATION logic gate; (a) Emission intensity changes of S3-FONs under different input condition (b) Circuit diagram (c) Truth table corresponding to logic gate.

5.3.2.7 Real Sample Analysis

The feasibility study of practicing the S3-FONs for recognising of Cu^{2+} and CN^- in real water sample was performed by spiking a known concentration of Cu^{2+} and CN^- in deionised water, tap water and river water (the Ganga river). Firstly the water samples were filtered to discard any particulate suspension proceeding to spiking the analyte (Cu^{2+} or CN^-) at optimum pH conditions and contact time. The results in terms of % recovery for Cu^{2+} are shown in Table 5.5 and for CN^- are shown in Table 5.6. The recovery values announce the potential of S3-FONs and S3-FONs-Cu^{2+} assembly for the detection of concerned ions in real samples.

Table: 5.5 Recovery analysis of spiked [Cu^{2+}] in deionized, tap and river water samples.

Spiked conc. (µM)	Deionized water		Tap water		River water	
	Found (µM)	Recovery[a] (%)	Found (µM)	Recovery[a] (%)	Found (µM)	Recovery[a] (%)
0	0.03		0.08		0.12	
0.2	0.197	98.5 ± 1.7	0.227	135.5 ± 2.4	0.310	155 ± 3.2
0.5	0.516	103 ± 3.1	0.553	110.6 ± 3.3	0.619	123.8 ± 3.7

Table: 5.6 Recovery analysis of spiked [CN^-] in deionized, tap and river water samples.

Spiked conc. (µM)	Deionized water		Tap water		River water	
	Found (µM)	Recovery[a] (%)	Found (µM)	Recovery[a] (%)	Found (µM)	Recovery[a] (%)
0	0.01		0.03		0.08	
0.2	0.199	99.5 ± 1.4	0.218	109 ± 1.5	0.223	111.5 ± 2.6
2	1.99	99.5 ± 2.1	2.15	107.5 ± 2.9	2.29	114 ± 2.1

[a]Mean value ± standard deviation (triplicate measurements)

5.3.2.8 Application of S3-FONs to Cellular Imaging

To test the feasibility of the Nanoprobe for intracellular Cu^{2+} and CN^- recognition bioimaging studies was performed in living HeLa cells. The cells treated by S3-FONs clearly exhibited green fluorescence. When 1 µM Cu^{2+} was incubated with HeLa cells for 30 minutes, the green color fluorescence diminished strongly. Further HeLa cells of the S3-FONs-Cu^{2+} complex were exposed with CN^- for 1 h, the observed cell exhibit green color fluorescence. The results proposed that the Nanoprobe could be used in the fluorescence recognition of Cu^{2+} and CN^- in living cell imaging application (Fig. 5.28).

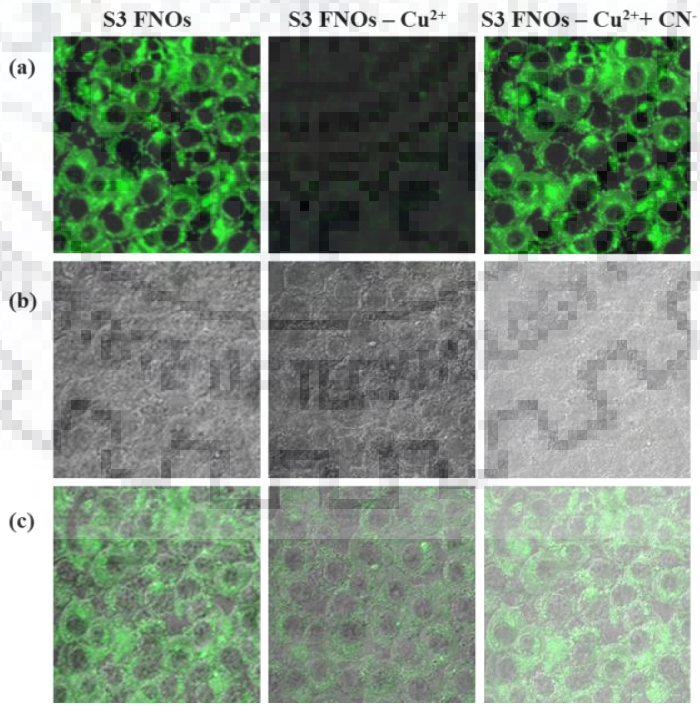

Fig. 5.28 Confocal laser scanning microscopy images of MCF-7 cells; (a) in the presence of S3-FONs (1 µM), after the addition of Cu^{2+} (10 µM) and after the addition of CN^- (20 µM) (b) Confocal phase contrast images (c) An overlay image.

5.4 CONCLUSION

In summary, we designed and synthesized novel ESIPT process based fluorescence receptors S1-S4, which exhibit AIEE based fluorescent properties in pure aqueous medium. Further AIE based fluorescent organic nanoparticles S3 was developed and characterized *via* various techniques. All ligands show as an effectual primary sensor for Cu^{2+} *via* turn OFF and a probable secondary sensor for CN^- *via* turn ON by metal displacement phenomena. The reversible "ON-OFF-ON" fluorescence responding by the sequential addition of Cu^{2+} and CN^- as input were exploited as an IMPLICATION logic gate at the molecular level and the fluorescence intensity signal as the output. Electrochemical study was also performed for the interaction between receptor S1 with Cu^{2+} and CN^-. Moreover S1 and S1-Cu^{2+} complex show venerable antifungal activities towards *Bipolaris oryzae* and *Rhizoctonia solani* strains. The proposed sensor detects both quantitative and qualitative determination of Cu^{2+} and CN^- concentrations in real samples. Confocal laser scanning microscopy stuffs presented here demonstrates that the S3-FONs are a novel and effective material for cellular imaging.

References

1. R. Martínez-Máñez, F. Sancenón, Fluorogenic and chromogenic chemosensors and reagents for anions, Chem. Rev. 103 (2003) 4419-4476.
2. S. I. Cerone, A. S. Sansinanea, S. A. Streitenberger, M. C. Garcia, A. J. Auza, Cytochrome c oxidase, Cu, Zn-superoxide dismutase and ceruloplasmin activities in copper-deficient bovines, Biol. Trace Elem. Res. 73 (2000) 269-278.
3. E. Gaggelli, H. Kozlowski, D. Valensin, G. Valensin, Copper homeostasis and neurodegenerative disorders (alzheimer's, prion, and parkinson's diseases and amyotrophic lateral sclerosis), Chem. Rev. 106 (2006) 1995-2044.
4. Y. Noda, M. Asada, M. Kubota, M. Maesako, K. Watanabe, M. Uemura, T. Kihara, S. Shimohama, R. Takahashi, A. Kinoshita, K. Uemura, Copper enhances APP dimerization and promotes Aβ production, Neurosci. Lett. 547 (2013) 10-15.
5. Y. Liu, X. Lv, Y. Zhao, J. Liu, Y. Q. Sun, P. Wang, W. Guo, A Cu (II)-based chemosensing ensemble bearing Rhodamine B fluorophore for fluorescence turn-on detection of cyanide, J. Mater. Chem. 22 (2012) 1747-1750.
6. P. Anzenbacher, J. Daniel, S. Tyson, K. Jursıkova, F. N. Castellano, Luminescence lifetime-based sensor for cyanide and related anions, J. Am. Chem. Soc. 124 (2002) 6232-6233.
7. B. Vennesland, E. E. Comm, C. J. Knownles, J. Westly, F. Wissing, Cyanide in biology, Academic Press, London 1981.
8. S. I. Baskin, T. G. Brewer, Cyanide poisoning, in medical aspects of chemical and biological warfare, Washington, DC (1997) 271-286.
9. R. A. Greenfield, B. R. Brown, J. B. Hutchins, J. J. Iandolo, R. Jackson, L. N. Slater, M. S. Bronze, Microbiological, biological, and chemical weapons of warfare and terrorism, Am. J. Med. Sci. 323 (2002) 326-340.
10. T. T. Christison, J. S. Rohrer, Direct determination of free cyanide in drinking water by ion chromatography with pulsed amperometric detection, J. Chromatogr. A 1155 (2007) 31-39.
11. R. D. Rockfln, E. L. Johnson, Determination of cyanide, sulfide, iodide, and bromide by ion chromatography with electrochemical detection, Anal. Chem. 55 (1983) 4-7.
12. M. Noroozifar, M. K. Motlagh, S. N. Hosseini, Flow injection analysis-flame atomic absorption spectrometry system for indirect determination of cyanide using cadmium carbonate as a new solid-phase reactor, Anal. Chim. Acta 528 (2005) 269-273.

13. J. H. Lee, A. R. Jeong, I. S. Shin, H. J. Kim, J. I. Hong, Fluorescence turn-on sensor for cyanide based on a cobalt (II)-coumarinylsalen complex, Org. Lett. 12 (2010) 764-767.
14. Z. Ekmekci, M. D. Yilmaz, E. U. Akkaya, A monostyryl-boradiazaindacene (BODIPY) derivative as colorimetric and fluorescent probe for cyanide ions, Org. Lett. 10 (2008) 461-464.
15. B. B. Shi, P. Zhang, T. B. Wei, H. Yao, Q. Lin, Y. M. Zhang, Highly selective fluorescent sensing for CN^- in water: utilization of the supramolecular self-assembly, Chem. Commun. 49 (2013) 7812-7814.
16. J. Luo, Z. Xie, J. W. Y. Lam, L. Cheng, H. Chen, C. Qiu, H. S. Kwok, X. Zhan, Y. Liu, D. Zhu, B. Z. Tang, Aggregation-induced emission of 1-methyl-1,2,3,4,5-pentaphenylsilole, Chem. Commun. 18 (2001) 1740-1741.
17. J. Huang, N. Sun, P. Chen, R. Tang, Q. Li, D. Ma, Z. Li, Largely blue-shifted emission through minor structural modifications: molecular design, synthesis, aggregation-induced emission and deep-blue OLED application, Chem. Commun. 50 (2014) 2136-2138.
18. W. Huang, H. Wang, L. Sun, B. Li, J. Su, H. Tian, Propeller-like D-p-A architectures: bright solid emitters with AIEE activity and large two-photon absorption, J. Mater. Chem. C 2 (2014) 6843-6849.
19. D. Li, J. Yu, R. Xu, Mesoporous silica functionalized with an AIE luminogen for drug delivery, Chem. Commun. 47 (2011) 11077-11079.
20. J. P. Lin, Y. Q. Long, Transition metal-free one-pot synthesis of 2-substituted 3-carboxy-4-quinolone and chromone derivatives, Chem. Commun. 49 (2013) 5313-5315.
21. H. Li, J. M. Tian, H. Y. Tang, S. Y. Pan, A. L. Zhang, J. M. Gao, Chaetosemins A-E, new chromones isolated from an Ascomycete Chaetomium seminudum and their biological activities, RSC Adv. 5 (2015) 29185-29192.
22. N. F. L. Machado, C. Ruano, J. L. Castro, M. P. M. Marquesa, J. C. Otero, Chromone-3-carboxylic acid as a potential electron scavenger: a surface-enhanced Raman scattering study, Phys. Chem. Chem. Phys. 13 (2011) 1012-1018.
23. H. Zhang, X. Xiao, M. M. Conte, Z. Khalil, R. J. Capon, Spiralisones A-D: acylphloroglucinol hemiketals from an Australian marine brown alga, Zonaria spiralis, Org. Biomol. Chem. 10 (2012) 9671-9676.
24. P. S. C. Medeiros, A. L. M. Batista de Carvalho, C. Ruano, J. C. Oterob, M. P. M. Marques, Raman microspectroscopy for probing the impact of a dietary antioxidant on human breast cancer cells, Food Funct. 7 (2016) 2800-2810.

25. C. Maicheen, J. Jittikoon, O. Vajragupta, J. Ungwitayatorn, Synthesis, topoisomerase I inhibitory and cytotoxic activities of chromone derivatives, Med. Chem. 9 (2013) 329-339.
26. L. J. Legoabe, A. Petzer, J. P. Petzer, Selected C7-substituted chromone derivatives as monoamine oxidase inhibitors, Bioorg. Chem. 45 (2012) 1-11.
27. T. Zhou, Q. Shi, K. H. Lee, Anti-AIDS agents 83. Efficient microwave-assisted one-pot preparation of angular 2,2-dimethyl-2H-chromone containing compounds, Tetrahedron Lett. 51 (2010) 4382-4386.
28. L. Liu, S. Liu, S. Niu, L. Guo, X. Chen, Y. Chen, Isoprenylated chromone derivatives from the plant endophytic fungus Pestalotiopsis fici, J. Nat. Prod. 72 (2009) 1482-1486.
29. H. Yan, H. Su, D. Tian, F. Miao, H. Li, Synthesis of triazolo-thiadiazole fluorescent organic nanoparticles as primary sensor toward Ag^{+} and the complex of Ag^{+} as secondary sensor toward cysteine, Sens. Actuators, B 160 (2011) 656-661.
30. F. Tang, C. Wang, J. Wang, X. Wang, L. Li, Fluorescent organic nanoparticles with enhanced fluorescence by self-aggregation and their application to cellular imaging, ACS Appl. Mater. Interfaces 6 (2014) 18337-18343.
31. B. K. An, S. K. Kwon, S. D. Jung, S. Y. Park, Enhanced emission and its switching in fluorescent organic nanoparticles, J. Am. Chem. Soc. 124 (2002) 14410-14415.
32. N. Maurya, A. K. Singh, Selective naked eye and "turn-on" fluorescence chemodosimeter for CN^{-} by activated Michael acceptor possessing different polars ubstituents: Reduced ICT-based signal transduction, Sens. Actuators, B 245 (2017) 74-80.
33. N. Maurya, A. K. Singh, Effective ensemble system for the identification of CN^{-} based on cobalt (II) complex: a logic gate mimic, New J. Chem. 41 (2017) 4814-4819.
34. W. J. Qu, G. T. Yan, X. L. Ma, T. B. Wei, Q. Lin, H. Yao, Y. M. Zhang, Cascade recognition of Cu^{2+} and $H_2PO_4^{-}$ with high sensitivity and selectivity in aqueous media based on the effect of ESIPT, doi.org/10.1016/j.snb.2016.09.173.
35. V. Bhalla, H. Arora, M. Kumar, Aggregates of a triphenylene based chemosensing ensemble for sensitive detection of cyanide ions in an aqueous medium, Dalton Trans. 42 (2013) 4450-4455.
36. W. Chen, Z. Zhang, X. Li, H. Agren, J. Su, Highly sensitive detection of low-level water content in organic solvents and cyanide in aqueous media using novel solvatochromic AIEE fluorophores, RSC Adv. 5 (2015) 12191-12201.

37. C. Chang, F. Wang, T. Wei, X. Chen, Benzothiazole-based fluorescent sensor for ratiometric detection of Zn(II) ion and secondary sensing PPi and its applications for biological imaging and PPase catalysis assays, Ind. Eng. Chem. Res.10.1021/acs.iecr.7b01209.
38. C. Chang, F. Wang, J. Qiang, Z. Zhang, Y Chen, W. Zhang, Y. Wang, X. Chen, Benzothiazole-based fluorescent sensor for hypochlorite detection and its application for biological imaging, Sens. Actuators, B 243 (2017) 22-28.
39. H. A. Benesi, J. H. Hildebrand, A spectrophotometric investigation of the interaction of iodine with aromatic hydrocarbons, J. Am. Chem. Soc. 71 (1949) 2703-2707.
40. N. Aggarwal, V. Sharma, H. Kaur, M. P. S. Ishar, Synthesis and evaluation of some novel chromone based dithiazoles as antimicrobial agents, Int. J. Med. Chem. 2013 http://dx.doi.org/10.1155/2013/815453.
41. J. H. Kini, V. K. K. Pai, Y. D. B. Devise, Synthesis and evaluation of antimicrobial activities of novel 8-imino chromone derivatives by physicochemical approach, J. Chem. Pharm. Res. 8 (2016) 1355-1364.
42. X. Chen, S. W. Nam, G. H. Kim, N. Song, Y. Jeong, I. Shin, S. K. Kim, J. Kim, S. Park, J. Yoon, A near-infrared fluorescent sensor for detection of cyanide in aqueous solution and its application for bioimaging, Chem. Commun. 46 (2010) 8953-8955.
43. Z. Xu, J. Pan, D. R. Spring, J. Cui, J. Yoon, Ratiometric fluorescent and colorimetric sensors for Cu based on 4,5-disubstituted-1,8-naphthalimide and sensing cyanide *via* Cu displacement approach, Tetrahedron 66 (2010) 1678-1683.
44. V. Bhalla, H. Singh, M. Kumar, Triphenylene based copper ensemble for the detection of cyanide ions, Dalton Trans. 41 (2012) 11413-11418.
45. J. F. Xu, H. H. Chen, Y. Z. Chen, Z. J. Li, L. Z. Wu, C. H. Tung, Q. Z. Yang, A colorimetric and fluorometric dual-modal chemosensor for cyanide in water, Sens. Actuators, B 168 (2012) 14-19.
46. R. Guliyev, O. Buyukcakir, F. Sozmen, O. A. Bozdemir, Cyanide sensing *via* metal ion removal from a fluorogenic BODIPY complex, Tetrahedron Lett. 50 (2009) 5139-5141.
47. M. Shahid, S. S. Razi, P. Srivastava, R. Ali, B. Maiti, A. Misra, A useful scaffold based on acenaphthene exhibiting Cu^{2+} induced excimer fluorescence and sensing cyanide *via* Cu^{2+} displacement approach, Tetrahedron 68 (2012) 9076-9084.
48. A. Helal, S. Kim, H. S. Kim, Sensing of cyanide using highly selective thiazole-based Cu^{2+} chemosensor, Bull. Korean Chem. Soc. 32 (2011) 3123-3126.

Appendix

Spectrum No. 1. FT-IR spectrum of receptor B1.

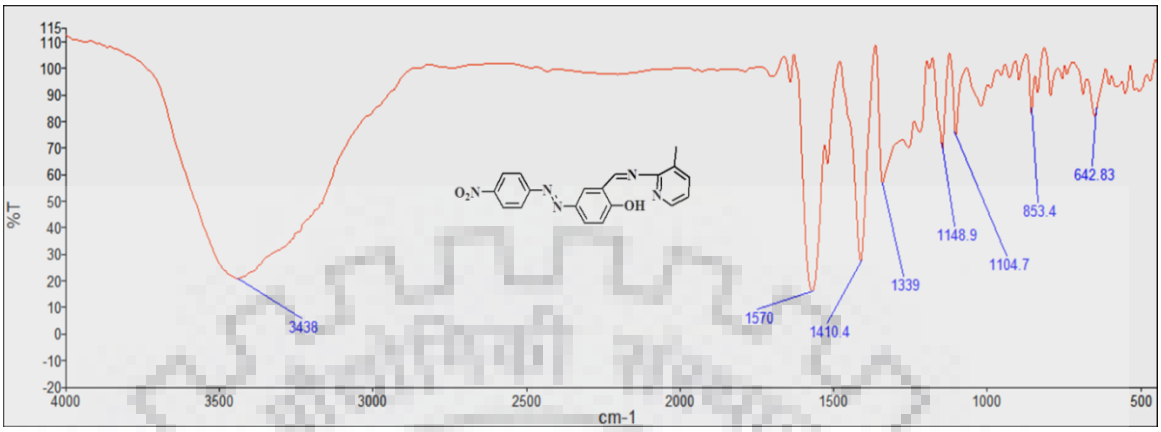

Spectrum No. 2. ^{1}H NMR spectrum of receptor B1 in $CDCl_3$.

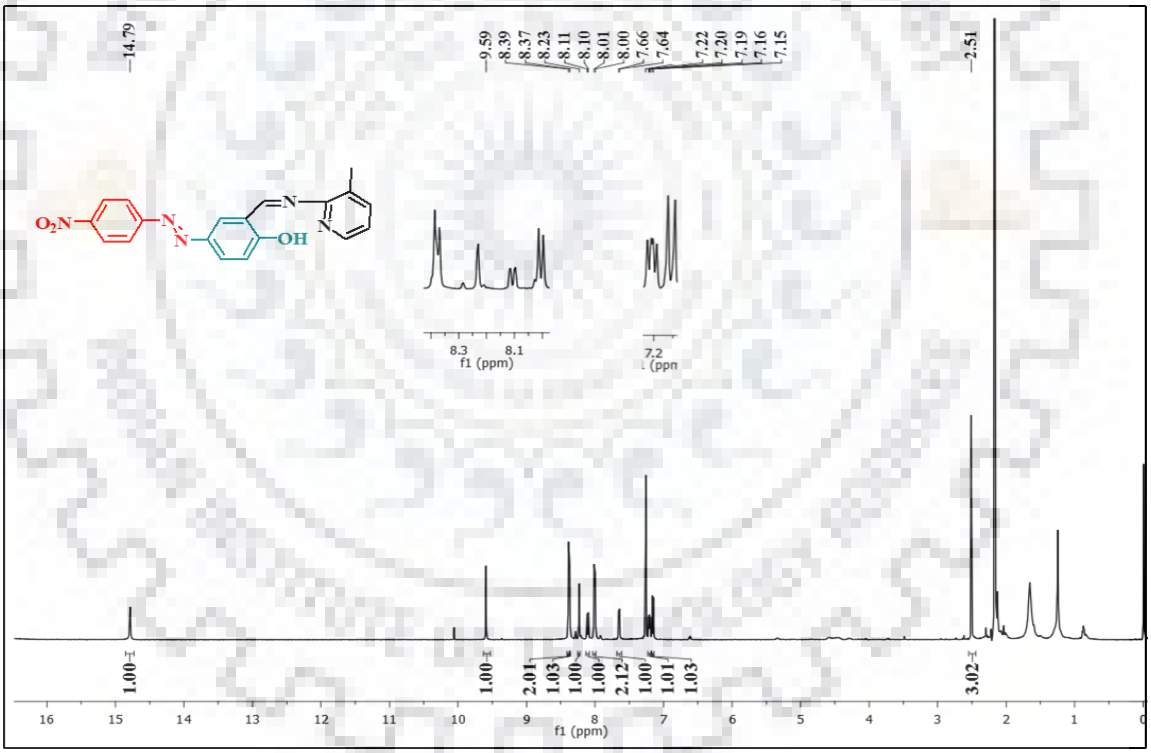

Spectrum No. 3. ^{13}C NMR spectrum of receptor B1 in $CDCl_3$.

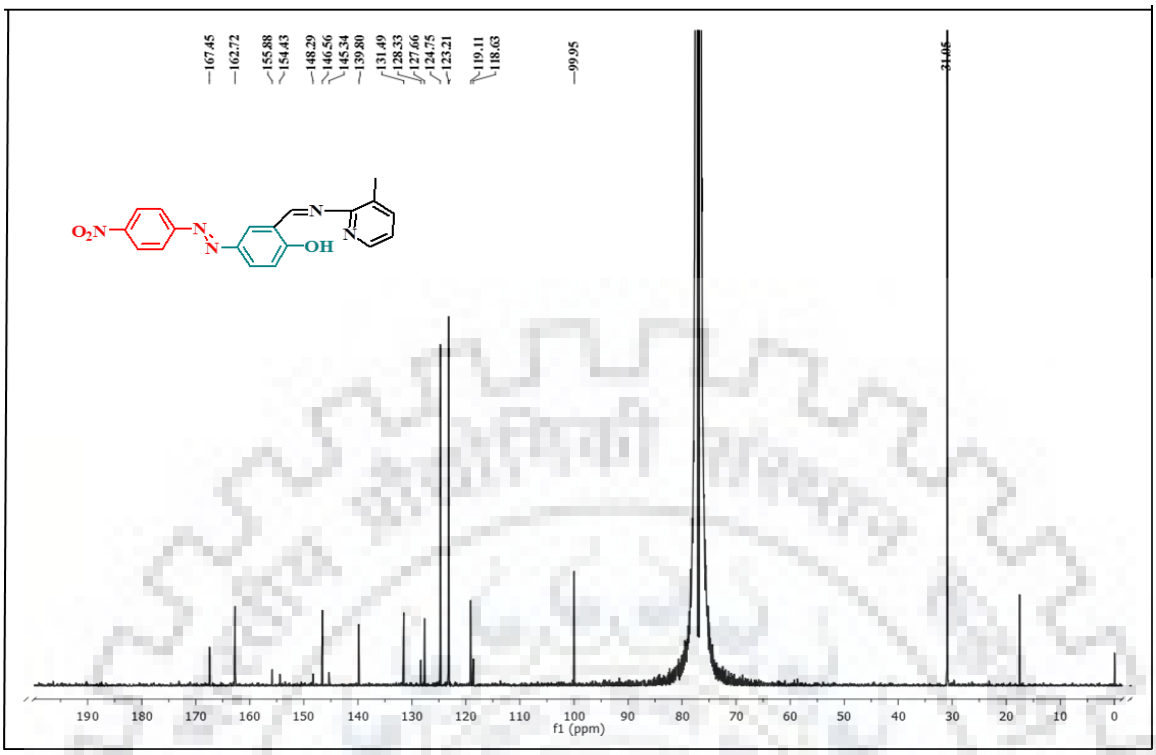

Spectrum No. 4. FT-IR spectrum of receptor B2.

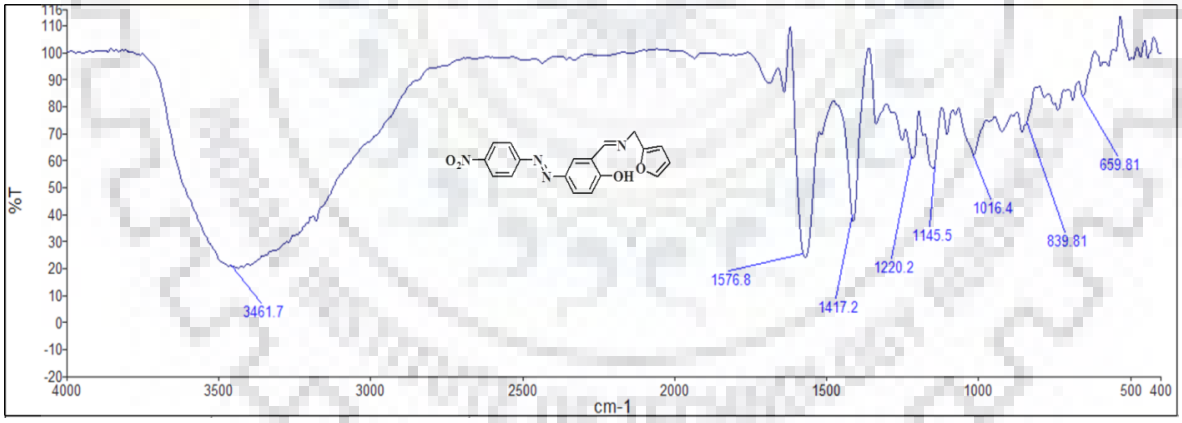

Spectrum No. 5. ^{1}H NMR spectrum of receptor B2 in DMSO d_6

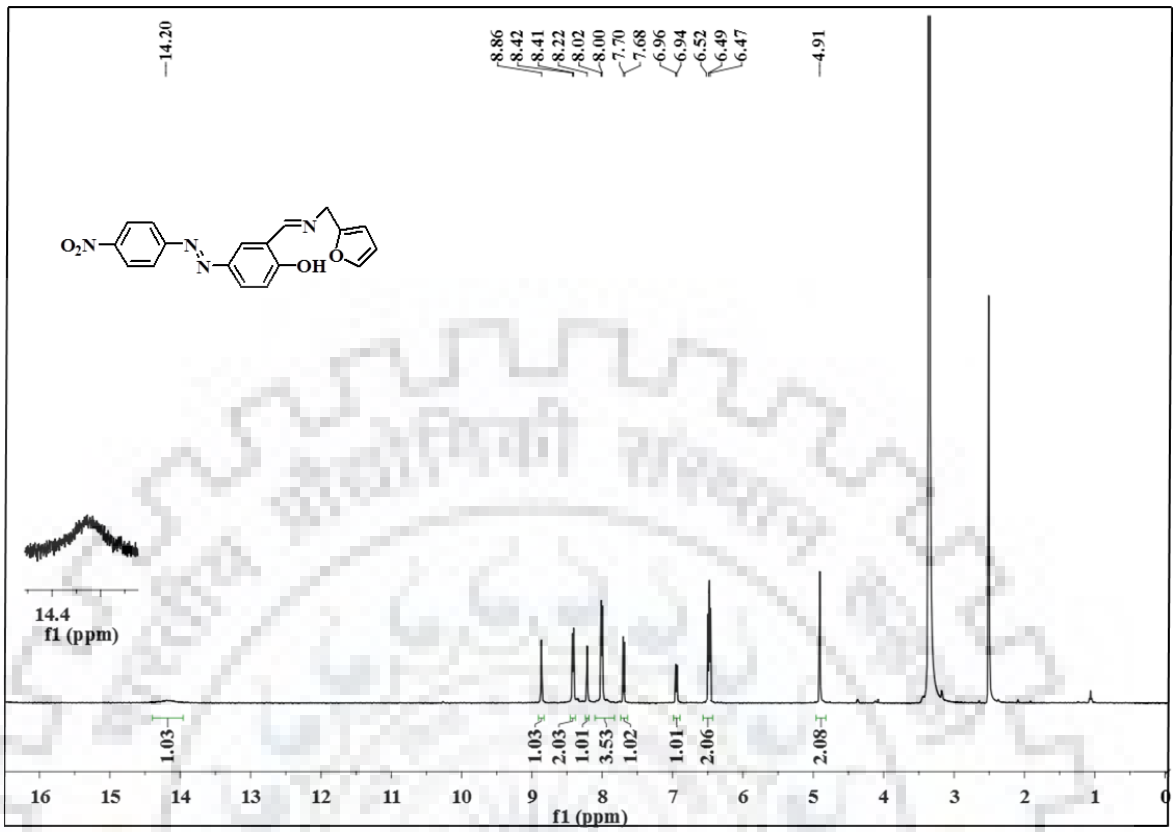

Spectrum No. 6. ^{13}C NMR spectrum of receptor B2 in DMSO d_6.

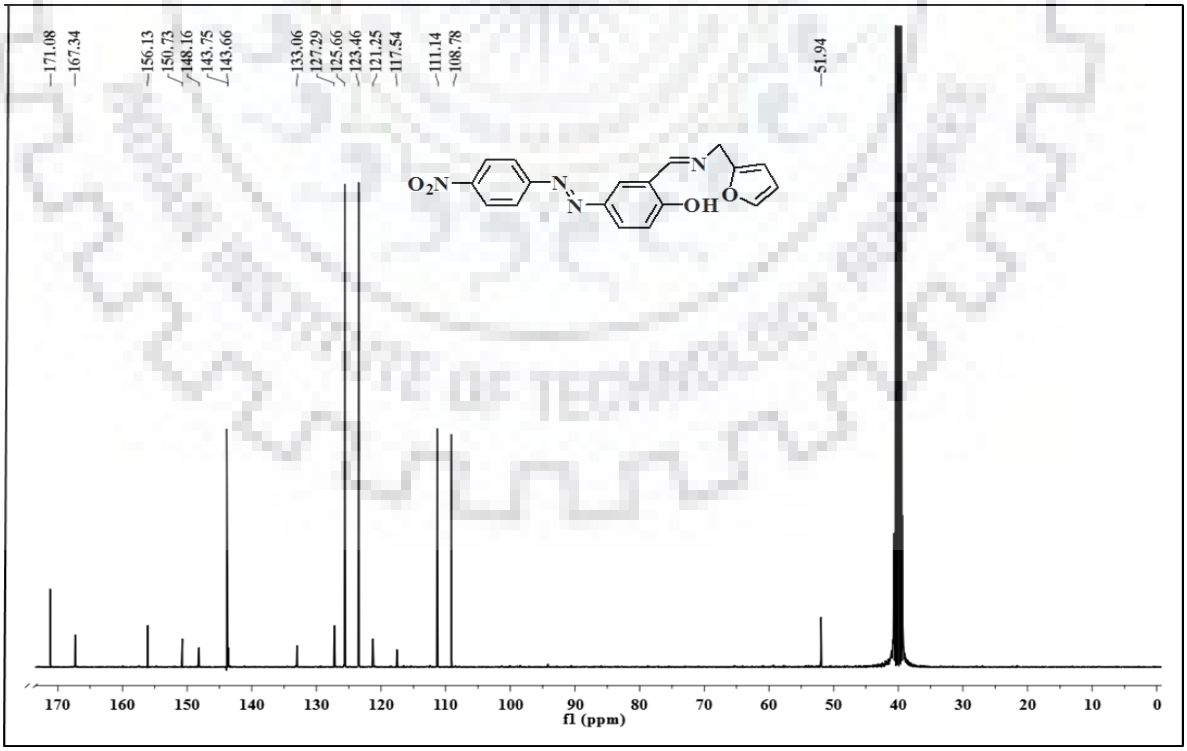

Spectrum No. 7. FT-IR spectrum of receptor B3.

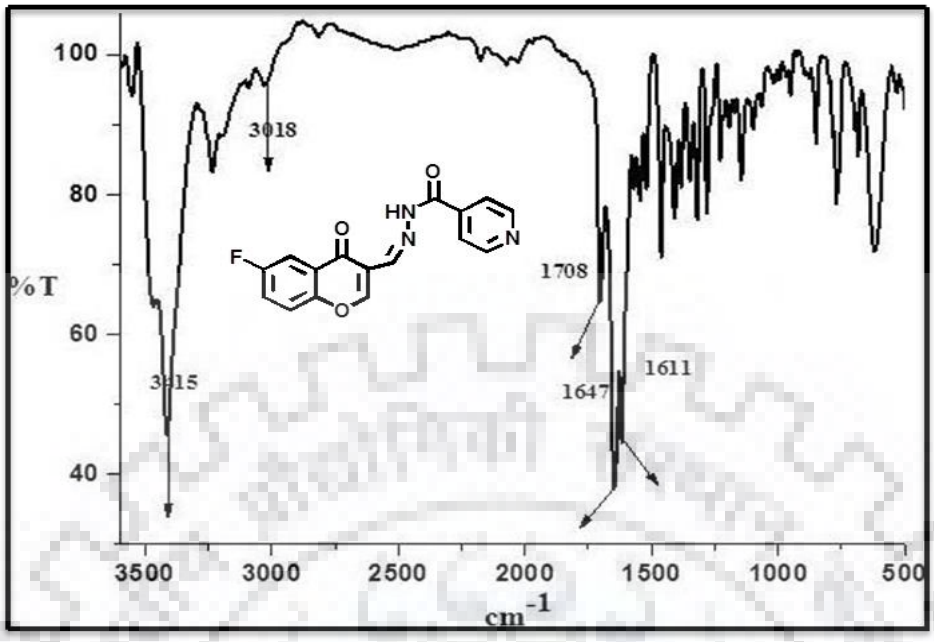

Spectrum No. 8. ^{1}H NMR spectrum of receptor B3 in DMSO d_6.

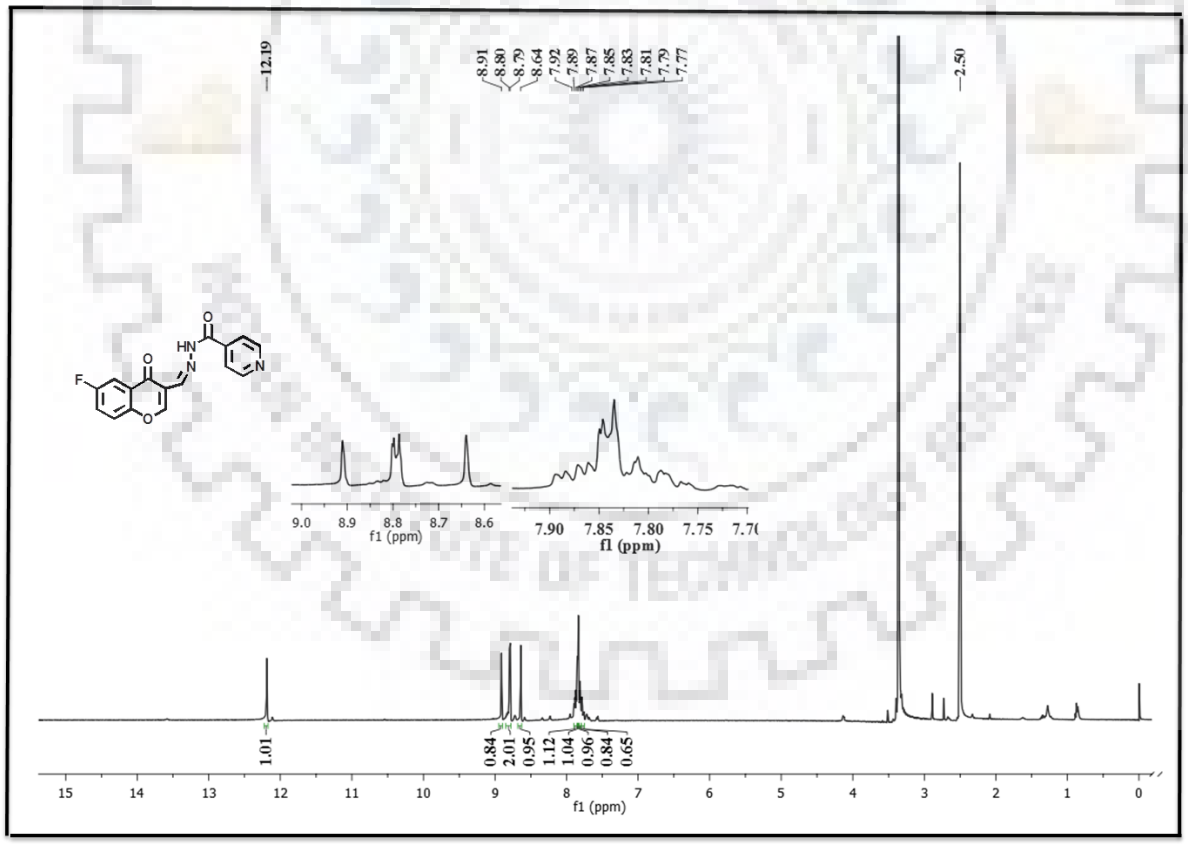

Spectrum No. 9. ^{13}C NMR spectrum of Receptor B3 in DMSO d_6.

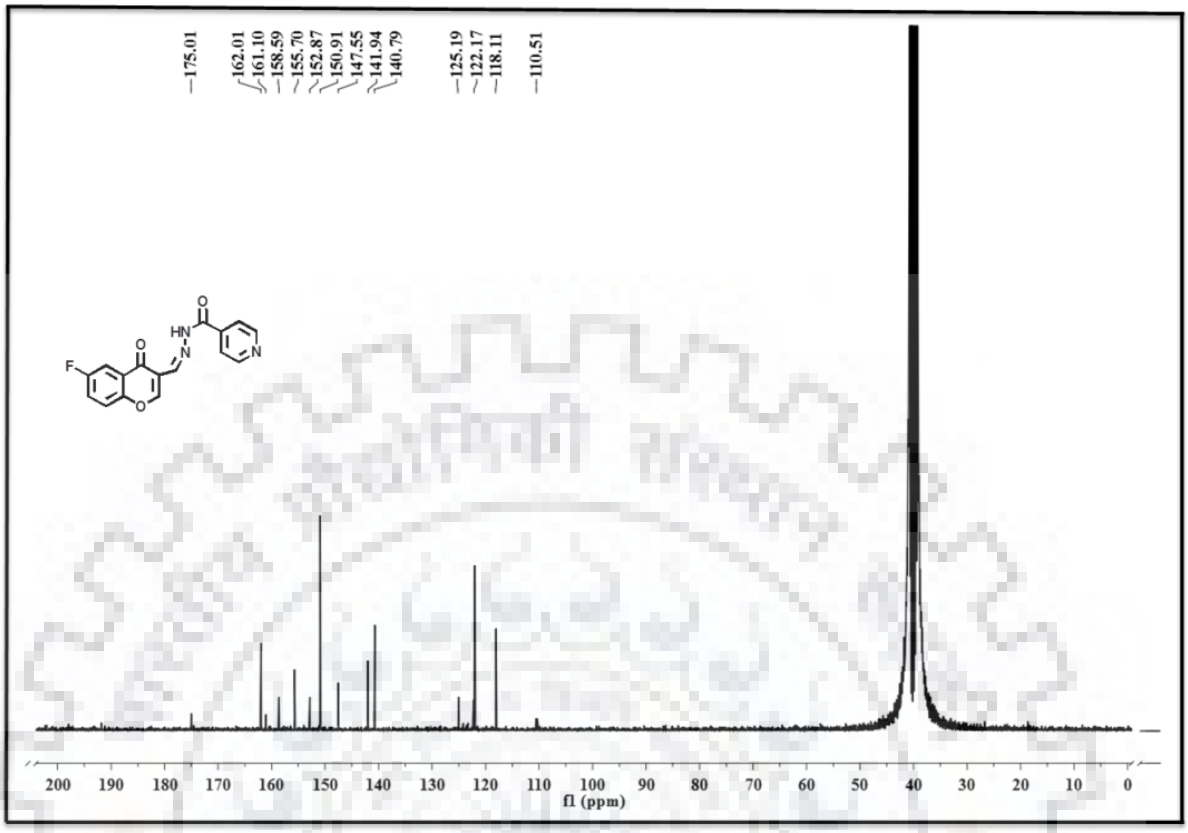

Spectrum No. 10. FT-IR spectrum of receptor B4

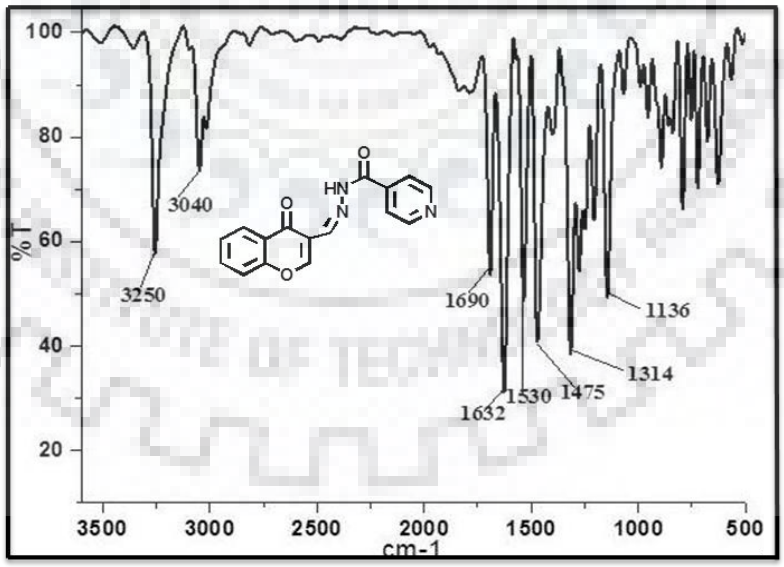

Spectrum No. 11. ^{1}H NMR spectrum of receptor B4 in DMSO d_6.

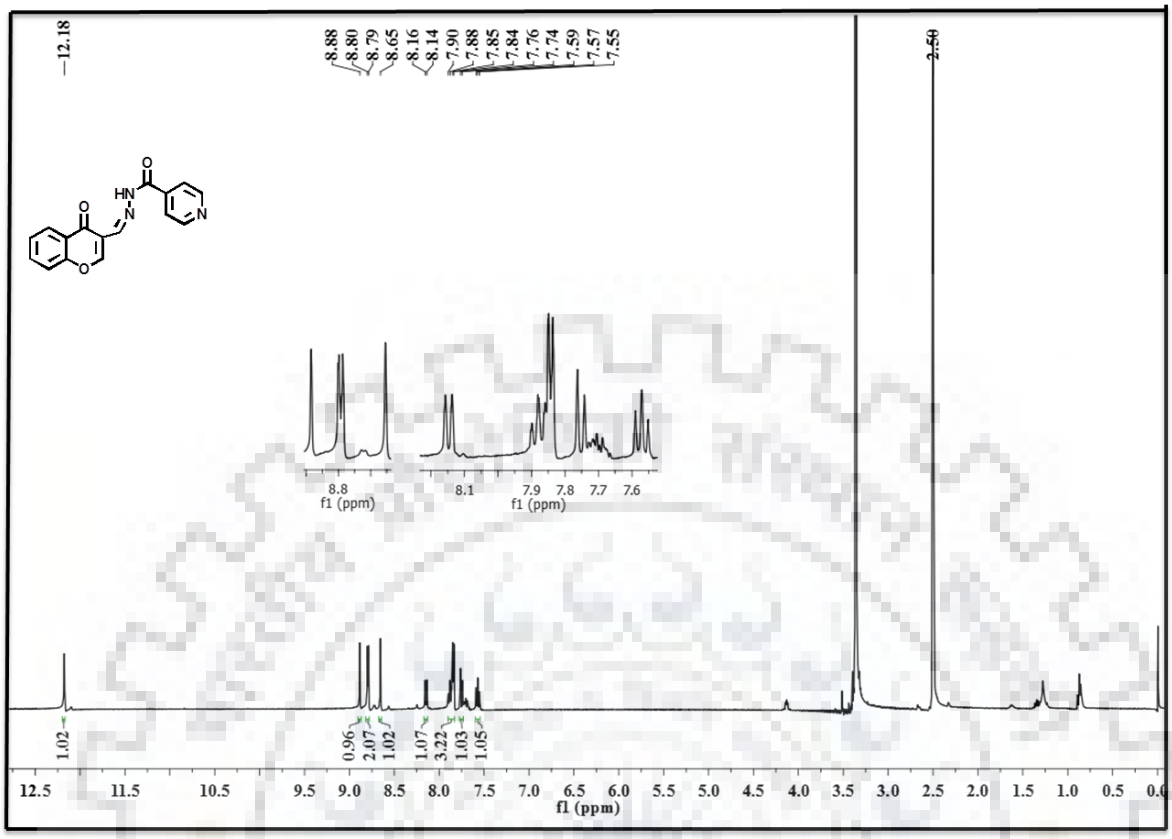

Spectrum No. 12. ^{13}C NMR spectrum of receptor B4 in DMSO d_6.

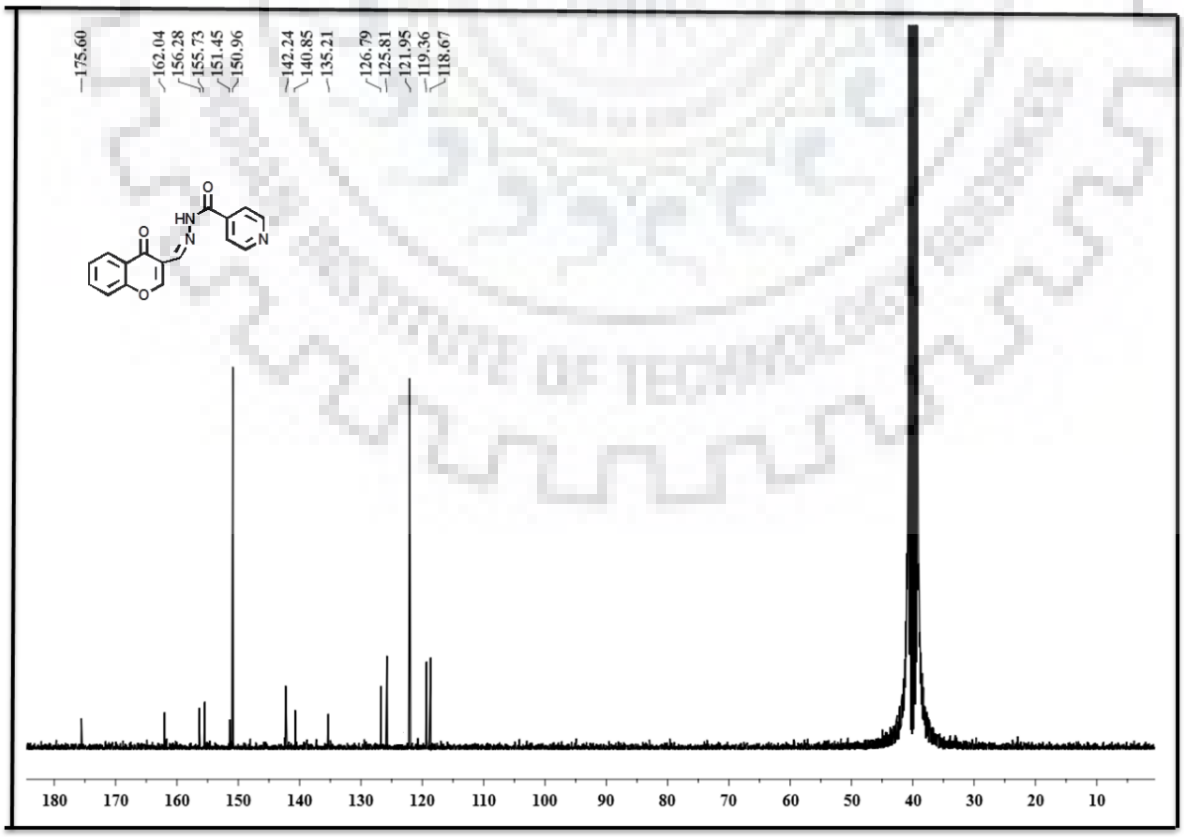

Spectrum No. 13. ^{1}H NMR spectrum of receptor 1 in $CDCl_3$.

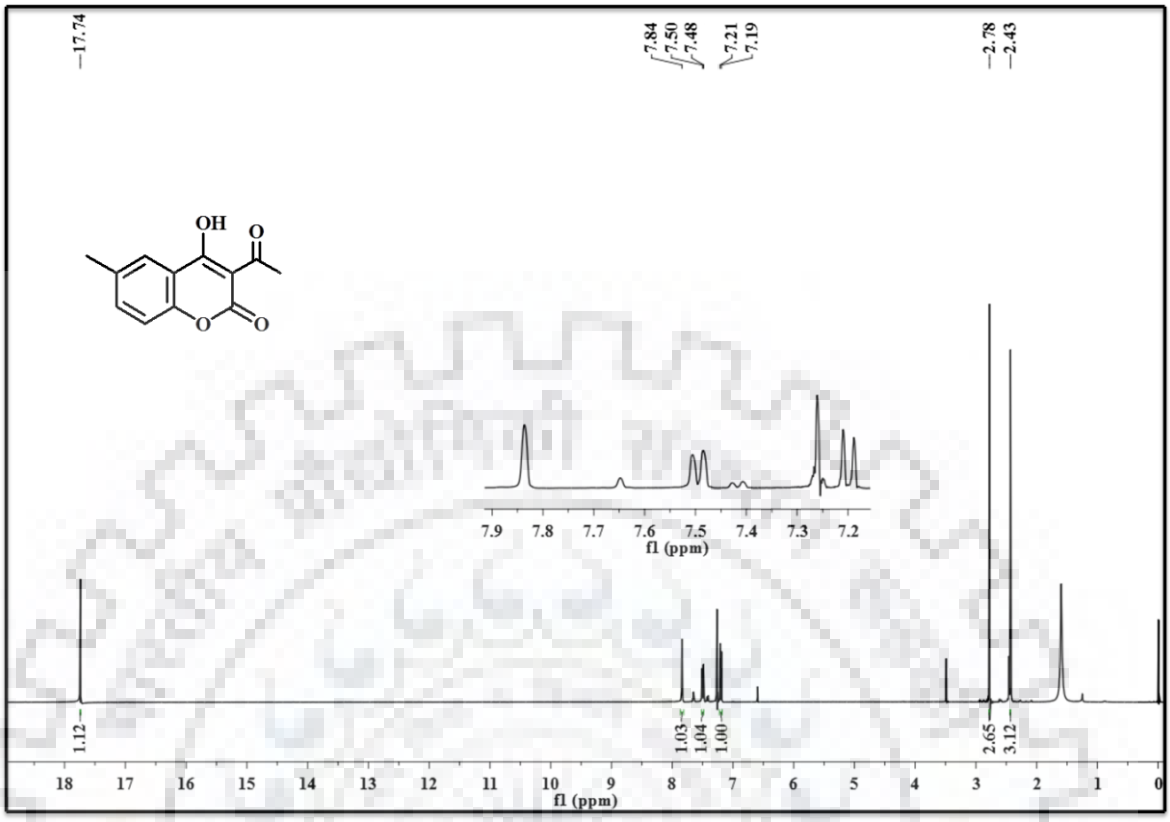

Spectrum No. 14. ^{13}C NMR spectrum of receptor 1 in $CDCl_3$.

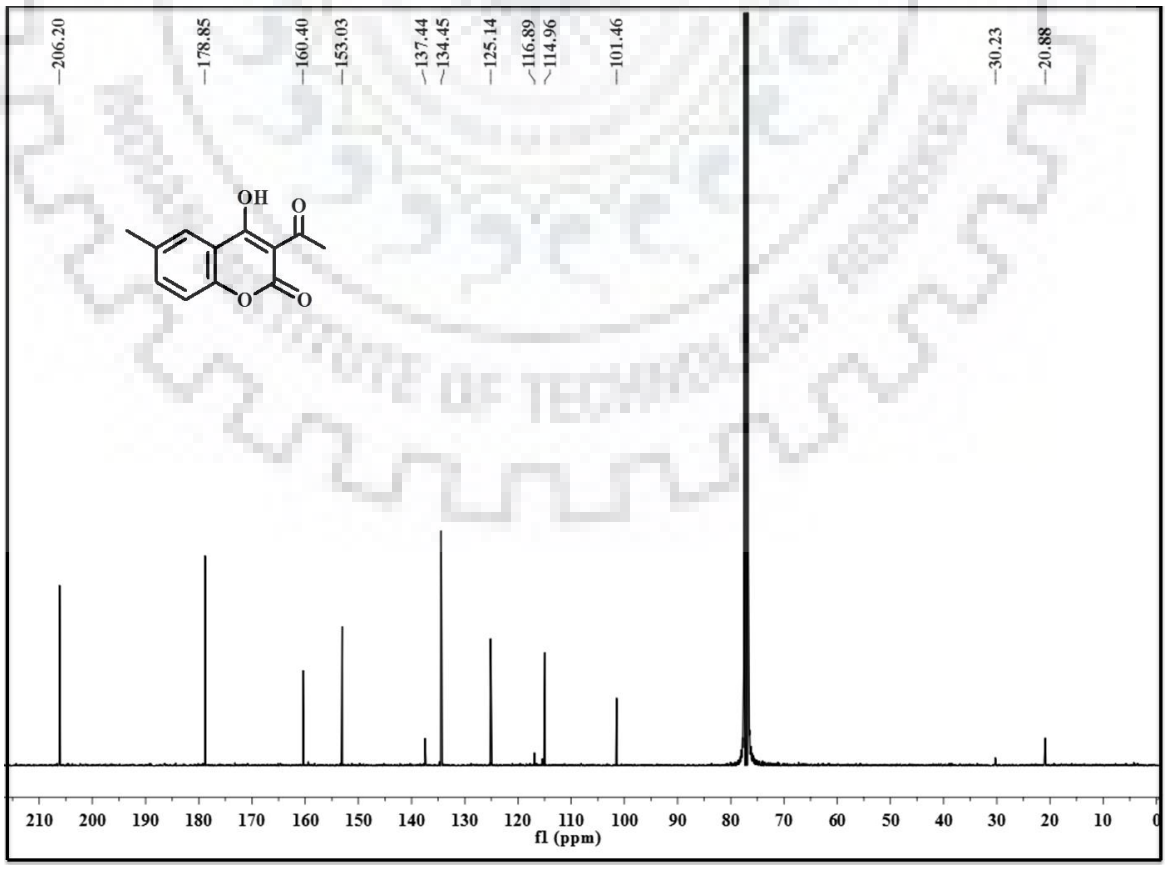

Spectrum No. 15. FT-IR spectrum of receptor 2a.

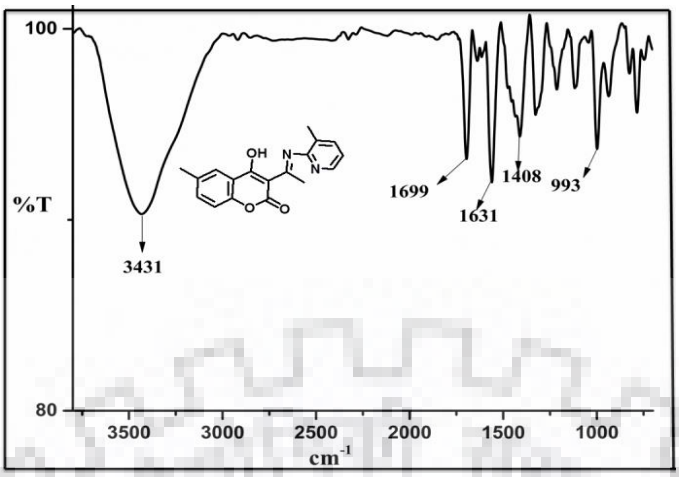

Spectrum No. 16. Mass spectrum of receptor 2a.

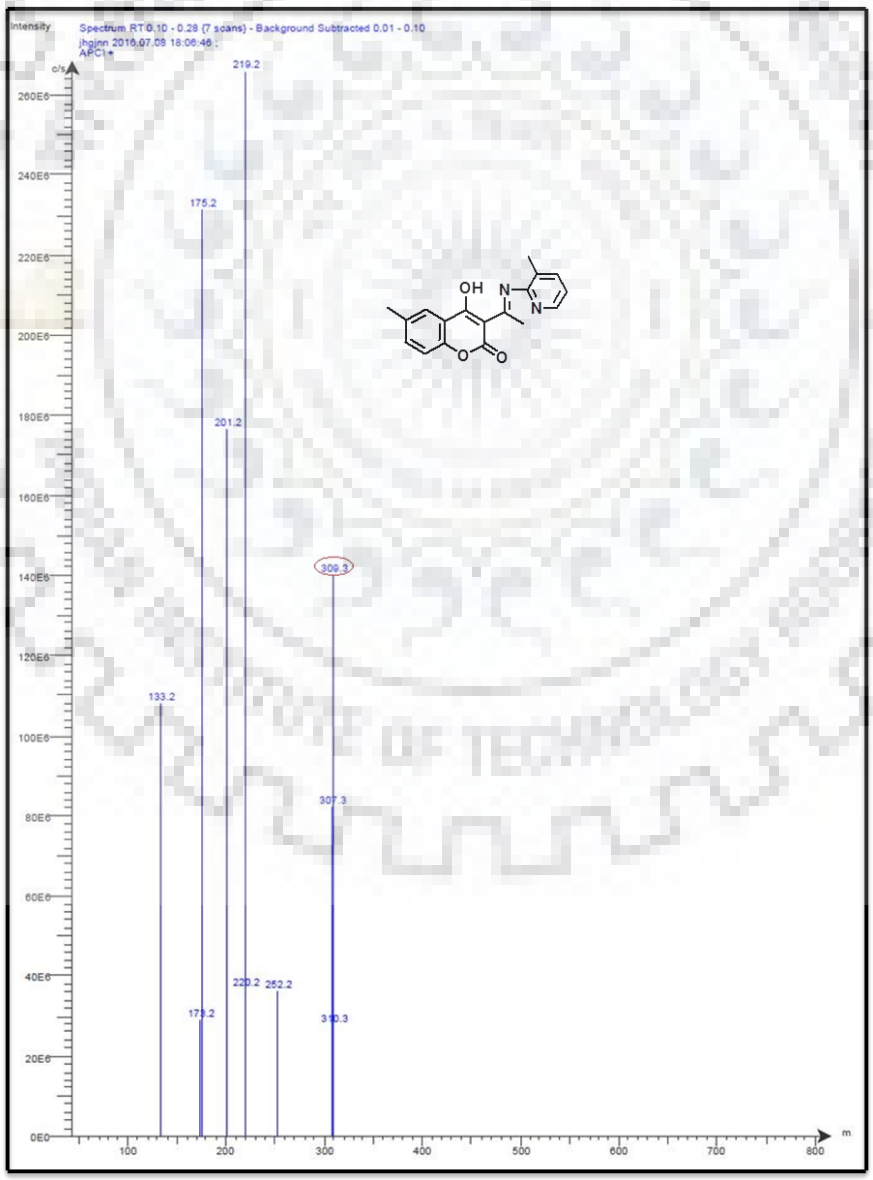

Spectrum No. 17. ^{1}H NMR spectrum of receptor 2a in DMSO d_6.

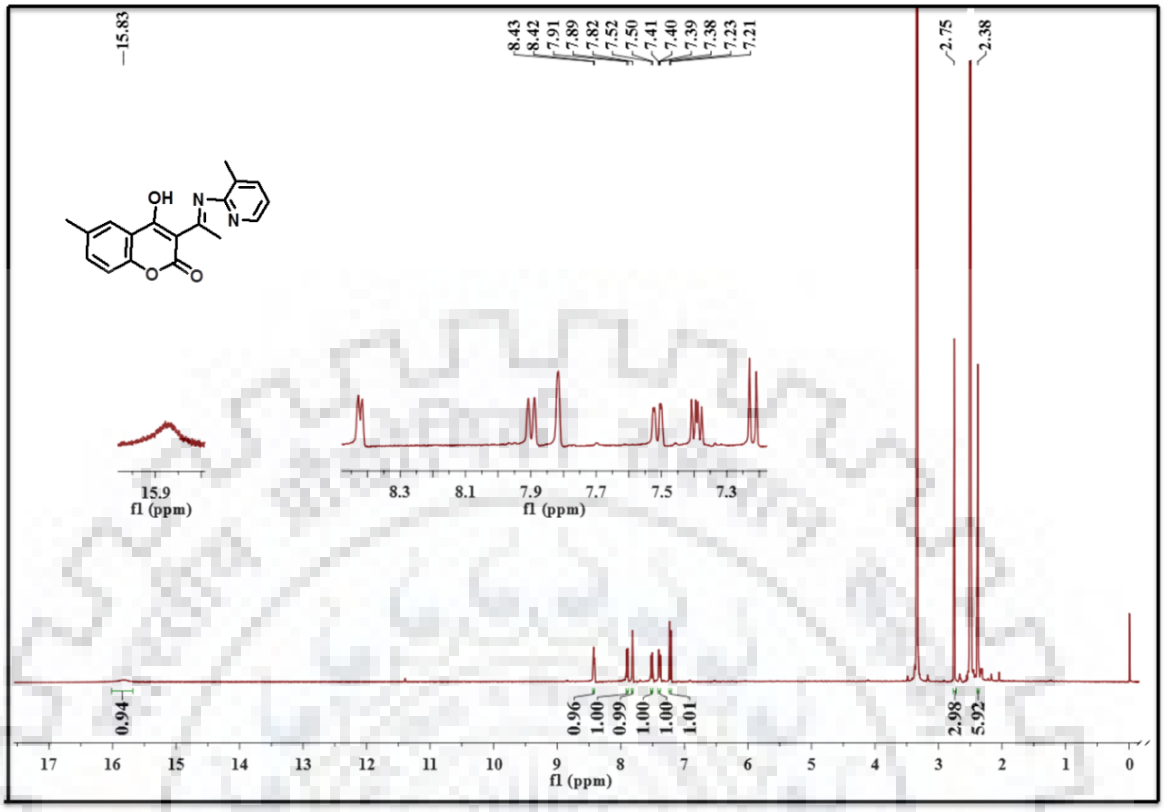

Spectrum No. 18. ^{13}C NMR spectrum of receptor 2a in $CDCl_3$.

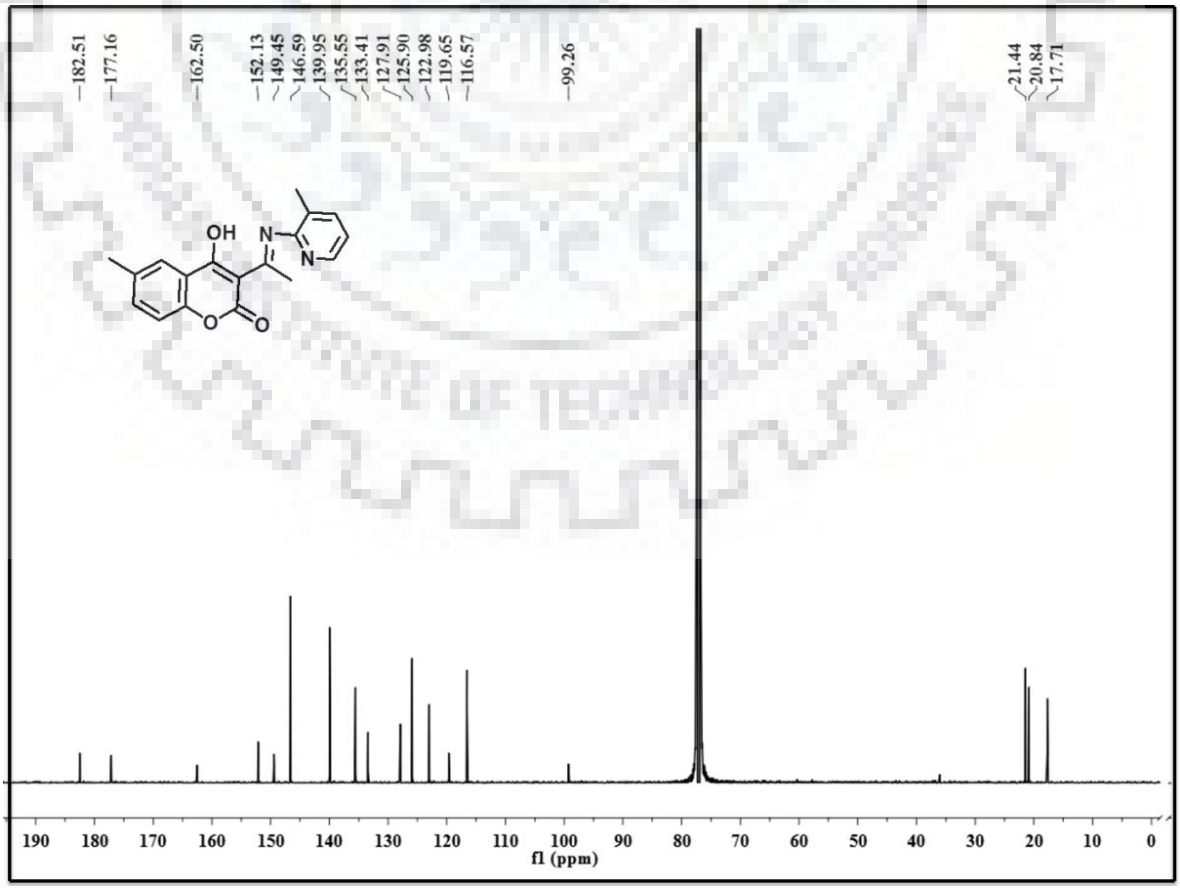

Spectrum No. 19. ^{1}H NMR spectrum of receptor 2b in $CDCl_3$.

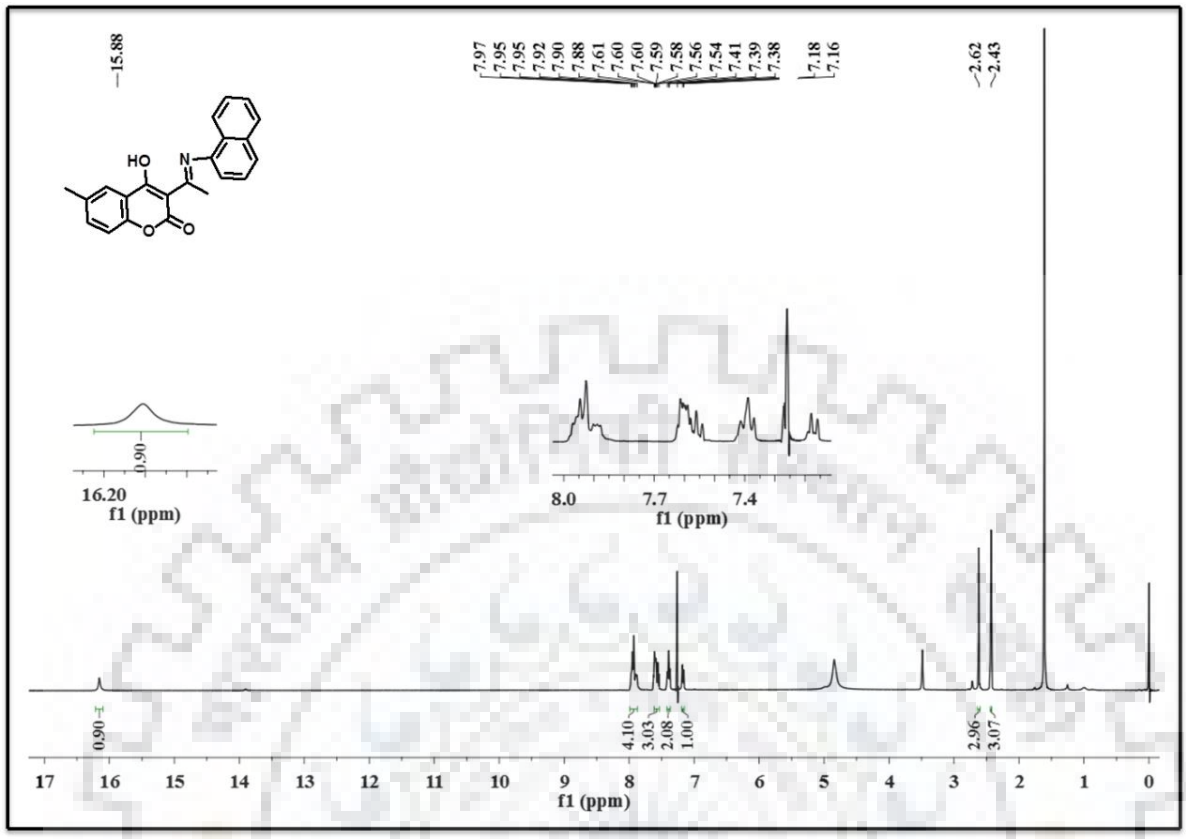

Spectrum No. 20. ^{13}C NMR spectrum of receptor 2b in $CDCl_3$.

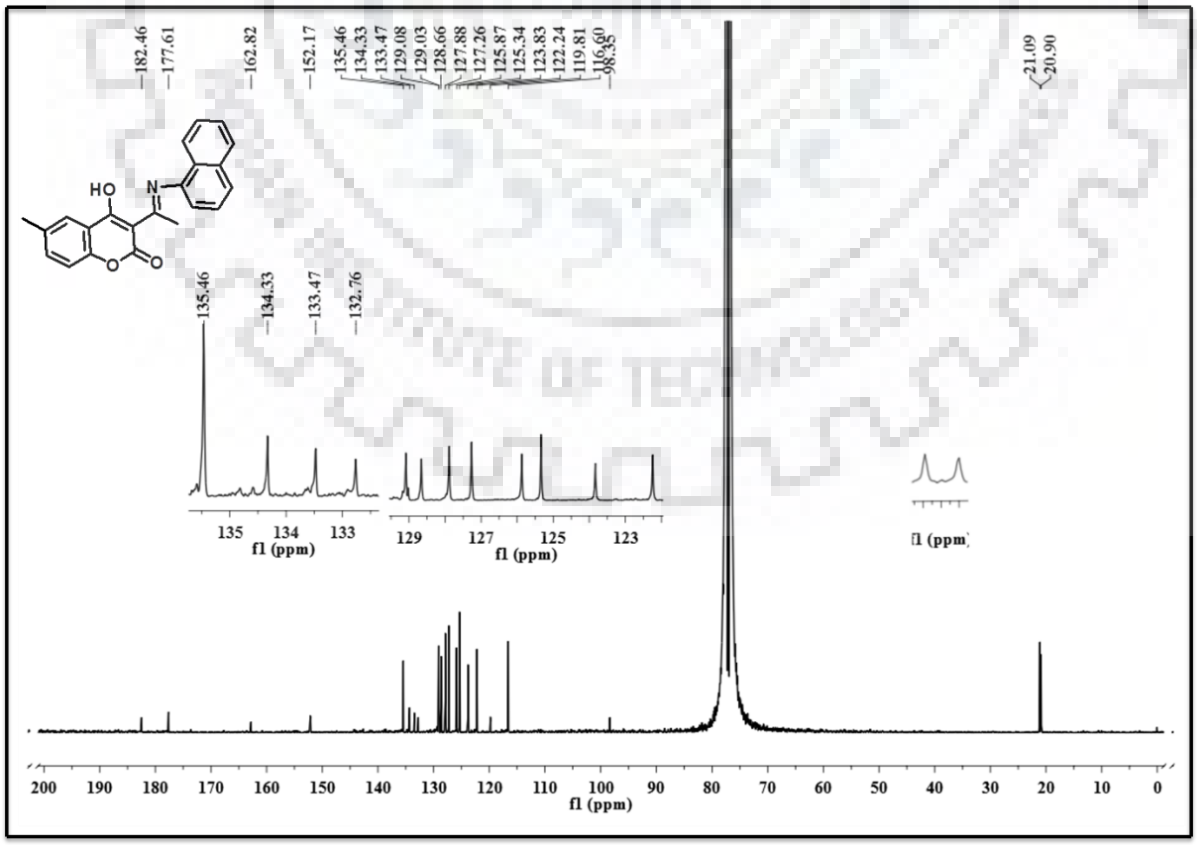

Spectrum No. 21. FT-IR spectrum of receptor L1.

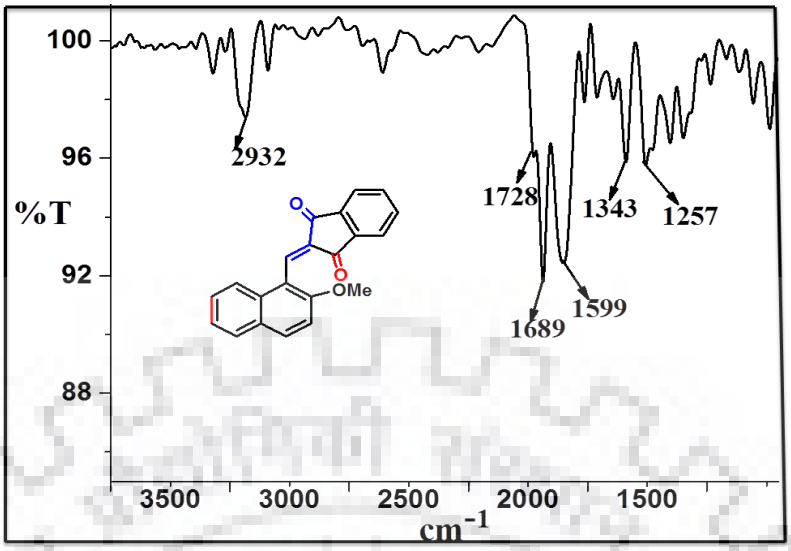

Spectrum No. 22. Mass spectrum of receptor of L1.

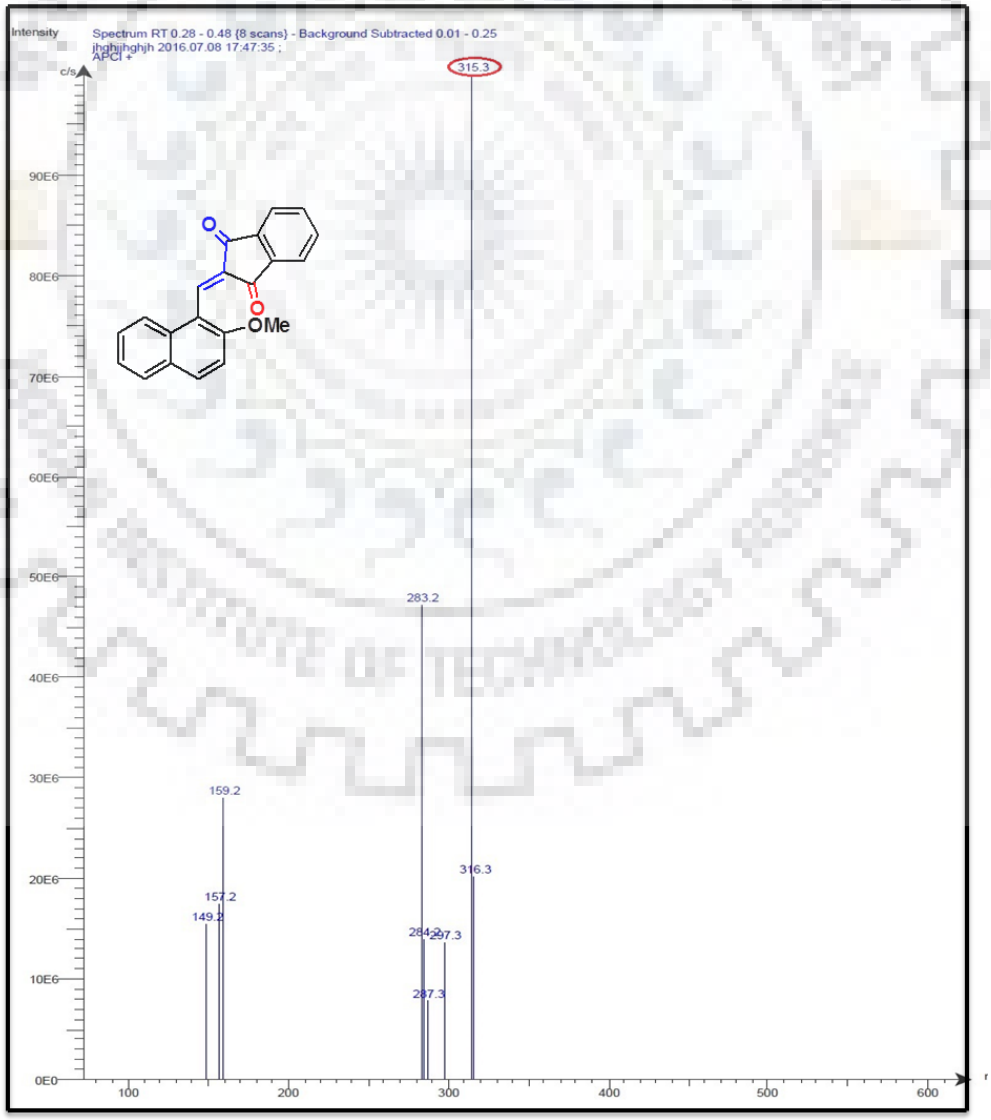

Spectrum No. 23. ^{1}H NMR spectrum of receptor L1 in $CDCl_3$.

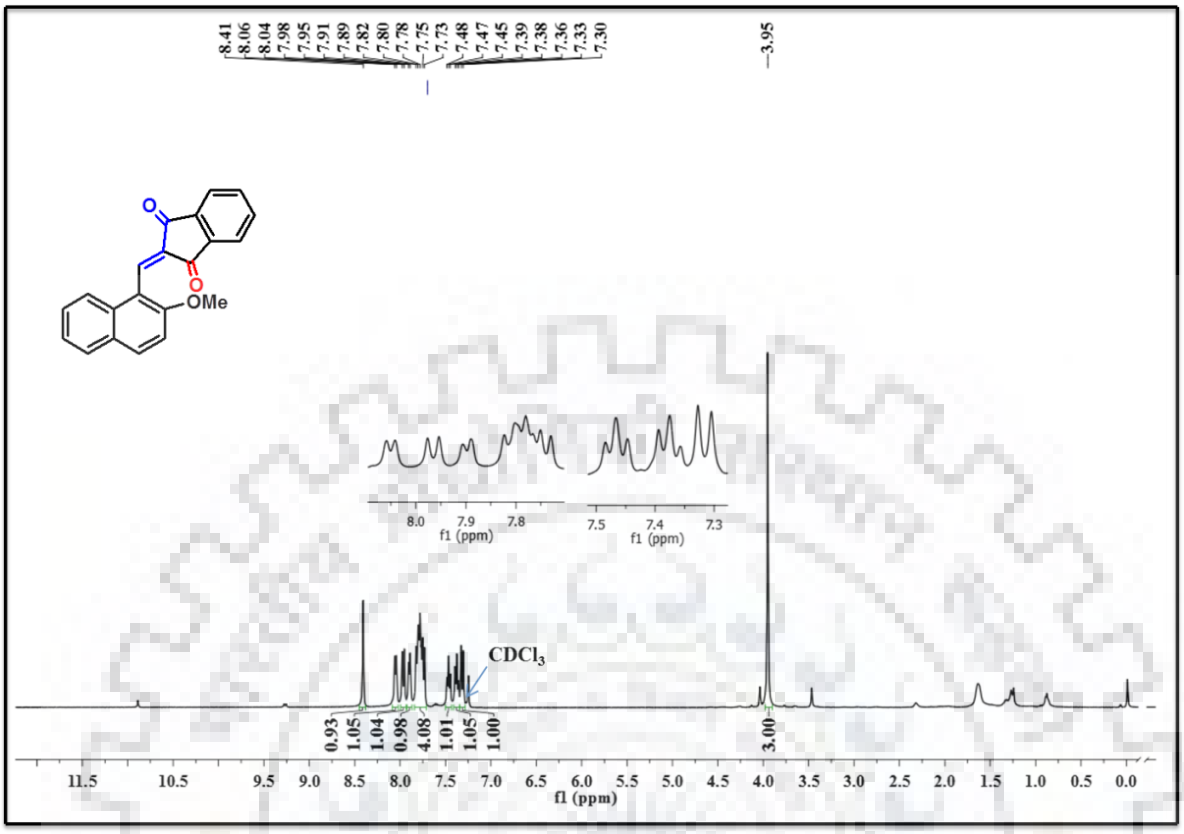

Spectrum No. 24. ^{13}C NMR spectrum of receptor L1 in $CDCl_3$.

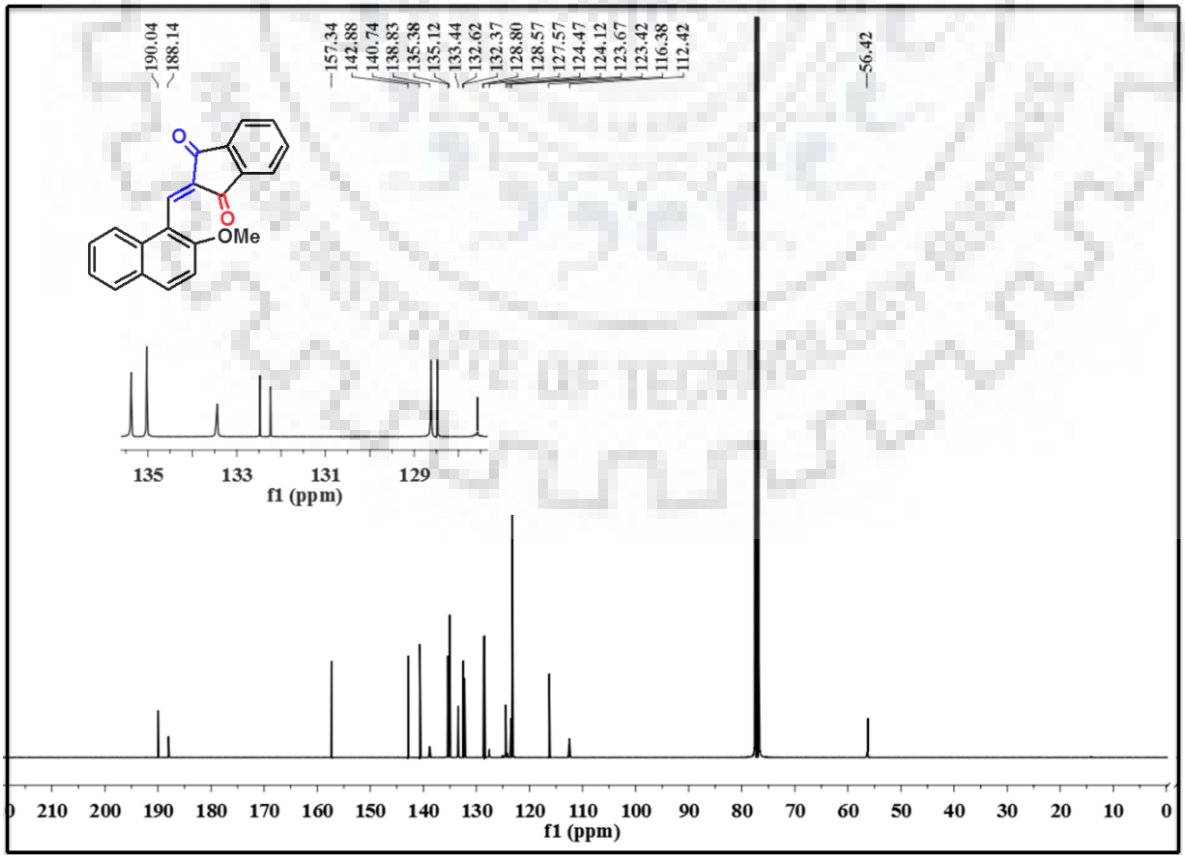

Spectrum No. 25. FT-IR spectrum of receptor L2.

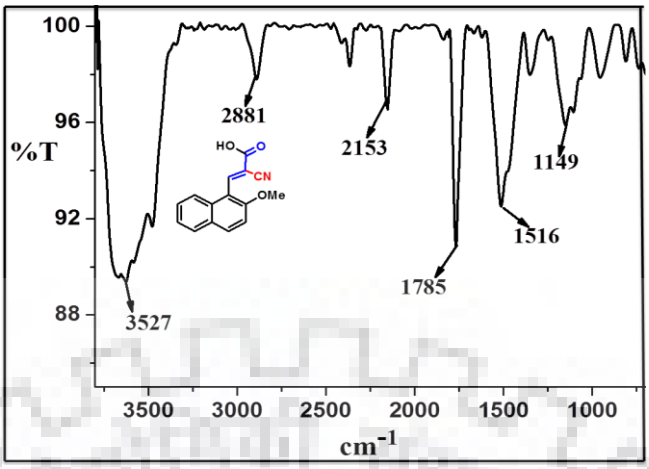

Spectrum No. 26. Mass spectrum of receptor of L2.

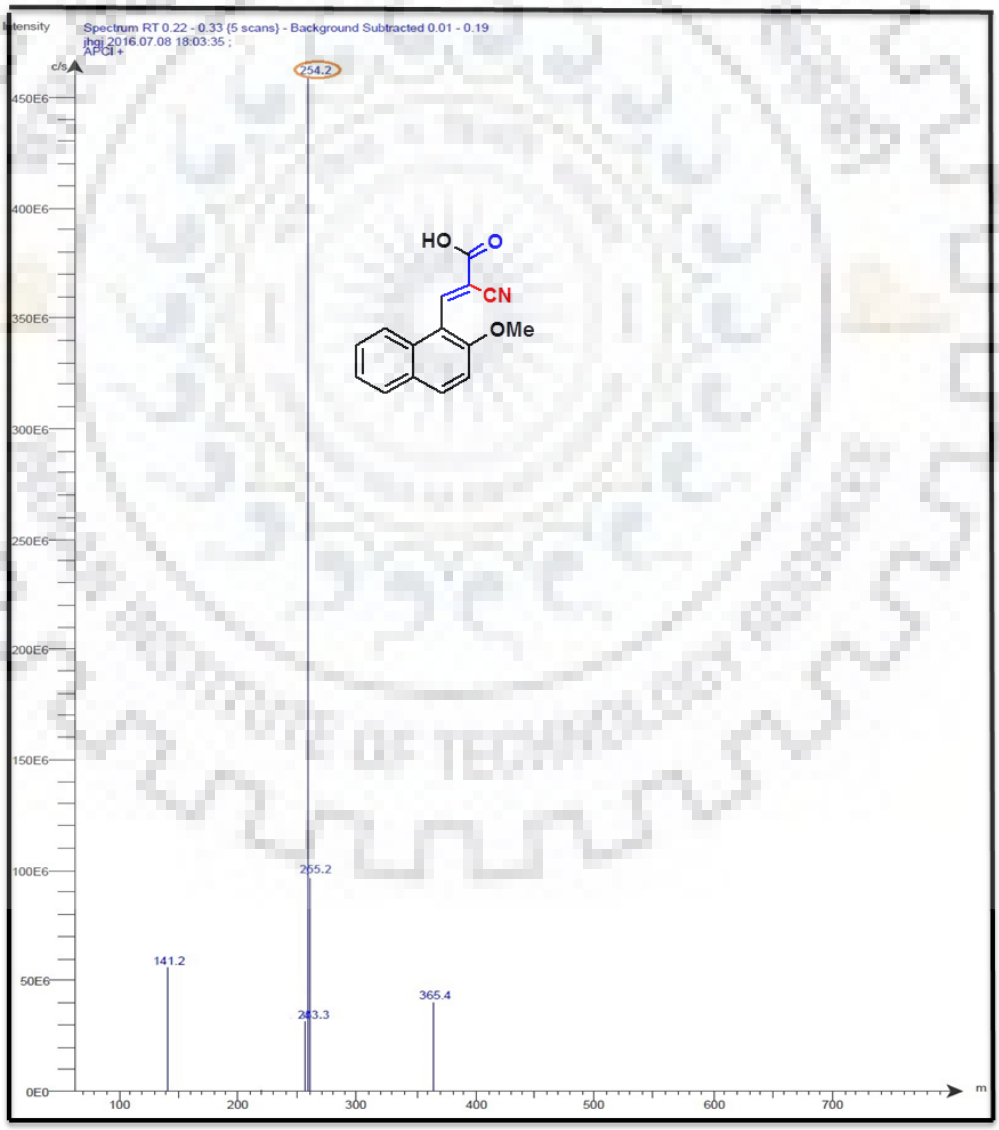

Spectrum No. 27. ^{1}H NMR spectrum of receptor L2 in $CDCl_3$.

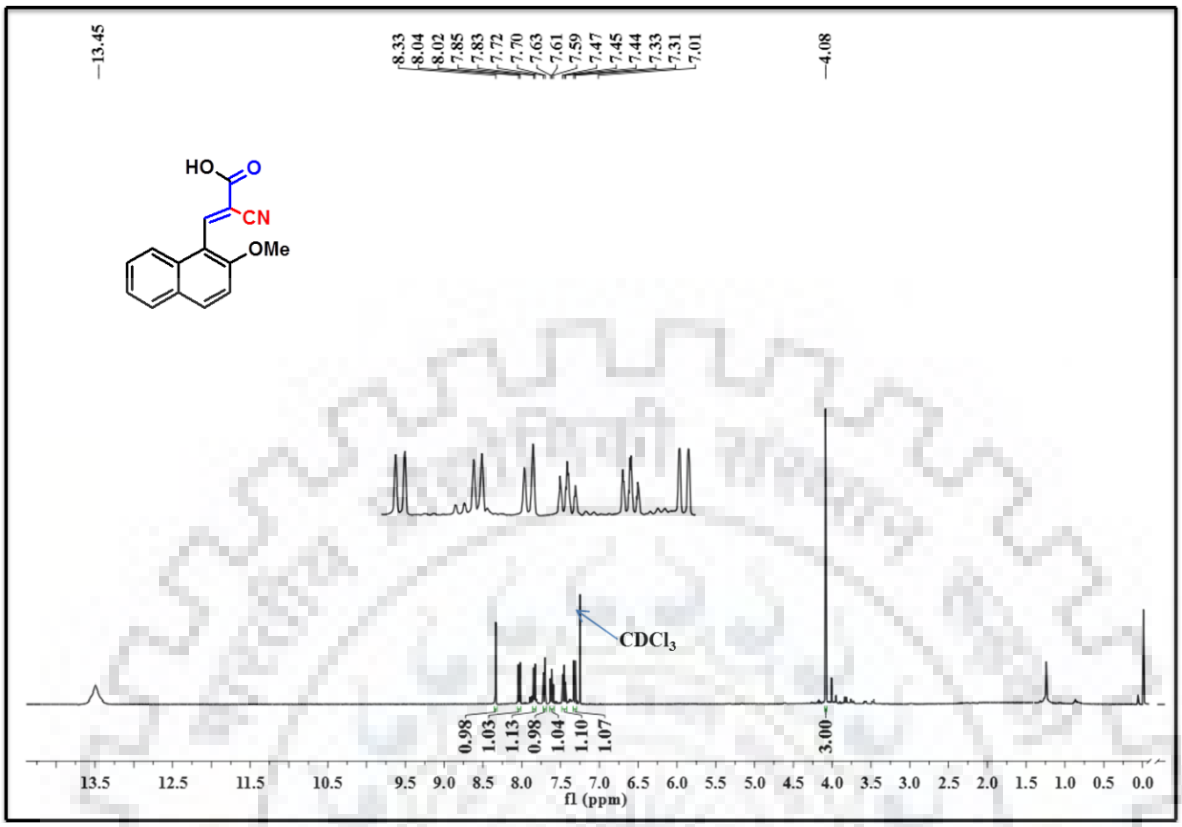

Spectrum No. 28. ^{13}C NMR spectrum of receptor L2 in $CDCl_3$.

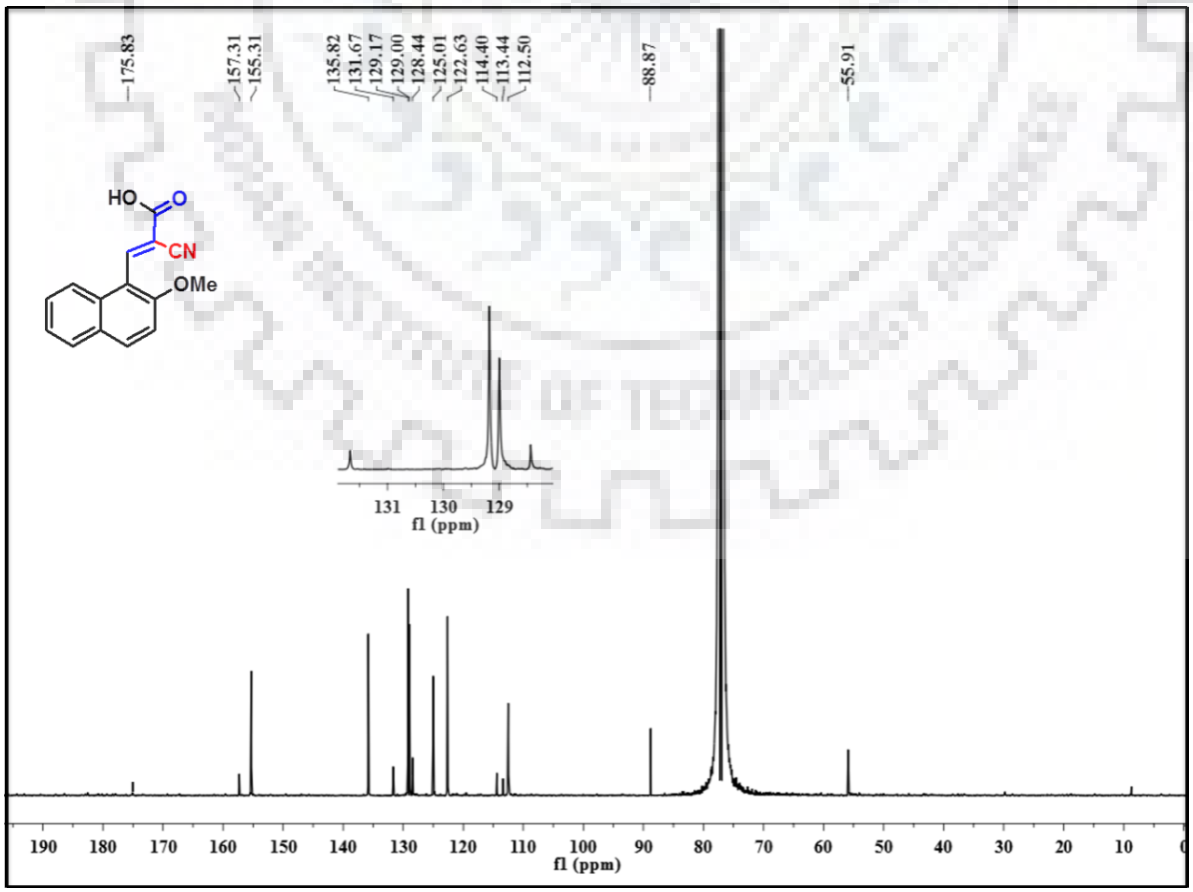

Spectrum No. 29. FT-IR spectrum of receptor L3.

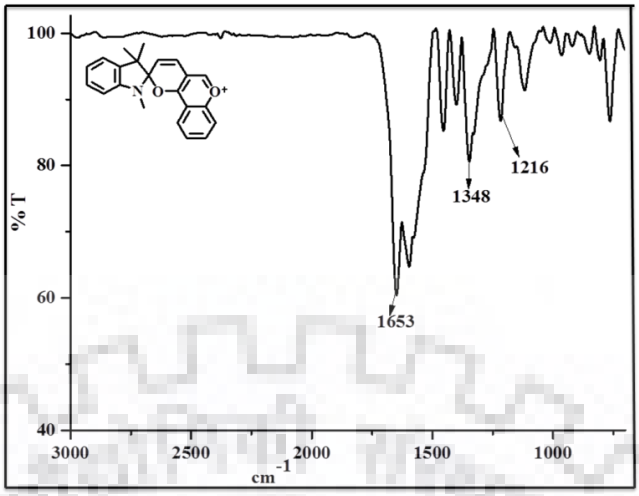

Spectrum No. 30. Mass spectrum of receptor of L3.

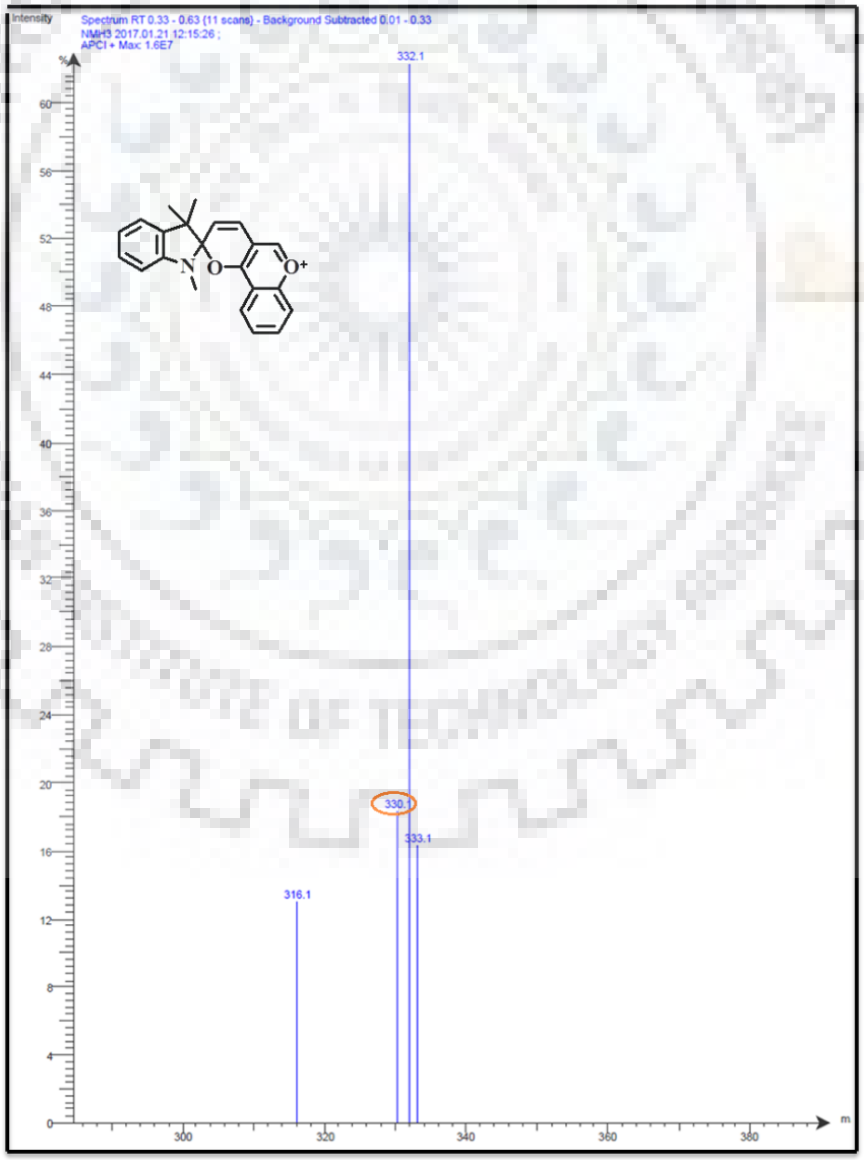

Spectrum No. 31. ^{1}H NMR spectrum of receptor L3 in $CDCl_3$.

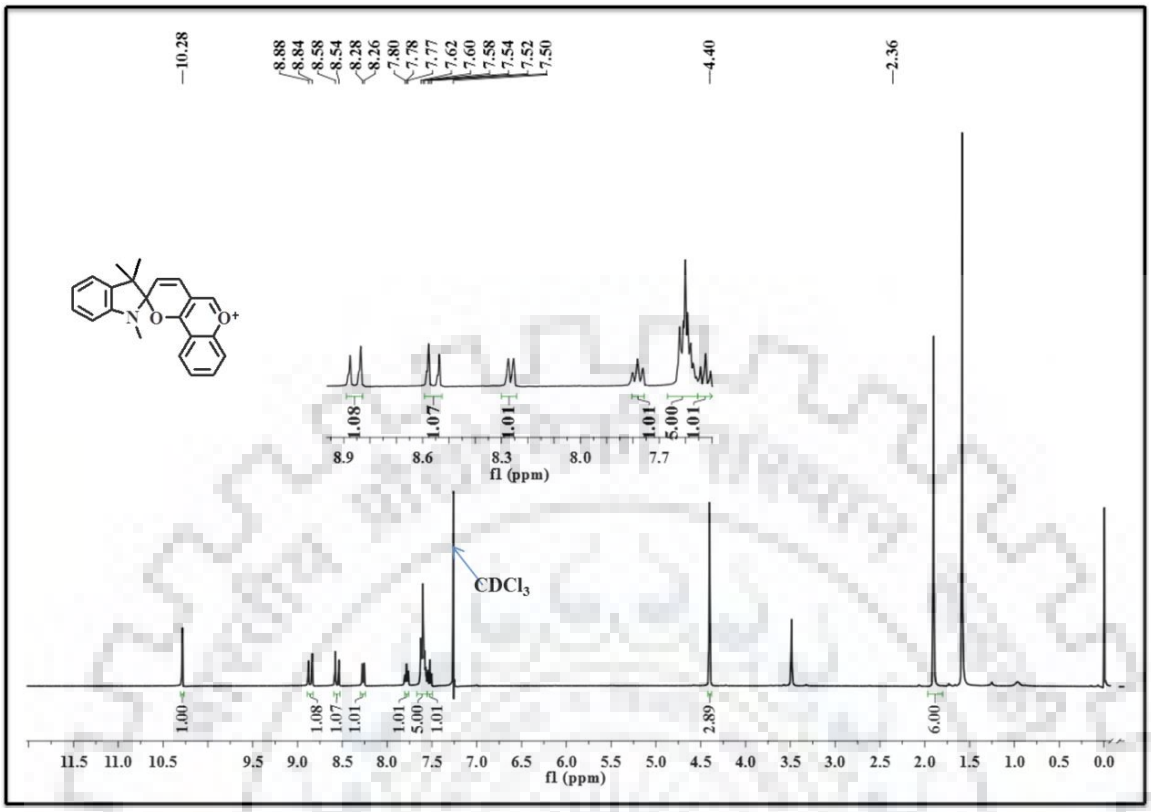

Spectrum No. 32. ^{13}C NMR spectrum of receptor L3 in $CDCl_3$ +DMSO d_6.

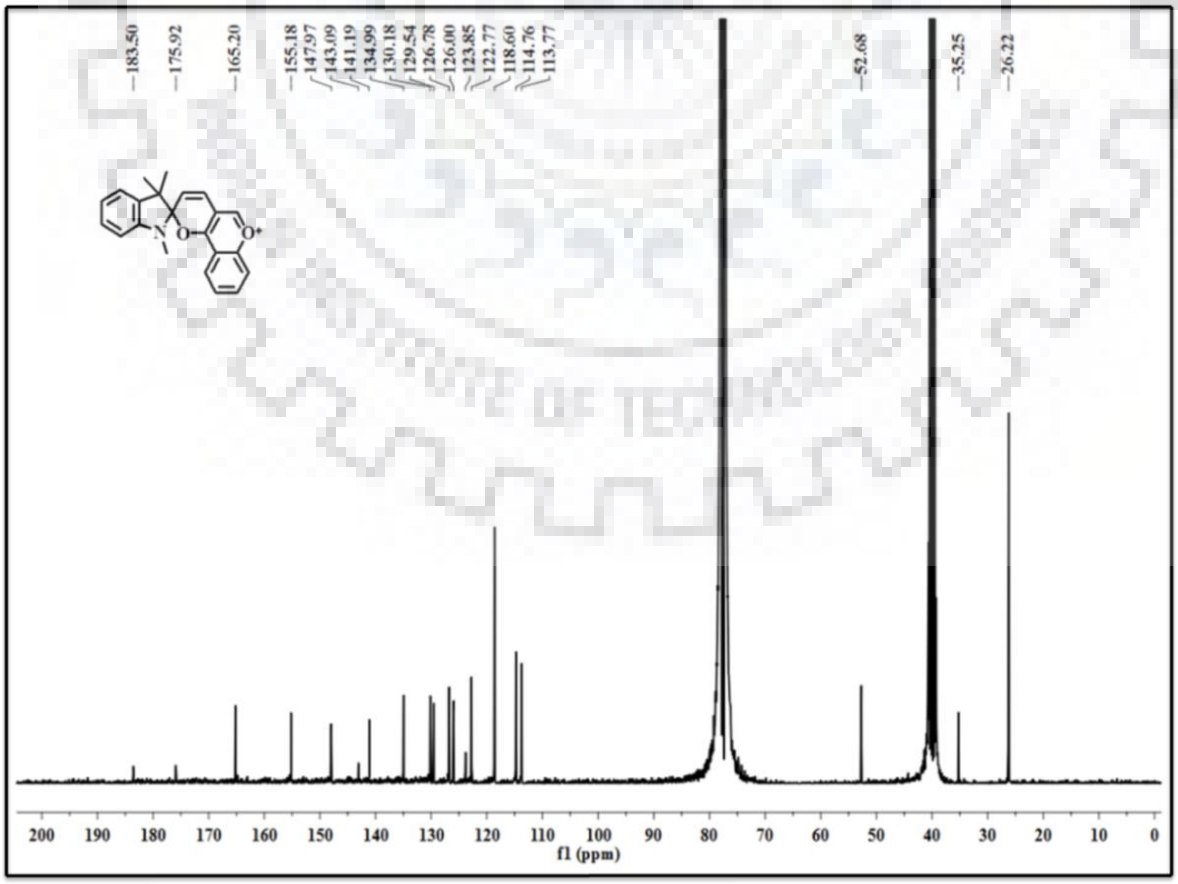

Spectrum No. 33. FT-IR spectrum of receptor L4.

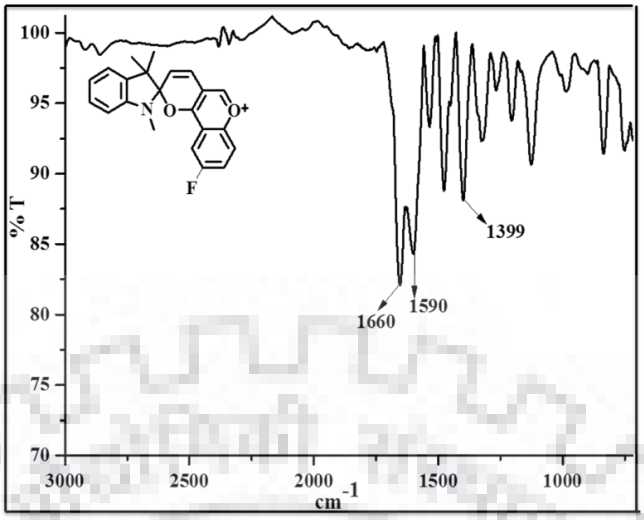

Spectrum No. 34. Mass spectrum of receptor L4.

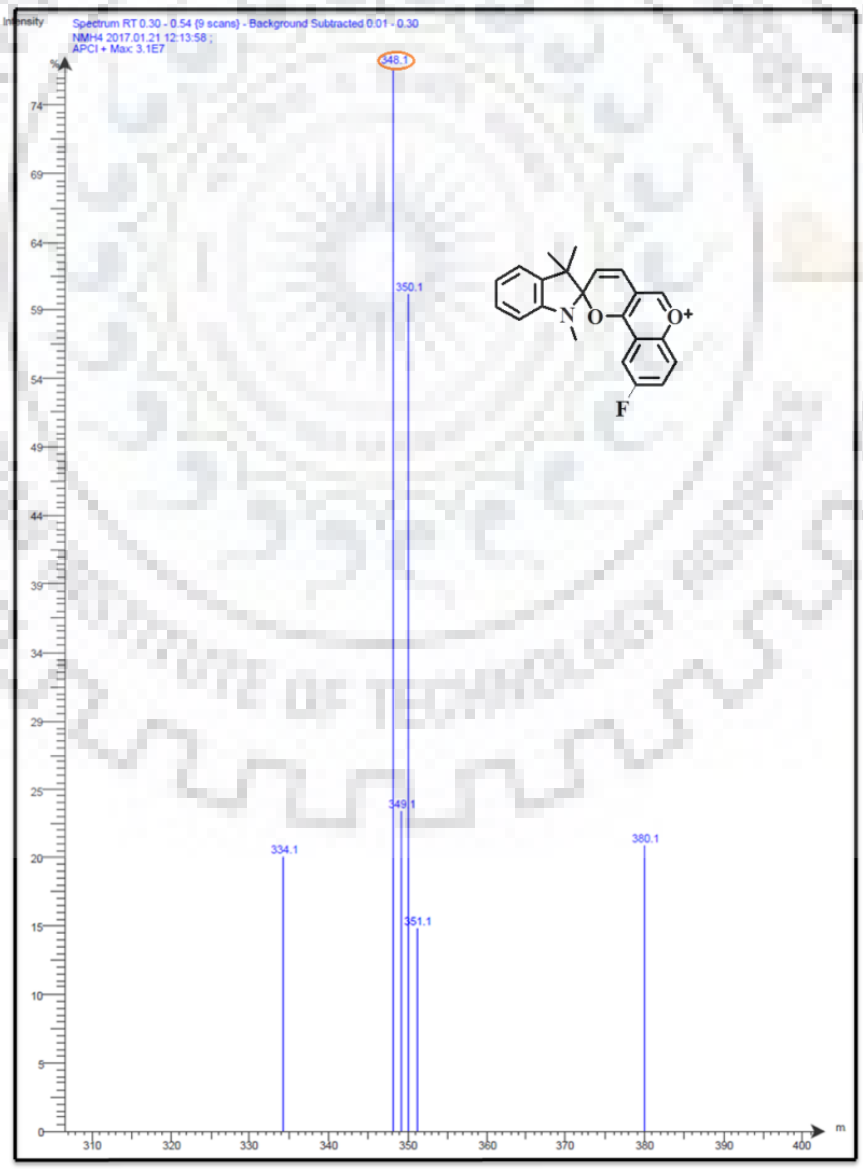

Spectrum No. 35. ^{1}H NMR spectrum of receptor L4 in DMSO $d_{6.}$

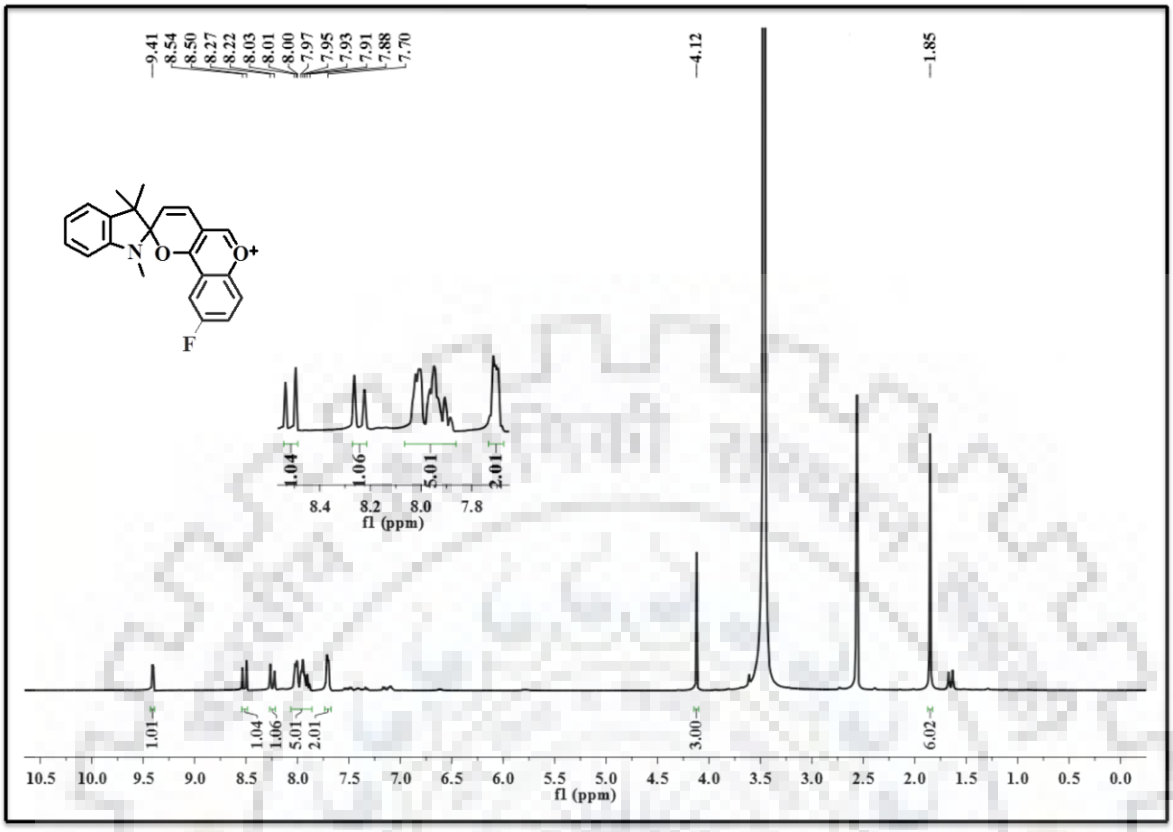

Spectrum No. 36. ^{13}C NMR spectrum of receptor L4 in DMSO $d_{6.}$

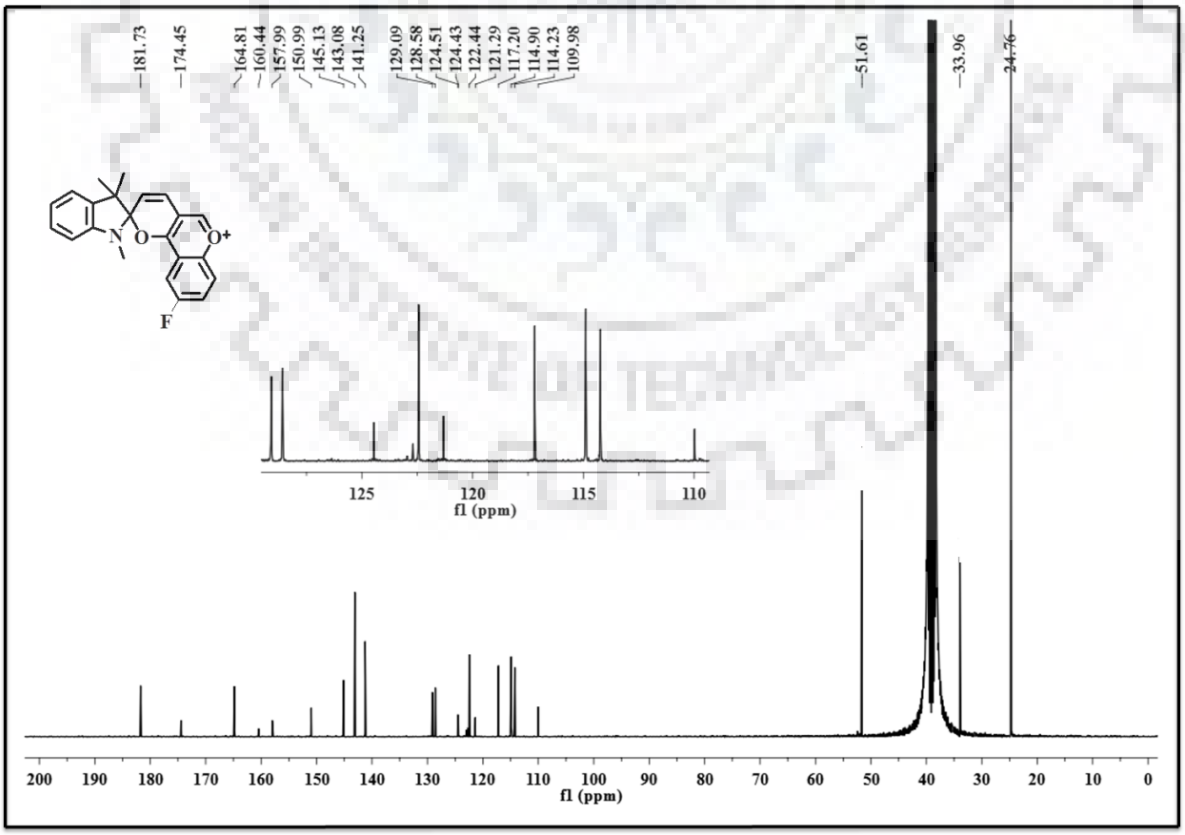

Spectrum No. 37. ^{1}H NMR spectrum of receptor S1 in $CDCl_3$.

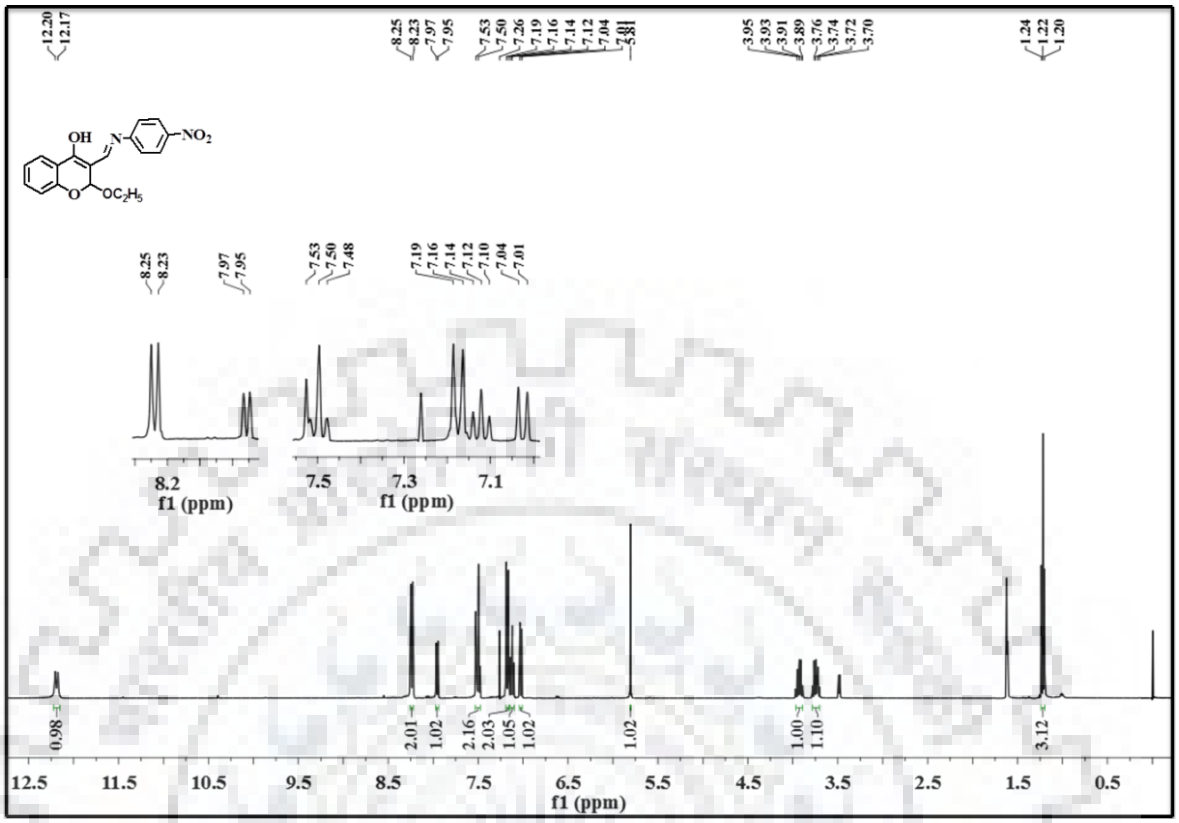

Spectrum No. 38. ^{13}C NMR spectrum of receptor S1 in $CDCl_3$.

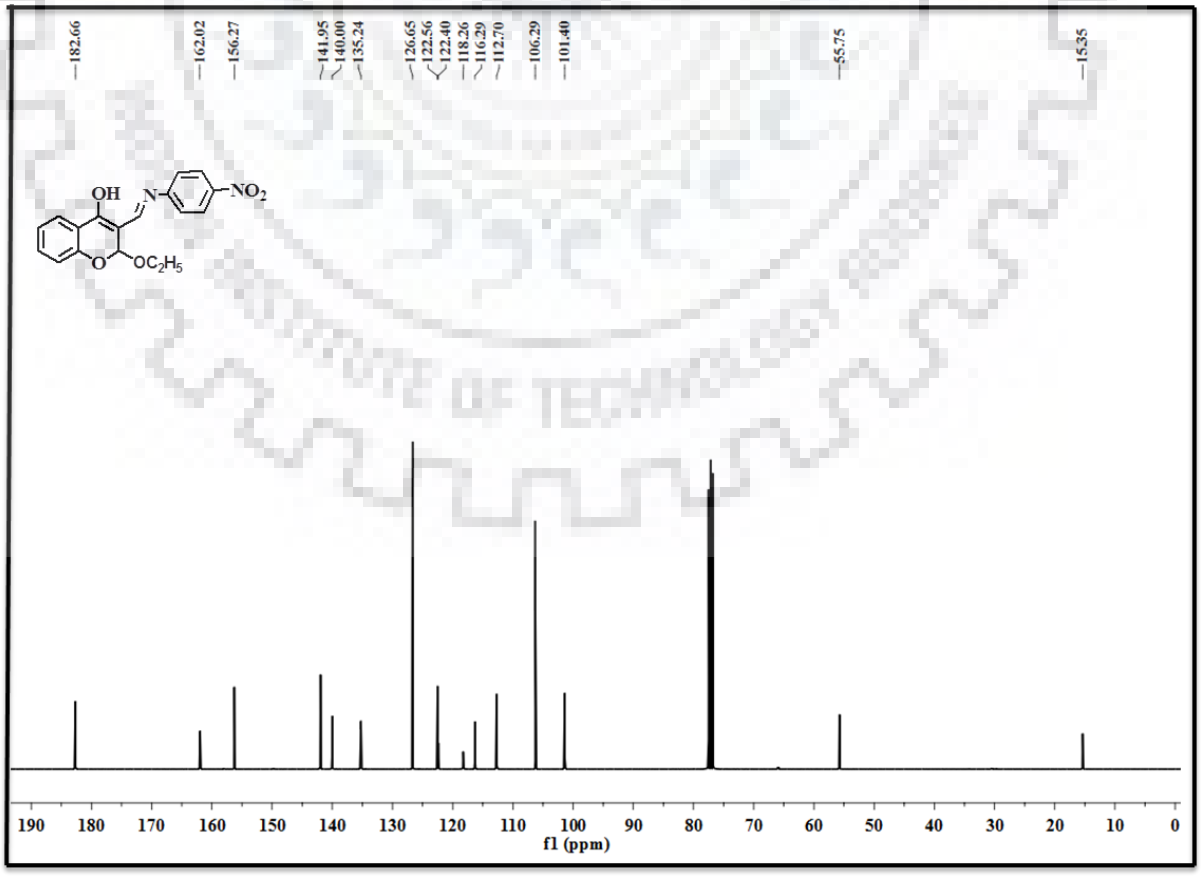

Spectrum No. 39. Mass spectrum of receptor S1.

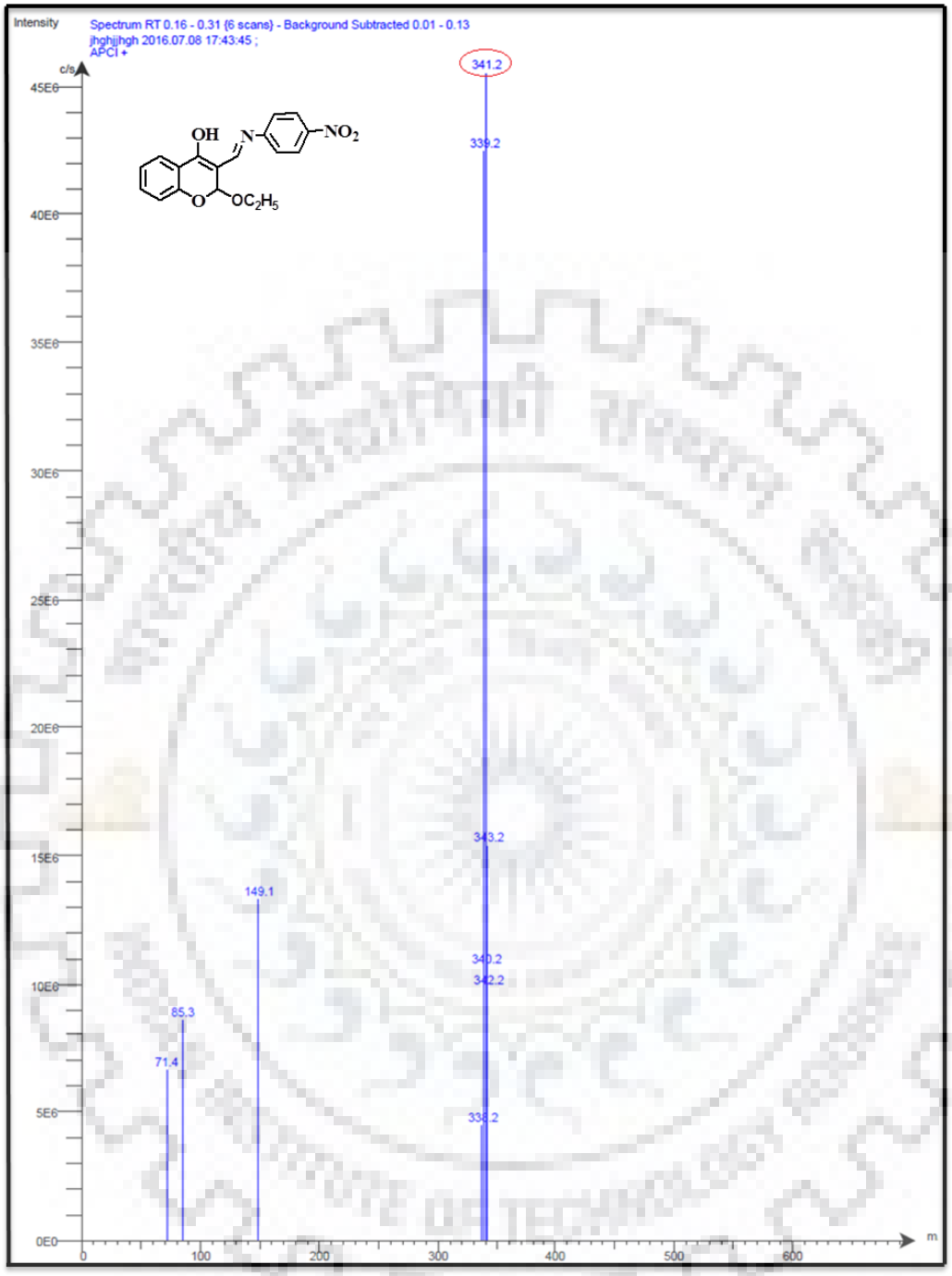

Spectrum No. 40. ^{1}H NMR spectrum of receptor S2 in DMSO d_6.

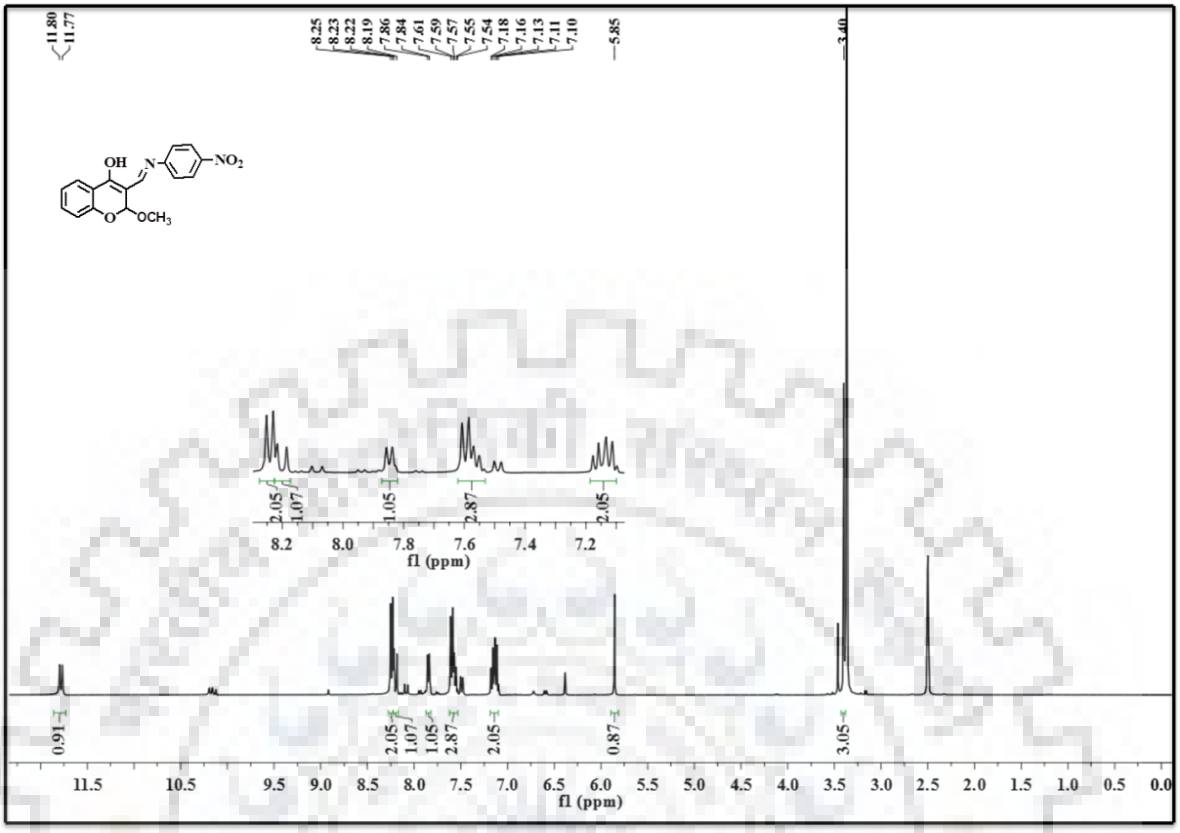

Spectrum No. 41. ^{1}H NMR spectrum of receptor S2 in DMSO d_6.

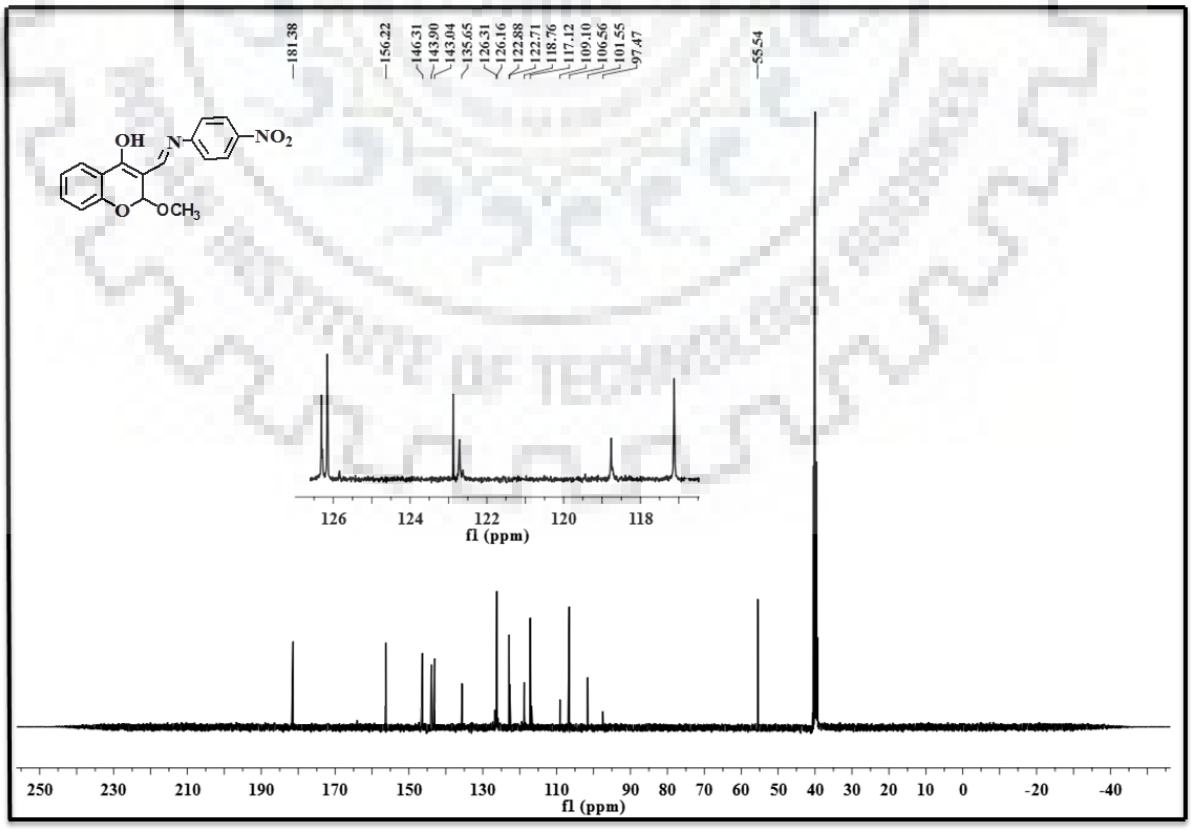

Spectrum No. 42. Mass spectrum of receptor S2.

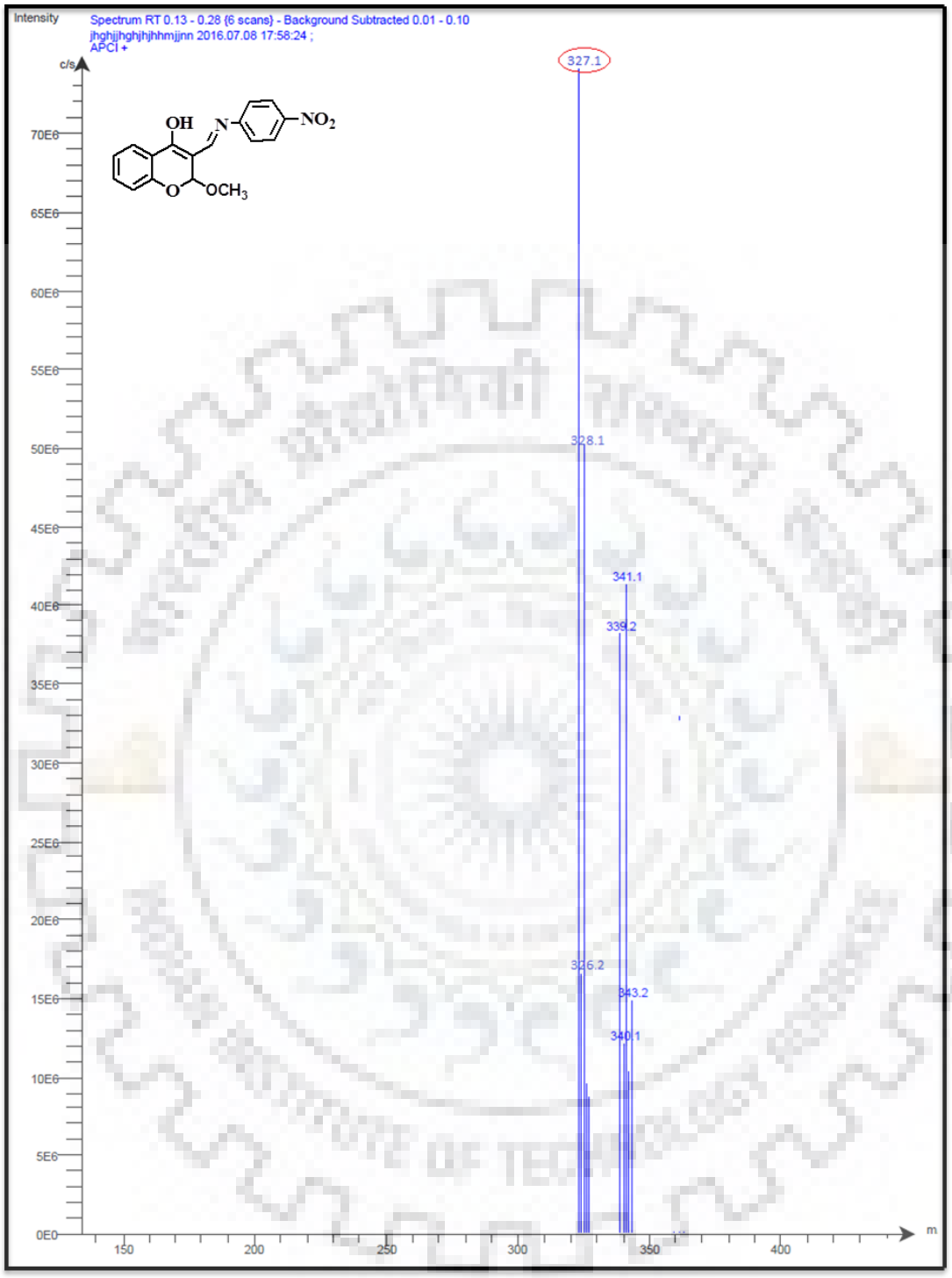

Spectrum No. 43. ^{1}H NMR spectrum of receptor S3 in DMSO d_6.

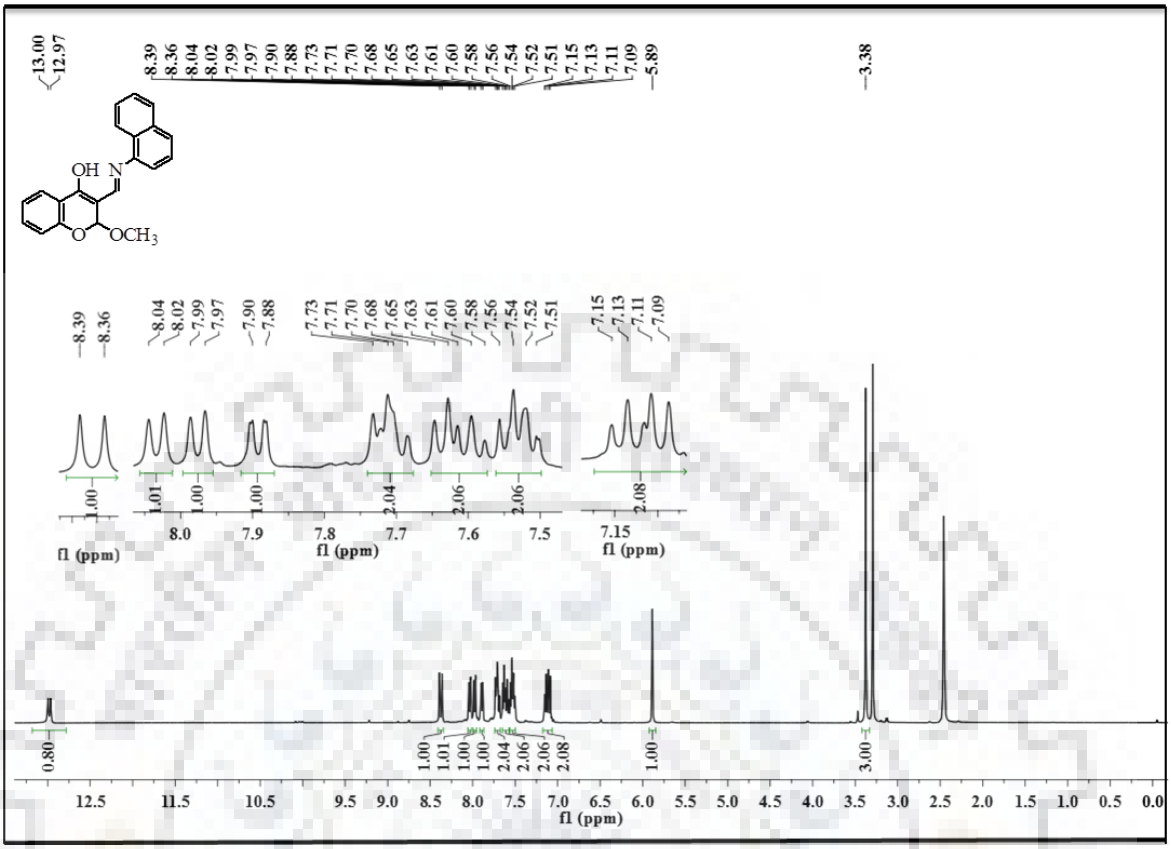

Spectrum No. 44. ^{13}C NMR spectrum of receptor S3 in DMSO d_6.

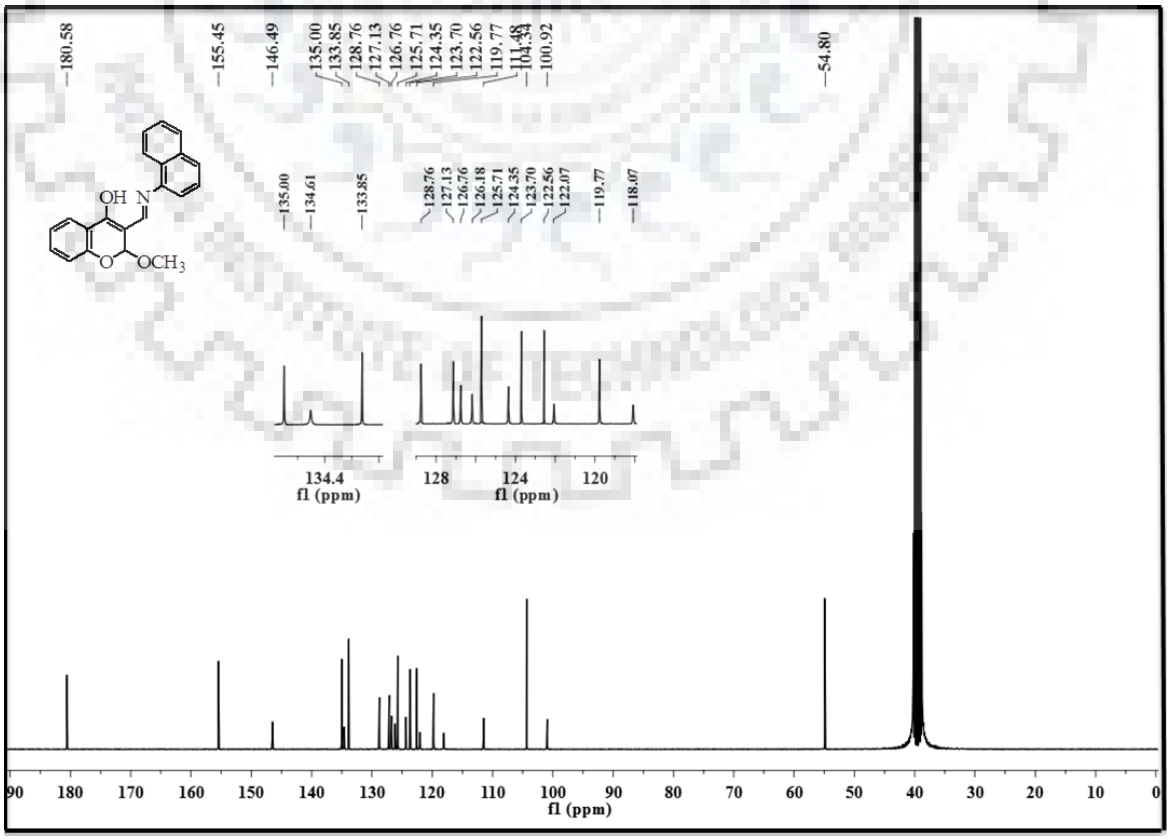

Spectrum No. 45. ^{1}H NMR spectrum of receptor S4 in DMSO d_6.

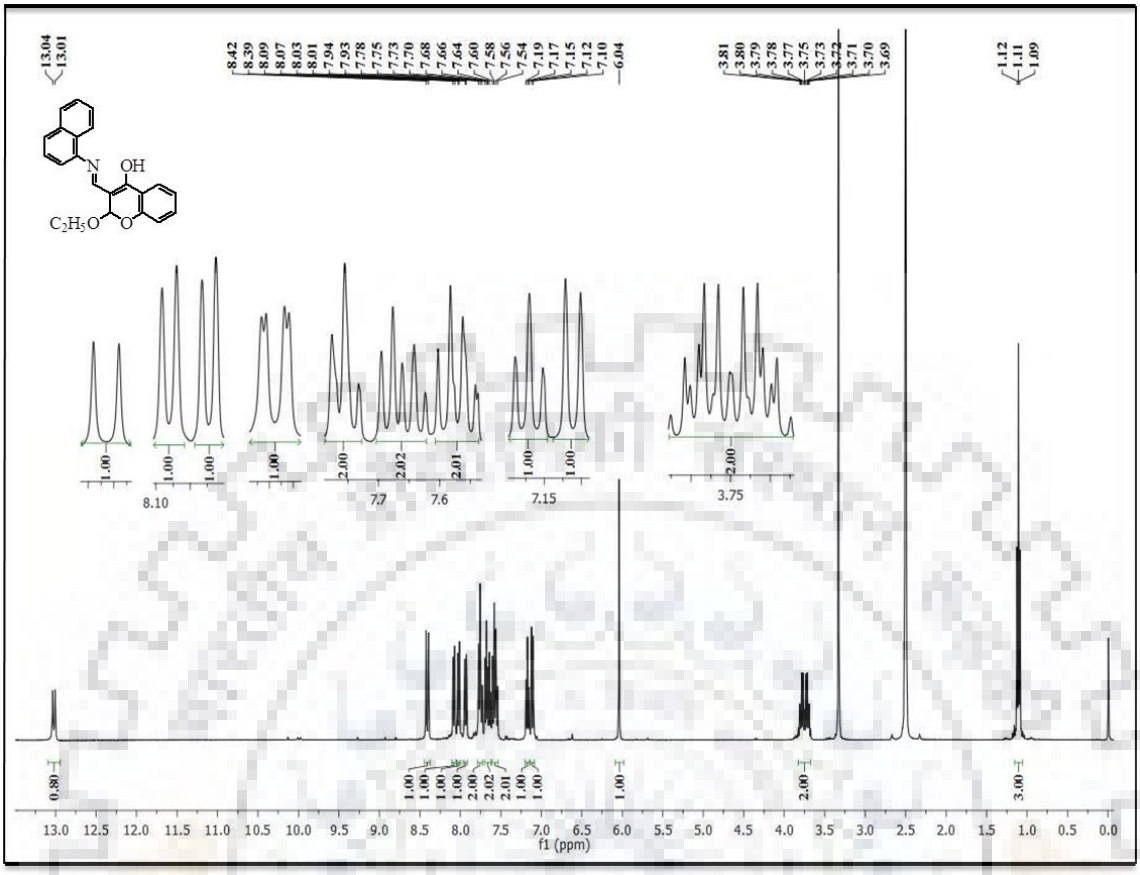

Spectrum No. 46. ^{13}C NMR spectrum of receptor S4 in $CDCl_3$.